Applied Geography 161 (2023) 103115

Contents lists available at ScienceDirect

Applied Geography

journal homepage: www.elsevier.com/locate/apgeog

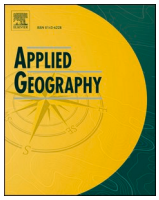

Greening of India: Forests or Croplands?

Jayanarayanan Kuttippurath *, Rahul Kashyap

CORAL, Indian Institute of Technology Kharagpur, Kharagpur, 721302, India

ARTICLE INFO

Handling Editor: J Peng

Keywords:
Greening
Croplands
Forests
Agriculture
Irrigation
LULC

ABSTRACT

There are substantial changes in global green cover owing to anthropogenic activities and climate change. Here, we estimate the long-term changes in India's green cover, and its contribution from croplands and forests using satellite-based Normalised Difference Vegetation Index (NDVI) and Leaf Area Index (LAI) for the period of 2000–2019. The change in Solar Induced Fluorescence (SiF) is also estimated to understand the variability in the photosynthetic activity and productivity. The increase in NDVI (10%), LAI (11%) and SiF (13%) suggests that India has been greening in the past two decades, which added 996640 km^2 of new leaf area during the period. The net vegetated land in India is substantially greening (62.5% area) and marginally browning (14% area). Interestingly, the magnitude of greening in croplands is twice the forests, and is predominant in Zaid (70% area) agricultural season. Therefore, the croplands drive (86.5% contribution) greening of India in the past two decades. The enhanced greening of croplands can be attributed to improved irrigation facilities, as demonstrated by the larger Net Irrigated Area (NIA) and Irrigated Sown Area (ISA). In addition, the effective cropland management, farm mechanisation and use of nitrogen fertilisers are also key to this cropland-based greening in India.

1. Introduction

The changes in the spatio-temporal patterns of temperature, rainfall, land use land cover (LULC) and biodiversity adversely affect the global forests and agriculture. Currently, the critical issues in food security are the land degradation and climate change (Watson et al., 2013; Meybeck et al., 2018; IPCC, 2019). Forests and agriculture account for nearly 80% of the geographical area of India, about 24.56% of which is forest and the remaining 55% is agriculture land (ISFR, 2019). Land use management is one of the important ways to increase the terrestrial vegetation and its productivity (Chen et al., 2019).

Satellite remote sensing offers a unique platform for earth observation across the domains and time periods (Kashyap et al., 2022; Roy et al., 2014; Sheffield et al., 2014). Typically, satellite-derived remote sensing indices such as Normalized Difference Vegetation Index (NDVI) and Leaf Area Index (LAI) are used as the indicators of changes in green cover (Burke & Lobell, 2017; Chen et al., 2019). Agricultural production is key for food security, which is usually analysed by the connection between crop yield and NDVI (Milesi et al., 2010; Teal et al., 2006). Many vegetation indices have been developed in the past, but NDVI is a reliable, well-tested and widely used parameter to study terrestrial vegetation. It is related to the structural properties of plants, such as LAI, live biomass, chlorophyll content, foliar nitrogen content and productivity (Roy et al., 2014; Sheffield et al., 2014). NDVI is an important parameter that represents aboveground primary production and thus, can be effectively employed to detect changes in the vegetation of terrestrial ecosystem (de Jong et al., 2011; Sarmah et al., 2018). LAI is one of the most important biophysical variables considered for characterising land surface ecosystems. It is closely linked to the terrestrial biophysical processes such as photosynthesis and evapotranspiration, and can be used to estimate net primary productivity (NPP) (Chen et al., 2019; de Jong et al., 2011).

The vegetation growth pattern is commonly used to monitor the productivity of natural forests and agricultural lands, and its temporal trends such as "declining or browning" and "increasing or greening" have been commonly used in the studies and reports; including the assessment of climate feedback (Cortés et al., 2021; Myneni et al., 1997). Note that the browning trends observed with the Moderate Resolution Imaging Spectroradiometer (MODIS) collection 5 data in some of the earlier studies were attributed to the sensor degradation with time (Wang et al., 2012; Zhang et al., 2017). The growing demand for food requires new and innovative technology that provide real-time monitoring of land, particularly the agricultural regions, for optimising sustainable management practices, agricultural efficiency and crop production (Atzberger, 2013; Burke & Lobell, 2017).

The atmosphere-land interactions are crucial for the functioning of

* Corresponding author.
E-mail address: jayan@coral.iitkgp.ac.in (J. Kuttippurath).

https://doi.org/10.1016/j.apgeog.2023.103115
Received 11 April 2023; Received in revised form 12 September 2023; Accepted 30 September 2023

climate and earth system through the exchanges of carbon, water, energy and momentum between the biosphere and atmosphere. Vegetation dynamics plays a significant role in regulating the climate system through these fluxes between land and atmosphere (Friedl et al., 2002; Fuchs et al., 2015; 2016; IPCC, 2019). However, recently, a great deal of change in the anthropogenic land use has been observed, and climate change has notably altered the global terrestrial biosphere (Zhu et al., 2016; Chen et al., 2019; IPCC, 2019). Most studies related to greening and browning have used only the NDVI and LAI data for India and South Asia. These studies have been conducted either for global land regions (Jiang et al., 2010; de Jong et al., 2011; Chen et al., 2019; Cortés et al., 2021) or some areas in India (Chakraborty et al., 2018; Mishra & Chaudhuri, 2015; Mishra & Mainali, 2017; Panday & Ghimire, 2012).

Currently, India is the most populated country and is one of the ecological hotspots of the world. Given the importance of croplands and forests for the national food security, sustainability and nature conservation, it is critical to understand the vegetation dynamics in India, as rapidly changing climate and human land management have greatly impacted the vegetation in India. Still, a dedicated study on the changes in the Indian terrestrial biosphere and its anthropogenic control is lacking. Some recent studies show greening of India in the past two decades (Kashyap et al., 2022, 2023a; Parida et al., 2020); making it the second largest contributor to the global greening (Chen et al., 2019). However, the contribution of croplands and forests to the net greening of India is largely unknown. Here, we analyse the long-term vegetation dynamics, and the contribution of croplands and forest to net greening, together with the biophysical aspects of greening in India for the last two decades. We also utilise both NDVI (surface greenness) and LAI (biophysical) metrices for estimating the changes in green cover and dynamics of vegetation growth in croplands and forests of India for the period from 2000 to 2019. On top of these, we also utilise the Solar Induced Fluorescence (SiF, photosynthesis and productivity) to complement the NDVI and LAI data to make our analysis more robust.

2. Data and methods

2.1. Green cover

There are several NDVI datasets available, including Advanced Very High-Resolution Radiometer (AVHRR), Generation of Global Inventory Modelling and Mapping Studies 3rd Version (GIMMS3g), Land Long-Term Data Record 4th Version (LTDR4) and MODIS. A validation study showed that these datasets had been compromised by temporal inconsistency for trend analysis due to sensor differences and sensor shifts among the platforms, except MODIS (Coppin et al., 2004; Prince et al., 2007). The MODIS collection 6 land and atmospheric data released in 2015 have significant improvement over the collection 5 data (Lyapustin et al., 2014). The study conducted by Tian et al. (2015) used NDVI and Enhanced Vegetation Index (EVI), and demonstrated the application of MODIS 6 for vegetation analysis. Here, the vegetation indices (VI) are acquired from the MODIS monthly (MOD13A1) data at 500 m pixel size (Didan, 2015). The seasonal NDVI data are computed by averaging the monthly NDVI data for winter (December, January and February), summer (March, April and May), monsoon (June, July and August) and post–monsoon (September, October and November) seasons at pan-India and regional scales, as shown in Fig. S1 and Table S1. Similarly, the seasonal LAI data are computed from the MODIS LAI product (MCD15A2H) (Myneni et al., 2015).

2.2. Photosynthetic activity and terrestrial productivity

We also examine the plant photosynthetic activity and terrestrial productivity by utilising the GOSIF v2 gridded SiF dataset as listed in Table 1. It is created by incorporating the Orbiting Carbon Observatory-2 (OCO-2) SIF with MODIS-based data and meteorological reanalysis (Li & Xiao, 2019). SiF is the radiation flux emitted in the form of light energy at 650–800 nm during the photosynthetic activity of plants. It is directly connected to the physiological process of plants and is therefore, a highly efficient proxy for plant photosynthesis, health and productivity (Porcar-Castell et al., 2014; Rascher et al., 2015). Currently, SiF is extensively utilised for detecting changes in surface greenness, due to its greater accuracy, as compared to the traditional reflectance-based indices (e.g. Kashyap et al., 2023b; Li et al., 2018; Xiao et al., 2019).

Table 1
Datasets, their resolution, purpose and the source from which they are acquired.

DATA	RESOLUTION	PURPOSE/USE	SOURCE
MODIS LULC	500 m	LULC data to extract Forest and Cropland	(https://lpdaacsvc.cr.usgs.gov/)
MODIS NDVI	500 m	NDVI & calculation of green cover change	(https://lpdaacsvc.cr.usgs.gov/)
MODIS LAI	500 m	LAI & calculation of green cover change	(https://lpdaacsvc.cr.usgs.gov/)
GOSIF SiF	0.5° × 0.5°	SiF & calculation of change in photosynthetic activity and productivity	(http://data.globalecology.unh.edu/)
Irrigated Area	250 m	Net Irrigated area & calculation of irrigated area change	(https://dx.doi.org/10.6084/m9.figshare.3790611.v1)
Major Food Crop types	0.1° × 0.1°	Delineate the spatial extent of major food crop types	(https://cds.climate.copernicus.eu/)
Agricultural data		Gross Sown area, area sown more than once, Net Irrigated area, food grain yield and food grain production	Ministry of Agriculture and Farmers Welfare, Government of India. (http://apps.iasri.res.in/agridata/20data/HOME_20.HTML) (https://www.indiastat.com/)

2.3. Delineation of the vegetated land and estimation of its long-term change

The MCD12Q1 is a global land cover product created using the supervised classification of MODIS reflectance data. The “cropland” type in this study is based on the International Geosphere-Biosphere Programme (IGBP) classification scheme of MCD12Q1, and is used because of the cropland class reliability (Fan & Liu, 2016). The forest cover types provided by the dataset are merged into a common forest class. The cropland class in the dataset is used to analyse the changes in agriculture areas, and the remaining classes are merged and reclassified as others. The forest and cropland dynamics are estimated using the MODIS Land Cover data (MCD12Q1). The years 2001, 2009 and 2019 are taken as the focal time periods for detecting the forest and cropland changes, as these cover the first and last years of our analysis and have an interval of a decade. The vegetation type map based on the MODIS Land Cover data (MCD12Q1 Version 6) International Geosphere-Biosphere Programme (IGBP) is shown in Fig. S2, with its details in Table S2. The major food crop types map of India based on the Copernicus global major food grain croplands productivity data are also shown in Fig. S3.

2.4. Quantification of changes in agriculture

The agricultural data such as Gross Sown Area (GSA), area sown more than once, food grain yield and food grain production are taken from the agricultural data book of the Ministry of Agriculture and Farmers Welfare, Government of India. The Net Irrigated Area (NIA) data for the period of 2000–2015 are taken from Ambika et al. (2016). The information about change in NIA for the period of 2000–2015 is obtained by the pixel-wise image differencing technique. Furthermore, the change in NIA (ΔNIA) is found for each climate homogeneous region of India. The percentage Irrigated Sown Area (ISWA) is obtained by

using GSA and NIA:

$$ISWA = \left(\frac{NIA}{GSA}\right)100\%$$

The regional contribution (RC) from each homogeneous climatic region of India for ΔNIA is,

$$RC_0 = \left(\frac{\Delta NIA_0}{\Delta NIA}\right)100\%$$

Where, 0 = any particular homogeneous region, ΔNIA_0 = ΔNIA for that particular homogeneous region (0), and ΔNIA = the change in NIA for whole India.

2.5. Estimation of long-term changes in green cover

We estimate the long-term change in surface greenness (NDVI), biophysical metric (LAI), and photosynthetic activity and productivity proxy (SiF) for the last two decades (2000–2019). The pixel-wise image differencing technique is applied to estimate the change in recent (2010–2019) from the previous decade (2000–2009). The change in NDVI, LAI and SiF is also estimated for the entire India and for specific regions (Fig. S1 and Table S1). In addition to the meteorological seasons, we also estimate these changes for the Indian agricultural seasons; Kharif (June–September), Rabi (October–February) and Zaid (March–May), as shown in the equation:

$$\Delta G\% = \frac{G_{(2010\text{–}2019)} - G_{(2000\text{–}2009)}}{G_{(2000\text{–}2009)}} \times 100$$

Here, ΔG% is the percentage change in the surface greenness (NDVI), biophysical metric (LAI), and photosynthetic activity and productivity proxy (SiF) for the period of 2000–2019. The long-term green cover change for the cropland is found by taking the average of each pixel of both NDVI and LAI, and then combining the long-term NDVI and LAI changes as shown above.

To understand the biophysical impact of greening and browning, we also estimate the net change in the leaf area (Δ LAI) for the period of 2000–2019, based on the equation in Chen et al. (2019):

$$\Delta LAI = \sum_{i=1}^{n} Ti \times Ai \times N$$

Where, *i* is a pixel with a statistically significant change, *n* refers to the total number of pixels in the region, *Ti* is the change in the pixel, *Ai* is the area of the pixel and *N* is the study period in number of years.

3. Results

3.1. Seasonal variability in green cover

The spatial variability of green cover in terms of NDVI, averaged for each pixel over the meteorological seasons of India is shown in Fig. 1. For the period 2000–2019, the non-vegetated (NDVI <0.25) land is found in the western Himalaya and northwest (NW) in all seasons. This is expanding from NW to the central (CI) and southern India (SI) in summer. Moderately vegetated land (NDVI = 0.25–0.5) is found in the regions of croplands, predominantly in summer and winter. Higher vegetation cover is found in the croplands for most of post-monsoon, areas of Indo-Gangetic Plain (IGP) and Tamil Nadu in winter, and some areas of IGP and CI in monsoon seasons. The minimum NDVI is smallest in winter and highest in post-monsoon, whereas the maximum NDVI is lowest in summer and highest in post-monsoon seasons. In summary, the seasonal variability of vegetated land is lowest in summer (mean NDVI = 0.35) and highest in post-monsoon (mean NDVI = 0.53).

The variability of LAI across the seasons for the Indian region during the of period 2000–2019 is shown in Fig. 2. Majority of the cropland

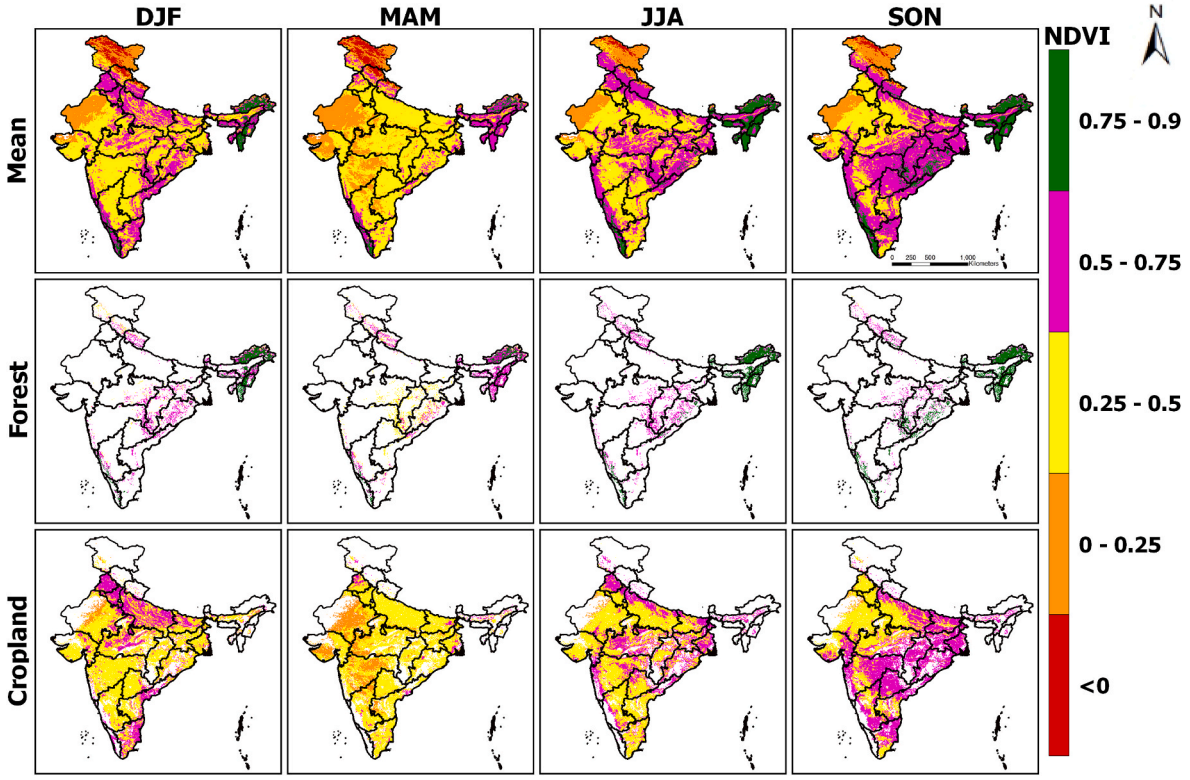

Fig. 1. Normalized Difference Vegetation Index (NDVI) (top panel), forest cover (middle panel) and croplands (bottom panel) during winter (December, January and February), summer (March, April and May), monsoon (June, July and August) and post–monsoon (September, October and November) seasons averaged over the period of 2000–2019 for the Indian region.

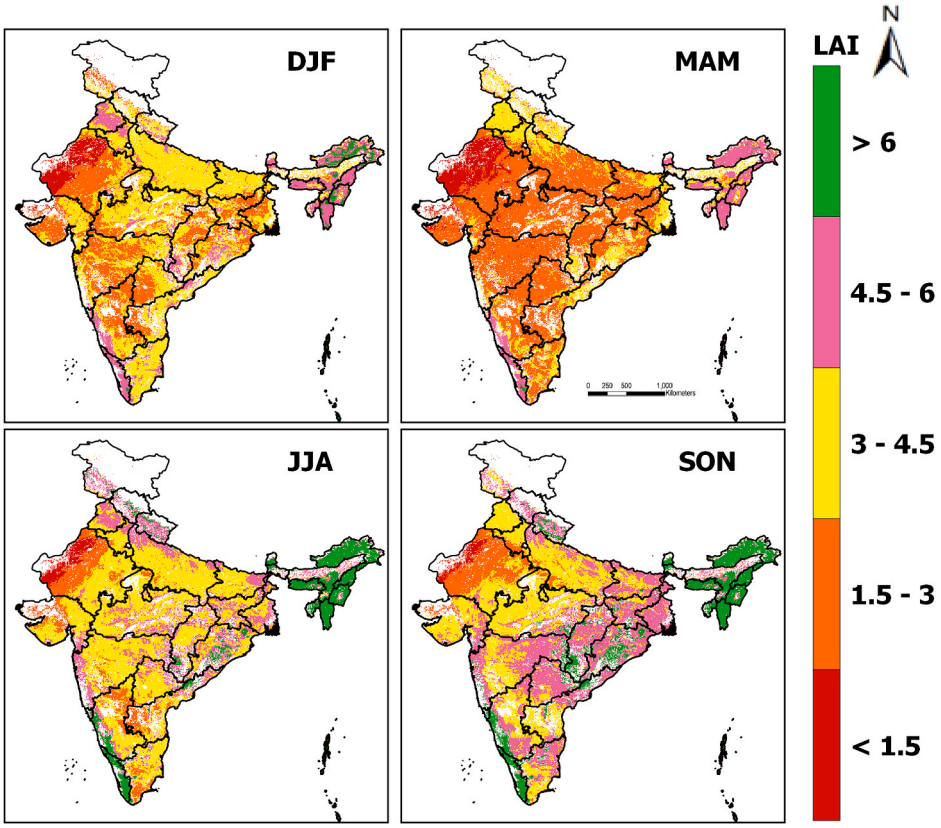

Fig. 2. Leaf Area Index (LAI) during winter (December, January and February), summer (March, April and May), monsoon (June, July and August) and post-–monsoon (September, October and November) seasons averaged over the period of 2000–2019 for the Indian region.

areas in monsoon and some areas of IGP, CI and SI in post-monsoon show moderate (3–4.5) LAI. The lowest (1.5–3) LAI is observed in NW in all seasons. It shows that the mean LAI is highest during post-monsoon and lowest in summer; consistent with the NDVI analysis. The state-wise net leaf area changes over the years 2000–2019 are presented in Table S3. The state of Rajasthan (133464.57 km^2) in NW, Madhya Pradesh (133464.57 km^2) and Maharashtra (105,429.79 km^2) in CI and Uttar Pradesh (96,371.79 km^2) in IGP have added the highest net leaf area during the study period (2000–2019). In contrast, the state of Mizoram (2.31 km^2) and Sikkim (27.27 km^2) in NE, Chandigarh (2.37 km^2) in IGP and Puducherry (61.36 km^2) in SI have added the lowest amount of net leaf area in the same period. The link between NDVI and LAI in all seasons is assessed for the period of 2000–2019 by using the correlation analysis and is shown in Fig. S4. The highest correlation coefficient (r) is obtained for the dry seasons, post-monsoon (0.745) and summer (0.741), and weakest correlation is found for the wet seasons, monsoon (0.675) and winter (0.658). A correlation of 0.704 is estimated between NDVI and LAI for the entire study period (2000–2019); demonstrating a very good agreement between them.

3.2. *Forests and croplands: seasonal variability*

Large areas of forest cover are observed in the western Himalaya (e. g. savanna, woody savanna, shrub lands and evergreen broadleaf forest) in all seasons, Central India in winter and monsoon, and Hilly and NE (e. g. evergreen broadleaf forests) in summer, as depicted in Figs. 1 and 2, Fig. S2 and Table S2. Very dense (NDVI = 0.75–0.9) vegetation (e.g. evergreen broadleaf forests) is observed in NE and the eastern Himalaya in all seasons, except for summer seasons. Areas of Central India (e.g. shrub lands, savanna dominated by woody perennials and deciduous broadleaf forests) in post-monsoon, and Western Ghats in monsoon and post-monsoon also show healthy forests (NDVI >0.75). Very dense forest (LAI >6) is observed in some areas of NE, eastern Himalaya, Western Ghats and CI in monsoon and post-monsoon seasons. Some regions in NE and Western Ghats in winter and summer, western Himalaya, some areas of IGP and CI in monsoon also have dense forests (LAI = 4.5–6.0).

Croplands with higher yield (NDVI = 0.5–0.75) are observed in much of IGP (e.g. wheat growing) and some areas in the southern peninsula (e. g. maize) in winter. The croplands of IGP (e.g. Punjab and Haryana) show the highest yield (LAI >4.5) in winter. Low yield is estimated (NDVI = 0.25–0.5, LAI = 1.5–3) in most croplands of the country in summer, and cropland yield is very small in some areas of NW and CI (NDVI = 0–0.25 and LAI = 1.5). During monsoon season, majority of croplands in the country have a moderate yield (LAI >3). However, higher yield (NDVI = 0.5–0.75 and LAI = 4.5–6) is observed in some areas of eastern India, IGP (e.g. rice and maize) and CI (e.g. soyabean, maize and wheat) during post-monsoon, as demonstrated in Figs. 1 and 2, Fig. S3. Most of the remaining areas are croplands with lower yields (NDVI = 0.25–0.5 and LAI = 1.5–3) in all seasons.

Since we examine the croplands in India, they are further explored in terms of the agricultural seasons Kharif, Rabi and Zaid of India, as shown in Fig. 3. In Zaid, most croplands in NW, CI, some areas in SI, and IGP have moderate crop cover (NDVI = 0.3–0.45), with some areas in NW are almost devoid of crop cover or they are in a severely stressed condition (NDVI = 0.15). High crop density or healthy crop growth (NDVI >0.45) is observed in IGP, NE and some areas of SI. In Kharif, majority of the croplands are healthy, and some areas in IGP exhibit the highest growth (NDVI = 0.6–0.75). However, some areas in NW and SI show lower crop density; showing signs of stress. In Rabi, IGP has dense crop cover and healthy growth with its peak density in Punjab and Haryana (NDVI = 0.6–0.75). Croplands in NW are sparse or severely stressed (NDVI <0.15). Therefore, it can be stated that the croplands are dense and in healthy condition in IGP, NE, areas of CI and SI. The croplands in areas of NW, CI and SI are in a state of moderate growth, although some

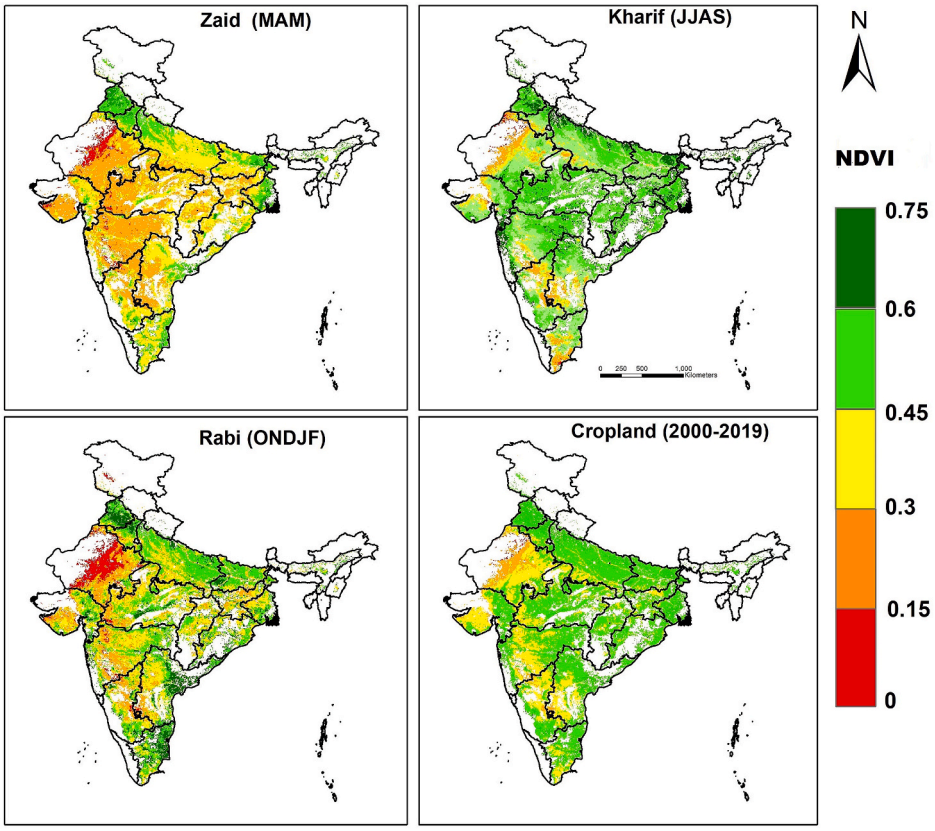

Fig. 3. Normalized Difference Vegetation Index (NDVI) in the croplands during the Indian agricultural seasons, Kharif (June–September), Rabi (October–February) and Zaid (March–May), averaged over the period of 2000–2019 for the Indian region.

areas in NW are under stress. The cropland productivity peaks in Kharif season with the maximum NDVI of 0.823, followed by Zaid (0.764) and Rabi (0.678). Kharif (0.495) has the highest mean NDVI, which also serves as a measure of gross farmland productivity, followed by Rabi (0.463) and Zaid (0.329) seasons.

3.3. Decadal change in the vegetated land

The spatial distribution of green cover and photosynthetic activity represented in terms of NDVI, LAI and SiF are presented in Fig. 4. The dense green cover with higher rates of photosynthesis and productivity is observed in HR, NE and some regions in CI and Western Ghats. The scanty vegetation with lower photosynthetic activity and productivity is observed in NW and the western CI and northern SI. The rest of the regions are vast croplands with moderate green cover, photosynthetic activity and productivity. The long-term trend in green cover represented by the decadal change in NDVI, LAI and SiF is presented in Fig. 4. The increase in NDVI/LAI/SiF (i.e. greening) is dominant in most of NW, IGP and CI, but decrease (i.e. browning) in much of HR, NE and SI. Some areas in the eastern or lower IGP also exhibit browning. It is evident that the areas of scanty green cover and lower photosynthetic activity and productivity, are greening. In contrast, the areas of denser green cover with higher rates of photosynthetic activity and productivity are browning.

The NDVI data are further analysed for all seasons in the previous (2000–2009) and recent (2010–2019) decades, as shown in Fig. S5. In winter and monsoon, NDVI is increased (greening) in IGP and some areas of CI, but most areas in post-monsoon for recent decade. For croplands, the minimum NDVI has increased for each season over the decades. In terms of decadal change, all seasons show an enhancement, except in summer. There is a marginal reduction (0.16%) in both NDVI and LAI for summer, but monsoon (11%), post-monsoon (5.8%) and winter (3.4%) show significant increase in NDVI in recent decade. However, in terms of LAI, the highest increase is found in post-monsoon (9.7%), followed by monsoon (4%) and winter (3.9%) in recent decade. In brief, enhanced greening is found in recent decade in all seasons, except in summer.

3.4. Decadal changes in forests and croplands

For forests, in 2000–2009, the minimum NDVI is smallest in winter and highest in post-monsoon seasons. The mean and maximum NDVI are lowest in summer (0.53) and highest (0.73) in post-monsoon, as listed in Table S4. In recent decade (2010–2019), the minimum and maximum NDVI are smallest in summer and highest in post-monsoon. Conversely, the mean NDVI is lowest for winter (0.58) and highest for post-monsoon (0.78). The increase in the peak NDVI (2.24%) indicates greening of forests in recent decade, which is highest in post-monsoon (3.3%) and then in winter (2.2%) and monsoon (2.1%). On the other hand, the LAI-based greening is found in all seasons, except in summer where it reduced by 1.6% in recent decade. Post-monsoon (2.9%) leads the LAI-based greening, followed by winter (2.5%), and monsoon (2%) during 2010–2019.

For croplands, in 2000–2009, the minimum and maximum NDVI are lowest for summer and highest for post-monsoon. The mean NDVI is smallest in summer (0.31) and highest in monsoon (0.47). In recent decade (2010–2019), the minimum and maximum NDVI are lowest for summer and highest for post-monsoon. The mean NDVI is lowest in summer (0.32) and highest in monsoon (0.5), as presented in Table S5. Recent decade (2010–2019) shows predominant greening of croplands with an estimated enhancement of 11.4% in NDVI and 12.1% in LAI. Both NDVI and LAI show greening in all seasons in recent decade, in which monsoon (20.4%), post-monsoon (10.8%) and winter (6%) exhibit substantial greening in terms of NDVI. The winter (22.1%), post-

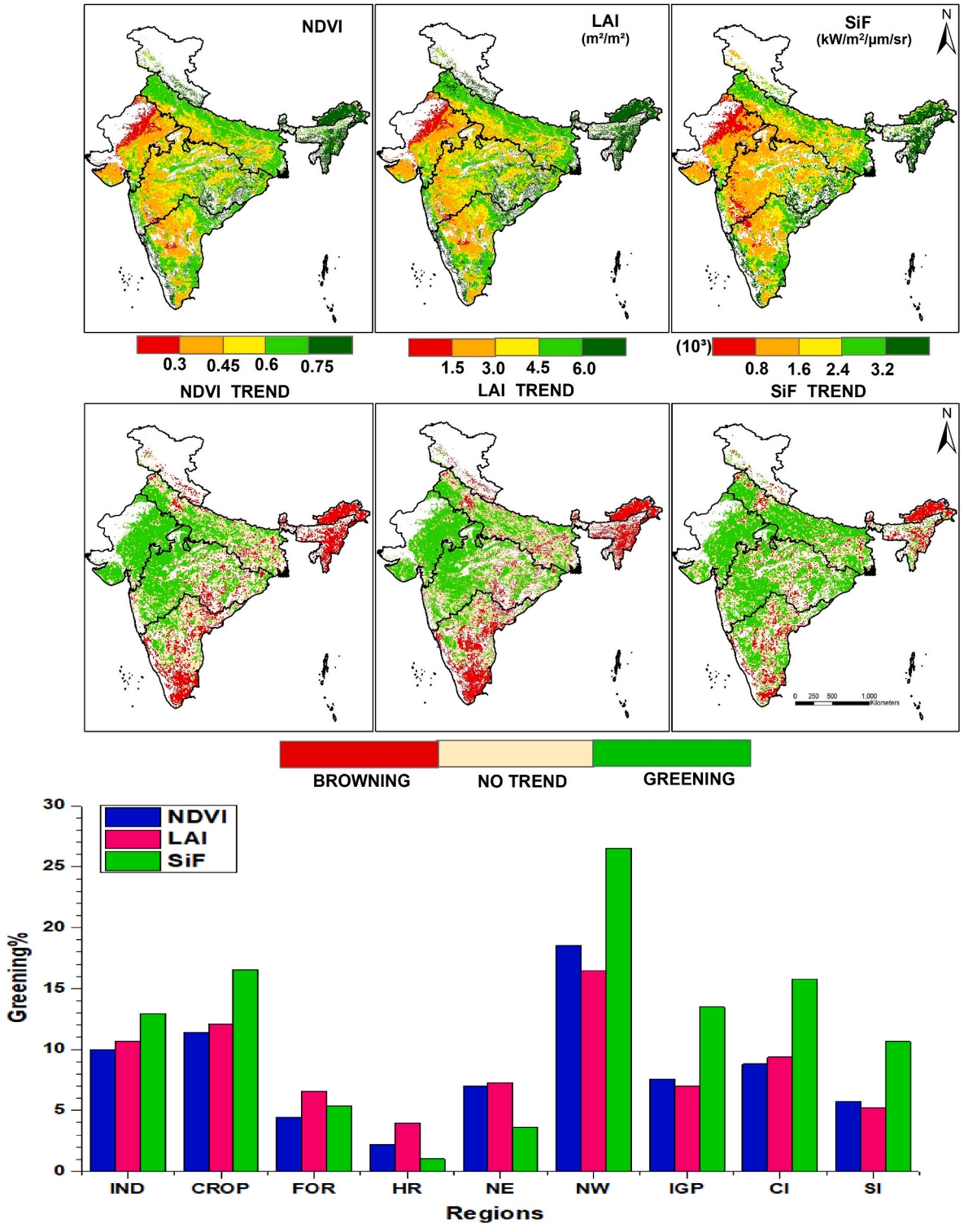

Fig. 4. Top: Green cover spatial variability exhibited by Normalized Difference Vegetation Index (NDVI), Leaf Area Index (LAI in m^2/m^2) and Solar Induced Fluorescence (SiF in $kW/m^2/\mu m/sr$) averaged over the period of 2000–2019 for the Indian region. Middle: The long-term change in green cover (greening/browning) exhibited with NDVI, LAI and SiF for the period of 2000–2019. Bottom: the increase (greening %) in NDVI, LAI and SiF for all vegetated lands of India (IND), croplands (CROP), forests (FOR) and the different regions of India: HR (Hilly), North east (NE), North west (NW), Indo Gangetic Plain (IGP), Central India (CI), and Southern/Peninsular India (SI) over the last two decades (2000–2019).

monsoon (12.4%) and monsoon (4.7%) seasons also show significant LAI-based greening in 2010–2019 as compared to that in 2000–2009. LAI increased by 4.8% for all vegetated lands, but 5.8% for croplands; suggesting the cropland-based greening in recent decade (2010–2019). Among the agricultural seasons, the highest increase in NDVI is observed in Zaid (3.3%), followed by Rabi (2.7%) and Kharif (1.1%) in recent decade.

Among the six homogeneous regions (Fig. S1 and Table S1), greening is dominant in NW (4.3%) and SI (3.6%) where the mean NDVI has increased by 0.025/dec in 2010–2019. Regarding the gross cropland

productivity, strong greening is found in Rabi (10.2%), and then in Kharif (8.6%) and Zaid (5%). The highest cropland greening is estimated in NW where the mean NDVI has increased by 15.5% (from 0.335 to 0.387) in recent decade. Some regions such as CI (8.8%, 0.41–0.446) and IGP (7.3%, 0.451–0.484) also show significant cropland greening. Conversely, the mountainous regions of Himalaya (6.6%, 0.483–0.515) and NE (3.8%, 0.53–0.55) exhibit relatively smaller changes in recent decade (2010–2019) from the previous decade (2000–2009), as forests are the predominant vegetation type there.

3.5. Greening of India

We quantify the greening of India in terms of long-term changes in NDVI, LAI and SiF during the period of 2000–2019 as exhibited in Fig. 4. All three metrices demonstrate substantial increase, with the highest enhancement in SiF (13%) and then in LAI (11%) and NDVI (10%). In terms of the cropland greening, SiF (16.6%) shows higher values than LAI (12.1%) and NDVI (11.4%). With respect to the forest greening, LAI (6.6%) exhibits the largest increase, followed by SiF (5.4%) and NDVI (4.5%). Henceforth, the greening is predominant in croplands, which is twice the forest during the last two decades in India. Here, NW has the highest increase in SiF (26.5%), NDVI (18.5) and LAI (16.4%), and HR has the lowest greening with marginal increase in LAI (3.9%), NDVI (2.1%) and SiF (1%).

In addition, we explore the greening of India in each season for the period of 2000–2019 using both NDVI and LAI. The NDVI-based greening is observed in all seasons, except for summer, in which it decreased by 0.34%. Substantial greening is observed during monsoon (21.9%), post-monsoon (11.6%) and winter (6.8%) seasons. The LAI-based greening shows the highest enhancement in post-monsoon (19%) and smallest in summer (3.8%) during 2000–2019. Significant LAI-based greening is also observed during monsoon (8%) and winter (7.8%). These analyses reveal that India has been greening, with an increase of about 996640 km^2 new leaf area, for the last two decades, as listed in Table S2.

The dynamics of net vegetated area comprising of forests and croplands in India is analysed for the periods of 2001–2009 and 2010–2019, and are shown in Fig. S6. In 2001, the total forest area was 353,403 km^2, which increased to 387,051.8 km^2 by 2019, about 9.52% increase during the period 2001–2019. On the other hand, in 2001, the total cropland area was 2426917 km^2, which increased to 2530036 km^2 by 2019, about 0.22%/yr increase during the period 2001–2019. Therefore, the vegetated land in India is increased by 4.92% during the past two decades.

3.6. What drives the greening?

The greening/browning in the croplands with respect to NDVI during the Indian agricultural seasons Kharif, Rabi and Zaid for the past 20 years (2000–2019) is presented in Fig. 5. In Zaid, there is predominant greening except for some areas in IGP and SI. In Kharif, most croplands are greening, except in some areas of IGP, CI and SI. In Rabi, greening is observed for NW and IGP, but browning in SI and CI. The highest greening area (70%) for the years 2000–2019 is found in Zaid, followed by Kharif (59.5%) and Rabi (54.8%), as given in Table 2.

The net vegetated land comprising of croplands and forests is largely greening (62.54%), and marginally (14%) browning in 2000–2019. In the forest lands, about 17.5% are greening and 47.43% are browning during the same period. Almost two-thirds (72.3%) of the croplands exhibit greening and 7.7% is browning. This suggests that a vast majority (86.5%) of greening in India is due to croplands. Among the regions, as listed in Table 2, large cropland greening is estimated in NW (83.5%), followed by IGP (64.5%) and CI (61.6%). In terms of agricultural seasons, Zaid shows the largest greening in NE (72.7%), IGP (70%) and Hilly (45.2%) regions, but Rabi in NW (89.6%) and CI (65.2%), and Kharif (48.7%) in SI.

We also investigate the factors responsible for cropland greening in India, as illustrated in Fig. 6. The Gross Sown Area (i.e., total harvested area) of India has increased by 8.4% (185.34 mha–200.95 mha) from 2001 to 2015. The total food grain production in India has increased by

Table 2
Cropland greening area (%) variability across seasons in various homogeneous regions during the period 2000–2019.

Regions	Greening Area (%)	Kharif (%)	Rabi (%)	Zaid (%)
Hilly (HR)	39.56	39.34	34.34	45.32
North East (NE)	41.57	40.11	12.40	72.72
Indo-Gangetic Plain (IGP)	64.55	61.69	62.21	69.96
North West (NW)	83.49	77.83	89.63	83.01
Central India (CI)	61.65	55.53	65.25	64.17
South India (SI)	41.88	48.68	28.77	48.20

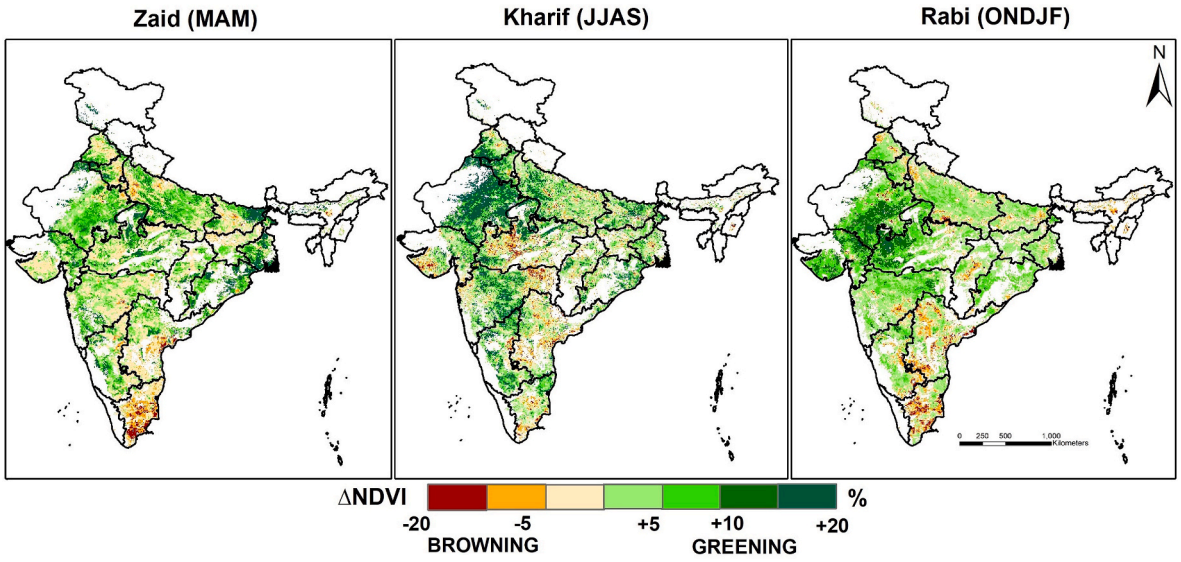

Fig. 5. Long-term green cover change (greening/browning) in the croplands based on the Normalized Difference Vegetation Index (NDVI) during the Indian agricultural seasons, Kharif (June–September), Rabi (October–February) and Zaid (March–May) averaged over the period of 2000–2019 for the Indian region.

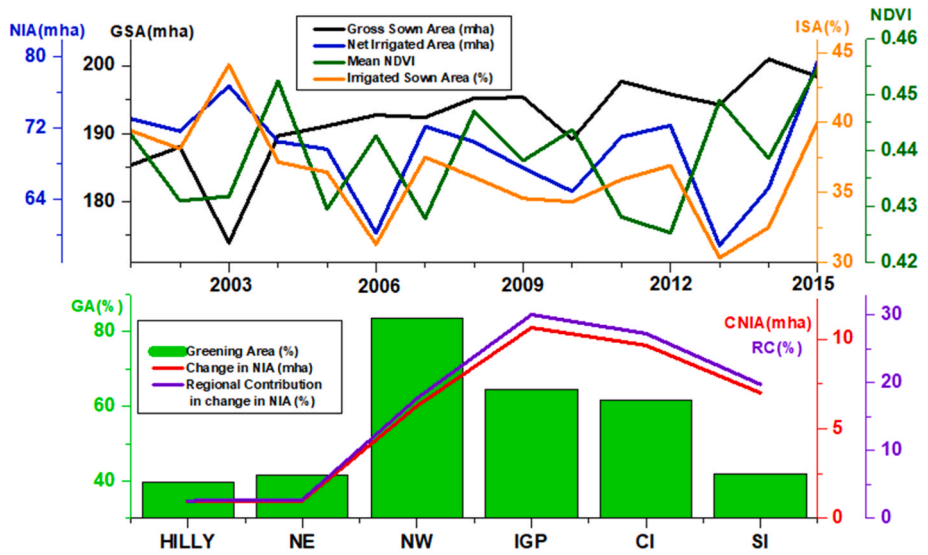

Fig. 6. Top: Temporal evolution of the mean Normalized Difference Vegetation Index (NDVI), Gross Sown Area (GSA), Net Irrigated Area (NIA) and the percentage of Irrigated Sown Area (ISA). Bottom: The percentage of greening area with change in the Net Irrigated Area (NIA), and the regional contribution of homogeneous regions of India; Hilly (HILLY), North east (NE), North west (NW), Indo Gangetic Plain (IGP), Central India (CI), and Southern/Peninsular India (SI), during the period of 2001–2015.

34% from 196 to 279 million tonnes during the period of 2000–2019. This is primarily because of the increase in the total harvested area through multiple cropping. The area sown more than once has increased by 38.6% (44 mha in 2000 to 61 mha in 2017), which also supports the idea that multiple cropping practices play a significant role in the greening. A substantial advancement (45.3%, 16 quintal/ha to 23.25 quintal/ha) in total food grain yield is observed during the period of 2000–2019. In recent decade (2010–2019), 24.82% increase in the total food grain yield is estimated, which can be due to the improvement in agricultural machinery, and is another reason for the greening in India.

The pixel-wise combination as the average of long-term change in NDVI and LAI is estimated for the three agricultural seasons in India to delineate the net green cover change, and is shown in Fig. 7. Most areas in NW, IGP and CI show greening, but browning is predominant in SI. Greening in recent decade (2010–2019) is found mostly in NW and IGP. In SI, croplands of Tamil Nadu and Andhra Pradesh depict browning. Analysis of the long-term changes in LAI for croplands also shows a similar trend and can be explained by increasing temperature, and decreasing precipitation and soil moisture there, which is known as the warming-induced moisture stress (Kashyap et al., 2022, 2023a; Parida et al., 2020). Croplands in NW, CI and some areas in IGP and SI, which are irrigated recently (2015), depict greening. Browning of croplands is observed in some areas of IGP, CI and SI, which were either irrigated in 2000 but not recently (2015) or non-irrigated. The increased food production is the outcome of expanded croplands supported by more irrigated lands.

NIA in India has increased by 10.79%, from 71.68 mha in 2001 to 79.42 mha by 2015. The ΔNIA is highest for IGP (10.64%) with a regional contribution (RC) of 30% to overall ΔNIA for the India vegetated lands. In addition, irrigation facilities in CI have improved (ΔNIA

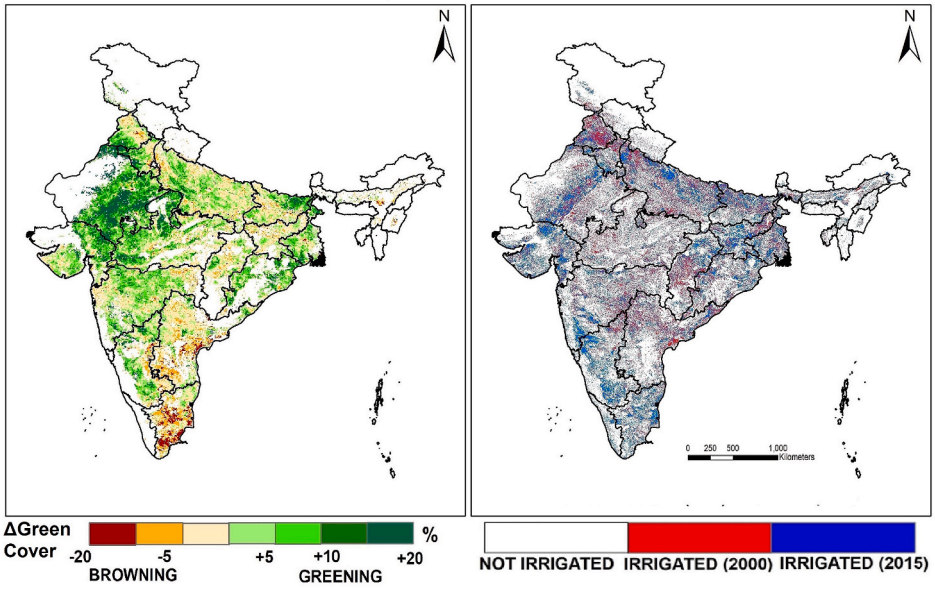

Fig. 7. Left. Long-term green cover change (greening/browning) in the cropland region based on the Normalized Difference Vegetation Index (NDVI) and Leaf Area Index (LAI) over the recent decades (2000–2019). Right. Change in the Net Irrigated Area (ΔNIA) over the years 2000–2015.

for CI = 9.65%), which contributes 27.23% to the net ΔNIA. The irrigation facilities in the hilly regions of Himalaya (ΔNIA = 0.97%, RC = 2.75%) and NE (ΔNIA = 0.97%, RC = 2.75%) show small improvement. The percentage of sown irrigated area has increased by 2% in the period of 2000–2015. In India, agriculture intensification is aided by the application of large amounts of fertiliser and the enhancement in irrigation facilities (both surface and groundwater). As a result, the lands in India, which were formerly fallow are now used to cultivate crops.

4. Discussion

4.1. Greening of India: climate Change and CO_2 fertilisation effect

In the context of changing climate, India is largely greening in recent decades (Bala et al., 2013; Kashyap et al., 2022, 2023a; Parida et al., 2020; Sarmah et al., 2018, 2021). In NW and CI, greening is observed due to improved soil moisture, i.e. moisture induced greening (Kashyap et al., 2022; Parida et al., 2020). The rising population and anthropogenic activities such as burning of fossil fuels, deforestation, soil-related factors (e.g. erosion, nutrient leaching, depleted soil organic carbon) and poor land management (e.g. clearing of vegetated land for commercial or agriculture purposes) have led to substantial rise in atmospheric CO_2 in India (Singh et al., 2022). The CO_2 in India is rising rapidly (2.1 ppm/yr) in recent decades (2002–2020) and is comparable to that of global tropics and mid-latitude regions (Kuttippurath et al., 2022). Apart from being a prominent greenhouse gas (GHG), atmospheric CO_2 plays a significant role in the global carbon cycle.

The "CO_2 fertilisation effect (CFE)" has two physiological effects because of the elevated levels of atmospheric CO_2 on plants. First, the enhancement in the terrestrial carbon assimilation by vegetation and higher productivity (Myneni et al., 1997; Zhu et al., 2016). Second, in higher CO_2 scenarios, leaves adjust to the ambient atmospheric conditions by limiting the stomatal conductance, which results in reduced water loss through transpiration and thus, enhance the ecosystem water use efficiency (Keenan et al., 2013; Cheng et al., 2017). Some studies report CFE as the major driver of global greening based on vegetation models and field observations (Zhu et al., 2016; Piao et al., 2020; Chen et al., 2022). Studies also find the contribution of CFE to greening of India and speculate that it would continue in future (Bala et al., 2013; Dubey & Ghosh, 2023). However, understanding the impact of elevated atmospheric CO_2 on plant growth, particularly in non-experimental settings, is currently limited. The impact varies based on plant species, ambient temperature, and the presence of adequate water and nutrient resources (McMurtrie et al., 2008; Wenzel et al., 2016). Apart from these, studies also report that there is a decline in global CFE in recent decades (Wang et al., 2020; Winkler et al., 2021). Furthermore, CFE drives greening in two ecosystem types, namely temperate forests and cool grasslands, but no visible long-term impacts in other biomes (Yang et al., 2016; Winkler et al., 2021). In future, the radiative effects of increasing atmospheric CO_2 may counter the CFE driven greening. Also, terrestrial ecosystems would be saturated to CFE in the warming scenario (Shi et al., 2021) and strengthen terrestrial carbon sinks in future (Keenan et al., 2016). Therefore, more field and modelling studies are needed on CFE to make robust conclusions.

4.2. Novelty of the study

Vegetative stages are characterised by the increasing NDVI and LAI (greening) during the growing period, followed by their decrease (browning) during the clearing and cultivation of crops. These analyses are key to understand the changes in vegetation and associated drivers (Kumar et al., 2013; Piao et al., 2020). Currently, almost one-third of the global vegetated land is greening due to changing climate (Zhang et al., 2017) and intensive land management (Chen et al., 2019). India has been largely greening in recent decades (Kashyap et al., 2022, 2023a; Parida et al., 2020), making it the second largest contributor to global greening (Chen et al., 2019). However, the question remains unanswered is that whether this greening is contributed by croplands or forests. In addition, most studies used a single metric to analyse the surface greenness and photosynthetic activity such as NPP (Bala et al., 2013), LAI (Chen et al., 2019), NDVI (Sarmah et al., 2018; Parida et al., 2020), FPAR (Kashyap et al., 2022) or GPP (Sarmah et al., 2021; Kashyap et al., 2023a). However, we apply three different remote sensing-based metrices, i.e. surface greenness (NDVI), biophysical metric (LAI), and photosynthetic activity and productivity proxy (SiF), to make a robust statistics on the long-term change in green cover and its anthropogenic drivers in India for the last two decades (2000–2019). Furthermore, we also present a detailed regional analysis of the long-term changes in green cover for all seasons.

4.3. Findings and implications

Our results reveal higher NDVI, LAI and SiF in the post-monsoon and monsoon seasons due to the favourable combination of moisture and temperature during the seasons, as also found in Bala et al. (2013), Parida et al. (2020) and Kashyap et al. (2022, 2023a). The surface greenness (NDVI) and biophysical metric (LAI) show a strong positive correlation as the changes in NDVI also reflect the temporal pattern of biophysical characteristics and phenological phases of vegetation growth (Ambika et al., 2016; Li et al., 2014; Sakamoto et al., 2005). India has been greening in recent decades with substantial enhancement in NDVI (10%), LAI (11%) and SiF (13%) and about 996640 km^2 of new leaf area is added in this period. India is substantially greening (62.54%) and marginally browning (14.08%) during 2000–2019, where the magnitude of greening in croplands is twice the forests. Our analysis reveals large-scale browning (47.43%) in forests, but a substantial part (72.26%) of croplands exhibits greening. Therefore, greening of India is driven by croplands (86.5% contribution) in recent decades.

Recent studies found that the greening in Europe is mainly due to the efficient management of land abandonment and afforestation (Buitenwerf et al., 2018; Fuchs et al., 2015, 2016). Central Asia is greening because of the positive changes in the socio-economic conditions (Venkatesh et al., 2022). In southeast Asia, China is greening largely owing to the better land use management and sustainable agricultural policies (Liu et al., 2020). In India, on the other hand, about 56% of agricultural yield depends on irrigation (Thakkar, 2000). Currently, India has the largest irrigated area (57 mha) and IGP is the most irrigated region in the world (Ambika et al., 2016; Ambika & Mishra, 2019, 2020). The advanced irrigation facilities lead to higher NIA, which makes increased GSA and ISA. Therefore, the enhanced cropland-based greening and food production of India can be largely attributed to improved irrigation facilities (Chen et al., 2019; Piao et al., 2020). In addition, the use of more nitrogen fertilisers, advanced farm mechanisation and effective land management are the other reasons for the enhanced cropland greening in India. In summary, the strong anthropogenic control over the green cover is highlighted by the cropland-based greening of India.

5. Conclusions

The greening and its contribution from croplands and forests are analysed using the surface greenness indicator (NDVI), biophysical metric (LAI), and photosynthetic activity and productivity proxy (SiF) for India in this study. The net vegetated land comprising of both croplands and forests is largely greening (62.54%) and marginally browning (14%) during the recent decades (2000–2019). In forests, 17.5% is greening, but a large area is browning (47.43%). In contrast, most of the croplands (72.3%) exhibit greening and some (7.7%) show browning. Also, the magnitude or intensity of greening in croplands is twice the forests during the same period. Among the agricultural seasons, Zaid shows the highest greening area (70%) during the period, followed by Kharif (59.52%) and Rabi (54.82%). With respect to the

regions, predominant cropland greening is estimated in NW (83.5%), IGP (64.6%) and CI (61.7%). Therefore, the greening of India is largely driven by croplands. The enhanced cropland greening of India can be attributed to improved irrigation facilities, effective cropland management, farm mechanisation, and the increased use of nitrogen fertilizers, which led to an increase in GSA, NIA, ISA and net vegetated area. The cropland driven greening of India highlights the massive anthropogenic influence on its green cover. Judicial use and effective management of land are essential to mitigate the threat of global warming and climate change, and thus, to achieve food security and sustainability.

CRediT authorship contribution statement

Jayanarayanan Kuttippurath: Conceptualization, Methodology, Supervision, Visualization, Writing– review & editing of the original draft. **Rahul Kashyap:** Conceptualization, Methodology, Data Analyses, Visualization, Software, Writing–original draft.

Data availability

All data are publicly available, and listed in Table 1.

Declaration of competing interest

The authors declare no conflict of interest and financial interests.

Acknowledgements

We thank the Director, Indian Institute of Technology Kharagpur (IIT Kgp), Chairman of CORAL IIT Kgp and the Ministry of Education (MoE) for facilitating the study. RK acknowledges the support from Prime Minister's Research Fellowship (PMRF). We acknowledge the support and help from Sarath Raj for Visualization and Software; Ajay Singh for agricultural data. We thank the NASA's LPDAAC team for providing the MODIS landcover, NDVI and LAI products, Krishnankutty Ambika A & Mishra V for making the high-resolution remote sensing based irrigated area data, Ministry of Agriculture and Farmers Welfare, Government of India for providing all the agriculture data. Special thanks to Jingfeng Xiao for making the SiF dataset publicly accessible.

Appendix A. Supplementary data

Supplementary data to this article can be found online at https://doi.org/10.1016/j.apgeog.2023.103115.

References

Ambika, A. K., & Mishra, V. (2019). Observational evidence of irrigation influence on vegetation health and land surface temperature in India. *Geophysical Research Letters, 46*(22), 13441–13451. https://doi.org/10.1029/2019GL084367

Ambika, A. K., & Mishra, V. (2020). Substantial decline in atmospheric aridity due to irrigation in India. *Environmental Research Letters, 15*(12), Article 124060. https://doi.org/10.1088/1748–9326/ABC8BC

Ambika, A. K., Wardlow, B., & Mishra, V. (2016). Remotely sensed high resolution irrigated area mapping in India for 2000 to 2015. *Scientific Data, 3*(1), Article 160118. https://doi.org/10.1038/sdata.2016.118

Atzberger, C. (2013). Advances in remote sensing of agriculture: Context description, existing operational monitoring systems and major information needs. *Remote Sensing, 5*(2), 949–981. https://doi.org/10.3390/RS5020949

Bala, G., Joshi, J., Chaturvedi, R. K., Gangamani, H. V., Hashimoto, H., & Nemani, R. (2013). Trends and variability of AVHRR–derived NPP in India. *Remote Sensing, 5*(2), 810–829. https://doi.org/10.3390/RS5020810

Buitenwerf, R., Sandel, B., Normand, S., Mimet, A., & Svenning, J. C. (2018). Land surface greening suggests vigorous woody regrowth throughout European semi–natural vegetation. *Global Change Biology, 24*(12), 5789–5801. https://doi.org/10.1111/GCB.14451

Burke, M., & Lobell, D. B. (2017). Satellite–based assessment of yield variation and its determinants in smallholder African systems. *Proceedings of the National Academy of Sciences of the United States of America, 114*(9), 2189–2194.

Chakraborty, A., Seshasai, M. V. R., Reddy, C. S., & Dadhwal, V. K. (2018). Persistent negative changes in seasonal greenness over different forest types of India using MODIS time series NDVI data (2001–2014). *Ecological Indicators, 85*, 887–903. https://doi.org/10.1016/J.ECOLIND.2017.11.032

Chen, C., Park, T., Wang, X., Piao, S., Xu, B., Chaturvedi, R. K., Fuchs, R., Brovkin, V., Ciais, P., Fensholt, R., Tømmervik, H., Bala, G., Zhu, Z., Nemani, R. R., & Myneni, R. B. (2019). China and India lead in greening of the world through land–use management. *Nature Sustainability, 2*(2), 122–129. https://doi.org/10.1038/s41893–019–0220–7

Chen, C., Riley, W. J., Prentice, I. C., & Keenan, T. F. (2022). CO2 fertilization of terrestrial photosynthesis inferred from site to global scales. *Proceedings of the National Academy of Sciences, 119*(10), Article e2115627119. https://doi.org/10.1073/pnas.2115627711

Cheng, L., Zhang, L., Wang, Y. P., Canadell, J. G., Chiew, F. H., Beringer, J., … Zhang, Y. (2017). Recent increases in terrestrial carbon uptake at little cost to the water cycle. *Nature Communications, 8*(1), 110. https://doi.org/10.1038/s41467-017-00114-5.

Coppin, P., Jonckheere, I., Nackaerts, K., Muys, B., & Lambin, E. (2004). Review ArticleDigital change detection methods in ecosystem monitoring: a review. *International Journal of Remote Sensing, 25*(9), 1565–1596.

Cortés, J., Mahecha, M. D., Reichstein, M., Myneni, R. B., Chen, C., & Brenning, A. (2021). Where are global vegetation greening and browning trends significant? *Geophysical Research Letters, 48*(6), Article e2020GL091496. https://doi.org/10.1029/2020GL091496

Didan, K. (2015). *MOD13C2 MODIS/terra vegetation indices monthly L3 global 0.05Deg CMG V006*. NASA EOSDIS Land Processes DAAC. from https://doi.org/10.5067/MODIS/MOD13C2.006. (Accessed 26 May 2022).

Dubey, N., & Ghosh, S. (2023). CO2 fertilization enhances vegetation productivity and reduces ecological drought in India. *Environmental Research Letters, 18*(6), Article 064025. https://doi.org/10.1088/1748-9326/acd5e7

Fan, X., & Liu, Y. (2016). A global study of NDVI difference among moderate-resolution satellite sensors. *ISPRS Journal of Photogrammetry and Remote Sensing, 121*, 177–191. https://doi.org/10.1016/j.isprsjprs.2016.09.008

Friedl, M. A., McIver, D. K., Hodges, J. C. F., Zhang, X. Y., Muchoney, D., Strahler, A. H., Woodcock, C. E., Gopal, S., Schneider, A., Cooper, A., Baccini, A., Gao, F., & Schaaf, C. (2002). Global land cover mapping from MODIS: Algorithms and early results. *Remote Sensing of Environment, 83*(1–2), 287–302. https://doi.org/10.1016/S0034–4257(02)00078–0

Fuchs, R., Herold, M., Verburg, P. H., Clevers, J. G. P. W., & Eberle, J. (2015). Gross changes in reconstructions of historic land cover/use for Europe between 1900 and 2010. *Global Change Biology, 21*(1), 299–313. https://doi.org/10.1111/GCB.12714

Fuchs, R., Schulp, C. J. E., Hengeveld, G. M., Verburg, P. H., Clevers, J. G. P. W., Schelhaas, M. J., & Herold, M. (2016). Assessing the influence of historic net and gross land changes on the carbon fluxes of Europe. *Global Change Biology, 22*(7), 2526–2539. https://doi.org/10.1111/GCB.13191

ISFR. (2019). *Indian state of forest report. Forest survey of India (FSI); Ministry of environment forest & climate change*. Government of India.

de Jong, R., de Bruin, S., de Wit, A., Schaepman, M. E., & Dent, D. L. (2011). Analysis of monotonic greening and browning trends from global NDVI time–series. *Remote Sensing of Environment, 115*(2), 692–702. https://doi.org/10.1016/J.RSE.2010.10.011

Jiang, L., Kogan, F.N., Guo, W., Tarpley, J.D., Mitchell, K.E., Ek, M.B., Tian, Y., Zheng, W., Zou, C.Z. and Ramsay, B.H., (2010). Real-time weekly global green vegetation fraction derived from advanced very high resolution radiometer-based NOAA operational global vegetation index (GVI) system. Journal of Geophysical Research: Atmospheres, 115(D11).

Kashyap, R., Kuttippurath, J., & Kumar, P. (2023a). Browning of vegetation in efficient carbon sink regions of India during the past two decades is driven by climate change and anthropogenic intrusions. *Journal of Environmental Management, 336*, Article 117655. https://doi.org/10.1016/j.jenvman.2023.117655

Kashyap, R., Kuttippurath, J., & Patel, V. K. (2023b). Improved air quality leads to enhanced vegetation growth during the COVID–19 lockdown in India. *Applied Geography, 151*, Article 102869. https://doi.org/10.1016/j.apgeog.2022.102869

Kashyap, R., Pandey, A. C., & Kuttippurath, J. (2022). Photosynthetic trends in India derived from remote sensing measurements during 2000–2019: Vegetation dynamics and key climate drivers. *Geocarto International*. https://doi.org/10.1080/10106049.2022.2060325

Keenan, T. F., Hollinger, D. Y., Bohrer, G., Dragoni, D., Munger, J. W., Schmid, H. P., & Richardson, A. D. (2013). Increase in forest water-use efficiency as atmospheric carbon dioxide concentrations rise. *Nature, 499*(7458), 324–327. https://doi.org/10.1038/nature12291

Keenan, T. F., Prentice, I. C., Canadell, J. G., Williams, C. A., Wang, H., Raupach, M., & Collatz, G. J. (2016). Recent pause in the growth rate of atmospheric CO2 due to enhanced terrestrial carbon uptake. *Nature Communications, 7*(1), Article 13428. https://doi.org/10.1038/ncomms13428

Kumar, L. T. V., Rao, K. K., Barbosa, H., & Jothi, E. P. (2013). Studies on spatial pattern of NDVI over India and its relationship with rainfall, air temperature, soil moisture adequacy and ENSO. *Geofizika, 30*(1).

Kuttippurath, J., Peter, R., Singh, A., & Raj, S. (2022). The increasing atmospheric CO2 over India: Comparison to global trends. *iScience, 25*(8). https://doi.org/10.1016/j.isci.2022.104863

Li, Q., Cao, X., Jia, K., Zhang, M., & Dong, Q. (2014). Crop type identification by integration of high–spatial resolution multispectral data with features extracted from coarse–resolution time–series vegetation index data. *International Journal of Remote Sensing, 35*(16), 6076–6088. https://doi.org/10.1080/01431161.2014.943325

Li, X., Xiao, J., He, B., Altaf Arain, M., Beringer, J., Desai, A. R., … Noe, S. M. (2018). Solar-induced chlorophyll fluorescence is strongly correlated with terrestrial photosynthesis for a wide variety of biomes: First global analysis based on OCO-2 and flux tower observations. *Global Change Biology, 24*(9), 3990–4008.

Liu, Z., Wang, J., Wang, X., & Wang, Y. (2020). Understanding the impacts of 'Grain for Green'land management practice on land greening dynamics over the Loess Plateau of China. *Land Use Policy, 99*, Article 105084. https://doi.org/10.1016/j.landusepol.2020.105084

Li, X., & Xiao, J. (2019). Mapping photosynthesis solely from solar–induced chlorophyll fluorescence: A global, fine–resolution dataset of gross primary production derived from OCO–2. *Remote Sensing, 11*(21), 2563. https://doi.org/10.3390/rs11212563

Lyapustin, A., Wang, Y., Xiong, X., Meister, G., Platnick, S., Levy, R., … Hall, F. (2014). Scientific impact of MODIS C5 calibration degradation and C6+ improvements. *Atmospheric Measurement Techniques, 7*(12), 4353–4365.

McMurtrie, R. E., Norby, R. J., Medlyn, B. E., Dewar, R. C., Pepper, D. A., Reich, P. B., & Barton, C. V. (2008). Why is plant-growth response to elevated CO2 amplified when water is limiting, but reduced when nitrogen is limiting? A growth-optimisation hypothesis. *Functional Plant Biology, 35*(6), 521–534. https://doi.org/10.1071/FP08128

Meybeck, A., Laval, E., Lévesque, R., & Parent, G. (2018). *Food security and nutrition in the age of climate change. Proeedings of the international symposium Organized by the Government of québec in Collaboration with FAO*.

Milesi, C., Samanta, A., Hashimoto, H., Kumar, K. K., Ganguly, S., Thenkabail, P. S., Srivastava, A. N., Nemani, R. R., & Myneni, R. B. (2010). Decadal variations in NDVI and food production in India. *Remote Sensing, 2*(3), 758–776. https://doi.org/10.3390/RS2030758

Mishra, N. B., & Chaudhuri, G. (2015). Spatio–temporal analysis of trends in seasonal vegetation productivity across Uttarakhand, Indian Himalayas, 2000–2014. *Applied Geography, 56*, 29–41. https://doi.org/10.1016/J.APGEOG.2014.10.007

Mishra, N. B., & Mainali, K. P. (2017). Greening and browning of the Himalaya: Spatial patterns and the role of climatic change and human drivers. *The Science of the Total Environment*, 326–339. https://doi.org/10.1016/J.SCITOTENV.2017.02.156

Myneni, R. B., Keeling, C. D., Tucker, C. J., Asrar, G., & Nemani, R. R. (1997). Increased plant growth in the northern high latitudes from 1981 to 1991. *Nature, 386*(6626), 698–702. https://doi.org/10.1038/386698a0

Myneni, R., Knyazikhin, Y., & Park, T. (2015). *MCD15A2H MODIS/Terra+Aqua leaf area Index/FPAR 8-day L4 global 500m SIN grid V006*. NASA EOSDIS Land Processes DAAC. . (Accessed 26 May 2022).

Panday, P. K., & Ghimire, B. (2012). Time-series analysis of NDVI from AVHRR data over the Hindu Kush-Himalayan region for the period 1982–2006. *International Journal of Remote Sensing, 33*(21), 6710–6721. https://doi.org/10.1080/01431161.2012.692836

Parida, B. R., Pandey, A. C., & Patel, N. R. (2020). Greening and browning trends of vegetation in India and their responses to climatic and non-climatic drivers. *Climate, 8*(8), 92. https://doi.org/10.3390/CLI8080092

Piao, S., Wang, X., Park, T., Chen, C., Lian, X. U., He, Y., … Nemani, R. R. (2020). Characteristics, drivers and feedbacks of global greening. *Nature Reviews Earth & Environment, 1*(1), 14–27. https://doi.org/10.1038/s43017-019-0001-x

Porcar-Castell, A., Tyystjärvi, E., Atherton, J., Van der Tol, C., Flexas, J., Pfündel, E. E., … Berry, J. A. (2014). Linking chlorophyll a fluorescence to photosynthesis for remote sensing applications: mechanisms and challenges. *Journal of Experimental Botany, 65*(15), 4065–4095. https://doi.org/10.1093/jxb/eru191

Prince, S. D., Wessels, K. J., Tucker, C. J., & Nicholson, S. E. (2007). Desertification in the Sahel: a reinterpretation of a reinterpretation. *Global Change Biology, 13*(7), 1308–1313.

Rascher, U., Alonso, L., Burkart, A., Cilia, C., Cogliati, S., Colombo, R., … Hyvärinen, T. (2015). Sun-induced fluorescence–a new probe of photosynthesis: First maps from the imaging spectrometer HyPlant. *Global Change Biology, 21*(12), 4673–4684. https://doi.org/10.1111/gcb.13017

Roy, D. P., Wulder, M. A., Loveland, T. R., C.E, W., Allen, R. G., Anderson, M. C., Helder, D., Irons, J. R., Johnson, D. M., Kennedy, R., Scambos, T. A., Schaaf, C. B., Schott, J. R., Sheng, Y., Vermote, E. F., Belward, A. S., Bindschadler, R., Cohen, W. B., Gao, F., … Zhu, Z. (2014). Landsat–8: Science and product vision for terrestrial global change research. *Remote Sensing of Environment, 145*, 154–172. https://doi.org/10.1016/J.RSE.2014.02.001

Sakamoto, T., Yokozawa, M., Toritani, H., Shibayama, M., Ishitsuka, N., & Ohno, H. (2005). A crop phenology detection method using time–series MODIS data. *Remote Sensing of Environment, 96*(3–4), 366–374. https://doi.org/10.1016/J.RSE.2005.03.008

Sarmah, S., Jia, G., & Zhang, A. (2018). Satellite view of seasonal greenness trends and controls in South Asia. *Environmental Research Letters, 13*, Article 034026. https://doi.org/10.1088/1748–9326/AAA866

Sarmah, S., Singha, M., Wang, J., Dong, J., Burman, P. K. D., Goswami, S., … Niu, S. (2021). Mismatches between vegetation greening and primary productivity trends in South Asia–A satellite evidence. *International Journal of Applied Earth Observation and Geoinformation, 104*, 102561. https://doi.org/10.1016/j.jag.2021.102561

Sheffield, J., Wood, E. F., Chaney, N., Guan, K., Sadri, S., Yuan, X., Olang, L., Amani, A., Ali, A., Demuth, S., & Ogallo, L. (2014). A drought monitoring and forecasting system for sub–sahara african water resources and food security. *Bulletin of the American Meteorological Society, 95*(6), 861–882. https://doi.org/10.1175/BAMS–D–12–00124.1

IPCC. (2019). In P. R. Shukla, J. Skea, E. Calvo Buendia, V. Masson–Delmotte, H.-O. Pörtner, D. C. Roberts, P. Zhai, R. Slade, S. Connors, R. van Diemen, M. Ferrat, E. Haughey, S. Luz, S. Neogi, M. Pathak, J. Petzold, J. Portugal Pereira, P. Vyas, E. Huntley, & J. Malley (Eds.), *Climate change and land: An IPCC special report on climate change, desertification, land degradation, sustainable land management,food security,and greenhouse gas fluxes in terrestrial ecosystems*.

Shi, H., Tian, H., Pan, N., Reyer, C. P., Ciais, P., Chang, J., … Hickler, T. (2021). Saturation of global terrestrial carbon sink under a high warming scenario. *Global Biogeochemical Cycles, 35*(10). https://doi.org/10.1029/2020GB006800. e2020GB006800.

Singh, A., Abbhishek, K., Kuttippurath, J., Raj, S., Mallick, N., Chander, G., & Dixit, S. (2022). Decadal variations in CO2 during agricultural seasons in India and role of management as sustainable approach. *Environmental Technology & Innovation, 27*, Article 102498. https://doi.org/10.1016/j.eti.2022.102498

Teal, R. K., Tubana, B., Girma, K., Freeman, K. W., Arnall, D. B., Walsh, O., & Raun, W. R. (2006). In–season prediction of corn grain yield potential using normalized difference vegetation index. *Agronomy Journal, 98*(6), 1488–1494. https://doi.org/10.2134/AGRONJ2006.0103

Thakkar, H. (2000). *Assessment of irrigation in India. World commission of dams*. College of Engineering: Purdue University, United States of America.

Tian, F., Fensholt, R., Verbesselt, J., Grogan, K., Horion, S., & Wang, Y. (2015). Evaluating temporal consistency of long-term global NDVI datasets for trend analysis. *Remote Sensing of Environment, 163*, 326–340.

Venkatesh, K., John, R., Chen, J., Xiao, J., Amirkhiz, R. G., Giannico, V., & Kussainova, M. (2022). Optimal ranges of social-environmental drivers and their impacts on vegetation dynamics in Kazakhstan. *Science of the Total Environment, 847*, Article 157562. https://doi.org/10.1016/j.scitotenv.2022.157562

Wang, D., Morton, D., Masek, J., Wu, A., Nagol, J., Xiong, X., … Wolfe, R. (2012). Impact of sensor degradation on the MODIS NDVI time series. *Remote Sensing of Environment, 119*, 55–61. https://doi.org/10.1016/j.rse.2011.12.001

Wang, S., Zhang, Y., Ju, W., Chen, J.M., Ciais, P., Cescatti, A., Sardans, J., Janssens, I.A., Wu, M., Berry, J.A. and Campbell, E., (2020). Recent global decline of CO2 fertilization effects on vegetation photosynthesis. Science, 370(6522), (1295-1300). doi:10.1126/science.abb7772.

Watson, J. E. M., Iwamura, T., & Butt, N. (2013). Mapping vulnerability and conservation adaptation strategies under climate change. *Nature Climate Change, 3*(11), 989–994. https://doi.org/10.1038/nclimate2007

Wenzel, S., Cox, P. M., Eyring, V., & Friedlingstein, P. (2016). Projected land photosynthesis constrained by changes in the seasonal cycle of atmospheric CO2. *Nature, 538*(7626), 499–501. https://doi.org/10.1038/nature19772

Winkler, A. J., Myneni, R. B., Hannart, A., Sitch, S., Haverd, V., Lombardozzi, D., … Kato, E. (2021). Slowdown of the greening trend in natural vegetation with further rise in atmospheric CO_2. *Biogeosciences, 18*(17), 4985–5010. https://doi.org/10.5194/bg-18-4985-2021

Xiao, J., Li, X., He, B., Arain, M. A., Beringer, J., Desai, A. R., … Varlagin, A. (2019). Solar-induced chlorophyll fluorescence exhibits a universal relationship with gross primary productivity across a wide variety of biomes. *Global Change Biology, 25*(4), e4–e6.

Yang, Y., Donohue, R. J., McVicar, T. R., Roderick, M. L., & Beck, H. E. (2016). Long-term CO2 fertilization increases vegetation productivity and has little effect on hydrological partitioning in tropical rainforests. *Journal of Geophysical Research: Biogeosciences, 121*(8), 2125–2140. https://doi.org/10.1002/2016JG003475

Zhang, Y., Song, C., Band, L. E., Sun, G., & Li, J. (2017). Reanalysis of global terrestrial vegetation trends from MODIS products: Browning or greening? *Remote Sensing of Environment, 191*, 145–155. https://doi.org/10.1016/j.rse.2016.12.018

Zhu, Z., Piao, S., Myneni, R. B., Huang, M., Zeng, Z., Canadell, J. G., … Cao, C. (2016). Greening of the Earth and its drivers. *Nature Climate Change, 6*(8), 791–795. https://doi.org/10.1038/nclimate3004

Journal of Environmental Management 336 (2023) 117655

Contents lists available at ScienceDirect

Journal of Environmental Management

journal homepage: www.elsevier.com/locate/jenvman

Research article

Browning of vegetation in efficient carbon sink regions of India during the past two decades is driven by climate change and anthropogenic intrusions

Rahul Kashyap, Jayanarayanan Kuttippurath *, Pankaj Kumar

CORAL, Indian Institute of Technology Kharagpur, Kharagpur, 721302, India

ARTICLE INFO

Keywords:
Carbon use efficiency (CUE)
Vegetation carbon dynamics (VCD)
Land-atmosphere interactions
Carbon cycle
Principal component analyses (PCA)
Causal discovery

ABSTRACT

Accurate estimation of carbon cycle is a challenging task owing to the complexity and heterogeneity of ecosystems. Carbon Use Efficiency (CUE) is a metric to define the ability of vegetation to sequester carbon from the atmosphere. It is key to understand the carbon sink and source pathways of ecosystems. Here, we quantify CUE using remote sensing measurements to examine its variability, drivers and underlying mechanisms in India for the period 2000–2019, by applying the principal component analyses (PCA), multiple linear regression (MLR) and causal discovery. Our analysis shows that the forests in the hilly regions (HR) and northeast (NE), and croplands in the western areas of South India (SI) exhibit high (>0.6) CUE. The northwest (NW), Indo-Gangetic plain (IGP) and some areas in Central India (CI) show low (<0.3) CUE. In general, the water availability as soil moisture (SM) and precipitation (P) promote higher CUE, but higher temperature (T) and air organic carbon content (AOCC) reduce CUE. It is found that SM has the strongest relative influence (33%) on CUE, followed by P. Also, SM has a direct causal link with all drivers and CUE; reiterating its importance in driving vegetation carbon dynamics (VCD) for the cropland dominated India. The long-term analysis reveals that the low CUE regions in NW (moisture induced greening) and IGP (irrigation induced agricultural boom) have an increasing trend in productivity (greening). However, the high CUE regions in NE (deforestation and extreme events) and SI (warming induced moisture stress) exhibit a decreasing trend in productivity (browning), which is a great concern. Our study, therefore, provides new insights on the rate of carbon allocation and the need of proper planning for maintaining balance in the terrestrial carbon cycle. This is particularly important in the context of drafting policy decisions for the mitigation of climate change, food security and sustainability.

1. Introduction

Human perturbations have led to highly capricious response of terrestrial vegetation to the changes in climate (Newbold et al., 2020). Modifications in the fluxes of momentum, water and energy in the earth system between land surface and atmosphere in recent decades have triggered significant variability in vegetation carbon dynamics (VCD) (He et al., 2018; Gang et al., 2022). Climate change has emerged as the most important and unpredictable factor that influences VCD. The scenario of limited water due to lower precipitation and warming of both atmosphere and land can decline terrestrial productivity (Gahlot et al., 2017; IPCC, 2019). Along with the changes in climate, various anthropogenic influences such as land use land cover change (LULCC), agricultural production and irrigation impacts VCD (Nemani et al., 2003; Chen et al., 2019).

Vegetation greening has a significant role in mitigation of global warming and climate change, because the terrestrial vegetation acts as a major carbon sink (Piao et al., 2020; Sarmah et al., 2021). South Asia has been greening in the last two decades (Parida et al., 2020; Kashyap et al., 2022) and much of it is contributed by India and China (Chen et al., 2019). However, quantification of this greening in terms of terrestrial carbon sequestration is largely unknown (Sarmah et al., 2021; Verma et al., 2022). The carbon cycle will be strongly impacted by the regional climate change in south Asia, and India is a region yet to be adequately explored with respect to carbon budget studies (Bala et al., 2013; Sarmah et al., 2021; Verma et al., 2022). Scarcity of data, extensive computational requirements and the complex land-atmosphere interactions in Indian region pose great challenges for undertaking such studies (Sarmah et al., 2021; Verma et al., 2022).

Carbon use efficiency (CUE) is a measure of the ability of vegetation to sequester atmospheric carbon and is estimated as the ratio of Net primary productivity (NPP) to Gross primary productivity (GPP) (De

* Corresponding author.
E-mail address: jayan@coral.iitkgp.ac.in (J. Kuttippurath).

https://doi.org/10.1016/j.jenvman.2023.117655
Received 2 November 2022; Received in revised form 25 February 2023; Accepted 1 March 2023
Available online 8 March 2023

Lucia et al., 2007). It gives the amount of carbon stored and used for growth out of the net carbon acquired by the ecosystem. CUE provides insight on the vegetation functioning as it is the rate of conversion of GPP to NPP or the splitting of GPP to NPP and autotrophic respiration (Ra) (He et al., 2018; Gang et al., 2022). Although it is a simple method as per concept, the estimation of CUE requires measurement of carbon uptake and its use for the growth, which makes it computationally very challenging (Migliavacca et al., 2021; Gang et al., 2022). GPP and NPP are the most important ecosystem variables that are studied extensively, as they are the fundamental ecological variables, which quantify the terrestrial carbon assimilation (Nemani et al., 2003; Bala et al., 2013). GPP is the rate of carbon dioxide captured by vegetation in a given period of time through photosynthesis. NPP is the residual of GPP after Ra, and is measured as the net production or accumulation of dry organic matter in vegetation (Roxburgh et al., 2005; Ballantyne et al., 2012). Terrestrial ecosystem carbon sink estimates, natural resource management and ecological studies are challenged by the high spatio-temporal variability of productivity (Ballantyne et al., 2012; Sarmah et al., 2021).

Direct measurement of GPP and NPP based on instruments at landscape, ecosystem and canopy level is still a daunting task. Therefore, quantification of global productivity highly relies on remote sensing measurements from space and model simulations (Ballantyne et al., 2012; Garbulsky et al., 2014). Satellite remote sensing enables larger sample size with unmatched global measurements for the synoptic monitoring of biosphere (Bala et al., 2013; Chen et al., 2019; Kashyap et al., 2022). Moreover, the unavailability of flux tower measurements in the regions of high carbon uptake makes remote sensing based VCD estimation inevitable (Sarmah et al., 2021; Verma et al., 2022).

Terrestrial carbon budgeting is vital for understanding of the land-atmosphere interactions, carbon sequestration, biosphere-climate feedback and climate change mitigation (Campbell et al., 2017; Newbold et al., 2020). We hypothesise that, VCD regulate the functioning of terrestrial ecosystems including carbon capture (GPP), storage (NPP) and rate of storage (CUE), and is influenced by certain drivers such as the fraction of photosynthetically active radiation (FPAR), temperature (T), precipitation (P), soil moisture (SM) and air organic carbon content (AOCC). Evaluation of CUE, its drivers and the underlying mechanisms are key to understand the terrestrial carbon cycle. It provides a better understanding of the changes in climate, and energy exchange between vegetation and atmosphere. Our study considers algorithms such as principal component analysis (PCA, rotated and unrotated), multiple linear regression (MLR) and causal discovery for understanding the drivers of CUE in India. This is the first of its kind analysis on CUE and its drivers in the Indian context and is the significance of this study.

2. Data and methodology

2.1. Data

The suitability and efficiency of Moderate Resolution Imaging Spectroradiometer (MODIS) data for studying large-scale terrestrial ecosystems are well established (e.g. Chen et al., 2019; Sarmah et al., 2021; Kashyap et al., 2022). MODIS GPP (MOD 17 A2HGF) and NPP (MOD 17 A3HGF) primary productivity data are considered here (Turner et al., 2006; Running et al., 2015). The Vegetation Index (VI) data taken are the MODIS based (MOD13A1) Normalised Difference Vegetation Index (NDVI) (e.g., Liu et al., 2017; Singh et al., 2022). The MCD12Q1 version 6 data provide land cover types using supervised classification. The land temperature (T) data are from the Global Land Data Assimilation System (GLDAS) NOAH 025 M 21 that are a blend of National Ocean and Atmospheric Administration and Global Data Assimilation System (NOAA/GDAS) atmospheric analysis (Wang et al., 2016; Xia et al., 2019). The precipitation (P) data are from the Global Precipitation Measurements (GPM, GPM_3IMERGDF L3), which is a multi-satellite integrated precipitation dataset with daily (mm/day) accumulated values (Xu et al., 2017). The GLDAS-based soil moisture data (SM) are also utilised in the study (Liu et al., 2019). The Modern Era Retrospective analysis for Research and Applications Version 2 (MERRA–2) air organic carbon content (AOCC) data are used for the atmospheric organic carbon estimates (Shikwambana, 2019), as listed in Table 1.

2.2. Methodology

2.2.1. Estimation of variability in productivity and CUE

This study is conducted for the Indian land region as shown in Fig. S1 and Table S1. The MODIS land cover data are used to mask the vegetated land comprising of forests and croplands. The MODIS GPP and NPP are based on the rate of dry matter formation from absorbed radiation, called the light use efficiency (LUE) model approach. This is the most commonly used method for productivity computation using remote sensing measurements (Wang et al., 2017; Sarmah et al., 2021; Verma et al., 2022). The MODIS-based gap-filled GPP data for winter (December, January, and February – DJF), summer (March, April, and May – MAM), monsoon (June, July, and August – JJA) and post-monsoon (September, October, and November – SON) seasons over the years 2000–2019 are averaged to obtain the respective seasonal means. However, the NPP data are considered only for the yearly and decadal averages, as there are no seasonal data. The trend in GPP is computed for three focal periods: study period (2000–2019), previous decade (2000–2009) and recent decade (2010–2019). The negative trend in productivity is called browning and positive trend is greening. The spatio-temporal analyses of CUE, its drivers and their temporal trends are also computed. Since, the NPP data are available in the yearly frequency, we estimated the seasonality/seasonal anomaly (Si, i for each season) in GPP as the departure from the mean in each season (Xi) from the annual mean (X). That is, $Si = X - Xi$. Since our analysis focuses on the seasonal VCD, we did not consider smaller temporal scales. Based on the seasonality in GPP, the seasonal variation in NPP and CUE are estimated. CUE is estimated as the ratio of NPP to GPP (De Lucia et al., 2007).

2.2.2. Connection, contribution and influence of drivers

PCA has been widely used in climate science for teleconnection analyses (Lim, 2015; Gao et al., 2017; Mezzina et al., 2020). To better understand the linkages among the drivers and CUE, we have performed both unrotated (UPCA) and rotated PCA (RPCA) in our analysis. The method is detailed in supplementary file. However, it should be noted

Table 1
Datasets with their resolution, purpose they serve in this study and source from which they are acquired.

Data Used	Resolution	Purpose	Source
MODIS NDVI	500 m	NDVI used for estimating FPAR	(https://lpdaacsvc.cr.usgs.gov/)
MODIS GPP	500 m	GPP, GPP trend, CUE estimation	(https://lpdaacsvc.cr.usgs.gov/)
MODIS NPP	500 m	NPP, CUE estimation	(https://lpdaacsvc.cr.usgs.gov/)
MODIS Land Cover	500 m	LULC data to extract vegetated land comprising of forests and croplands	(https://lpdaacsvc.cr.usgs.gov/)
GPM Level-3 precipitation	0.1° × 0.1°	Precipitation, relationship with CUE	(https://daac.gsfc.nasa.gov/)
GLDAS Temperature	0.25° × 0.25°	Temperature, relationship with CUE	(https://daac.gsfc.nasa.gov/)
MERRA– 2 Air organic carbon	0.5° × 0.625°	Air organic carbon, relationship with CUE	(https://daac.gsfc.nasa.gov/)
GLDAS Soil Moisture	0.25 × 0.25°	Soil Moisture, relationship with CUE	(https://daac.gsfc.nasa.gov/)

that relationship between PCA output and physical processes is not straightforward (Spensberger et al., 2020).

The relative contribution and influence of drivers to productivity (P) and CUE variability are estimated using the modified multiple linear region (MLR, Kashyap et al., 2022) where the normalised trend (trend/range) is used in place of trend unlike the conventional MLR (e.g. Kuttippurath and Nair, 2017; Kuttippurath et al., 2021) as detailed in supplementary file.

2.2.3. Causal discovery of drivers

Sensitivity of ecological systems and their interactions with both climate and anthropogenic processes have a nonlinear relationship and is very complex (Gahlot et al., 2017). Correlation is insufficient for detecting the complex and nonlinear associations with drivers with substantial autocorrelation, which does not necessarily imply causation (Runge et al., 2019). True causality necessitates not just the establishment of relationship among the variables, but also provides its direction (e.g. Kumar et al., 2022). This study uses one such causal model within Pearl Causality (PC) framework to discover the potential drivers of CUE and PCMCI is the most widely used algorithm in climate science for causal discovery (e.g. Krich et al., 2020; Verma et al., 2022).

In the first stage, the PCMCI algorithm identifies each driver's parents by performing an iterative conditional independence test by calculating the partial correlation between two time series. In the second stage, it assesses the statistical significance of causal links using momentary conditional independence (MCI) tests, and then estimates the strength of causal links using multiple linear regression (MLR). To determine causality, the PCMCI method employs a number of statistical tests, including linear partial correlations (Par-Corr) and nonlinear independence tests such as Gaussian process regressions and distance correlation (GPDC) and conditional mutual information (CMI). The PCMCI algorithm has two free parameters that the user must choose: maximum time delay (T_{max}) and significance threshold (ά), which define the acceptable level of false-positive link discovery. For identifying causal links, this study employs PCMCI+ (a PCMCI extension) to allow the discovery of contemporaneous links based on linear Par-corr tests (Muñoz et al., 2021). Kwiatkowski-Phillips-Schmidt-Shin (KPSS) test and the Augmented Dickey-Fuller (ADF) unit root test are used to examine the stationarity of the dataset prior to the causal analysis.

3. Results

3.1. Seasonal and decadal variability in terrestrial productivity

The average GPP in various seasons for India during the period 2000–2019 is shown in Fig. 1. In winter, high (>250 gC/m^2/yr) GPP in Punjab and Haryana and moderate GPP (100–250 gC/m^2/yr) in the rest of Indo-Gangetic plain (IGP) are observed. This is due to the rabi agriculture in this season, which is supported by optimum T (15–20 °C) and moderate SM (50–75 kg/m^2) that lead to higher (>0.7) FPAR there, as shown in Figs. S2 and S3. In summer, majority of the lands show lower GPP (<100 gC/m^2/yr) due to little P (<0.5 mm/day), lower SM (<75 kg/m^2), moderate FPAR (0.4–0.6) and very high AOCC (>20 mg/m^2). In monsoon, NE (>500 gC/m^2/yr), CI, and the western and eastern Ghats exhibit high GPP (>250 gC/m^2/yr) owing to higher P (>7.5 mm/day) and SM (>125 kg/m^2). However, higher T (>30 °C), lower SM (50–75 kg/m^2) and high AOCC (15–20 mg/m^2) lead to moderate (100–250 gC/m^2/yr) GPP in NW, IGP and some areas in SI. In post-monsoon, NE (>500 gC/m^2/yr), the eastern coasts and SI show higher GPP (>250 gC/m^2/yr) because of relatively high P (>5 mm/day) and SM (>125 kg/m^2)

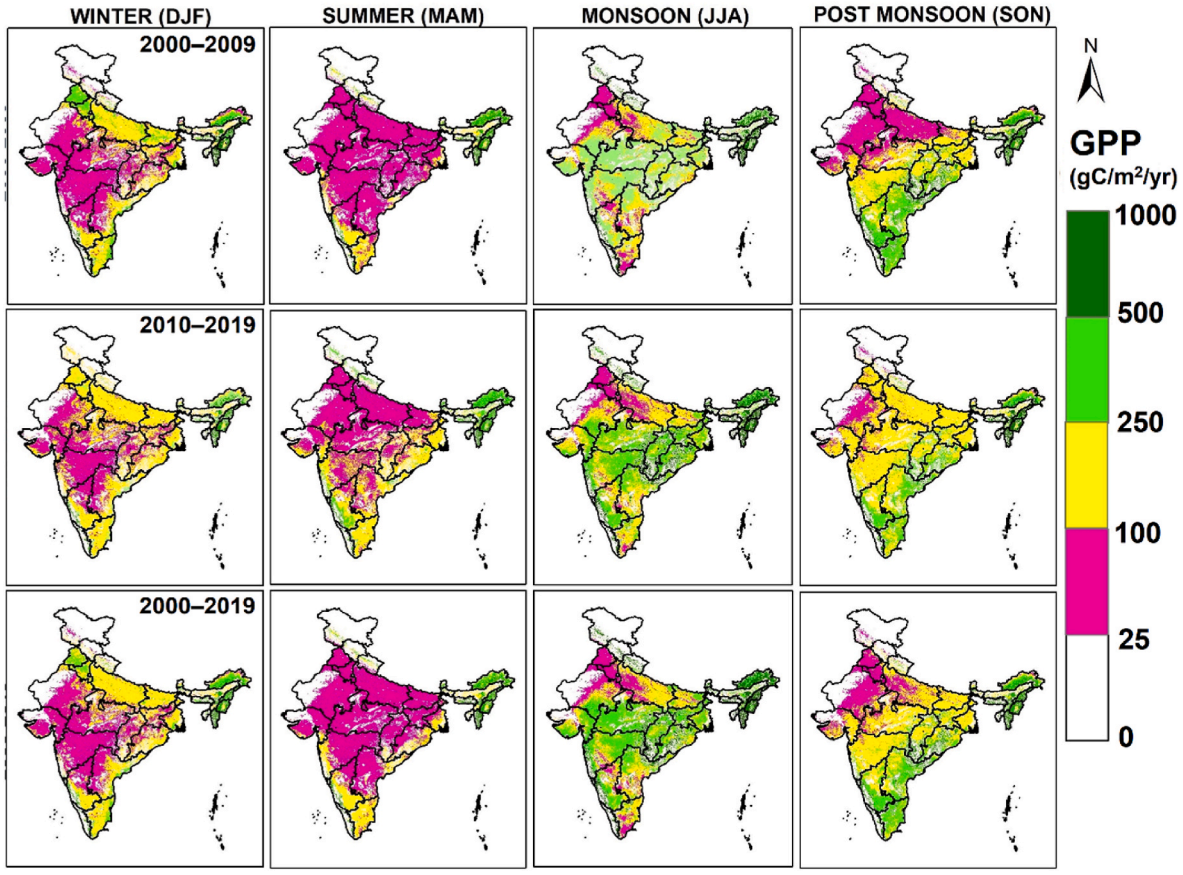

Fig. 1. Gross Primary Productivity (GPP) during winter (December, January and February), summer (March, April and May), monsoon (June, July and August) and post–monsoon (September, October and November) seasons for the period 2000–2009 (top panel), 2010–2019 (middle panel) and 2000–2019 (bottom panel).

there.

The spatio-temporal variability in terrestrial primary productivity i.e. GPP (Fig. 1) and NPP (Fig. 2) for both focal periods: (i) previous decade (2000–2009) and (ii) recent decade (2010–2019) are also estimated. In winter, NW and IGP (Punjab and Haryana) depict enhanced GPP, but it is lower in the northern SI for recent decade in comparison to the previous decade. During summer, GPP is lower in NE and higher in the western areas of SI in recent decade. In monsoon and post-monsoon seasons, majority of the regions exhibits an increase in GPP in recent decade, except in SI. The NPP for the period 2000–2019 exhibits a specific spatial pattern in India, as illustrated in Fig. 2. For instance, high (>200 gC/m^2/yr) NPP is observed in the forest areas of HR (western Himalaya) and NE. Croplands, mainly in CI and SI, also exhibit high NPP. In previous decade, NW and some areas in IGP exhibited lower NPP (<100 gC/m^2/yr), whereas NE, coastal areas, SI and some regions in IGP show higher NPP (>200 gC/m^2/yr). Interestingly, the western Himalaya, IGP, CI and northern SI show an increase in NPP in recent decade. Similar, results are also observed for GPP, with a strong increase in NW and IGP, but a substantial reduction in NE and SI regions.

3.2. Carbon Use Efficiency (CUE) of vegetation

3.2.1. Seasonal variability in CUE

The seasonal variability of CUE in the vegetated Indian landmass for the period 2000–2019 is illustrated in Fig. 3. In winter, the colder regions (5–10 °C) of NW with little P (0–0.5 mm/day) show very small (0.15–0.3) CUE (Figs. S2 and S3). Most areas in IGP, CI and some areas in SI with limited P (0–0.5 mm/day) and SM (50–75 kg/m^2) exhibit moderate (0.3–0.45) CUE. On the contrary, the croplands in SI with optimum T (10–20 °C) and moderate SM (50–75 kg/m^2) promote higher (0.6–0.75) CUE there. The forests in the western Himalaya with higher P (2.5–5 mm/day) and very small AOCC (5–15 mg/m^2) show the highest (0.75–0.9) CUE among the regions. During summer, limited P (0.5–2.5 mm/day) and SM (25–50 kg/m^2) with high T (30–40 °C) and AOCC (25–35 mg/m^2) lead to very small (0.15–0.3) CUE in some areas of IGP and NW. The availability of moisture in terms of P (0.5–2.5 mm/day) and SM (50–100 kg/m^2) outplays the warm summer conditions (30–40 °C) to produce moderate (0.3–0.45) CUE in most areas of CI and SI. Conversely, the low T (5–15 °C), high P (2.5–7.5 mm/day) and moderate AOCC (15–25 mg/m^2) in the Himalaya results in very high (0.75–0.9) CUE in these regions.

In monsoon season, northern IGP with lower SM (25–50 kg/m^2) show very small (0.15–0.3) CUE. Although there is high T (30–40 °C), the water availability in terms of both P (2.5–5 mm/day) and SM (75–125 kg/m^2) results in higher (0.45–0.6) CUE in SI. Some coastal regions experience higher P (7.5–30 mm/day) that promote high (0.6–0.75) CUE there. Very high SM (>100 kg/m^2) in the western areas of SI promote higher CUE (>0.6) in both monsoon and post-monsoon seasons. The eastern Himalaya has this cultivation season supported by sufficient P (15–30 mm/day) and SM (75–100 kg/m^2) lead to high CUE in those regions. During post-monsoon, limited SM (50–75 kg/m^2) in northern IGP produce low (0.15–0.3) CUE. Favourable P (2.5–5 mm/day) and SM (75–125 kg/m^2) promote high (0.45–0.75) CUE in CI. Forests in HR (western Himalaya) with high P (5–30 mm/day) and lower T (5–15 °C) lead to very high (0.75–0.9) CUE in the region. The spatial variability in CUE is in accordance with that of GPP and NPP, and with its drivers in each region. Henceforth, there exists a close link between CUE and GPP-NPP variability.

3.2.2. Vegetation carbon dynamics

Vegetation carbon dynamics (VCD) regulates the functioning of terrestrial ecosystems that includes carbon capture (GPP), storage (NPP) and rate of storage (CUE) as the ratio of NPP to GPP. Here, VCD is shown in terms of the long-term trend in GPP and spatial variability in CUE (Fig. 4). Positive trend in GPP (greening) is estimated in IGP (Punjab, Haryana and UP) northwest (Rajasthan), west (Maharashtra), CI (MP) and SI (Karnataka). Negative trend in GPP (browning) is observed in IGP (Bihar, Jharkhand, West Bengal), CI (Chhattisgarh and Orissa), NE and SI (Tamil Nadu and Andhra Pradesh). The CUE variability in India in the last two decades (2000–2019) shows a specific pattern. For instance, the regions such as NW, IGP and some areas in CI exhibit small (<0.3) CUE, but higher CUE (0.45–0.6) in CI and SI. Croplands in the western areas of SI (0.6–0.75), and forests in the Himalaya and NE (0.6–0.9) show very high CUE. Therefore, greening is found in the regions of lower CUE and browning in higher CUE regions. This is a major concern as there is a need of proper planning and management to protect the green cover in these areas of higher CUE.

3.2.3. Vegetation types and CUE

Apart from climate variability, vegetation type also plays a key role in VCD (Yao et al., 2018). The CUE is a function of ecozones and vegetation types (De Lucia et al., 2007). The Indian landmass has rich and varied vegetated land such as forests, croplands, agroforestry and plantations, and each type with specific role in carbon sequestration (Murthy et al., 2013; Le Quéré et al., 2018). The major vegetation types in India are shown in Fig. S4 and are listed in Table S2. In the western Himalaya, savanna, woody savanna, shrublands and evergreen broadleaf forest exhibit very high CUE (0.75–0.9), as shown in Fig. 4. These regions are majorly alpine forests dominated by trees such as pine and oak. The evergreen broadleaf forests in the eastern Himalaya exhibit higher (>0.75) CUE. In CI, shrublands, savanna dominated by woody perennials and deciduous broadleaf forests also show higher (>0.6) CUE. The savannas, grasslands and croplands in CI and SI regions show CUE of 0.6 or higher. Croplands exhibit moderate (0.3–0.45) CUE in IGP,

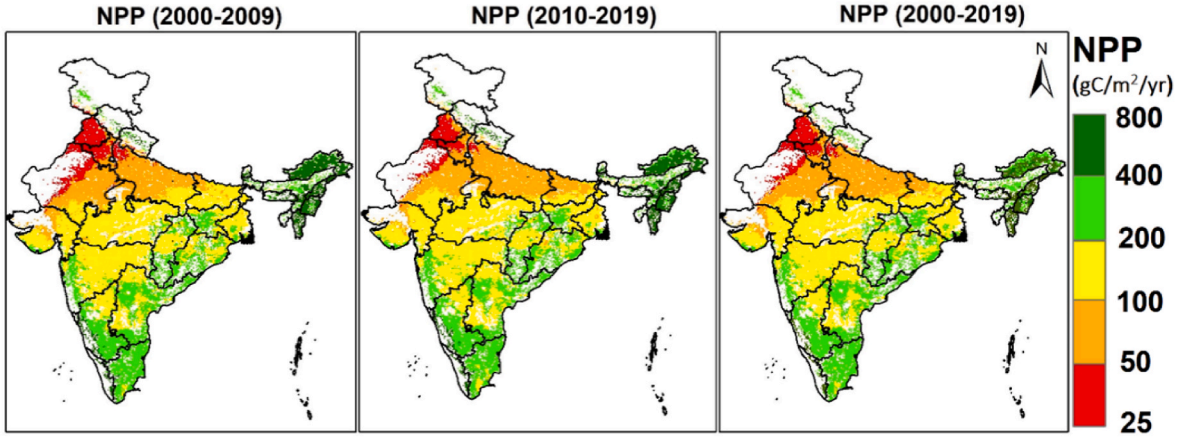

Fig. 2. Net Primary Productivity (NPP) averaged over the periods 2000–2009, 2010–2019 and 2000–2019.

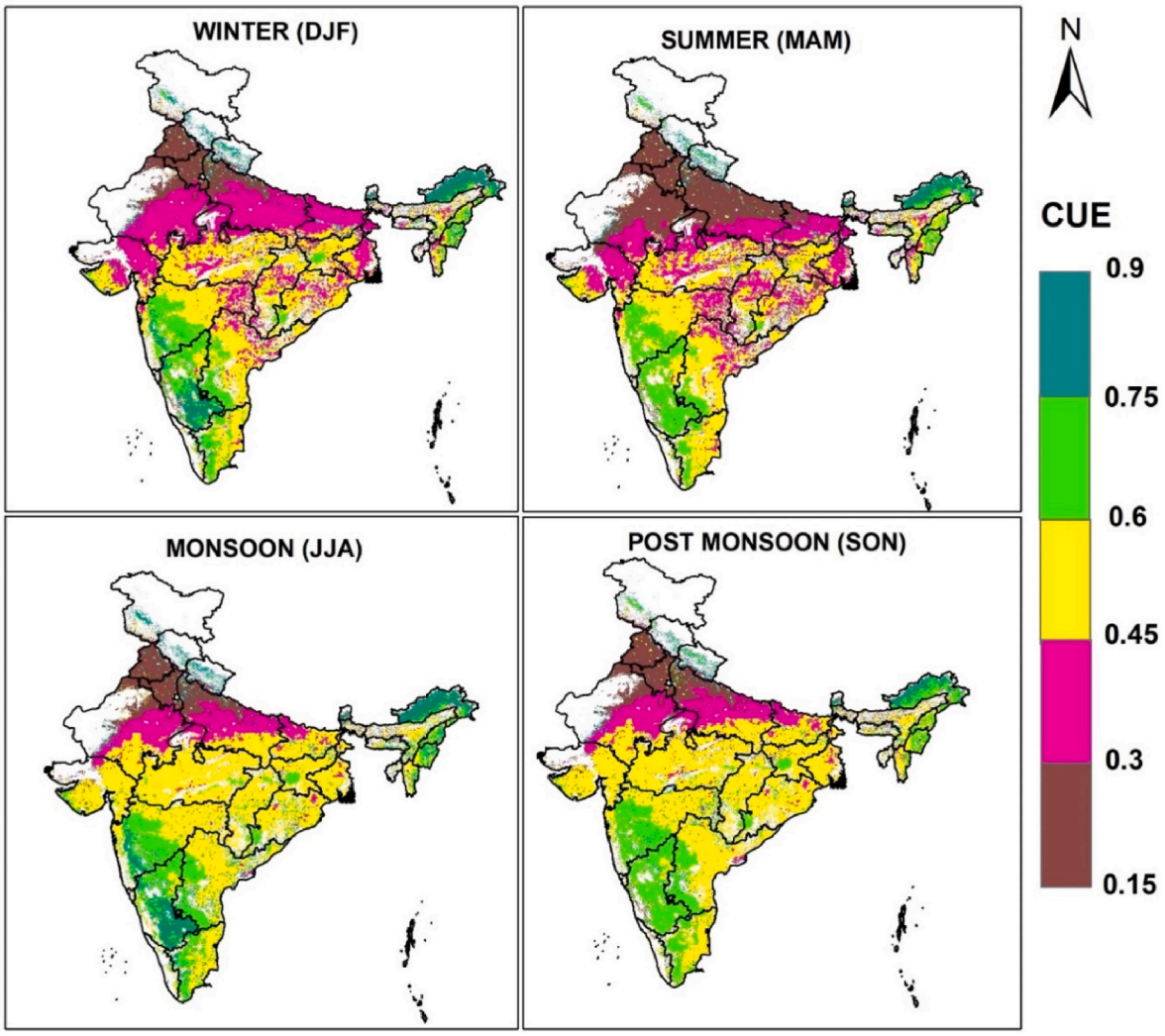

Fig. 3. The Carbon Use Efficiency (CUE) during winter (December, January and February), summer (March, April and May), monsoon (June, July and August) and post-monsoon (September, October and November) seasons averaged over the last 20 years (2000–2019).

CI and western coastal plains. The croplands in the western NW have low CUE (0.15–0.3). In general, forests exhibit higher CUE than that by croplands. Therefore, vegetation type is also a major factor in determining the CUE of ecosystems. VCD and CUE are ecosystem-specific parameters and they vary for different biomes and vegetation types (He et al., 2018; Gang et al., 2022). Henceforth, the selection of plant type is very important in reforestation, agroforestry and plantation activities, particularly for climate change mitigation measures.

3.3. CUE: variability, role of drivers and underlying mechanisms

3.3.1. Interannual variability

CUE is greatly affected by climate drivers such as T and P (He et al., 2018; Gang et al., 2022). The changing climate has highly influenced VCD with a reduction in NPP during the drought years (Bala et al., 2013; Gang et al., 2022). There are negative impacts of T extremes on cropland productivity (Lobell and Gourdji, 2012). Here, the interannual variability in CUE is explored in relation to its drivers in FPAR, SM, P, T and AOCC, as demonstrated in Fig. 5. The years 2003–2008, 2010, 2011, 2013 and 2014 with higher water availability (P and SM) and higher FPAR show higher CUE. However, CUE is lower in the years 2000–2002, 2009, 2012 and 2015 due to the reduction in water availability. The years of predominant warming such as 2002, 2009 and 2016 show the combined effect of limited P and high T, where the resulting low SM and FPAR lead to small CUE (warming induced moisture stress). In addition, these years also have higher AOCC, which negatively affect CUE. The water availability accompanied by cooling has led to higher CUE (moisture induced greening) in 2004, 2011 and 2013, as also found in other studies (e.g. Pérez-Girón et al., 2020, 2022).

3.3.2. Connection with drivers

PCA is carried out to understand the connection of CUE with its drivers, as shown in Fig. 5. Here, both UPCA and RPCA are performed with two PCs, namely PC1 and PC2 based on eigen values. PC1 is defined in UPCA by SM (0.84), P (0.66) and CUE (0.61) with positive correlation, whereas T (−0.83) and AOCC (−0.66) are correlated negatively with PC1. It shows that the water availability components in SM and P exhibit comparable variability as for CUE. This is expected as P drives SM and both have strong positive association with CUE. However, the negative correlation of T and AOCC with PC1 suggests that these factors have a detrimental effect on the variability of CUE and other variables in PC1. Due to the overwhelming negative influence of T and AOCC, FPAR (−0.38) shows a weak negative correlation with PC1. PC2 is largely determined by the variability of CUE (0.65), FPAR (0.81) and P (0.49); indicating that FPAR has a positive impact on the variability of CUE.

To better understand the relationship among the drivers and CUE, we used the varimax approach to rotate the PCs. In RPCA, it is observed that CUE (0.88), P (0.82) and SM (0.81) have a very strong positive

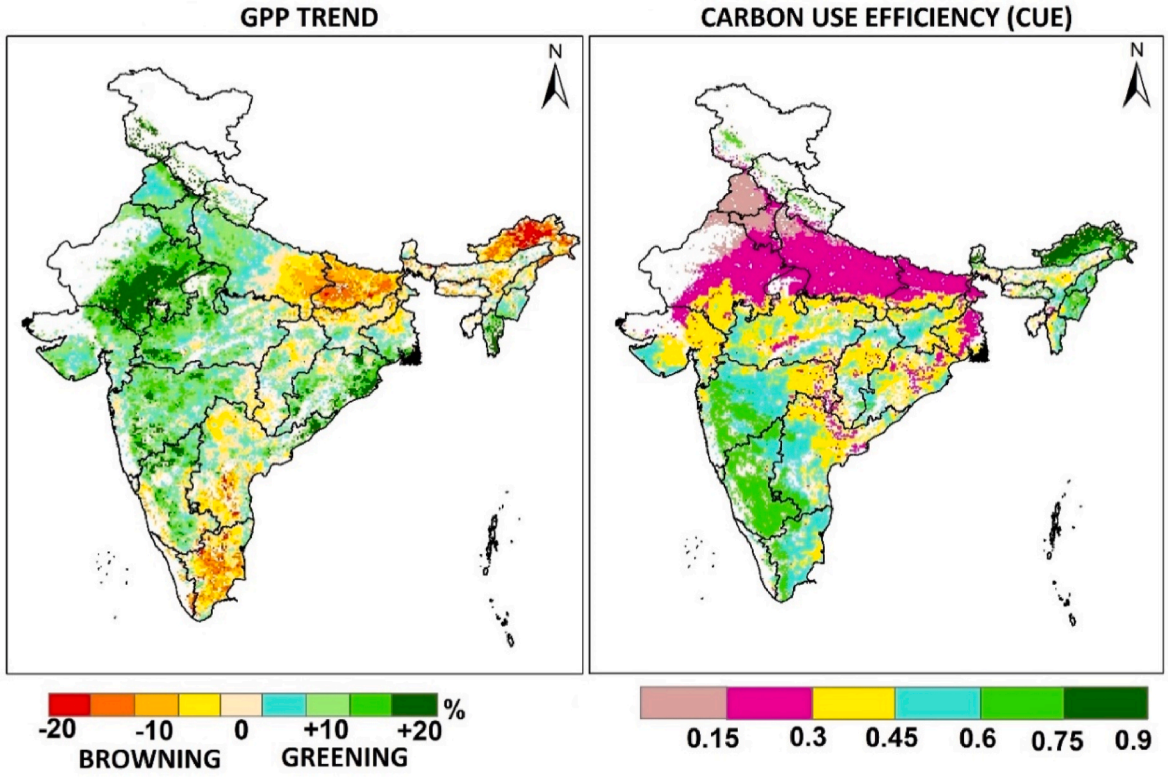

Fig. 4. Gross Primary Productivity (GPP) trend (decreasing– browning; increasing – greening). The ratio of NPP to GPP gives the Carbon Use Efficiency (CUE) for the period 2000–2019.

correlation with PC1, which indicates that these variables are highly connected among themselves. T (−0.41) has a negative correlation with PC1 as higher T will adversely affect CUE. PC2 is also distinguished by a strong positive correlation with FPAR (0.85), AOCC (0.84) and T (0.8). However, T (−0.41) also influences PC1 negatively as higher T will adversely affect SM, P and CUE. AOCC (−0.15) exhibits weak negative correlation with PC1, which suggests that it has a weak negative connection with CUE. Henceforth, PCA analysis demonstrates that both SM and P have strong positive association with CUE. This points out the close connection between carbon and water cycles in cropland dominated India.

3.3.3. Contribution and influence of drivers

CUE and VCD are regulated by the changes in terrestrial productivity, which is influenced by the spatial and temporal variability in drivers. SM (32.83%) is the most dominant driver of CUE in cropland dominated India; indicating a close link between carbon and water cycles. P (26.13%), FPAR (22.32%), and AOCC (16.47%) make significant contributions to CUE variability. The relative influence (positive/negative) of the drivers on the GPP trend and CUE is shown in Fig. 6. The positive influence of SM and T dominates over the negative influence of P and AOCC; leading to increase in productivity (greening) called moisture induced greening, which is observed in NW (Parida et al., 2020; Kashyap et al., 2022). In CI, positive influence of AOCC might be the reason for greening due the cooling effect there, which is also replicated by anthropogenic aerosol (brown haze) in this region (e.g. Kuttippurath and Raj, 2021). The enhanced productivity (greening) in IGP can be attributed to the anthropogenic intrusions such as the improvement in irrigation facilities, enhanced farm mechanisation and application of nitrogen-based fertilizers (Nayak et al., 2013; Ambika and Mishra., 2020). The negative influence of SM and T (warming induced moisture stress) is dominant over the positive influence of P, and that lead to reduced productivity (browning) in SI. The warming induced moisture stress is prevalent in this region, which is predominant in the areas of Tamil Nadu (e.g. Parida et al., 2020; Kashyap et al., 2022). In NE and eastern areas of IGP, large-scale anthropogenic activity (shifting cultivation and land abandoning) has led to green cover loss and browning. The NE region has severe consequences of human induced LULCC as the loss of vegetation cover drives extreme events such as fires and landslides in these ecologically fragile regions (Sannigrahi et al., 2020; Kashyap et al., 2021).

3.3.4. Causal discovery of drivers

The causal graphs/network are developed by considering various maximum time delay (T_{max}) or lag and significance threshold (ά) to understand the non-linear role of drivers in terrestrial VCD. As ά is increased from 0.1 to 0.05 and further to 0.01, the number of causal links diminishes and only the strong links remain. Also, the causal graphs at different T_{max} (lag) provide insights on the mechanisms influencing CUE and terrestrial VCD at different temporal scales ranging from T_{max} = 1–3 months, as shown in Fig. S5. Here, we have shown the causal graph for T_{max} = 4 (Fig. 7), where a number of causal structures are established at ά = 0.1. P does not have a direct causal link with CUE, but it drives SM that has a direct link with CUE with lag of 2 months. P also has a link with FPAR, which has a direct positive connection with CUE in a 1-month lag. FPAR is used as a proxy for photosynthesis and higher P would support more photosynthesis and faster carbon uptake (i.e. higher CUE). P has a negative link with T (lag = 1 month), which has direct negative link with CUE (lag = 2 months). Therefore, P affects CUE indirectly through other drivers. T has a strong negative link with FPAR, as photosynthetic activity responds well only to the optimum range of T, and therefore, CUE has a direct negative link with T. Furthermore, T has a negative link with SM, which has a direct positive link with CUE; explaining the negative link between T and CUE. AOCC also has a direct negative link with CUE, as biomass burning in extensive croplands and wild fires in forests release the stored carbon stocks captured by the vegetation and reduces CUE. Similar causal links are also observed for ά = 0.05 and for ά = 0.01.

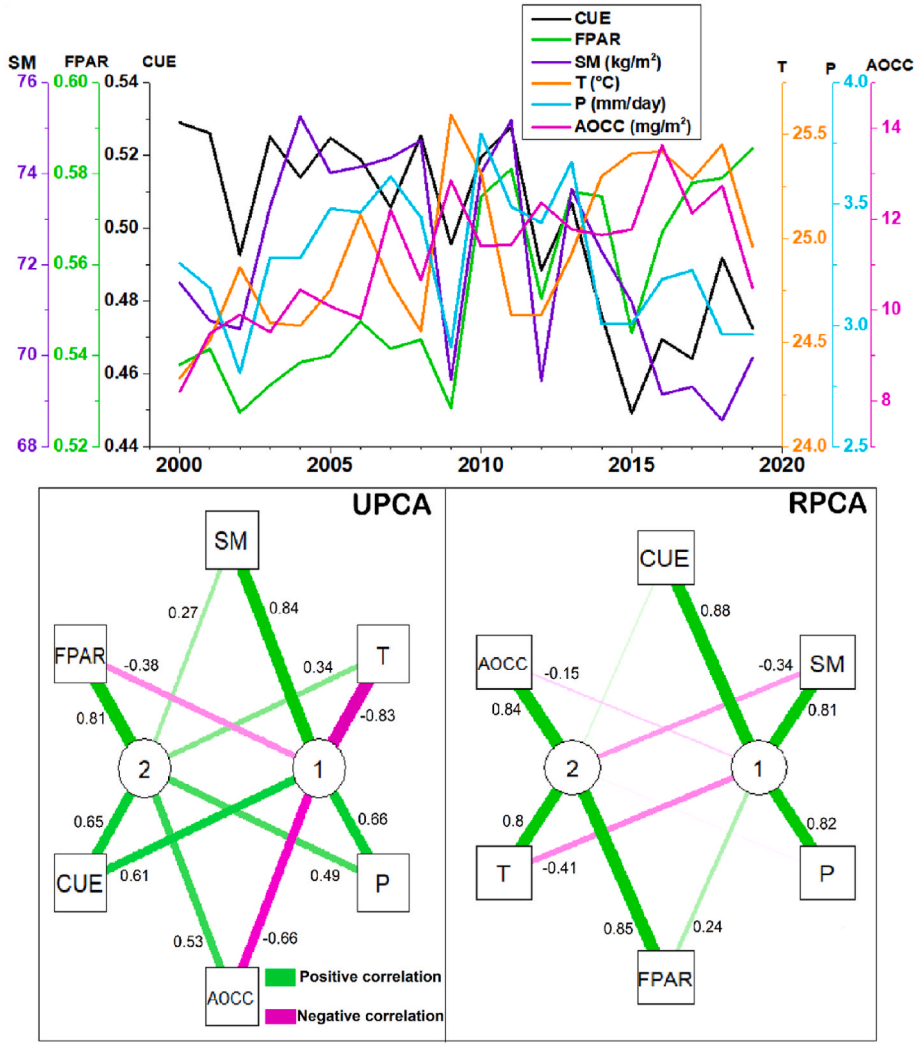

Fig. 5. Interannual variability in Carbon Use Efficiency (CUE) and its drivers– Fraction of Photosynthetically Active Radiation (FPAR), Precipitation (P), Temperature (T), Soil Moisture (SM) and Air Organic Carbon Content (AOCC) (top panel). The Principal Component Analysis (PCA) comprising of Unrotated PCA (UPCA) and Rotated PCA (RPCA) shows the links among CUE and its drivers. Here, the green and magenta lines represent positive and negative correlations, respectively. The thickness of the lines is a measure of the strength of the link represented in terms of correlation coefficients. (For interpretation of the references to colour in this figure legend, the reader is referred to the Web version of this article.)

4. Discussion

4.1. Background and our findings

India is second to China in global greening as revealed by the satellite-based leaf area index (LAI) analysis (Chen et al., 2019). However, quantification of this greening in terms of terrestrial VCD is still uncertain (Sarmah et al., 2021; Verma et al., 2022). Therefore, we utilised the MODIS data to understand the changes in terrestrial productivity for the last two decades. To find the carbon sequestration potential of vegetated land, CUE is estimated, for the first time for India.

Regarding the productivity, Singh et al. (2011) utilised satellite data and model results, and found a positive trend of 8.5%/dec in NPP for India during the period 1981–2000. Another study by Nayak et al. (2013), by using model results, showed that the increase in agricultural production is the major reason for enhanced NPP in India during the period 1981–2006. Bala et al. (2013) reported about 4%/dec increase of NPP in India based on the AVHRR satellite data for the period 1982–2006. Our analysis also shows that there is about 13% increase in NPP during the study period (2000–2019). In addition, Bala et al. (2013) showed that the seasonal cycle of terrestrial productivity is strongly influenced by SM in India. Kashyap et al. (2022) also revealed that SM is the dominant driver of photosynthetic trend in India during the last two decades. The carbon-water cycle interactions in India is complex and exhibit high regional variability owing to the conventional irrigation pattern in the croplands (Verma et al., 2022). Our analyses show that SM has a dominant role in driving VCD and thus, expose a strong link between carbon and water cycle in India. However, Sarmah et al. (2021) found that there is a mismatch between the greening trends and terrestrial carbon uptake in south Asia. The greening is largely observed in the croplands, which has limited carbon uptake potential. This is also reciprocated in our study as the high CUE regions are browning. This is a big concern for the terrestrial VCD with implications for anthropogenic climate change.

4.2. Novelty and wider implications

Most studies have relied on either correlation (Bala et al., 2013) or partial correlation (Sarmah et al., 2021) for finding the role of potential drivers in the variability of terrestrial productivity. A recent study by Verma et al. (2022) utilised causal discovery to find the drivers of GPP. However, there were limited number of drivers with known influence. Our analysis is not centred around the causal approach, but we utilise the method to examine the robustness of our results derived using various statistical techniques such as the correlation analysis, MLR and PCA. Our study provides new insights on the rate of carbon allocation and conversion to new biomass in ecosystems. Furthermore, it brings into light the ecologically vulnerable regions (NE, eastern IGP and some areas in SI), which requires immediate attention to increase the green cover for maintaining balance in the terrestrial carbon cycle, and also to mitigate carbon-induced climate change. Since India has various vegetation types, our study would also serve as a reference for quantification

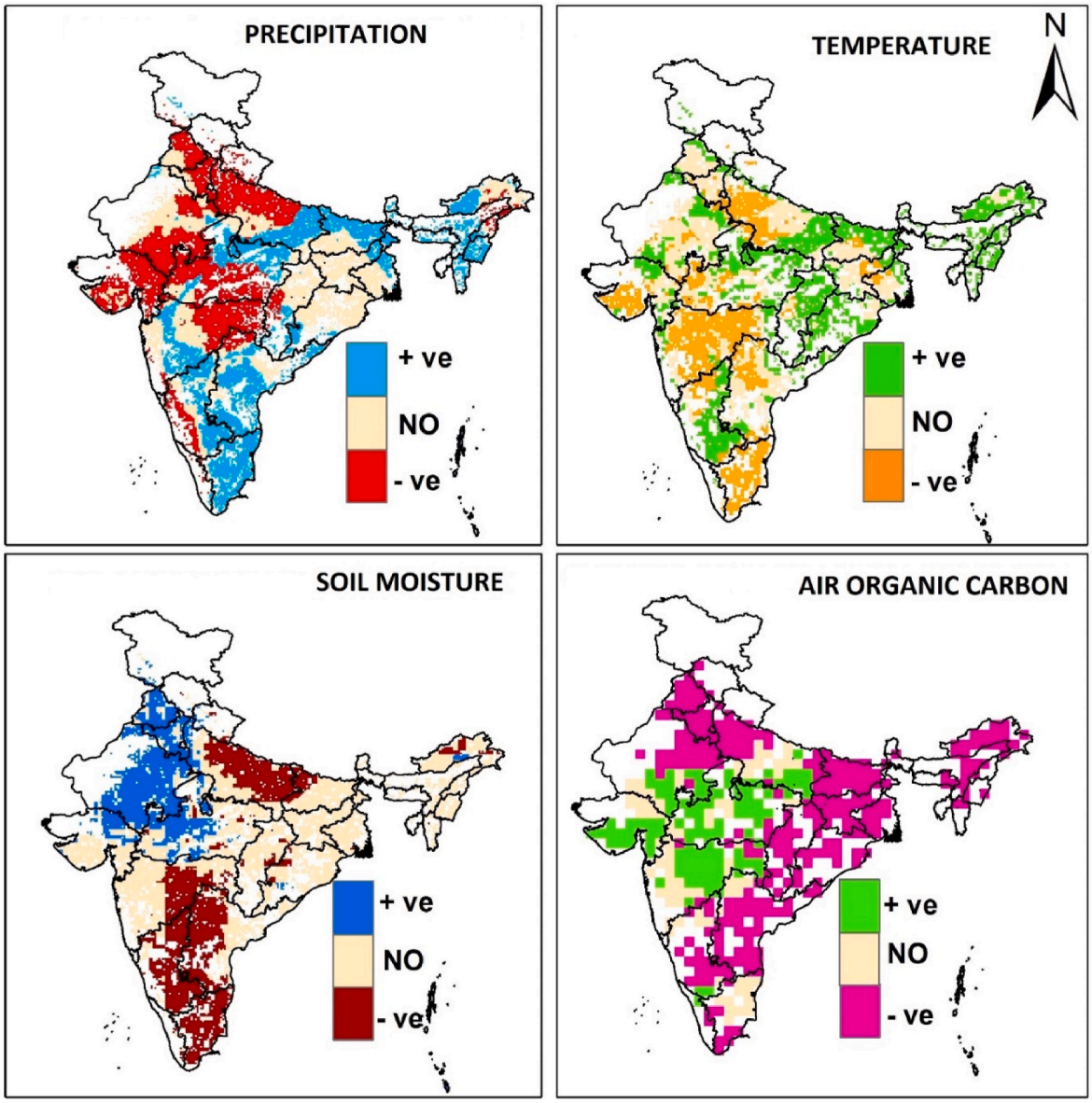

Fig. 6. Relative influence (negative/positive) of the spatial trend in climate drivers– precipitation (drying/showering), temperature (cooling/warming), soil moisture (drying/moistening), and air organic carbon content (high/low) on the productivity trend (browning/greening) and Carbon Use Efficiency (CUE) over the period 2000–2019.

and understanding the mechanisms influencing VCD at regional and global scales. Additionally, our analyses would enhance the performance of Earth System models by providing better model input for carbon fluxes between land and atmosphere. The balance in the terrestrial carbon cycle is key to achieve ambient atmospheric and environmental conditions. Weakening of efficient vegetation carbon sinks is a great concern for sustainability, global warming and climate change. Knowledge about the country-wide terrestrial VCD is very important to draft policies for mitigating climate change impacts on food production and to achieve sustainable development goals (SDGs).

4.3. Constraints

Improved spatial resolution of the datasets would give more detailed information on terrestrial VCD. This study assumes the seasonal variability in NPP to be the same as that of GPP for estimating CUE as there are no seasonal datasets for NPP. The contribution of drivers estimated here is the "relative contribution" where the sum of contribution of all drivers is 100%. As there can be other drives, this assessment does not claim exact contribution of any driver in regulating VCD. Since the MODIS data are available from 2000 onwards, and the years 2020 and 2021 have the influence of COVID-induced lockdown (Kashyap et al., 2023), the period 2000–2019 is considered in our analysis. Ground-based measurements of productivity might provide better results, but those are not available for the Indian region to assess VCD. Therefore, the above -mentioned limitations could influence the uncertainty of the estimates.

5. Conclusions

The vegetation carbon dynamics (VCD) regulates functioning of terrestrial ecosystems, as it includes carbon capture (GPP), storage (NPP) and rate of storage (CUE). Here, we have utilised PCA, MLR and causal discovery to examine the key drivers of CUE variability in India for the period 2000–2019. Water availability (SM and P) promotes higher CUE, but higher T and AOCC reduce CUE. There is an increase in

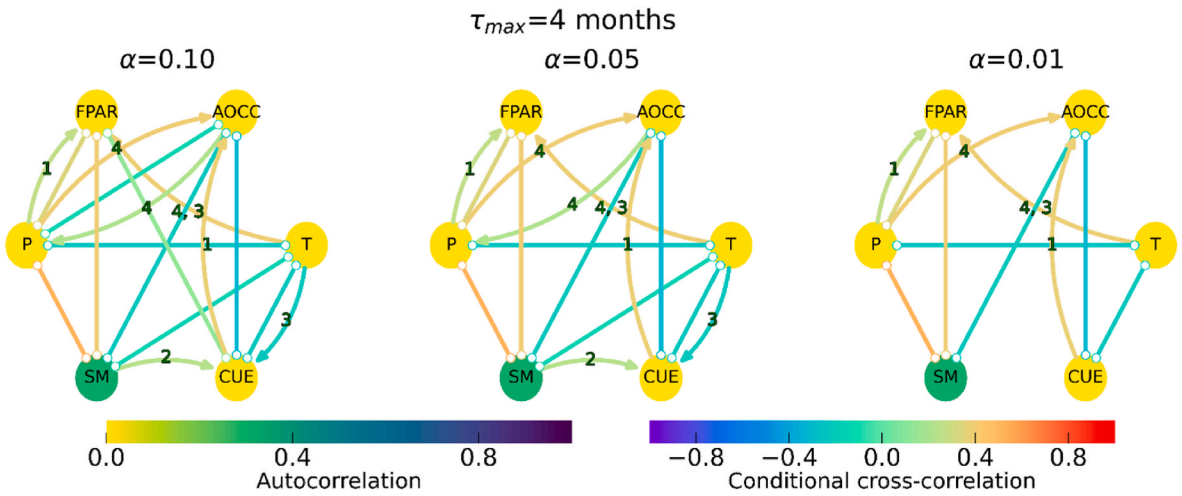

Fig. 7. Causal graphs representing the links for relation of Carbon Use Efficiency (CUE) with its drivers, and interrelationship among Fraction of Photosynthetically Active Radiation (FPAR), Precipitation (P), Temperature (T) Soil Moisture (SM) and Air Organic Carbon Content (AOCC). Here, the maximum time delay is T_{max} and significance threshold is ά.

productivity (greening) in regions of lower CUE in NW (moisture induced greening) and IGP (irrigation induced agricultural boom). However, a reduced productivity (browning) is found in regions of higher CUE such as NE, lower IGP (deforestation and extreme events) and SI (warming induced moisture stress). Apart from climate drivers, anthropogenic intrusions (e.g. land use change, irrigation, farm mechanisation and pollution) also play a role in regulating VCD. Since browning is found in regions of higher CUE, it is a major concern as it indicates weakening of efficient terrestrial carbon sinks. Thus, there is a need of proper planning to protect the green cover in the areas of higher CUE.

This study, therefore, recommends preservation of green cover for maintaining balance in the terrestrial carbon cycle. The preservation of indigenous green cover and afforestation, particularly in the regions of higher vegetation CUE, is very important as it would reduce the carbon footprints in the world of global warming, rising population and high pollution. Our analysis provides new insights on the rate of carbon allocation and help to accurately quantify the ability of vegetation to convert carbon to new biomass in ecosystems. Accurate quantification of CUE for different ecozones and vegetation types would enhance the performance of Earth System Models by providing better input for land-atmosphere interactions. These findings would enable us to counter the challenges of food security, global warming, climate change, and attain sustainability by drafting and implementing relevant policies.

Credit authors statement

RK: Conceptualization, Methodology, Data Analyses, Visualization, Validation, Software, Writing–original draft. **JK:** Conceptualization, Methodology, Visualization, Supervision, review and editing of the original draft. **PK**: Data Analyses, Visualization and Software.

Declaration of competing interest

The authors declare that they have no known competing financial interests or personal relationships that could have appeared to influence the work reported in this paper.

Data availability

All data are publicly available, but can also be made available on request. All data are listed in Table 1.

Acknowledgements

We thank the Director, Indian Institute of Technology Kharagpur (IIT Kgp), Chairman of CORAL IIT Kgp and the Ministry of Education (MoE) for facilitating the study. RK acknowledges the support from Prime Minister's Research Fellowship (PMRF), MoE and PK acknowledges the support from MoE, IIT KGP. We thank the NASA's LPDAAC team for providing the MODIS landcover, NDVI, GPP and NPP products. Giovanni's online data system developed and maintained by the NASA GES DISC for providing the GPM level–3 precipitation data, GLDAS for providing temperature and soil moisture content datasets and MERRA 2 air organic carbon content datasets. We thank the anonymous reviewers and the editor for their comments to improve the quality of this study.

Appendix A. Supplementary data

Supplementary data to this article can be found online at https://doi.org/10.1016/j.jenvman.2023.117655.

References

Ambika, A.K., Mishra, V., 2020. Substantial decline in atmospheric aridity due to irrigation in India. Environ. Res. Lett. 15 (12), 124060 https://doi.org/10.1088/1748-9326/abc8bc.

Bala, G., Joshi, J., Chaturvedi, R.K., Gangamani, H.V., Hashimoto, H., Nemani, R., 2013. Trends and variability of AVHRR– derived NPP in India. Rem. Sens. 5 (2), 810–829. https://doi.org/10.3390/rs5020810.

Ballantyne, A.Á., Alden, C.Á., Miller, J.Á., Tans, P.Á., White, J.W.C., 2012. Increase in observed net carbon dioxide uptake by land and oceans during the past 50 years. Nature 488 (7409), 70–72. https://doi.org/10.1038/nature11299.

Campbell, J.E., Berry, J.A., Seibt, U., Smith, S.J., Montzka, S.A., Launois, T., Belviso, et al., 2017. Large historical growth in global terrestrial gross primary production. Nature 544 (7648), 84–87. https://doi.org/10.1038/nature22030.

Chen, C., Park, T., Wang, X., Piao, S., Xu, B., Chaturvedi, R.K., et al., 2019. China and India lead in greening of the world through land–use management. Nat. Sustain. 2 (2), 122–129. https://doi.org/10.1038/s41893-019-.

De Lucia, E.H., Drake, J.E., Thomas, R.B., Gonzalez-Meler M I Q U E L., 2007. Forest carbon use efficiency: is respiration a constant fraction of gross primary production? Global Change Biol. 13 (6), 1157–1167. https://doi.org/10.1111/j.1365-2486.2007.01365.x.

Gahlot, S., Shu, S., Jain, A.K., Baidya Roy, S., 2017. Estimating trends and variation of net biome productivity in India for 1980–2012 using a land surface model. Geophys. Res. Lett. 44 (22), 11–573. https://doi.org/10.1002/2017GL075777.

Gang, C., Wang, Z., You, Y., Liu, Y., Xu, R., Bian, Z., et al., 2022. Divergent responses of terrestrial carbon use efficiency to climate variation from 2000 to 2018. Global Planet. Change 208, 103709. https://doi.org/10.1016/j.gloplacha.2021.103709.

Gao, T., Yu, J.Y., Paek, H., 2017. Impacts of four northern–hemisphere teleconnection patterns on atmospheric circulations over Eurasia and the Pacific. Theor. Appl. Climatol. 129 (3), 815–831. https://doi.org/10.1007/s00704-016-1801-2.

Garbulsky, M.F., Filella, I., Verger, A., Peñuelas, J., 2014. Photosynthetic light use efficiency from satellite sensors: from global to Mediterranean vegetation. Environ. Exp. Bot. 103, 3–11. https://doi.org/10.1016/j.envexpbot.2013.10.009.

He, Y., Piao, S., Li, X., Chen, A., Qin, D., 2018. Global patterns of vegetation carbon use efficiency and their climate drivers deduced from MODIS satellite data and process–based models. Agric. For. Meteorol. 256, 150–158. https://doi.org/10.1016/j.agrformet.2018.03.009.

IPCC, 2019. Climate Change and Land: an IPCC Special Report on Climate Change, Desertification, Land Degradation, Sustainable Land Management, Food Security, and Greenhouse Gas Fluxes in Terrestrial Ecosystems.

Kashyap, R., Pandey, A.C., Kuttippurath, J., 2022. Photosynthetic trends in India derived from remote sensing measurements during 2000–2019: vegetation dynamics and key climate drivers. Geocarto Int. 1–17. https://doi.org/10.1080/10106049.2022.2060325.

Kashyap, R., Pandey, A.C., Parida, B.R., 2021. Spatio–temporal variability of monsoon precipitation and their effect on precipitation triggered landslides in relation to relief in Himalayas. Spat Inf Res 29 (6), 857–869. https://doi.org/10.1007/s41324-021-00392-8.

Kashyap, R., Kuttippurath, J., Patel, V.K., 2023. Improved air quality leads to enhanced vegetation growth during the COVID–19 lockdown in India. Appl. Geogr., 102869 https://doi.org/10.1016/j.apgeog.2022.102869.

Krich, C., Runge, J., Miralles, D.G., Migliavacca, M., Perez–Priego, O., El–Madany, T., Mahecha, M.D., et al., 2020. Estimating causal networks in biosphere–atmosphere interaction with the PCMCI approach. Biogeosciences 17 (4), 1033–1061. https://doi.org/10.5194/bg-17-1033-2020.

Kumar, P., Kuttippurath, J., Mitra, A., 2022. Causal discovery of drivers of surface ozone variability in Antarctica using a deep learning algorithm. Environ SciProcess Impacts 24 (3), 447–459. https://doi.org/10.1039/D1EM00383F.

Kuttippurath, J., Murasingh, S., Stott, P.A., Sarojini, B.B., Jha, M.K., Kumar, P., et al., 2021. Observed rainfall changes in the past century (1901–2019) over the wettest place on Earth. Environ. Res. Lett. 16 (2), 024018 https://doi.org/10.1088/1748-9326/abcf78.

Kuttippurath, J., Nair, P.J., 2017. The signs of Antarctic ozone hole recovery. Sci. Rep. 7 (1), 1–8. https://doi.org/10.1038/s41598-017-00722-7.

Kuttippurath, J., Raj, S., 2021. Two decades of aerosol observations by AATSR, MISR, MODIS and MERRA–2 over India and Indian Ocean. Remote Sens. Environ. 257, 112363 https://doi.org/10.1016/j.rse.2021.112363.

Le Quéré, C., Andrew, R.M., Friedlingstein, P., Sitch, S., Hauck, J., Pongratz, J., Arneth, A., et al., 2018. Global carbon budget 2018. Earth Syst. Sci. Data 10 (4), 2141–2194. https://doi.org/10.18160/GCP-2018.

Lim, Y.K., 2015. The East atlantic/west Russia (EA/WR) teleconnection in the north–atlantic: climate impact and relation to rossby wave propagation. Clim. Dynam. 44, 3211–3222. https://doi.org/10.1007/s00382-014-2381-4.

Liu, S., Cheng, F., Dong, S., Zhao, H., Hou, X., Wu, X., 2017. Spatiotemporal dynamics of grassland aboveground biomass on the Qinghai–Tibet Plateau based on validated MODIS NDVI. Sci. Rep. 7 (1), 1–10. https://doi.org/10.1038/s41598-017-04038-4.

Liu, Y., Liu, Y., Wang, W., 2019. Inter–comparison of satellite–retrieved and Global Land Data Assimilation System–simulated soil moisture datasets for global drought analysis. Remote Sens. Environ. 220, 1–18. https://doi.org/10.1016/j.rse.2018.10.026.

Lobell, D.B., Gourdji, S.M., 2012. The influence of climate change on global crop productivity. Plant Physiol. 160 (4), 1686–1697. https://doi.org/10.1104/pp.112.208298.

Mezzina, B., Garcia–Serrano, J., Blade, I., Kucharski, F., 2020. Dynamics of the ENSO teleconnection and NAO variability in the North Atlantic–European late winter. J. Clim. 33, 907–923. https://doi.org/10.1175/JCLI-D-19-0192.1.

Migliavacca, M., Musavi, T., Mahecha, M.D., Nelson, J.A., Knauer, J., Baldocchi, D.D., et al., 2021. The three major axes of terrestrial ecosystem function. Nature 598 (7881), 468–472. https://doi.org/10.1038/s41586-021-03939-9.

Muñoz, E., Poveda, G., Arbeláez, M.P., Vélez, I.D., 2021. Spatiotemporal dynamics of dengue in Colombia in relation to the combined effects of local climate and ENSO. Acta Trop. 224, 106136 https://doi.org/10.1016/j.actatropica.2021.106136.

Murthy, I.K., Gupta, M., Tomar, S., Munsi, M., Tiwari, R., Hegde, G.T., Ravindranath, N. H., 2013. Carbon sequestration potential of agroforestry systems in India. J. Earth Sci. Climatic Change 4 (1), 1–7. https://doi.org/10.4172/2157-7617.1000131.

Nayak, R.K., Patel, N.R., Dadhwal, V.K., 2013. Inter-annual variability and climate control of terrestrial net primary productivity over India. Int. J. Climatol. 33 (1), 132–142. https://doi.org/10.1002/joc.3414.

Nemani, R.R., Keeling, C.D., Hashimoto, H., Jolly, W.M., Piper, S.C., Tucker, C.J., et al., 2003. Climate-driven increases in global terrestrial net primary production from 1982 to 1999. Science 300 (5625), 1560–1563. https://doi.org/10.1126/science.1082750.

Newbold, T., Tittensor, D.P., Harfoot, M.B., Scharlemann, J.P., Purves, D.W., 2020. Non–linear changes in modelled terrestrial ecosystems subjected to perturbations. Sci. Rep. 10 (1), 1–10. https://doi.org/10.1038/s41598-020-70960-9.

Parida, B.R., Pandey, A.C., Patel, N.R., 2020. Greening and browning trends of vegetation in India and their responses to climatic and non–climatic drivers. Climate 8 (8), 92. https://doi.org/10.3390/cli8080092.

Pérez-Girón, J.C., Alvarez-Alvarez, P., Díaz-Varela, E.R., Lopes, D.M.M., 2020. Influence of climate variations on primary production indicators and on the resilience of forest ecosystems in a future scenario of climate change: application to sweet chestnut agroforestry systems in the Iberian Peninsula. Ecol. Indicat. 113, 106199 https://doi.org/10.1016/j.ecolind.2020.106199.

Pérez-Girón, J.C., Díaz-Varela, E.R., Álvarez-Álvarez, P., 2022. Climate-driven variations in productivity reveal adaptive strategies in Iberian cork oak agroforestry systems. Ecosystems 9, 100008. https://doi.org/10.1016/j.fecs.2022.100008.

Piao, S., Wang, X., Park, T., Chen, C., Lian, X.U., He, Y., Bjerke, J.W., Myeni, R.B., et al., 2020. Characteristics, drivers and feedbacks of global greening. Nat. Rev. Earth Environ. 1 (1), 14–27. https://doi.org/10.1038/s43017-019-0001-x.

Roxburgh, S.H., Berry, S.L., Buckley, T.N., Barnes, B., Roderick, M.L., 2005. What is NPP? Inconsistent accounting of respiratory fluxes in the definition of net primary production. Funct. Ecol. 19 (3), 378–382. https://www.jstor.org/stable/3599129.

Runge, J., Bathiany, S., Bollt, E., Camps–Valls, G., Coumou, D., Deyle, E., Zscheischler, J., et al., 2019. Inferring causation from time series in Earth system sciences. Nat. Commun. 10 (1), 1–13. https://doi.org/10.1038/s41467-019-10105-3.

Running, S., Mu, Q., Zhao, M., 2015. MOD17A2H MODIS/Terra Gross Primary Productivity 8– Day L4 Global 500m SIN Grid V006. NASA EOSDIS L. Process. DAAC.

Sannigrahi, S., Pilla, F., Basu, B., Basu, A.S., Sarkar, K., Chakraborti, S., et al., 2020. Examining the effects of forest fire on terrestrial carbon emission and ecosystem production in India using remote sensing approaches. Sci. Total Environ. 725, 138331 https://doi.org/10.1016/j.scitotenv.2020.138331.

Sarmah, S., Singha, M., Wang, J., Dong, J., Burman, P.K.D., Goswami, S., Ge, Y., Ilyas, S., Niu, S., 2021. Mismatches between vegetation greening and primary productivity trends in South Asia-A satellite evidence. Int. J. Appl. Earth Obs. Geoinf. 104, 102561 https://doi.org/10.1016/j.jag.2021.102561.

Shikwambana, L., 2019. Long-term observation of global black carbon, air organic carbon and smoke using CALIPSO and MERRA– 2 data. Remote Sens. Lett. 10 (4), 373–380. https://doi.org/10.1080/2150704X.2018.1557789.

Singh, A., Abbhishek, K., Kuttippurath, J., Raj, S., Mallick, N., Chander, G., Dixit, S., 2022. Decadal variations in CO2 during agricultural seasons in India and role of management as sustainable approach. Environ. Technol. Innovat. 27, 102498 https://doi.org/10.1016/j.eti.2022.102498.

Singh, R.P., Rovshan, S., Goroshi, S.K., Panigrahy, S., Parihar, J.S., 2011. Spatial and temporal variability of net primary productivity (NPP) over terrestrial biosphere of India using NOAA–AVHRR based GloPEM model. J. Ind. Soc. Remote Sens. 39, 345–353. https://doi.org/10.1007/s12524-011-0123-1.

Spensberger, C., Reeder, M.J., Spengler, T., Patterson, M., 2020. The connection between the Southern Annular Mode and a feature–based perspective on Southern Hemisphere midlatitude winter variability. J. Clim. 33, 115–129. https://doi.org/10.1175/JCLI-D-19-0224.1.

Turner, D.P., Ritts, W.D., Cohen, W.B., Gower, S.T., Running, S.W., Zhao, M., et al., 2006. Evaluation of MODIS NPP and GPP products across multiple biomes. Remote Sens. Environ. 102 (3– 4), 282–292. https://doi.org/10.1016/j.rse.2006.02.017.

Verma, A., Chandel, V., Ghosh, S., 2022. Climate drivers of the variations of vegetation productivity in India. Environ. Res. Lett. 17 (8), 084023 https://doi.org/10.1088/1748-9326/ac7c7f.

Wang, L., Li, X., Chen, Y., Yang, K., Chen, D., Zhou, J., et al., 2016. Validation of the global land data assimilation system based on measurements of soil temperature profiles. Agric. For. Meteorol. 218, 288–297. https://doi.org/10.1016/j.agrformet.2016.01.003.

Wang, L., Zhu, H., Lin, A., Zou, L., Qin, W., Du, Q., 2017. Evaluation of the latest MODIS GPP products across multiple biomes using global eddy covariance flux data. Rem. Sens. 9 (5), 418. https://doi.org/10.3390/rs9050418.

Xia, Y., Hao, Z., Shi, C., Li, Y., Meng, J., Xu, T., et al., 2019. Regional and global land data assimilation systems: innovations, challenges, and prospects. J. Meteorol. Res. 33 (2), 159–189. https://doi.org/10.1007/s13351-019-8172-4.

Xu, R., Tian, F., Yang, L., Hu, H., Lu, H., Hou, A., 2017. Ground validation of GPM IMERG and TRMM 3B42V7 rainfall products over southern Tibetan Plateau based on a high-density rain gauge network. J. Geophys. Res. Atmos. 122 (2), 910–924. https://doi.org/10.1002/2016JD025418.

Yao, Y., Wang, X., Li, Y., Wang, T., Shen, M., Du, M., He, H., Li, Y., Piao, S., et al., 2018. Spatiotemporal pattern of gross primary productivity and its covariation with climate in China over the last thirty years. Global Change Biol. 24 (1), 184–196. https://doi.org/10.1111/gcb.13830.

Resources, Conservation & Recycling 222 (2025) 108478

Contents lists available at ScienceDirect

Resources, Conservation & Recycling

journal homepage: www.sciencedirect.com/journal/resources-conservation-and-recycling

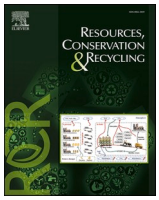

Full length article

Weakening of forest carbon stocks due to declining Ecosystem Photosynthetic Efficiency under the current and future climate change scenarios in India

Rahul Kashyap, Jayanarayanan Kuttippurath *

CORAL, Indian Institute of Technology Kharagpur, Kharagpur 721302, India

ARTICLE INFO

Keywords:
Carbon cycle
Ecosystem photosynthetic efficiency
Forest resilience
Machine learning
CMIP6
Dynamic global vegetation model (DGVM)

ABSTRACT

Despite lying in the tropics of higher carbon uptake, Indian forest carbon stocks are underexplored. We investigate the translation of greenness to carbon uptake (Ecosystem Photosynthetic Efficiency, EPE) and its impact on forest carbon (CUE) and water use (WUE) efficiencies in the current and future climate. We find hindered ability of Indian forests to translate greening into carbon uptake, due to a marked decline (-5 %) in EPE during recent decade (2010–2019) from the previous (2000–2009). The reduced EPE deteriorates forest health [(CUE, -4.5 %), (WUE, -3 %)] driven by soil drying (-2 %) and enhanced evaporative stress (+8 %). Granger Causality and Random Forest (RF) analyses reveal soil moisture (SM) as the key driver of EPE. Only 16 % of the Indian forests exhibits high integrity due to anthropogenic interventions. The CMIP6 and LPJ-GUESS model projections suggest weakening of forest carbon sinks in India and calls for sustainable actions to achieve the target of net-zero emissions by 2070.

1. Introduction

The stability of global climate system and carbon cycle is controlled by terrestrial ecosystems as they act as major carbon sinks, regulate the fluxes of carbon, water, energy and momentum between the land and atmosphere, and are home to vast varieties of habitats (Friedlingstein et al., 2024; Bar-On et al., 2025). Forests act as global carbon sinks, capturing almost 50 % of fossil-fuel emissions with tropical forest deforestation and degradation releasing almost 2/3rd of it (Pan et al., 2024). Thus, forests capture around 30 % of the anthropogenic carbon dioxide (CO_2) emissions (Ruehr et al., 2023; Bar-On et al., 2025). Therefore, utilising the carbon sequestration capacity of forests is a crucial element of strategies to alleviate climate change and a fundamental aspect of policy development (IPCC, 2021; Friedlingstein et al., 2024). Simultaneously, climate change in the warming world and enhanced dryness stress have adverse impacts on forests (Bauman et al., 2022; Yan et al., 2025). In the future, global warming will intensify aridity stress, which would decrease vegetation greenness, carbon uptake and perturb the terrestrial carbon cycle (Reichstein et al., 2013; Seneviratne et al., 2021).

Global carbon sinks have been stable for past three decades (1990–2019) with regional biome level changes such as gain in temperate, and decline in boreal and tropical intact forests (Pan et al., 2024; Feng et al., 2024). However, growing climatic extremes (Tao et al., 2022; Feng et al., 2024), accelerated tropical deforestation (Qin et al., 2021; Zhao et al., 2024) and ageing forests (Yang et al., 2023) could disrupt the land carbon sinks (Pan et al., 2024). India lies in the tropical regions of higher carbon uptake and contributes about 7 % to the global carbon sinks (Harris and Gibbs, 2021), even with its mere 2 % of the global forest cover (ISFR, 2021). India reports 21.71 % of land area as forests and is the 8th largest in terms of global forest cover (ISFR, 2021). Additionally, India hosts 4 of the 36 biodiversity hotspots, and 2 of 8 hottest biodiversity hotspots in the world (Kong et al., 2021). Concurrently, India is the second largest contributor to the global greening (Chen et al., 2019) and one of the hotspots of land-atmosphere coupling (Humphrey et al., 2021).

India has been greening in recent decades due to climate change (Parida et al., 2020; Kashyap et al., 2022, 2023a) and anthropogenic activities (Kuttippurath and Kashyap, 2023). However, this is largely (86.5 %) cropland-based driven by improved irrigation and better land management (Kuttippurath and Kashyap, 2023). Some recent studies report mismatch in the greening and carbon uptake (Sarmah et al., 2021;

* Corresponding author.
E-mail address: jayan@coral.iitkgp.ac.in (J. Kuttippurath).

https://doi.org/10.1016/j.resconrec.2025.108478
Received 8 July 2024; Received in revised form 15 June 2025; Accepted 19 June 2025

Das et al., 2023) and carbon sink regions (Kashyap et al., 2023a) in India. Also, the carbon uptake by Indian ecosystems is projected to decline in the future climate scenarios (Bejagam et al., 2024). This calls for a dedicated study that thoroughly investigates the translation of greenness to carbon uptake in Indian forests and its drivers in the current and future climate scenarios. However, the translation of greenness to carbon uptake is rather complex (Walther et al., 2016; Zeng et al., 2023), as the photosynthesis and carbon uptake are very sensitive to environmental changes (Walther et al., 2016; Yan et al., 2019). Environmental factors have the potential to cause a substantial change in the carbon uptake even before inflicting any observable change in the vegetation greenness (Wei et al., 2022; Zhang et al., 2024). Ecosystem Photosynthetic Efficiency (EPE) is a metric used to understand this intricate relationship between greenness and carbon uptake (Zhang et al., 2024; Wang et al., 2023).

We, for the first time, estimate the translation of greenness to carbon uptake (EPE), and its impact on the health and functioning [Carbon Use Efficiency (CUE) and Water Use Efficiency (WUE)] of Indian forest ecosystems. We quantify the contribution, relation, association and sensitivity of ecosystem functioning metrics (EPE, CUE and WUE) to various climate drivers. Additionally, we estimate the resilience of forest carbon stocks to drying, warming, aridity and wildfires. We also unravel the anthropogenic influence on forest ecosystems in India. Apart from these, we examine the future of forest carbon stocks in India based on the Coupled Model Intercomparison Project Phase 6 (CMIP6) projection data and a process-based ecosystem model, Lund-Potsdam-Jena General Ecosystem Simulator (LPJ-GUESS), results. These findings will provide new insight into the complex relationship between greenness and carbon uptake. This will facilitate the implementation of strategic management and effective policies to preserve forest ecosystems, food security, achieve net zero target and to promote sustainability in India and other similar bioclimatic regions worldwide.

2. Data and methods

2.1. Data

2.1.1. Land cover, greenness, photosynthesis and carbon uptake

We utilise a wide range of datasets including satellite measurements and reanalyses as listed in **Table S1.** A synoptic scale observation for comprehensive monitoring of the terrestrial biosphere on a global scale are achieved through satellite remote sensing (Crowther et al., 2015; Chen et al., 2019). The effectiveness of moderate resolution imaging spectroradiometer (MODIS) for the tropical regions of high carbon uptake is well established (Sarmah et al., 2021; Kashyap et al., 2023a). Here, we utilise the MODIS Land Cover Type (MCD12Q1) Version 6 dataset that enables a comprehensive representation of global land cover types based on supervised classification of the surface reflectance data. Since this study is focused on forest ecosystems, we mask the other classes. The most widely used proxy of surface greenness is the Normalised Difference Vegetation Index (NDVI) as it represents vegetation vigour due to its association with chlorophyll content, foliar nitrogen and leaf characteristics of the plant (Parida et al., 2020; Kuttippurath and Kashyap, 2023). We utilise the MODIS MOD13A1 NDVI for this purpose. We also consider the biophysical metric, Leaf Area Index (LAI) based on MODIS MCD15A2H LAI as it is one of the key parameters to quantify the greenness and biomass of the ecosystem due to its close association with the plant biophysical processes (Chen et al., 2019; Kuttippurath and Kashyap, 2023). To effectively quantify the plant photosynthetic activity, it is crucial to estimate the fraction of photosynthetically active radiation (FPAR) that plants absorb from the solar energy (Kashyap et al., 2022, 2025). The NDVI-FPAR relation is linear in most cases and FPAR could be evaluated more accurately using NDVI as detailed in Supplementary material. We also utilise the Net Primary Productivity (NPP) from MODIS (MOD 17 A3HGF) as it is one of the most fundamental ecological variables used to quantify the plant carbon uptake, measured as the residual of Gross Primary Productivity (GPP, MOD 17 A2HGF) after autotrophic respiration (Ra) (Nemani et al., 2003; Kashyap et al., 2023a). Additionally, we analyse the Solar-Induced Fluorescence (SIF) data from GOSIF v2 gridded dataset (Li and Xiao, 2019; Kashyap et al., 2023b). SIF is the radiation flux emitted as light energy in the wavelength range 650–800 nm during photosynthesis (Rascher et al., 2015) and is considered an efficient indicator of photosynthetic activity (Shekhar et al., 2022).

2.1.2. Ecosystem characteristics

The ecosystem characteristics taken in account are canopy cover, Vegetation Continuous Fields (VCF) and above ground biomass (AGB). The canopy cover is the proportion of the land that is having forest canopy represented in terms of percentage (%) for the year 2010 obtained from the Global Forest Watch (GFW). The Vegetation Continuous Fields (VCF) product is a comprehensive description of the Earth's surface, encompassing three distinct components of ground cover (tree, non-tree and bare) surfaces. Here, we consider MODIS VCF (MOD44B Version 6.1) as it is the primary dataset known as the percent tree cover layer that provide the percentage of each pixel covered by a tree canopy. The biomass is a measure of the carbon stock in the plant. Here we use the AGB data derived from GlobBiomass for the year 2010 (Santoro et al., 2021). We also consider the forest age data to examine the structure, carbon sequestration ability, recovery post-disturbance by climate change and anthropogenic intrusions of Indian forest ecosystems. These data are an ensemble of the global forest inventories, biomass and climate data and are obtained from the Max Planck Institute of Biogeochemistry (MPI-BGC) for the year 2010 (Besnard et al., 2021).

2.1.3. Meteorology, aridity, fire and topography

The moisture availability is assessed based on the precipitation (P) data from the Global Precipitation Measurement (GPM) and the soil moisture (SM) data from the Global Land Data Assimilation System (GLDAS). The aridity is quantified in terms of Climatic Water Deficit (CWD) and Vapour Pressure Deficit (VPD) obtained from the TerraClimate database. CWD is a measure of land evaporative aridity quantified as the difference between the potential evapotranspiration (PET) and actual evapotranspiration (AET). Basically, CWD is the amount of water that would have potentially evaporated/transpired to the atmosphere, if it was available (Huang et al., 2021; Kashyap and Kuttippurath, 2024a). VPD is a measure of atmospheric evaporative demand or atmospheric aridity as it is the difference between the saturated and ambient vapour pressure conditions at a particular temperature (Bauman et al., 2022). VPD is considered to have a strong control on the vegetation stomatal opening and thus influence the exchange of carbon and water between the biosphere and atmosphere (Bauman et al., 2022; Yan et al., 2025). The temperature (T) data is obtained from fifth generation European Centre for Medium-Range Weather Forecast Reanalysis (ERA-5). The evapotranspiration (ET) data are obtained from MODIS (MOD16 A3HGF) to account for ET and estimate WUE (Kashyap and Kuttippurath, 2024a, b). We also consider the fire counts from MODIS Fire Information for Resource Management System (FIRMS) to account for the impact of wildfires on the ecosystem health (Giglio et al., 2016; Kashyap and Pandey, 2021). To have a clear understanding of the impact of topography and terrain on the variability of forest types and their health, we utilise the elevation data based on the Advanced Space-borne Thermal Emission and Reflection Radiometer (ASTER) Global Digital Elevation 4 Model (GDEM) Version 3 (ASTGTM) data (Farr et al., 2007).

2.1.4. Anthropogenic activity

To account for anthropogenic influence on the forests we consider two indices, the Human Modification Index (HMI) and Forest Landscape Integrity Index (FLII) for the year 2016. HMI is obtained from the Socioeconomic Data and Applications Center (SEDAC) and it ranges from 0 to 1, which represents the cumulative measure of human modification

on land accounting for a total of 13 anthropogenic stressors divided into 5 categories such as (i) human settlement, (ii) agriculture, (iii) transportation, (iv) mining and energy production and (v) electrical infrastructure (Kennedy et al., 2019). FLII is the first estimate of ecological integrity of global forests, where it accounts for the observed and inferred human pressure (infrastructure, agriculture and tree cover loss) accounting for the loss of forest connectivity (ratio of current to potential forest connectivity), for the year 2019. It ranges from 0 to 10, where low is 0–6, moderate is 6–9.6 and high is 9.6–10 (Grantham et al., 2020). Furthermore, we also estimate the change in human population in the year 2019 from 2000, based on the pixel-wise image differencing technique, for the Indian forest regions, which is a proxy for examining the anthropogenic interventions in these natural ecosystems.

2.1.5. Future projections from the CMIP 6 models

We consider the future projection data for LAI, GPP, NPP and ET from the models CNRM (1.40° × 1.40°), ACCESS (1.875° × 1.25°), MPI-ESM (1.88° × 1.86°) and Can-ESM (2.81° × 2.77°), as these are high resolution models with good reliability for the Indian region (Bejagam et al., 2024). We use the data from high-resolution CMIP6 models such as GFDL, CNRM, CM61HR and HadGEM for P and T for high emissions scenarios (Shared Socioeconomic Pathways, SSP585) detailed in **Table S2**.

2.2. Methods

We use a suite of statistical techniques such as correlation, multiple linear regression (MLR), machine learning (ML) based Random Forest (RF) model, Granger Causality, Growth Rate (GR) estimation and Resilience method to make our analysis robust to draw solid conclusions. The key methodological approaches are given below.

2.2.1. Regional and spatio-temporal variability estimation

First, we present the spatial variability in the forest cover in India in terms of their broad geographic/climatic zones, forest types and elevation zones. Then, we present VCF, canopy cover and biomass and estimate their regional variability. Then, we compute the spatio-temporal variability in greenness, photosynthesis and productivity (FPAR, SIF, LAI and NPP). We utilise the image differencing technique to estimate the change in greenness, photosynthesis and productivity in recent decade (2010–2019) from its previous decade (2000–2009). The decadal change in moisture availability (P and SM), aridity (CWD and VPD) and T are also estimated using the Eq. (2):

$$\%\ X_{R-P} = \frac{X_R - X_P}{X_P} \times 100 \quad (1)$$

Here, X is any variable like LAI or NPP, R is the mean of X in recent decade (2010–2019), and P is the mean of X in the previous decade (2000–2009).

To delineate the regional variability in different bioclimatic regions, we estimate the normalised regional anomaly (NRA) of the changes in various variables, as per Eq. (2):

$$NRA = (I_m - X_m)/X_m \quad (2)$$

Here, I_m = mean change value for any bioclimatic forest region of India and X_m = mean change value for the Indian forests.

We estimate forest loss based on pixel-wise image differencing technique and the pixels of forest regions converted to non-forest pixels are delineated as “forest loss” based on MODIS Land Cover Type between the years 2001 and 2019.

2.2.2. Estimation of forest health and functioning

We estimate three metrics of ecosystem health and functioning namely, EPE, CUE and WUE. EPE is the translational ability of greenness to productivity by plants. It is computed as the ratio of SIF to LAI previously (Wei et al., 2022; Wang et al., 2023; Zhang et al., 2024). However, being a weak signal, at times SIF is not accurately captured and is not always a surrogate for the amount of carbon assimilated by ecosystems particularly in high biomass regions like forests (MacBean et al., 2018; Zeng et al., 2023). Therefore, we estimate EPE as the ratio of carbon uptake (NPP) to greenness (LAI) for the forest ecosystems as per Eq. (3):

$$\mathrm{EPE} = \frac{\mathrm{NPP}}{\mathrm{LAI}} \quad (3)$$

The ecosystem CUE is the measure of the rate or the ability of the vegetation to sequester carbon from the atmosphere (Gang et al., 2022; Kashyap et al., 2023a). It is basically the rate of conversion of GPP to NPP in ecosystems estimated as per Eq. (4):

$$\mathrm{CUE} = \frac{\mathrm{NPP}}{\mathrm{GPP}} \quad (4)$$

The ecosystem WUE is the amount of carbon assimilated to the water lost through transpiration during photosynthesis by the plant (Keenan et al., 2013; Kashyap and Kuttippurath, 2024a). It is a key ecohydrological metric that interlinks the carbon and water cycles, and is estimated as per Eq. (5):

$$\mathrm{WUE} = \frac{\mathrm{NPP}}{\mathrm{ET}} \quad (5)$$

We also compute the future EPE, CUE and WUE based on the future LAI, GPP, NPP and ET data from the model projections. We estimate the change EPE, CUE and WUE among the decades from the historical (2015–2019) to the future periods such as the decades of mid-century (2040–2050) and end-century (2090–2100).

2.2.3. Relation with drivers: Correlation and Granger Causality

To decipher the associations of drivers with EPE we perform Parsons’s correlation analysis. However, since correlation does not imply causation, we further investigate the existence of causal relationships among EPE and its drivers based on Granger causality. We consider Granger causality test based on the concepts of "cause" and "effect". Granger causality is affirmed wherein the potential to predict future responses of variable Y enhances by accounting all relevant information, except for the present value of variable X (Granger, 1969) as detailed in Supplementary material. To conduct a Granger causality test, a bivariate model is established between the time series (X and Y) that are stationary as per Eqs. (6) and (7):

$$Y_t = \sum_{i=1}^{n} a_i Y_{t-i} + \sum_{i=1}^{n} b_i X_{t-i} + \varepsilon_t \quad (6)$$

$$X_t = \sum_{i=1}^{n} c_i X_{t-i} + \sum_{i=1}^{n} d_i Y_{t-i} + \delta_t \quad (7)$$

where, X and Y are two stationary time series; a, b, c and d are coefficients; and ε and δ are white noise. For X to Granger cause Y, $b_i \neq 0$; for Feedback between X and Y, $d_i \neq 0$. To comprehend the temporal delay in Ganger Causality, a maximum lag of 4 months is assigned.

2.2.4. Contribution of drivers: Random Forest and MLR

The capability of machine learning (ML) to effectively handle multidimensional data has made it very useful for modelling systems that exhibit complex nonlinear structures. The Random Forest (RF) is an ensemble model that integrates boosting and regression trees (Breiman, 2001). A total of 500 trees are generated, with two variable splitting in each tree. These data are partitioned into two subsets: 30 % for testing and 70 % for training purposes. In this study, a methodology based on precision is employed to estimate the relative contribution of each driver on EPE, CUE, and WUE. In R Studio version 4.2.1, we employ the RF model along with the "randomForest" and "caret" packages to assess the relative significance of each variable based on independent data

samples. In RF, each tree has its own independent out-of-the-bag data sample that were not included in the initial build. The first step involves evaluating the specimen obtained directly from the bag in terms of its predictive accuracy. Afterwards, the stability of all other variables is maintained, while the values of the variables in the outlier sample are generated randomly. We assess the accuracy of predicted values by calculating the average decrease in precision across all trees. The value indicator is further divided into various categories of the outcomes. It can be deduced that the stochastic rearrangement of a variable leads to the total elimination of its predictive capability. The importance of a variable is a measure of the degree to which its omission results in a decrease of precision, as per Eq. (8):

$$I_x = \sum_{k=1}^{K} \left[\frac{1}{K} \left({MSE_k}^{xprem} - MSE_k \right) \right] \quad (8)$$

Here, I_x is the variable importance or contribution, K is the number of trees in the forest, ${MSE_k}^{xprem}$ is the estimation error with predictor x being eliminated for the k^{th} decision tree, and MSE_k is the forecasting error with all predictors included in the k^{th} decision tree.

The RF model's default hyperparameters are chosen for their exceptional efficiency in executing the algorithm (e.g. Kashyap and Kuttippurath, 2024a, b). Additionally, we employ MLR to estimate the influence of the drivers and complement the findings drawn from the RF model as explained in Supplementary material.

2.2.5. Sensitivity to drivers

We estimate the sensitivity of forest health and functioning (EPE, CUE and WUE) to its drivers such as P, SM, CWD, VPD, FPAR, T and fire count (FC) as per Eq. (9):

$$Sx = \frac{\Delta S}{\Delta X} \quad (9)$$

Here, Sx is the sensitivity of S to X, and S is either of EPE, CUE or WUE and X is its driver (P, SM, CWD, VPD, FPAR, T and FC). The change in S (ΔS) and X (ΔX) are the percentage change in recent decade (2010–2019) from the previous decade (2000–2009) (Kashyap et al., 2025).

2.2.6. Growth Rate analysis

The Growth Rate (GR) concept is widely used in economics to compute the intermediate variations and overall cumulative changes over a period. Recently, this technique has also been employed to investigate the atmospheric CO_2 concentration changes (Keenan et al., 2016). It is estimated as the difference in the value (X) in the current (t) from the previous (t-1) period, as shown in Eq. (10):

$$X_{GR} = X_t - X_{t-1} \quad (10)$$

Here, X_{GR} is the growth rate (GR) in X (EPE and its drivers) between time periods t and t-1.

We also estimate the cumulative growth rate (CGR, Eq. (11)) and mean growth rate (MGR, Eq. (12)) for the study period (2000–2019).

$$CGR = \sum_{i=1}^{n} X_{GR} \quad (11)$$

$$MGR = \left(\sum_{i=1}^{n} X_{GR} \right) \Big/ n \quad (12)$$

Here, n is the number of years of the study.

2.2.7. Forest Resilience

The ability or potential of an ecosystem to maintain its state and functioning amidst a disturbance is termed as resilience (Holling, 1973). Resilience method has gained a wide popularity in studies pertaining to ecosystems (Sharma and Goyal, 2018; Kashyap and Kuttippurath, 2024a). Here we, estimate the forest resilience to P drying, SM stress, surface warming, CWD, VPD and wildfires. Since, it is a long-term analysis and we cannot consider every event as it would be for a small period and on a regional scale, we rely on the worst affected year. First, we find the largest negative anomaly (P and SM) and positive anomaly (CWD, VPD, T and fire count (FC)). Then, the we compute the ratio (Ri) of the worst affected year (Y_x) to the overall mean of the period (Y_m). The non-dimensional quantity Ri is called as the coefficient of resilience as per Eq. (13):

$$R_i = \frac{Y_x}{Y_m} \quad (13)$$

The Ri threshold of 0.8–0.9 is moderately resilient, while higher than that is resilient and lower is non-resilient (Sharma and Goyal, 2018; Kashyap and Kuttippurath, 2024a).

2.2.8. Process based ecosystem model

LPJ-GUESS is a process based dynamic global vegetation model (DGVM) that analyses the dynamics of vegetation, biogeochemistry of the ecosystem and water cycling. By utilising available data on regional climate conditions and atmospheric CO_2, it is possible to make predictions regarding the structural, compositional and functional properties of the indigenous ecosystems found within the primary climate zones of our planet. In LPJ-GUESS models trees as age cohorts that are identical within each cohort (age class) but differ across multiple replicate patches. It gives outputs such as the composition and coverage of vegetation, categorised by major plant functional types (PFTs) (Smith et al., 2014). We employ the LPJ-GUESS (version 3.0) model to estimate LAI, NPP, biomass, leaf carbon and nitrogen ratios (leaf C:N) for six selected forest sites in India, one each in six different bio-climatic regions, as detailed in Supplementary material (**Table S3**). We initially run the model for 1000 years as a "spin up" to tune the model up for each forest site and then run in the "transient phase" for 20, 50, and 100 years to match the periods of 2015–2019, 2040–2050, and 2050–2100, respectively. We use a pre-defined climate [(precipitation (P) and temperature (T)] through "Run GetClim" module, which uses default atmospheric CO_2 concentrations for the "spin up". In the "transient phase", we run the model initially for the "climate change" scenario. We employ the available P (GPM) and T (ERA-5 2 m) data to compute their anomaly for the period 2015–2019 and multi-model (GFDL, CNRM, CM61HR, HadGEM) ensemble of P and T from CMIP6 climate projections for the future runs i.e. 2040–2050, and 2050–2100. We also run the LPJ-GUESS model for "no-climate change" scenario when the P and T anomalies are set at 0.

3. Study area

3.1. Zones, PFTs and elevation

The forested ecosystems in India are spatially categorised into six bioclimatic regions: (i) Western Himalaya (WH), (ii) Eastern Himalaya (EH), (iii) North East (NE), (iv) Indo-Gangetic Plain (IGP), (v) Central India (CI), and (vi) Western Ghats and Peninsula (WGP) (**Fig. S1a**). Evergreen Needleleaf Forests (ENF) are found in the foothills of WH in the moderate elevation zones (600–1200 m). Evergreen Broadleaf Forests (EBF) are found mostly in EH, NE and western ghats (WG) in a wide range of elevations (600–2400 m). Deciduous Needleleaf Forests (DNF), are found in moderate elevation zones (600–1200 m) of lower WH and CI. Deciduous Broadleaf Forests (DBF) are majorly found in the low elevation areas (< 600 m) of CI, IGP and WGP. Mixed Forests (MF) are a blend of evergreen and deciduous tree types (40–60 % of each) found in all forested regions and are the predominant forest types in WH and EH in the high (1200–4800 m) elevation and CI in low (300–600 m) elevation areas (**Fig. S1b, S1c**)

3.2. Canopy, Vegetation Continuous Fields and biomass

For the Indian forests, we find the mean the canopy cover as 55.6 %, VCF as 52.5 % and AGB as 589 Mg/ha. In terms of spatial variability, there is a homogeneous pattern among canopy, VCF and AGB (**Fig. S1d, e, f**). Among the regions, EH with forest types such as EBF and MF have the highest VCF (68.5 %), canopy (77.8 %) and AGB (786 Mg/ha). NE is the other region with EBF, MF and DBF, has high VCF (59 %), canopy

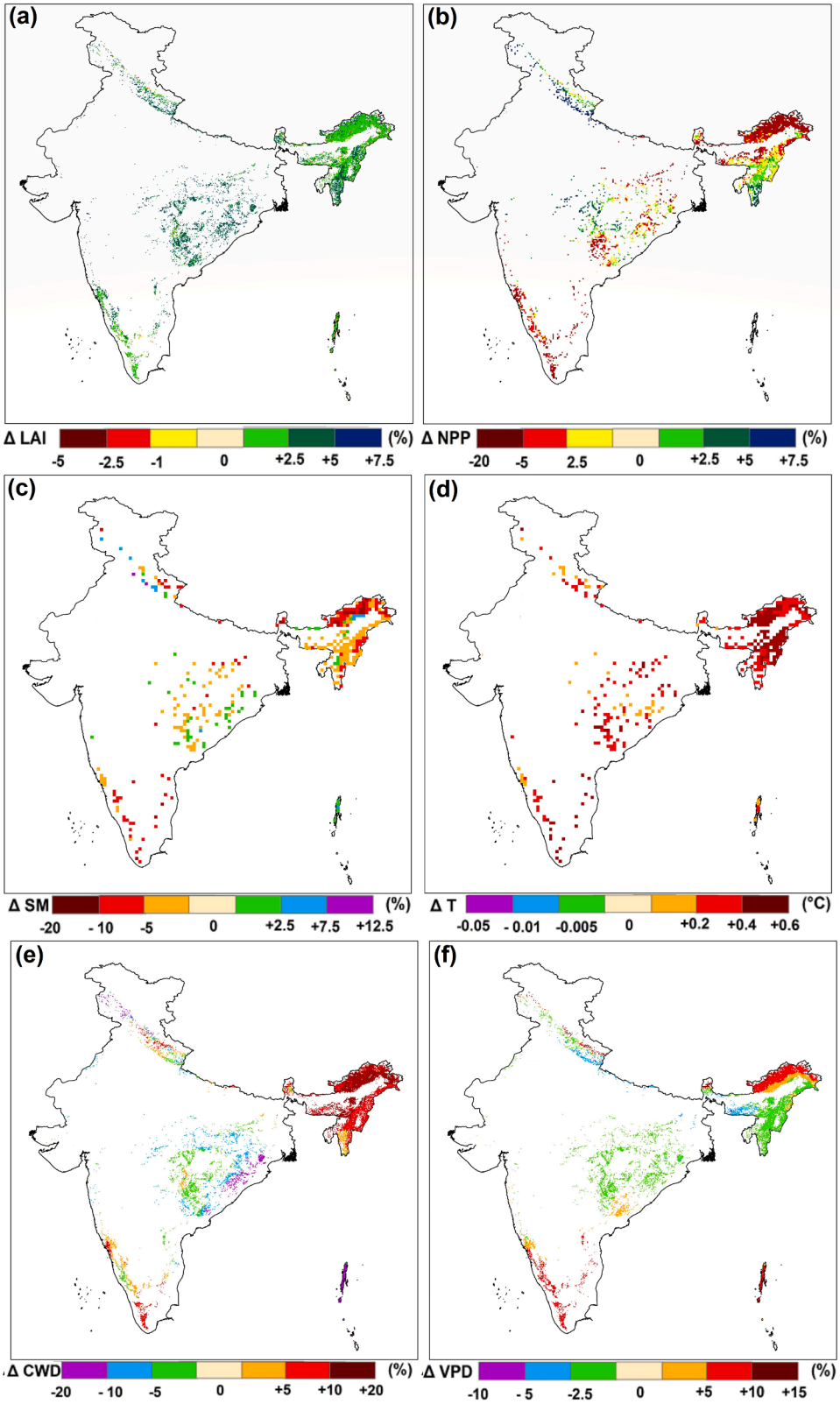

Fig. 1. Change (%) in (a) Leaf Area Index (LAI), (b) Net Primary Productivity (NPP), (c) Soil Moisture (SM), (d) Temperature (T), (e) Climatic Water Deficit (CWD) and (f) Vapour Pressure Deficit (VPD) in recent decade (2010–2019) from the previous decade (2000–2009) for Indian forests.

(69.8 %) and AGB (662 Mg/ha). WGP forests have high VCF (45 %) and canopy (50.7 %). In contrast, CI with forest types such as DBF and MF has the lowest VCF (29.7 %), canopy (36.4 %) and AGB (378 Mg/ha).

3.3. Greenness, photosynthesis, carbon uptake and climate

Here, high FPAR (0.75–09), SIF (0.3–0.4 W/m^2/m/sr), LAI (5.5–7 m^2/m^2) and NPP (900–1500 gC/m^2/yr) are observed in majority of the forested areas in EH, NE, and WGP (**Fig. S2**). These are the regions of high moisture availability [P (> 10 mm/day), SM (> 80 kg/m2)], moderate ET (750–1500 mm) and optimum T (16–25 °C). Moreover, these are also the regions of lower aridity [lower CWD (< 30 mm) and VPD (<0.8 kPa)]. Contrarily, low FPAR (< 0.65), SIF (< 0.2 W/m^2/m/sr), LAI (< 4.5) and NPP (< 500 gC/m^2/yr) are exhibited by the forests in the south WH and majority of CI. Limited moisture availability [P (< 6 mm/day), SM (< 60 kg/m^2)], lower ET (< 750 mm), higher T (>25 °C) added by higher aridity [(CWD > 45 mm), (VPD > 1.3 kPa)] are the reasons for this (**Figs. S3, S4**). It is evident that the forest ecosystems with ample moisture availability, optimum warmth and lower aridity show higher greenness, photosynthetic activity and carbon uptake.

4. Results

4.1. Decline in forest carbon uptake despite greening

The forests in India experience a rise in FPAR (2.3 %), SIF (2.2 %) (**Fig. S5**), and LAI (3.1 %) (Fig. 1a) in recent decade (2010–2019) from the previous decade (2000–2009). In terms of spatial heterogeneity, large increase (2.5–7.5 %) in FPAR, SIF and LAI is observed in majority of forests in CI and some areas of WH. Marginal (< 2.5 %) increase in FPAR, SIF and LAI is found in some forests of WH, EH, NE and WGP. LAI exhibits an increase in all six bioclimatic regions, with its highest in WH (4 %) and WGP (2.9 %). Similarly, FPAR and SIF also show an increase in most regions; suggesting the greening of Indian forests. However, the forests in India experience a decline (−1.4 %) in carbon uptake (NPP) during recent decade from the previous (Fig. 1b). Substantial increase (2.5–7.5 %) in NPP is observed in some forest regions of WH, CI and NE, but marginal (< 2.5 %) increase in some areas of WH, NE and CI. This increase is overridden by large decline (−5 to −20 %) in NPP observed for most forests of EH, WGP and some in CI and IGP. Small (< −5 %) decline in NPP is found in some areas of NE, CI and WGP. In terms of regional heterogeneity, except for WH (0.3 %), all other regions exhibit decrease in NPP, and is prominent in EH (−1.8 %), WGP (−1.5 %) and IGP (−1.4 %). This decline in carbon uptake with hotspots in the pristine forests of EH and WGP is also in the regions of high SM stress (−20 to −5 %), intense warming (0.2–0.6 °C), and enhanced land (CWD) and atmospheric aridity (VPD), about 10–20 % (Fig. 1c, d, e, f)

In terms of the temporal variability (**Fig. S6**) there is a homogeneity among photosynthesis (FPAR), greenness (LAI), and carbon uptake (NPP) in the previous decade (2000–2009), but not in recent decade (2010–2019). While, FPAR, and LAI exhibit substantial recovery post-2012, NPP fails to do so. To find the reason for this, we investigate the temporal variability in NPP with its drivers (**Figs. S6, S7**) such as moisture availability (P and SM), temperature (T), ET, aridity (CWD and VPD). The year 2012 exhibits a marked decline in moisture availability, higher warming and large VPD that drives sharp reduction in NPP. The forest NPP recovered up to a certain extent in 2013, but then again declined in 2014 and continued to 2016 due to very high VPD in 2014. Since 2015, enhanced warming and ET deplete SM and thus, drive the reduction in forest carbon uptake. It suggests that enhanced greenness has not translated into carbon stocks by the forests in India, and this mismatch is stronger in the pristine forests of EH and WGP.

4.2. Forest health and drivers

To explore the reason for the inability of forests to translate greening into carbon uptake, we examined the forest health and functioning metrics in terms of their photosynthetic ability (EPE, Fig. 2a), carbon sequestration (CUE, **Fig. S8**) and water use (WUE, **Fig. S8**). We find that the forests dominated by EBF in EH, NE and WGP have high (1250–2000) EPE. Conversely, low (< 750) EPE is found in the forests dominated by MF in the lower WH and CI. Most areas in CI and some areas in eastern peninsula dominated by DBF exhibit moderate (750–1250) EPE. Likewise, high (0.7–0.9) CUE is observed for forests in most regions of EH, some areas in WH, EH, NE and WGP dominated by MF and EBF. However, low (< 0.45) CUE is found in forests of lower WH and CI dominated by DBF. Very high (2–3) WUE is observed in forests of WH and EH dominated by MF. Forests in NE and WGP also exhibit large (1.5–2) WUE dominated by EBF, but majority of forests in CI and lower WH show low (< 0.75) WUE and are dominated by DBF.

We then investigate the relation of EPE with its drivers (**Fig. S9**) and find that SM (0.64) and T (−0.55) have strong positive and negative relations, respectively. CWD (0.41) and P (0.31) have the positive control, contrary to negative influence of VPD (−0.2) and ET (−0.14). We further explore the causal relationship of EPE with its drivers based on Granger Causality test at 0–4 months temporal lag (Fig. 2b). The results reveal that EPE has causal association with SM, T, ET, CWD and VPD. Interestingly, P has no direct causal relation with EPE, but influences EPE through other drivers such as SM and T. SM and T emerge as major drivers as they have causal link with other drivers. Furthermore, to quantify the control of various drivers, we estimate the relative importance based on RF (Fig. 2c). We find, the most dominant driver of EPE is SM (26.6 %), followed by VCF (19.4 %) and T (13.1 %). Amongst others, P (8.7 %), FPAR (8.7 %), VPD (8.6 %), VCF (8.4 %) and CWD (6 %) are very important to EPE variability. We also employ MLR to estimate the influence of drivers to EPE variability and find similar results to that of RF (**Table S4**). Likewise, SM is the key to the variability in both CUE (31.3 %) and WUE (32 %). Temperature also has a notable control on forest CUE (17.8 %) and WUE (16.8 %). FPAR and VCF are more important to the variability in CUE (14 %, 9.2 %) than WUE (10.7 %, 7.5 %). In contrast, VPD and P have a stronger control on WUE (12.6 %, 7.8 %) than CUE (11.2 %, 4.6 %), whereas CWD has a stronger control on CUE (5.3 %) than WUE (5.1 %) (**Fig. S8**).

4.3. Declining forest health

To understand the changes in health of forest ecosystems, we estimate the change (Fig. 3a, b, c), in EPE, CUE and WUE in recent decade (2010–2019) from the previous decade (2000–2009). The forests in India experience a notable decline in all three metrics of ecosystem health with the largest reduction in EPE (−5 %), followed by CUE (−4.5 %) and WUE (−3 %). In terms of spatial heterogeneity, a substantial decline (−5 to −20 %) in EPE is observed in most of EH, CI, WGP, IGP and some areas in NE. A small (< −5 %) decline in EPE is found in some areas of WH, NE and CI. Some areas in WH exhibit a large increase (2.5–7.5 %) in EPE and some areas in NE and CI show marginal (< 2.5 %) increase in EPE. Likewise, a substantial decline (−5 to −20 %) in CUE is observed in some areas of WH, EH, NE, CI and WGP. A small (< −5 %) decline in CUE is also found in some areas of WH, NE and CI. Some areas in WH exhibit a high increase (2.5–7.5 %) in CUE and some areas in CI find a marginal (< 2.5 %) increase in CUE. A substantial reduction (−5 to −20 %) in WUE is observed in most of WH, CI and some areas in NE. A small (< −5 %) decline in WUE is also found in some areas of EH, NE, CI and WGP. Some areas in EH, NE, IGP and eastern peninsula show an increase in WUE. In terms of temporal variability (Fig. 3d), there is an evident decline in all three (EPE, CUE and WUE) forest health metrics in recent decade (2010–2019). As found in NPP (**Fig. S6**), it never recovered after the big drop in 2012, with recurring reductions in 2014–2016 and 2019.

The decline in the health of Indian forests is due to reduced moisture availability [P (−1.1 %), SM (−2.2 %)], increased aridity [CWD (8.2 %) and VPD (0.4 %)], surface warming (0.125 % or 0.36 °C) and frequent

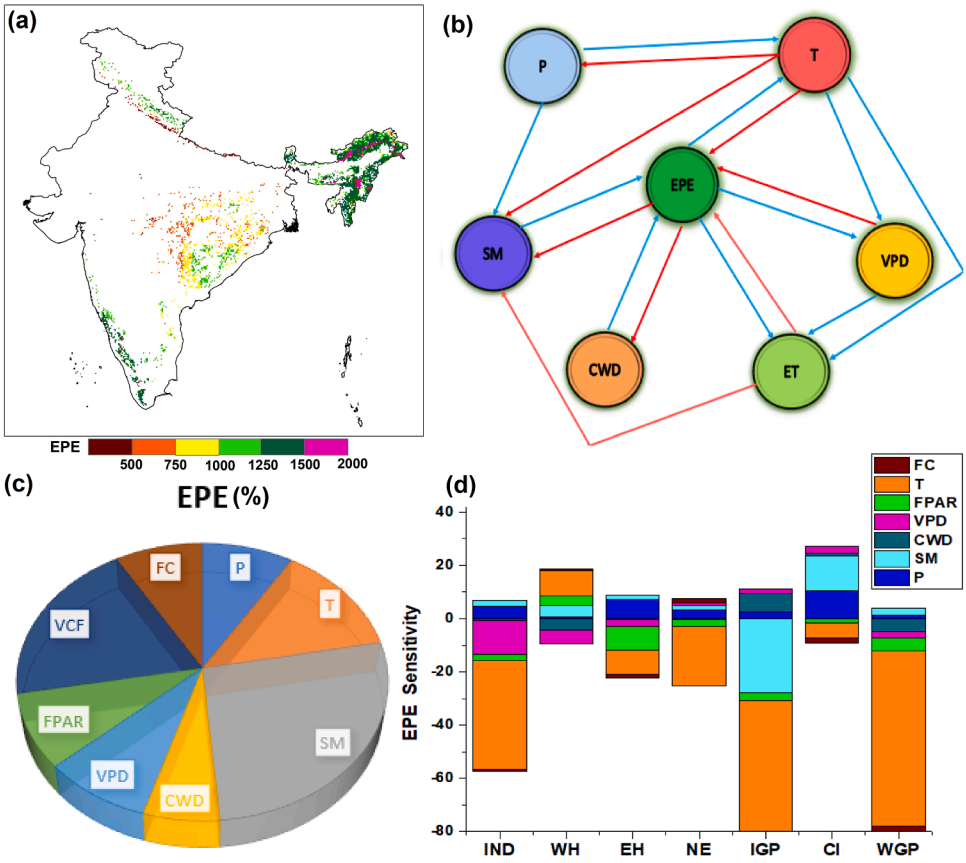

Fig. 2. (a) Ecosystem Photosynthetic Efficiency (EPE), (b) Granger Causality results for relation of EPE (blue line: positive impact, red line: negative impact) with drivers at 0–4 months temporal lag. (c) Random Forest based relative contribution (%) of drivers to EPE variability, (d) Sensitivity of EPE to its drivers- Precipitation (P), Soil Moisture (SM), Temperature (T), Climatic Water Deficit (CWD), Vapour Pressure Deficit (VPD), Fraction of Photosynthetically Active Radiation (FPAR), Vegetation Continuous Fields (VCF) and Fire Counts (FC) for Indian forests during the period 2000–2019.

wildfires (8.7 %) in recent decade (2010–2019) from the previous decade (2000–2009) (Fig. 3e). In terms of regional heterogeneity, all regions except WH [(EPE (+7.2 %) and CUE (+12.3 %)], have reduced EPE and CUE. The regions such as EH (−9 %), WGP (−8 %) and IGP (−7.8 %) show a very large, and CI (−5.4 %) and NE (−3.3 %) exhibit a marked decline in EPE. Likewise, the largest reduction in CUE is observed in WGP (−6 %) and EH (−4.4 %). This is due to enhanced moisture stress and increased wildfires in the warmer and drier climate. NRA in the changes also reveal similar results, with the largest EPE (−4 %) decline among the bioclimatic regions in EH due to a substantial increase in aridity [CWD (18 %), VPD (3.3 %)], warming (T, 0.9 %) and drying [SM (−2.7 %), P (−0.16 %)]. WGP also exhibits a marked decline in EPE (−3 % NRA) due to predominant P drying (−5.8 %), SM stress (−0.63 %) and enhanced atmospheric aridity (VPD, 3 %) (**Fig. S10**).

4.4. Forest health: Sensitivity and Resilience

To understand impact of these changes and the ability of the forests to maintain their health, we estimate the sensitivity of EPE to its drivers (Fig. 2d). EPE exhibits very high negative sensitivity to T (−41) and VPD (−13), but low sensitivity to FPAR (−2.2), CWD (−0.63) and wildfires (−0.59). Conversely, EPE has positive sensitivity to moisture availability [(P, 4.5) and (SM, 2.3)]. CUE and WUE also exhibit similar sensitivities to their drivers but of a smaller magnitude (**Fig. S11**). On regional scale, both EPE and CUE shows very high negative sensitivity to T in WGP (−66, −48.3), IGP (−60.5, −28.5) and NE (−22.4, −19.4). Interestingly, CUE (16.5) and EPE (9.6) exhibit high positive sensitivity to T, but WUE shows high negative (−13.7) sensitivity to T in WH. Except in WGP, WUE has positive sensitivity to both VPD (7.7) and CWD (5.9), which is highest in CI (Figs. 2d **and S11**).

Furthermore, the forest resilience to the moisture deficit (P, SM), warming (T), aridity (CWD, VPD) and wildfire (FC) are shown in Fig. 4. We find forests in most of lower WH, some areas in EH, NE and most of CI are non-resilient to P deficit (Fig. 4a). Likewise, forest ecosystems in most areas of WH, NE and CI are non-resilient to SM drying (Fig. 4b). Majority of forest ecosystems in WH, CI and some areas in EH and WGP are non-resilient to CWD (Fig. 4c). Likewise, there are regions such as WH, eastern CI, IGP and some areas in EH and NE, where forests are non-resilient to VPD stress (Fig. 4d). Forests in most of EH, WGP, some areas in NE and WH are non-resilient to warming (Fig. 4e). The forests non-resilient to wildfires are largely in EH, WG and some areas in WH and CI (Fig. 4f). The Indian forests are vulnerable to these extremes in various regions.

4.5. Forest health: Human influence and Integrity

The forests are not just impacted by climate change but also by human activities. To find the extend of human intervention on forests, we consider two indices, HMI and FLII, (Fig. 5). The forests in most of lower WH, IGP and WGP exhibit higher (0.35–0.6), and EH and lower NE exhibit lower human modifications (HMI < 0.25) (Fig. 5a). In India, most (56.34 % area) forests show moderate (8–9.6) and some (27.43 % area) in NE and CI exhibit low (0–6) integrity (FLII) (Fig. 5b). Conversely, some (16.22 % area) forests in EH and CI exhibit high (9.6–10) integrity. On regional scale, forests in EH has the smallest modifications (HMI=0.16) and thus exhibits largest integrity (FLII=8.2), but forests in CI exhibit high modifications (HMI=0.4) and low integrity (FLII=5.5). Likewise, forests in IGP exhibits lowest

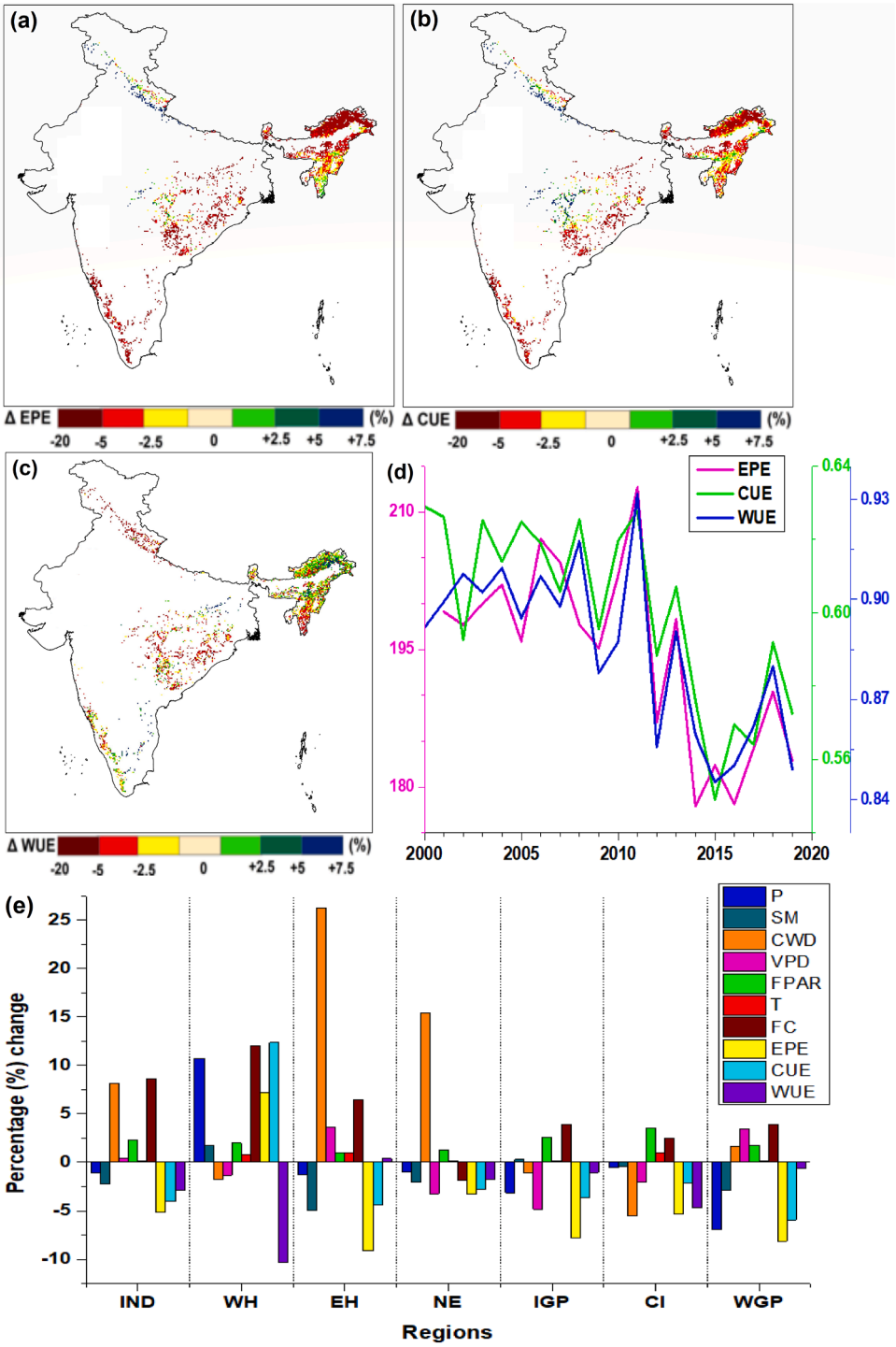

Fig. 3. Change (%) in (a) Ecosystem Photosynthetic Efficiency (EPE), (b) Carbon Use Efficiency (CUE) and (c) Water Use Efficiency (WUE) in recent decade (2010–2019) from the previous decade (2000–2009), (d) Temporal evolution in EPE, CUE and WUE during the period 2000–2019, (e) Percentage change in EPE, CUE, WUE and their divers- Precipitation (P), Soil Moisture (SM), Temperature (T), Climatic Water Deficit (CWD), Vapour Pressure Deficit (VPD), Fraction of Photosynthetically Active Radiation (FPAR), Vegetation Continuous Fields (VCF) and Fire Counts (FC) in recent decade (2010–2019) from the previous decade (2000–2009) for various regions in India (IND), and Western Himalaya (WH), Eastern Himalaya (EH), North East (NE), Indo-Gangetic Plain (IGP) Central India (CI) and Western Ghats and Peninsula (WGP).

integrity (FLII= 3.9) and large modifications (HMI=0.38). This hints at potential forest fragmentation by humans with hotspots in IGP and CI. Interestingly, despite high modifications (HMI= 0.37), forests in WH exhibits large (FLII= 7.7) integrity, which is opposite in the forests of NE (FLII= 6.2 and HMI= 0.28) (Fig. 5c, d). Furthermore, we also find a substantial increase in human population in the Indian forests during the period 2000–2019. The forests in HR, NE, IGP, CI and WGP exhibit a huge population explosion (40–60 %) (**Fig. S12**). These regions are also the hotspots of human modification and forest fragmentation (Figs. 5 **and S12**).

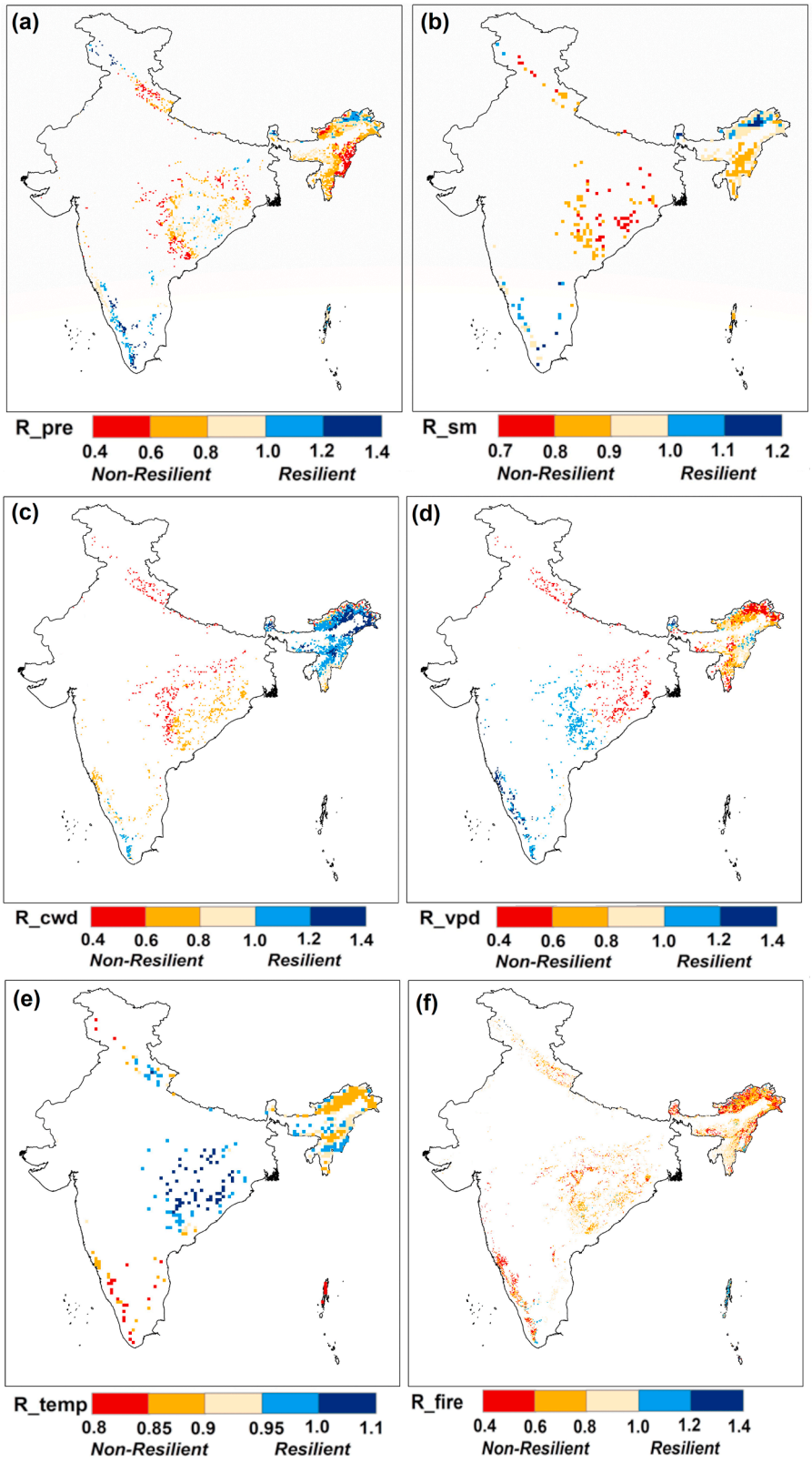

Fig. 4. Forest Resilience (R) to (a) Precipitation (R_pre) drying, (b) Soil Moisture stress (R_sm) , (c) land evaporative aridity (R_cwd), (d) atmospheric aridity (R_vpd), (e) warming (R_temp) and (f) wildfires (R_fire) during the period 2000–2019.

4.6. Forest health: Growth Rate, age and the future

The Growth Rate (GR) analysis during the period 2000–2019 reveals greening of Indian forests with positive CGR in NDVI (2.7 %), VCF (2 %), LAI (7.4 %) and SIF (6.1 %). However, this greening is not being efficiently translated in carbon uptake as exhibited by the negative CGR in NPP (−3.54 %) and a reduction in translation of greenness to carbon uptake (EPE, −2.67 %), which substantially deteriorates forest health

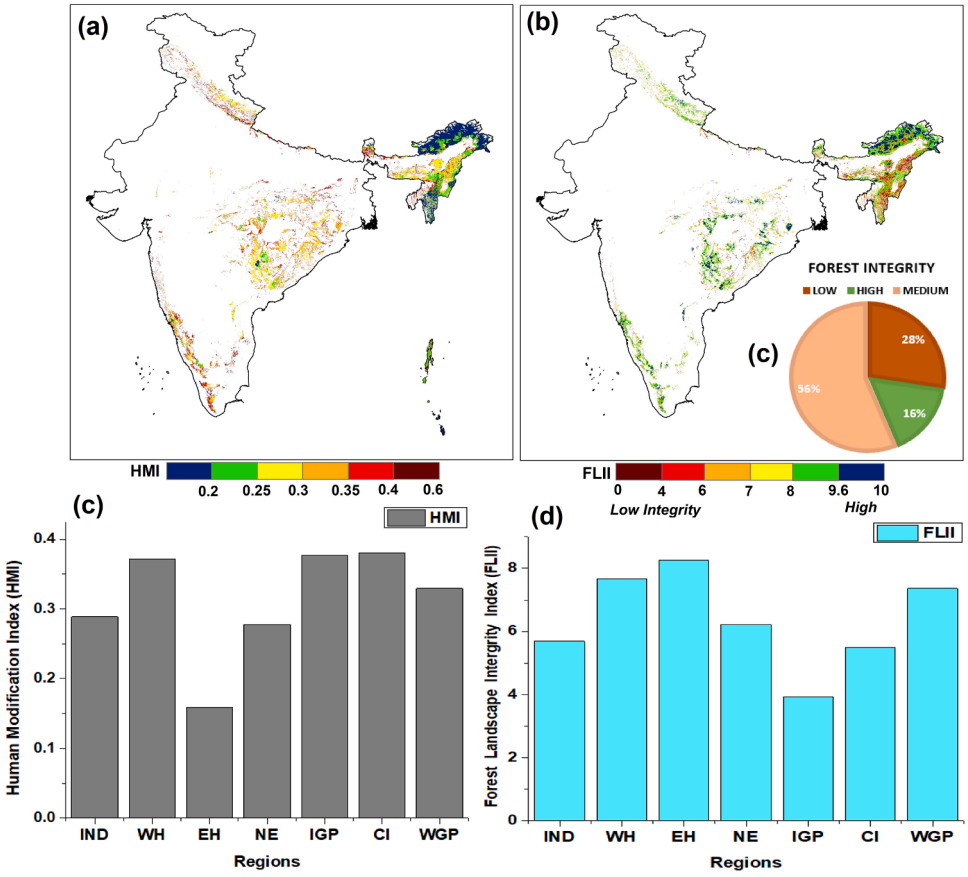

Fig. 5. (a) Human Modification Index (HMI), (b) Forest Landscape Integrity Index (FLII), and (c) area (%) in various FLII categories (low, medium and high forest integrity), and (d) HMI and (e) FLII for India (IND), and Western Himalaya (WH), Eastern Himalaya (EH), North East (NE), Indo-Gangetic Plain (IGP) Central India (CI) and Western Ghats and Peninsula (WGP).

[negative CGR in CUE (−10.75 %) and WUE (−5.8 %)] in India. This is driven by positive CGR in aridity [VPD (9.9 %), CWD (5.1 %)], T (2.26 %) and wildfires (12.34 %), and negative CGR in moisture availability [SM (−2.47 %), P (−2.1 %)] as depicted in Fig. 6b Apart from the climate drivers, there are human interventions that negatively impact the forest structure and functioning. To closely examine this, we analyse the forest age (Fig. 6a) and forest loss (**Fig. S13)** in India. We find that most forests in India are middle aged (30–60 years), and are mainly found in the foothills of WH, most of EH, NE, CI and northern WGP. The forests in India are young (< 30 years) in the regions of southern WGP, eastern CI, and IGP. In contrast, old age (60–150 years) forests are predominantly found in the Himalaya (northern WH and EH). We find forest loss as the conversion of forests to non-forest lands during the period from 2001 to 2019, primarily in CI (23 % NRA) and WGP (10 % NRA). This explains the decline in EPE in Indian forests with its peak in the pristine forests of EH and WGP. Thus, we find declining forest carbon sink potential in India despite greening due to both changing climate and anthropogenic intrusions. Henceforth, the future fate of forest carbon stocks in India in this scenario needs to be explored.

In order to investigate the future of forest ecosystems in India, we employ CMIP6 future projections and LPJ-GUESS process-based ecosystem model results. From the CMIP6 (**Fig. S14**), we find increase in all parameters except CUE (−0.6 %) in the end of the century (P3, 2090–2100) from the base period (P1, 2015–2019). Furthermore, we split the time span into two focal periods, i.e., F1 is mid-century (P2, 2040–2050) from the base period (P1, 2015–2019); and F2 is end-century (P3) from P2. We find large increase in all parameters in F1 wherein, greenness (LAI, 6 %), carbon uptake (NPP, 23 %) and conversion (EPE, 8.6 %) are prominent. In F2, there is smaller increase in NPP (10.7 %) despite larger increase in LAI (14 %) due to reduction in EPE (−1.35 %). Among the two focal periods (Fig. 6c), there is predominant decline in carbon uptake (−12.3 %), despite greening (8.2 %) due to decline in EPE (−10 %). The decrease in EPE also degrades forest health (CUE, −3.8 %) and (WUE, −5 %).

We run the LPJ-GUESS DGVM, for examining the effect of climate change on forests. Therefore, the model is run for both no-climate change (**Fig. S15**), and climate change scenarios (Fig. 6d). In no-climate change scenario, there are very small and inconsistent changes among the parameters in the period (P3-P1). In contrast, we find increase in all parameters (LAI, NPP, biomass and leaf C:N) in the period (P3-P1) in the climate change scenario. As done before, we split the time span into two focal periods (F1 and F2) for detailed investigation. Interestingly, there is a substantial increase in each parameter [(LAI, 10.6 %), (NPP, 14.2 %), (biomass, 20 %) and (leaf C:N, 10.4 %)] in F1. However, there is decline in each parameter [(LAI, −3.7 %), (NPP, −0.9 %), (biomass, 20 %) and (leaf C:N, 10.4 %)] in F2 (**Fig. S14**). Between the two focal periods (F1 and F2), there is a substantial decline in all parameters such as greenness (−14.3 %), carbon uptake (−15 %), biomass (−23.2 %) and leaf C:N (−13.8 %) in the climate change context. Contrarily, in no-climate change scenario, there are very small changes in all parameters, where carbon uptake has smaller decline than in the climate change run (Fig. 6d). Therefore, both LPJ DGVM results and CMIP6 future projections reveal that the strength of Indian forest carbon sinks is declining in the future.

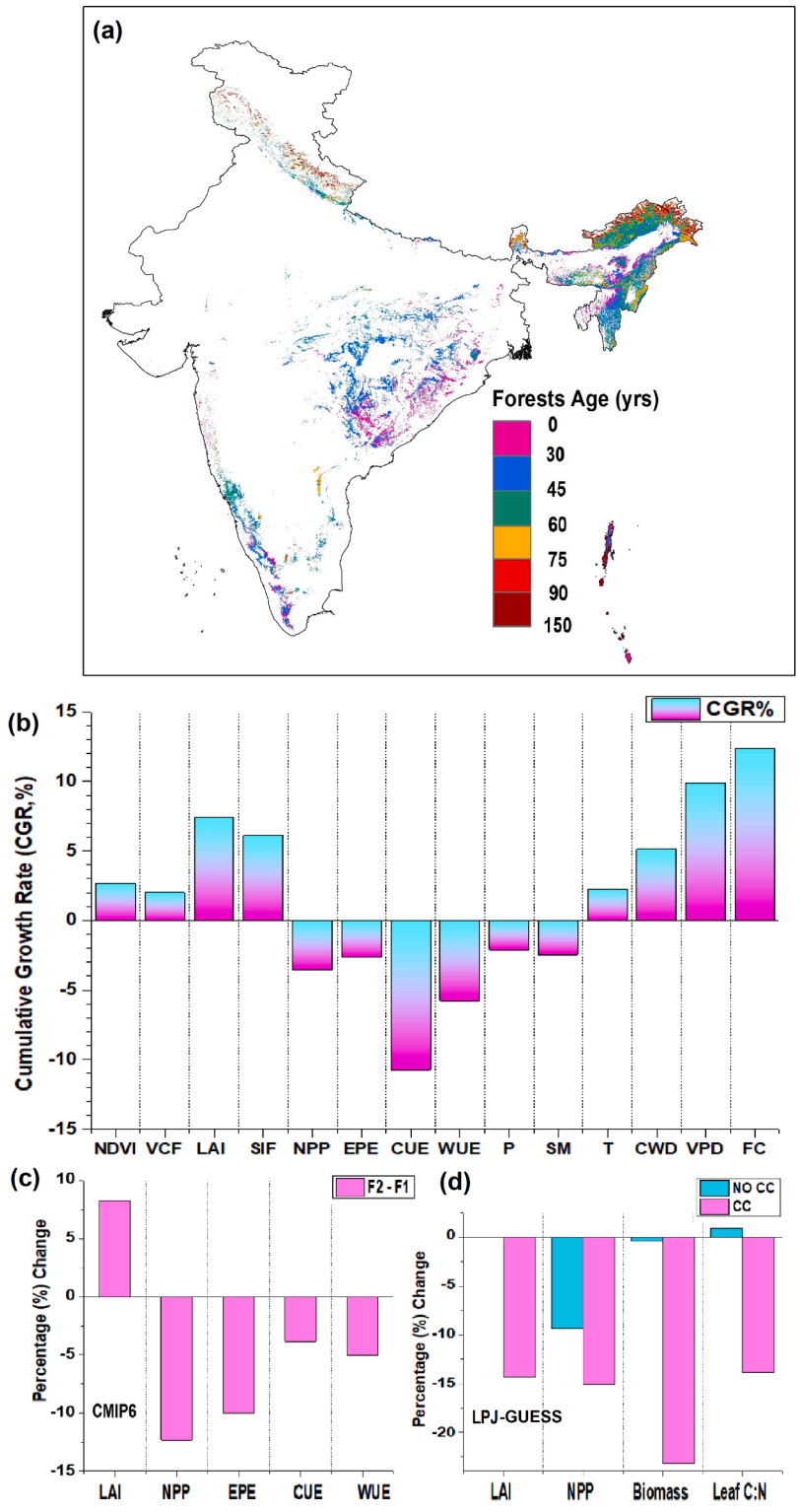

Fig. 6. (a) Forest Age (in years) in the year 2010, (b) Cumulative Growth Rate in vegetation greenness and photosynthesis [(Normalised Difference Vegetation Index: NDVI), (Vegetation Continuous Fields: VCF), (Leaf Area Index: LAI) and (Solar-Induced Fluorescence: SIF)], functioning and health [(Net Primary Productivity: NPP), (Ecosystem Photosynthetic Efficiency: EPE), (Carbon Use Efficiency: CUE) and (Water Use Efficiency: WUE)] and their climate drivers [(Precipitation: P), (Soil Moisture: SM), (Temperature: T), (Climatic Water Deficit: CWD), (Vapour Pressure Deficit: VPD) and (Fire Counts: FC)] for the period 2000–2019. Percentage (%) change in (c) greenness (LAI), carbon uptake (NPP), EPE, CUE and WUE from the CMIP6 model results, (d) LAI, NPP, and biomass and leaf carbon:nitrogen ratio (Leaf C:N) from the LPJ-GUESS model simulations between mid-century (P2, 2040–2050) to end-century (P3, 2090–2100) i.e. focal period 2 (F2) from mid-century to base period (P1, 2015–2019) i.e. focal period 1 (F1) in no climate change (NO CC) and climate change (CC) runs.

5. Discussion

5.1. Indian forest carbon stocks: significance

The global atmospheric CO_2 and average temperature have risen substantially since the industrial revolution (IPCC, 2021; Friedlingstein et al., 2024). India is no different, as the CO_2 concentration in India has been increasing rapidly (2.1 ppm/yr) over the past few decades (2002–2020) similar to those in the global tropical and mid-latitudes (Kuttippurath et al., 2022). This increase in atmospheric CO_2 in India can be attributed to anthropogenic emissions, agricultural and soil emissions, and inadequate land management practices (Singh et al., 2022). Since the Kyoto Protocol (1997), there has been a notable emphasis on forests for the purpose of carbon sequestration and mitigation of global warming (IPCC, 2021; Friedlingstein et al., 2024). Under the Bonn Challenge (2011) and Land Degradation Neutrality (LDN) goals (2015), India is committed to restore 26 million hectares of degraded land by 2030. Also, maintaining forest carbon sinks and their resilience to climate change and human interventions is key to attain India's target of net zero emissions by 2070 (ISFR, 2021, 2023). South Asia continues to be a carbon sink with India being the largest contributor, both as a source and a sink (Jain et al., 2025). However, despite lying in the tropical region of higher carbon uptake, the fate of forest carbon stocks in the current and future climate change sceanrios is largely underexplored for India, and therefore, this is the first comprehensive study in this regard.

5.2. Mismatch between forest greening and carbon uptake

We find that there is greening of Indian forests in terms of increase in greenness and photosynthesis (FPAR, LAI and SIF) consistent with our previous finding Kuttippurath and Kashyap (2023). The Indian forests are greening in recent decades due to several land development initiatives such as the National Afforestation Programme (NAP) and Green India Mission (GIM) implemented by the Ministry of Environment, Forest and Climate Change (MoEFCC) focused on plantations and afforestation drives (ISFR, 2021, 2023; Pasha and Dadhwal, 2024). However, there is a decline in forest carbon uptake (NPP) of Indian forests despite greening. The limited cropland canopy carbon uptake and low GPP in forests resulted in weak carbon uptake in India during recent decades (Sarmah et al., 2021). Interestingly, there is a mismatch between the greening and carbon sink potential in India (Kashyap et al., 2023a). A recent study also finds this inability of translation of greenness to productivity in major forests of India due to warming. It states that, above a threshold temperature, GPP decreases and wherein respiration becomes stable and reduce NPP (Das et al., 2023). Apart from warming, there must be other ecosystem processes and certain biophysical mechanisms that inhibits the carbon uptake despite increased greenness in Indian forests.

5.3. Declining forest carbon stocks: Climate change and anthropogenic intrusions

To further investigate this, we estimate EPE (translation of greenness to carbon uptake) for the first time for Indian forests and find that EPE has declined substantially in recent decade (2010–2019) from the previous (2000–2009). Interestingly, the largest decline in EPE is for the pristine forests of EH, WGP and IGP which also have the highest EPE. This explains the hindered ability of Indian forests to translate greenness to carbon uptake during recent decade. In addition, declining EPE adversely impacts the forest health with reduction in CUE and WUE, predominant in the pristine forests of WGP and EH. The decline in forest ecosystem health can be attributed to the reduced moisture availability, increased aridity, enhanced warming and frequent wildfires in recent decade (2010–2019). Correlation analysis and Granger Causality test reveal SM and T as the key drivers of EPE. We also find SM (26.7 %) to have a stronger control on EPE than T (13.2 %) for the Indian forests, as per RF analysis. The forest health metrics (EPE, CUE and WUE) exhibit higher negative sensitivity to T and VPD, low negative sensitivity to FPAR, CWD and wildfires, and positive sensitivity to P and SM. Interestingly, the sensitivity of EPE to its drivers surpasses that of CUE and WUE. Rising moisture stress and intense warming adversely affect the health and functioning of terrestrial ecosystems in India (Das et al., 2023; Kashyap and Kuttippurath, 2024a, b). Accelerated warming and wildfires have depleted the forests and negatively impacted the carbon sinks in recent decades (Haughan et al., 2022) in India, particularly with wildfire hotspots in WH, EH and CI (Sannigrahi et al., 2020), and more frequent fires are expected in the warmer and drier future climate (Bar et al., 2024). Frequent landslides in the Himalayan region can also deplete the carbon sinks (Kashyap et al., 2021). The forests are non-resilient to moisture stress, aridity, warming and wildfires, with hotspots in the pristine forests of EH and WGP.

Furthermore, there are noticeable human modifications leading to forest fragmentation (loss of integrity) with hotspots in IGP and CI. Nevertheless, some forests (16.2 % area) in India have high forest integrity, though much lower than the global average of 40 % (Grantham et al., 2020). We find young forests (< 30 years) in the regions of predominant forest loss in CI and WGP. Also, there has been a substantial decline in the large and mature trees in India, which are replaced with small plantations in recent decade (Brandt et al., 2024). The large-scale anthropogenic intrusions such as deforestation owing to the traditional agricultural practices (slash and burn, and shifting jhum cultivation) (Sparsha and Parida, 2024), plantation expansion, encroachment, mining activities and other developmental activities have led to forest degradation in the ecologically sensitive regions of EH, NE, CI and WG (Reddy et al., 2018; ISFR, 2023). Since 2012, the Western Ghats are designated as the UNESCO World Heritage site for being one the planet's most biologically diverse hotspots, but the region experienced 7 % deforestation during 2001–2020 (Pasha and Dadhwal, 2024) with a notable decline in moderately dense and open forests (ISFR, 2023). Concurrently, there is an increase in plantation trees outside the forests and savanna in India (ISFR, 2023; Pasha and Dadhwal, 2024).

5.4. Future of forest carbon stocks: Implications and Recommendations

From the CMIP6 model results we find a marked decline in carbon uptake (NPP, −12.3 %), despite greening (LAI, +8.2 %) in Indian forests between mid-century (2040–2050) to end-century (2090–2100) from mid-century to base period (2015–2019). This is due to the reduction in translation of greenness to carbon uptake (EPE, −10 %) that leads to reduced carbon (CUE, −3.8 %) and water (WUE, −5 %) sequestration of the forests while maintaining carbon uptake. Likewise, the results from a process-based DGVM in LPJ-GUESS exhibit a substantial decline in carbon uptake (−15 %), biomass (−23.2 %) and leaf C:N (−13.8 %) during the same period. This indicates the weakening of the forest carbon sinks and declining forest health is likely to be stronger in the future due to climate change and anthropogenic interventions in India. A recent study also finds a declining NPP growth rate from 2021 to 2099 for the Indian terrestrial ecosystems and attributes it to weakening CO_2 fertilization effect (CFE) (Bejagam et al., 2024). This is in coherence with the limited and reduced CFE due to rising nutrient and water limitations in the current and future climate (Wang et al., 2020; Winkler et al., 2021). Additionally, the radiative effects of increasing CO_2 as a potent greenhouse gas (GHG) would drive unprecedented warming and counterbalance the fertilization effects (Peñuelas et al., 2017; Shi et al., 2021).

The degradation of forest resources is a concern for the economy of a country and would eventually impact its timber production, market price, planting intensity and lives of forest dwellers in India. Additionally, it threatens the indigenous biodiversity and pushes them towards extinction. Also, degradation of forests in ecologically fragile regions like EH, NE and WG can lead to more frequent climatic extremes in the

future. Furthermore, forests possess a restricted capacity for carbon storage, which is insufficient to effectively address the rise in atmospheric CO_2. Furthermore, a substantial part of carbon is stored in non-living systems on land (Bar-On et al., 2025). Henceforth, it is imperative to avoid misconstruing forest-based climate mitigation as a solution to current anthropogenic carbon emissions levels (Canadell, 2025). The ageing tropical forests might get saturated as carbon sinks in the future (Yang et al., 2023; Wigneron et al., 2024). Conversely, endeavours to counteract deforestation and enhance carbon reserves should be promoted as valuable and efficient approaches to counterbalance the residual emissions to achieve the target of net-zero emissions by 2070 in India. Henceforth, there is a need for better management of land-based carbon emissions and advanced technologies for carbon capture and sequestration. Additionally, the afforestation programmes should be more scientific and focused on maintaining the existing forest areas, including the historical natural forests. Furthermore, studies on forest carbon dynamics should be encouraged for the Indian region integrating remote sensing observations and ground-based measurements.

5.5. Limitations

The study employs remote sensing measurements, which have uncertainties such as saturation and insufficient sensitivity in the dense canopy regions. There is a severe lack of ground-based measurements for the estimation of carbon and water fluxes for the Indian region. Therefore, satellite data with higher resolution and more surface measurements would improve our understanding of Indian forest carbon dynamics. The CMIP6 model results are subject to limitations like insensitive to efficiently account for dryness stress such as SM, VPD and compound SM-VPD stresses on vegetation (Liu et al., 2023; Song et al., 2024) and they overestimate the future greening (Wu et al., 2022). The CMIP6 models are also subject to limited ability to simulate the extreme events such as mega-droughts, heatwaves, intense wildfires, human mismanagements, destructive logging, insect and disease outbreaks, and forest diebacks (Zhao et al., 2020; Wu et al., 2022). These models also face challenges in simulating the influence of climate oscillations like El Niño Southern Oscillation (ENSO), which substantially impact photosynthesis (Kashyap and Kuttippurath, 2025) and carbon stocks (Wigneron et al., 2020) in the topical regions of higher carbon uptake. In addition, the CMIP6 model results are constrained by coarse resolution and thus, it affects the accuracy of simulations on regional scales. Process-based ecosystems models like LPJ-GUESS are originally calibrated for global climate regions and henceforth, they might not very efficiently capture regional variability, particularly for a very complex vegetation-climate-human interaction landscape like India. The statistical and ML techniques employed in this study are subject to some limitations as they are largely data-driven, which demand more measurements to produce robust results. The natural variability in forests such as succession, defoliation, regeneration, changes in soil composition, altered nutrient cycle and plant species distribution are very complex and are not accounted for in these analyses, which could also add some uncertainty in the results. The study period is based on the availability of data post-MODIS era (since 2000), and the years post-2019 such as 2020 and 2021 are not considered as they exhibit high anomalies due to the impact of COVID-19 lockdown (Kashyap et al., 2023b).

6. Conclusions

Forests are major carbon sinks and are considered as nature-based solutions (NbS) to combat climate change. We, for the first time, thoroughly investigate the structure (greenness), functioning (carbon uptake), translation of greenness to carbon uptake (EPE), health (CUE and WUE), climate and anthropogenic drivers of change, and spatio-temporal evolution in the current and future climate scenarios for the Indian forests. We employ a suite of statistical and ML techniques on a range of remote sensing, reanalysis, the CMIP6 model projections and the LPJ-GUESS process based vegetation model data. We find limited ability of Indian forest ecosystems to translate the greenness to carbon uptake in recent decades (2000–2019). Previous studies have reported mismatch between greening and carbon uptake and hindered translation of greening to enhanced carbon uptake in India and attributed it the impacts of climate change driven warming. However, we compute a novel metric-the Ecosystem Photosynthetic Efficiency (EPE) to explicitly explain the inhibited translation of the structure and functioning of Indian forests. We find substantial decline in EPE during recent decade (2010–2019) from the previous decade (2000–2009), predominant in the hotspots of highest EPE such as EH, WGP and IGP. The decrease in EPE also drives reduction in CUE and WUE of the forests. Our analysis finds that the decline in forest health and functioning (EPE, CUE and WUE) is due to enhanced moisture stress, rising aridity and increased wildfires, in addition to rapid surface warming. Forest health and functioning exhibit high negative sensitivity to T and VPD, low negative sensitivity to FPAR, CWD and wildfires, and high positive sensitivity to moisture availability (P and SM). Forests ecosystems are non-resilient to drying, aridity, warming and frequent wildfires in most regions, with the pristine forests in EH and WGP being the hotspots. Additionally, human-driven modifications have led to loss of forest integrity, with IGP and CI as its hotspots. Both CMIP6 projections and process based DGVM in LPJ-GUESS results reveal that there is a notable decrease in the carbon uptake, despite greening due to the decline in EPE, which reduces CUE and WUE between mid-century (2040–2050) to end-century (2090–2100) from mid-century to the historical period (2015–2019). This suggests that the forest carbon sinks in India are weakening under the current and future climate change scenarios.

The study has some limitations due to the uncertainties in the remote sensing, reanalyses, and the model data. The lack of ground-based data in India and limitations of the statistical and ML methods adds to these uncertainties. Therefore, these findings call for establishment of an efficient network of ground-based stations in the Indian region, as its forests are weakening as carbon sinks, home to rich biodiversity and support food and livelihood of billions in the country. Future studies should integrate remote sensing data with in-situ measurements with a focus on the ecologically fragile and climate extreme prone pristine forests of Himalaya and Western Ghats. In the future, accelerated deforestation and forest degradation due to changing climate, rising extremes, agricultural expansion, plantation growth and rapid developmental activities can lead to savannisation of Indian forests. Henceforth, there is an urgent need for preservation of indigenous forests, sustainable and judicious use of forest resources, improved forest management practices, scientific afforestation programmes, substantial reduction in carbon emissions and better carbon capture technologies to achieve sustainability and the target of net zero emissions in India by the year 2070.

CRediT authorship contribution statement

Rahul Kashyap: Writing – review & editing, Writing – original draft, Visualization, Software, Methodology, Formal analysis, Data curation, Conceptualization, Investigation. **Jayanarayanan Kuttippurath:** Writing – review & editing, Visualization, Supervision, Resources, Methodology, Conceptualization.

Declaration of competing interest

The authors declare that they have no known competing financial interests or personal relationships that could have appeared to influence the work reported in this paper.

Acknowledgments

We thank the Director, Indian Institute of Technology Kharagpur (IIT

Kgp), Chairman of CORAL IIT Kgp and the Ministry of Education (MoE) for facilitating the study. RK acknowledges the support from Prime Minister's Research Fellowship (PMRF), MoE. We thank all the data providing sources like NASA's LPDAAC team for providing the MODIS land cover, NDVI, LAI, GPP, NPP, ET, ASTER DEM and VCF products. We also thank Giovanni's online data system, developed and maintained by the NASA GES DISC, for providing the GPM level-3 precipitation data; GLDAS for providing SM datasets; ERA-5 for air temperature data; TerraClimate for CWD and VPD datasets; SEDAC for HMI data; GFW for canopy cover data; GlobBiomass for AGB data; CMIP6 for providing future projections; WorldPop for population data, MPI-BGC for forest age data. We also sincerely thank the team that developed LPJ-GUESS DVGM. Special thanks to Jingfeng Xiao for SIF, and Hedley Grantham for making FLII datasets as available publicly.

Supplementary materials

Supplementary material associated with this article can be found, in the online version, at doi:10.1016/j.resconrec.2025.108478.

Data availability

All data are publicly available, and listed in Table S1.

References

Bar, S., Acharya, P., Parida, B.R., Sannigrahi, S., Maiti, A., Barik, G., Kumar, N., 2024. Investigation of fire regime dynamics and modeling of burn area over India for the twenty-first century. Environ. Sci. Pollut. Res. 31 (41), 53839–53855. https://doi.org/10.1007/s11356–024–32922–w.

Bar-On, Y.M., Li, X., O'sullivan, M., Wigneron, J.P., Sitch, S., Ciais, P., Fischer, W.W., et al., 2025. Recent gains in global terrestrial carbon stocks are mostly stored in nonliving pools. Science (1979) 387 (6740), 1291–1295. https://doi.org/10.1126/science.adk1637.

Bauman, D., Fortunel, C., Delhaye, G., Malhi, Y., Cernusak, L.A., Bentley, L.P., McMahon, S.M., et al., 2022. Tropical tree mortality has increased with rising atmospheric water stress. Nature 608 (7923), 528–533. https://doi.org/10.1038/s41586–022–04737–7.

Bejagam, V., Sharma, A., Wei, X., 2024. Projected decline in the strength of vegetation carbon sequestration under climate change in India. Sci. Total Environ. 916, 170166. https://doi.org/10.1016/j.scitotenv.2024.170166.

Besnard, S., Koirala, S., Santoro, M., Weber, U., Nelson, J., Gütter, J., Carvalhais, N., et al., 2021. Mapping global forest age from forest inventories, biomass and climate data. Earth Syst. Sci. Data Discuss. 2021, 1–22. https://doi.org/10.5194/essd-13-4881-2021.

Brandt, M., Gominski, D., Reiner, F., Kariryaa, A., Guthula, V.B., Ciais, P., Fensholt, R., et al., 2024. Severe decline in large farmland trees in India over the past decade. Nat. Sustain. 7 (7), 860–868. https://doi.org/10.1038/s41893–024–01356–0.

Breiman, L., 2001. Random forests. Mach. Learn. 45, 5–32. https://doi.org/10.1023/A:1010933404324.

Canadell, J.G., 2025. Looking beyond the trees for carbon storage. Science (1979) 387 (6740), 1252–1253. https://doi.org/10.1126/science.adw3259.

Chen, C., Park, T., Wang, X., Piao, S., Xu, B., Chaturvedi, R.K., Myneni, R.B., et al., 2019. China and India lead in greening of the world through land–use management. Nat. Sustain. 2 (2), 122–129. https://doi.org/10.1038/s41893–019–0220–7.

Crowther, T.W., Glick, H.B., Covey, K.R., Bettigole, C., Maynard, D.S., Thomas, S.M., Bradford, M.A., et al., 2015. Mapping tree density at a global scale. Nature 525 (7568), 201–205. https://doi.org/10.1038/nature14967.

Das, R., Chaturvedi, R.K., Roy, A., Karmakar, S., Ghosh, S., 2023. Warming inhibits increases in vegetation net primary productivity despite greening in India. Sci. Rep. 13 (1), 21309. https://doi.org/10.1038/s41598–023–48614–3.

Farr, T.G., Rosen, P.A., Caro, E., Crippen, R., Duren, R., Hensley, S., Alsdorf, D., et al., 2007. The shuttle radar topography mission. Rev. Geophys. 45 (2). https://doi.org/10.1029/2005RG000183.

Feng, Y., Ciais, P., Wigneron, J.P., Xu, Y., Ziegler, A.D., van Wees, D., Zeng, Z., et al., 2024. Global patterns and drivers of tropical aboveground carbon changes. Nat. Clim. Chang. 14 (10), 1064–1070. https://doi.org/10.1038/s41558–024–02115–x.

Friedlingstein, P., O'sullivan, M., Jones, M.W., Andrew, R.M., Hauck, J., Landschützer, P., Zeng, J., et al., 2024. Global carbon budget 2024. Earth Syst. Sci. Data Discuss. 2024, 1–133. https://doi.org/10.5194/essd–17–965–2025.

Gang, C., Wang, Z., You, Y., Liu, Y., Xu, R., Bian, Z., Zhang, M., et al., 2022. Divergent responses of terrestrial carbon use efficiency to climate variation from 2000 to 2018. Glob. Planet Change 208, 103709. https://doi.org/10.1016/j.gloplacha.2021.103709.

Giglio, L., Schroeder, W., Justice, C.O., 2016. The collection 6 MODIS active fire detection algorithm and fire products. Remote Sens. Environ. 178, 31–41. https://doi.org/10.1016/j.rse.2016.02.054.

Granger, C.W., 1969. Investigating causal relations by econometric models and cross-spectral methods. Econometr. J. Econometr. Soc. 424–438. https://www.jstor.org/stable/1912791.

Grantham, H.S., Duncan, A., Evans, T.D., Jones, K.R., Beyer, H.L., Schuster, R., Watson, J.E.M., et al., 2020. Anthropogenic modification of forests means only 40% of remaining forests have high ecosystem integrity. Nat. Commun. 11 (1), 5978. https://doi.org/10.1038/s41467–020–19493–3.

Harris, N., Gibbs, D., 2021. Forests absorb twice as much carbon as they emit each year. World Resour. Inst. (WRI) Insights. January 21. https://www.wri.org/insights/forests–absorb–twice–much–carbon–they–emit–each–year.

Haughan, A.E., Pettorelli, N., Potts, S.G., Senapathi, D., 2022. The role of climate in past forest loss in an ecologically important region of South Asia. Glob. Chang. Biol. 28 (12), 3883–3901. https://doi.org/10.1111/gcb.16161.

Holling, C.S., 1973. Resilience and stability of ecological systems. Annu. Rev. Ecol. Syst. 4 (1), 1–23. https://doi.org/10.1017/9781009177856.038.

Huang, M., Zhai, P., Piao, S., 2021. Divergent responses of ecosystem water use efficiency to drought timing over Northern Eurasia. Environ. Res. Lett. 16 (4), 045016. https://doi.org/10.1088/1748–9326/abf0d1.

Humphrey, V., Berg, A., Ciais, P., Gentine, P., Jung, M., Reichstein, M., Frankenberg, C., et al., 2021. Soil moisture–atmosphere feedback dominates land carbon uptake variability. Nature 592 (7852), 65–69. https://doi.org/10.1038/s41586–021–03325–5.

IPCC, 2021. Climate change 2021: the physical science basis. Contribution of Working Group I to the 6th Assessment Report of the Intergovernmental Panel on Climate Change. Cambridge Press, Cambridge, UK.

ISFR, 2021. India State of the Forest Report. Forest Survey of India, The Ministry of Environment, Forest and Climate Change (MoEFCC). Govt. of India, Dehradun. https://fsi.nic.in/forest–report–2021.

ISFR, 2023. India State of the Forest Report. Forest Survey of India, The Ministry of Environment, Forest and Climate Change (MoEFCC). Govt. of India, Dehradun. https://fsi.nic.in/uploads/isfr2023/isfr_book_eng–vol–1_2023.pdf.

Jain, A.K., Seshadri, S., Anand, J., Chandra, N., Patra, P.K., Canadell, J.G., Tiwari, Y.K., et al., 2025. South Asia's ecosystems are a net carbon sink, but the region is a major net GHG source to the atmosphere. Glob. Biogeochem. Cycles 39 (4). https://doi.org/10.1029/2024GB008261 e2024GB008261.

Kashyap, R., Pandey, A.C., 2021. Spatio–temporal variability assessment of pre–monsoon temperature to deduce their impact on Forest Fire events in relation to relief across himalayan region. J. Geomat. 15 (2), 106–114. https://isgindia.org/volume–15–no–2–october–2021.

Kashyap, R., Kuttippurath, J., Patel, V.K., 2025. Agriculture intensification and moisture–induced Thar desert greening: implications for energy balance, socio–economy, and biodiversity. GIsci. Remote Sens. 62 (1), 2483458. https://doi.org/10.1080/15481603.2025.2483458.

Kashyap, R., Kuttippurath, J., 2025. Tropical cyclones enhance photosynthesis in moisture–stressed regions of India. NPJ Clim. Atmos. Sci. 8 (1), 115. https://doi.org/10.1038/s41612–025–00988–z.

Kashyap, R., Kuttippurath, J., 2024a. Unraveling the sensitivity and response of ecosystems to rising moisture stress in India. Ecosyst. Health Sustain. 9, 0180. https://doi.org/10.1016/j.jenvman.2023.117655.

Kashyap, R., Kuttippurath, J., 2024b. Warming-induced soil moisture stress threatens food security in India. Environ. Sci. Pollut. Res. 31 (49), 59202–59218. https://doi.org/10.1007/s11356–024–35107–7.

Kashyap, R., Kuttippurath, J., Kumar, P., 2023a. Browning of vegetation in efficient carbon sink regions of India during the past two decades is driven by climate change and anthropogenic intrusions. J. Environ. Manage. 336, 117655. https://doi.org/10.1016/j.jenvman.2023.117655.

Kashyap, R., Kuttippurath, J., Patel, V.K., 2023b. Improved air quality leads to enhanced vegetation growth during the COVID–19 lockdown in India. Appl. Geogr. 151, 102869. https://doi.org/10.1016/j.apgeog.2022.102869.

Kashyap, R., Pandey, A.C., Kuttippurath, J., 2022. Photosynthetic trends in India derived from remote sensing measurements during 2000–2019: vegetation dynamics and key climate drivers. Geocarto Int. 37 (26), 11813–11829. https://doi.org/10.1080/10106049.2022.2060325.

Kashyap, R., Pandey, A.C., Parida, B.R., 2021. Spatio-temporal variability of monsoon precipitation and their effect on precipitation triggered landslides in relation to relief in Himalayas. Spat. Inf. Res. 29 (6), 857–869. https://doi.org/10.1007/s41324–021–00392–8.

Keenan, T.F., Hollinger, D.Y., Bohrer, G., Dragoni, D., Munger, J.W., Schmid, H.P., Richardson, A.D., 2013. Increase in forest water–use efficiency as atmospheric carbon dioxide concentrations rise. Nature 499 (7458), 324–327. https://doi.org/10.1038/nature12291.

Keenan, T.F., Prentice, I.C., Canadell, J.G., Williams, C.A., Wang, H., Raupach, M., Collatz, G.J., 2016. Recent pause in the growth rate of atmospheric CO2 due to enhanced terrestrial carbon uptake. Nat. Commun. 7 (1), 13428. https://doi.org/10.1038/ncomms13428.

Kennedy, C.M., Oakleaf, J.R., Theobald, D.M., Baruch-Mordo, S., Kiesecker, J., 2019. Managing the middle: a shift in conservation priorities based on the global human modification gradient. Glob. Chang. Biol. 25 (3), 811–826. https://doi.org/10.1111/gcb.14549.

Kong, X., Zhou, Z., Jiao, L., 2021. Hotspots of land–use change in global biodiversity hotspots. Resour. Conserv. Recycl. 174, 105770. https://doi.org/10.1016/j.resconrec.2021.105770.

Kuttippurath, J., Kashyap, R., 2023. Greening of India: forests or croplands? Appl. Geogr. 161, 103115. https://doi.org/10.1016/j.apgeog.2023.103115.

Kuttippurath, J., Peter, R., Singh, A., Raj, S., 2022. The increasing atmospheric CO2 over India: comparison to global trends. iScience 25 (8). https://doi.org/10.1016/j.isci.2022.104863.

Li, X., Xiao, J., 2019. Mapping photosynthesis solely from solar-induced chlorophyll fluorescence: a global, fine–resolution dataset of gross primary production derived from OCO–2. Remote Sens. 11 (21), 2563. https://doi.org/10.3390/rs11212563 *(Basel)*.

Liu, X., Sun, G., Fu, Z., Ciais, P., Feng, X., Li, J., Fu, B., 2023. Compound droughts slow down the greening of the Earth. Glob. Chang. Biol. 29 (11), 3072–3084. https://doi.org/10.1111/gcb.16657.

MacBean, N., Maignan, F., Bacour, C., Lewis, P., Peylin, P., Guanter, L., Disney, M., et al., 2018. Strong constraint on modelled global carbon uptake using solar–induced chlorophyll fluorescence data. Sci. Rep. 8 (1), 1973. https://doi.org/10.1038/s41598–018–20024–w.

Nemani, R.R., Keeling, C.D., Hashimoto, H., Jolly, W.M., Piper, S.C., Tucker, C.J., Running, S.W., et al., 2003. Climate-driven increases in global terrestrial net primary production from 1982 to 1999. Science (1979) 300 (5625), 1560–1563. https://doi.org/10.1126/science.1082750.

Pan, Y., Birdsey, R.A., Phillips, O.L., Houghton, R.A., Fang, J., Kauppi, P.E., Murdiyarso, D., et al., 2024. The enduring world forest carbon sink. Nature 631 (8021), 563–569. https://doi.org/10.1038/s41586–024–07602–x.

Parida, B.R., Pandey, A.C., Patel, N.R., 2020. Greening and browning trends of vegetation in India and their responses to climatic and non–climatic drivers. Climate 8 (8), 92. https://doi.org/10.3390/cli8080092.

Pasha, S.V., Dadhwal, V.K., 2024. National analysis on variations in estimates of forest cover dynamics over India (2001–2020) using multiple techniques and data sources. Spat. Inf. Res. 32 (4), 451–461. https://doi.org/10.1007/s41324–024–00570–4.

Peñuelas, J., Ciais, P., Canadell, J.G., Janssens, I.A., Fernández-Martínez, M., Carnicer, J., Sardans, J., et al., 2017. Shifting from a fertilization-dominated to a warming-dominated period. Nat. Ecol. Evol. 1 (10), 1438–1445. https://doi.org/10.1038/s41559-017-0274-8.

Qin, Y., Xiao, X., Wigneron, J.P., Ciais, P., Brandt, M., Fan, L., Moore III, B., et al., 2021. Carbon loss from forest degradation exceeds that from deforestation in the Brazilian Amazon. Nat. Clim. Chang. 11 (5), 442–448. https://doi.org/10.1038/s41558–021–01026–5.

Rascher, U., Alonso, L., Burkart, A., Cilia, C., Cogliati, S., Colombo, R., Zemek, F., et al., 2015. Sun-induced fluorescence-a new probe of photosynthesis: first maps from the imaging spectrometer HyPlant. Glob. Chang. Biol. 21 (12), 4673–4684. https://doi.org/10.1111/gcb.13017.

Reddy, C.S., Saranya, K.R.L., Pasha, S.V., Satish, K.V., Jha, C.S., Diwakar, P.G., Murthy, Y.K., et al., 2018. Assessment and monitoring of deforestation and forest fragmentation in South Asia since the 1930s. Glob. Planet Change 161, 132–148. https://doi.org/10.1016/j.gloplacha.2017.10.007.

Reichstein, M., Bahn, M., Ciais, P., Frank, D., Mahecha, M.D., Seneviratne, S.I., Wattenbach, M., et al., 2013. Climate extremes and the carbon cycle. Nature 500 (7462), 287–295. https://doi.org/10.1038/nature12350.

Ruehr, S., Keenan, T.F., Williams, C., Zhou, Y., Lu, X., Bastos, A., Terrer, C., et al., 2023. Evidence and attribution of the enhanced land carbon sink. Nat. Rev. Earth Environ. 4 (8), 518–534. https://doi.org/10.1038/s43017–023–00456–3.

Sannigrahi, S., Pilla, F., Basu, B., Basu, A.S., Sarkar, K., Chakraborti, S., Roy, P.S., et al., 2020. Examining the effects of forest fire on terrestrial carbon emission and ecosystem production in India using remote sensing approaches. Sci. Total Environ. 725, 138331. https://doi.org/10.1016/j.scitotenv.2020.138331.

Santoro, M., Cartus, O., Carvalhais, N., Rozendaal, D.M., Avitabile, V., Araza, A., Willcock, S., et al., 2021. The global forest above-ground biomass pool for 2010 estimated from high–resolution satellite observations. Earth Syst. Sci. Data 13 (8), 3927–3950. https://doi.org/10.5194/essd–13–3927–2021.

Sarmah, S., Singha, M., Wang, J., Dong, J., Burman, P.K.D., Goswami, S., Niu, S., et al., 2021. Mismatches between vegetation greening and primary productivity trends in South Asia-a satellite evidence. Int. J. Appl. Earth Observ. Geoinf. 104, 102561. https://doi.org/10.1016/j.jag.2021.102561.

Seneviratne, S.I., Zhang, X., Adnan, M., Badi, W., Dereczynski, C., Di Luca, A., Zhou, B. et al. (2021). Weather and climate extreme events in a changing climate (Chapter 11). 10.1017/9781009157896.013.

Sharma, A., Goyal, M.K., 2018. Assessment of ecosystem resilience to hydroclimatic disturbances in India. Glob. Chang. Biol. 24 (2), e432–e441. https://doi.org/10.1111/gcb.13874.

Shekhar, A., Buchmann, N., Gharun, M., 2022. How well do recently reconstructed solar–induced fluorescence datasets model gross primary productivity? Remote Sens. Environ. 283, 113282. https://doi.org/10.1016/j.rse.2022.113282.

Shi, H., Tian, H., Pan, N., Reyer, C.P., Ciais, P., Chang, J., Yang, J., et al., 2021. Saturation of global terrestrial carbon sink under a high warming scenario. Glob. Biogeochem. Cycles 35 (10), e2020GB006800. https://doi.org/10.1029/2020GB006800.

Singh, A., Abbhishek, K., Kuttippurath, J., Raj, S., Mallick, N., Chander, G., Dixit, S., 2022. Decadal variations in CO2 during agricultural seasons in India and role of management as sustainable approach. Environ. Technol. Innov. 27, 102498. https://doi.org/10.1016/j.eti.2022.102498.

Smith, B., Wårlind, D., Arneth, A., Hickler, T., Leadley, P., Siltberg, J., Zaehle, S., 2014. Implications of incorporating N cycling and N limitations on primary production in an individual–based dynamic vegetation model. Biogeosciences 11 (7), 2027–2054. https://doi.org/10.5194/bg–11–2027–2014.

Song, J., Zhou, S., Yu, B., Li, Y., Liu, Y., Yao, Y., Fu, B., et al., 2024. Serious underestimation of reduced carbon uptake due to vegetation compound droughts. NPJ Clim. Atmos. Sci. 7 (1), 23. https://doi.org/10.1038/s41612–024–00571–y.

Sparsha, S., Parida, B.R., 2024. Vegetation browning trend progressively leading to forest degradation in eastern Himalaya in response to climatic and anthropogenic drivers. Remote Sens. Appl. Soc. Environ. 35, 101209. https://doi.org/10.1016/j.rsase.2024.101209.

Tao, S., Chave, J., Frison, P.L., Le Toan, T., Ciais, P., Fang, J., Saatchi, S., et al., 2022. Increasing and widespread vulnerability of intact tropical rainforests to repeated droughts. Proc. Natl. Acad. Sci. 119 (37), e2116626119. https://doi.org/10.1073/pnas.2116626119.

Walther, S., Voigt, M., Thum, T., Gonsamo, A., Zhang, Y., Köhler, P., Guanter, L., et al., 2016. Satellite chlorophyll fluorescence measurements reveal large-scale decoupling of photosynthesis and greenness dynamics in boreal evergreen forests. Glob. Chang. Biol. 22 (9), 2979–2996. https://doi.org/10.1111/gcb.13200.

Wang, S., Zhang, Y., Ju, W., Chen, J.M., Ciais, P., Cescatti, A., Peñuelas, J., et al., 2020. Recent global decline of CO2 fertilization effects on vegetation photosynthesis. Science (1979) 370 (6522), 1295–1300. https://doi.org/10.1126/science.abb7772.

Wang, B., Xue, S., Niu, Z., 2023. Increasing trend in ecosystem-scale photosynthetic efficiency in the Yellow River Basin since 2000 caused by afforestation and climate change. Ecoscience 30 (3–4), 223–233. https://doi.org/10.1080/11956860.2024.2303187.

Wei, F., Wang, S., Fu, B., Wang, L., Zhang, W., Wang, L., Fensholt, R., et al., 2022. Divergent trends of ecosystem-scale photosynthetic efficiency between arid and humid lands across the globe. Glob. Ecol. Biogeogr. 31 (9), 1824–1837. https://doi.org/10.1111/geb.13561.

Wigneron, J.P., Ciais, P., Li, X., Brandt, M., Canadell, J.G., Tian, F., Fensholt, R., et al., 2024. Global carbon balance of the forest: satellite–based L–VOD results over the last decade. Front. Remote Sens. 5, 1338618. https://doi.org/10.3389/frsen.2024.1338618.

Wigneron, J.P., Fan, L., Ciais, P., Bastos, A., Brandt, M., Chave, J., Fensholt, R., et al., 2020. Tropical forests did not recover from the strong 2015–2016 El Niño event. Sci. Adv. 6 (6), eaay4603. https://doi.org/10.1126/sciadv.aay4603.

Winkler, A.J., Myneni, R.B., Hannart, A., Sitch, S., Haverd, V., Lombardozzi, D., Brovkin, V., et al., 2021. Slowdown of the greening trend in natural vegetation with further rise in atmospheric CO 2. Biogeosciences 18 (17), 4985–5010. https://doi.org/10.5194/bg-18-4985-2021.

Wu, J., Wang, D., Li, L.Z., Zeng, Z., 2022. Hydrological feedback from projected Earth greening in the 21st century. Sustain. Horiz. 1, 100007. https://doi.org/10.1016/j.horiz.2022.100007.

Yan, D., Scott, R.L., Moore, D.J.P., Biederman, J.A., Smith, W.K., 2019. Understanding the relationship between vegetation greenness and productivity across dryland ecosystems through the integration of PhenoCam, satellite, and eddy covariance data. Remote Sens. Environ. 223, 50–62. https://doi.org/10.1016/j.rse.2018.12.029.

Yan, Y., Liu, Z., Chen, L., Chen, X., Lin, K., Zeng, Z., Ma, Z., et al., 2025. Earth greening and climate change reshaping the patterns of terrestrial water sinks and sources. Proc. Natl. Acad. Sci. 122 (11), e2410881122. https://doi.org/10.1073/pnas.241088112.

Yang, H., Ciais, P., Frappart, F., Li, X., Brandt, M., Fensholt, R., Wigneron, J.P., et al., 2023. Global increase in biomass carbon stock dominated by growth of northern young forests over past decade. Nat. Geosci. 16 (10), 886–892. https://doi.org/10.1038/s41561–023–01274–4.

Zeng, Y., Hao, D., Park, T., Zhu, P., Huete, A., Myneni, R., Chen, M., et al., 2023. Structural complexity biases vegetation greenness measures. Nat. Ecol. Evol. 7 (11), 1790–1798. https://doi.org/10.1038/s41559–023–02187–6.

Zhang, Y., Liu, X., Wang, L., Zeng, X., Zhao, L., Wu, X., et al., 2024. Reductions in forest resilience: unraveling the decoupling between gross primary productivity and photosynthetic efficiency. Geophys. Res. Lett. 51 (16), e2024GL110148. https://doi.org/10.1029/2024GL110148.

Zhao, Q., Zhu, Z., Zeng, H., Zhao, W., Myneni, R.B., 2020. Future greening of the Earth may not be as large as previously predicted. Agric. For. Meteorol. 292, 108111. https://doi.org/10.1016/j.agrformet.2020.108111.

Zhao, Z., Ciais, P., Wigneron, J.P., Santoro, M., Brandt, M., Kleinschroth, F., Li, W., et al., 2024. Central African biomass carbon losses and gains during 2010–2019. One Earth 7 (3), 506–519. https://doi.org/10.1016/j.oneear.2024.01.02101.

Environmental Science and Pollution Research (2024) 31:59202–59218
https://doi.org/10.1007/s11356-024-35107-7

RESEARCH ARTICLE

Warming-induced soil moisture stress threatens food security in India

Rahul Kashyap[1] · **Jayanarayanan Kuttippurath**[1]

Received: 12 February 2024 / Accepted: 17 September 2024 / Published online: 30 September 2024

Abstract

Soil moisture (SM) interconnects various components of the Earth system and drives the land–atmosphere feedbacks and food production. However, around 40% of global vegetated land experiences SM drying. India is one of the global hotspots of land–atmosphere interactions and an extensively agrarian economy, but underexplored in terms of SM dynamics and its ramifications on food security. Here, we examine the mechanism of SM drying and its implications on cropland productivity in India based on remote sensing measurements and land surface model simulations in recent decades (2000–2019) and future projection of the 21st century. We find SM reduction predominantly in monsoon (4.5%) and winter (3%) seasons that are in the major agricultural seasons of Kharif and Rabi, respectively. Machine learning (ML)-based random forest (RF) reveals that temperature (T, 30.76%) is the dominant driver of SM variability, and then precipitation (P, 26.34%), evapotranspiration (ET, 26.08%) and surface greenness (16.82%). Concurrently, India experiences severe warming in terms of land (0.59 ℃/dec), soil (0.48 ℃/dec) and soil heat flux (SHF, 0.16 W/m^2/dec) during 2000–2019. Partial correlation analysis between SM and T limiting the influence of P reveals a strong negative (> -0.5) relationship in the agriculture intensive regions of Indo-Gangetic Plain (IGP) and South India (SI). Drying owing to warming and increased SHF, termed as warming-induced moisture stress, reduces gross primary productivity (GPP) (i.e. browning) and yield of major food crops of wheat, rain-fed rice, maize and soyabean, predominantly in SI and eastern IGP. Granger Causality shows that warming-induced soil moisture stress has a maximum temporal lag of 1 month. In a warming world, the ever-growing population demands more food, and therefore, the warming-induced soil moisture stress is a serious threat to food security in India and similar agro-climatic regions of the world. This calls for climate-resilient agriculture, better agronomic management, improved irrigation and adoption of water-efficient crops.

Keywords Agricultural droughts · Causality · Cropland productivity · Global warming · Machine learning

Introduction

Soil moisture (SM) is an important entity in the global climate system as it interconnects the hydrosphere, atmosphere, lithosphere and biosphere (Humphrey et al. 2021). SM plays a vital role in the land–atmosphere feedbacks and food production (Humphrey et al. 2021; Krishnamurthy et al. 2022). SM regulates the fluxes of moisture, energy, momentum between land and atmosphere, and controls the terrestrial biogeochemical cycles (Green et al. 2019). Therefore, changes in SM can alter these fluxes and impact water and carbon cycles (Zhou et al. 2021; Patel et al. 2024). SM also plays a vital role in ecosystem functioning (Green et al. 2019; Humphrey et al. 2021), crop yield (Krishnamurthy et al. 2022) and extreme events such as droughts (Trenberth et al. 2014; Ault 2020) and heatwaves (Zhou et al. 2024). Therefore, SM is an essential climate variable (ECV) of the land–atmosphere interactions. However, the drastic reduction of SM intensified in recent decades, by which almost 40% of the global land region is drying (Lal et al. 2023; Peng et al. 2023). This SM drying is attributed to decline in precipitation (P), increase in evapotranspiration (ET) and warming (Deng et al. 2020; Lal et al. 2023). Global warming leads to an increase in ET, which further increases the intensity and frequency of SM drying (Lal et al. 2023). Anthropogenic warming may be a major cause for SM drying (Marvel et al. 2019). Also,

Responsible Editor: Kitae Baek

✉ Jayanarayanan Kuttippurath
jayan@coral.iitkgp.ac.in

[1] CORAL, Indian Institute of Technology Kharagpur, Kharagpur 721302, India

the intensive agricultural practices based on the enhanced nitrogenous fertilisers have led to the expansion of arable lands and disturbed soil–water balance owing to high SM consumption (Liu et al. 2015; Samaniego et al. 2018).

Global croplands are facing frequent flash droughts in recent decades (Mahto and Mishra 2023) with southeast Asia as a major hotspot of water and food crisis due to climate change (Lobell et al. 2008) and recent engrossment in aridity (Kashyap and Kuttippurath 2024). Furthermore, the warming in this region is projected to result in more intense and frequent flash droughts that would decline crop yield (Mishra et al. 2014; Mahto and Mishra 2023). In India, monsoon precipitation is the primary source of moisture during the Kharif season. However, crop production during the dry season (Rabi) largely depends on the SM availability (Mishra 2020; Shah et al. 2021). Apart from the changes in monsoon rainfall (Nair et al. 2018; Mishra 2020), there is a significant warming (Kumar et al. 2023) and increase in ET during recent decades in India (Patel and Kuttippurath 2022). The dry season warming exuberates the SM drying in India (Mishra 2020). Concurrently, India exhibits substantial changes in vegetation during recent decades (Chen et al. 2019; Parida et al. 2020; Kuttippurath and Kashyap 2023) and studies highlight the importance of SM in driving photosynthetic activity (Kashyap et al. 2022), productivity (Dubey and Ghosh 2023), carbon dynamics (Kashyap et al. 2023a), ecosystem health (Kashyap and Kuttippurath 2024) and land–atmosphere feedbacks (Sebastian et al. 2023) in India.

Low SM leads to vegetation droughts in a minimum of 50% of the total area in 16 out of 24 major river basins in India, with more than half of the total area for each vegetation type exhibits a lack of resilience (Jha et al. 2019). In the anthropogenic climate change scenario, the carbon–water cycle coupling has strengthened due to rising moisture stress in India (Kashyap and Kuttippurath 2024). A few studies attempt to investigate the influence of SM variability on vegetation in India (Pangaluru et al. 2019; Bhimala et al. 2020). SM limitations predominantly control vegetation productivity in India (Dubey and Ghosh 2023). Additionally, soil-vegetation moisture capacitator effect maintains dry season productivity and land–atmosphere feedbacks in India (Sebastian et al. 2023). Henceforth, SM is a crucial factor that affect carbon capture, crop growth and the net food production in India. Henceforth, there is a need of a dedicated study that provides a holistic insight on SM changes, mechanisms and implications in terms of food security in India.

We hypothesise that in a warming world with erratic rainfall can increase ET and cause soil drying that would adversely affect vegetation productivity and crop yield. Therefore, we find the variability and changes of SM across space and time in India, based on remote sensing measurements (ESA CCI) and process-based land surface model simulations for the past two decades (2000–2019). The role of key climate drivers (P, temperature [T] and ET) and anthropogenic drivers such as gross sown area (GSA), net irrigated area (NIA) and irrigated sown area (ISA) in regulating SM is also explored using the partial correlation, multiple linear regression (MLR), pixel wise change detection, machine learning (ML)-based random forest (RF) technique and Granger Causality. To examine the implications of SM changes on food security, the interrelationship between SM and gross primary productivity (GPP) is assessed. The changes in major food crop yield for wheat, rain-fed rice, maize and soyabean are also estimated. The future scenario is examined in the context of climate change impact on SM and its implications for food security in India in the 21st century. The study has high significance for agricultural decisionmaking, cropland management, sustainable agricultural practices, land resource conservation and carbon sequestration in the warming world.

Data and methodology

Data

Soil moisture and meteorological data

A suite of datasets from both satellite and reanalysis are used in this study (Table 1). The estimation of SM and its changes is of paramount significance for attaining water and food security in the changing climate (Seneviratne et al. 2010; Furtak and Wolińska 2023). However, SM measurements have always been very challenging. Traditionally ground-based in situ measurements were used but it is very costly, time-consuming, labour-intensive and not feasible for large-scale studies. Currently, single satellite SM estimates such as Soil Moisture Active Passive (SMAP) (Entekhabi et al. 2010) and Soil Moisture and Ocean Salinity (SMOS) (Kerr et al. 2010) are developed for detecting SM variability. However, these datasets are for the last decade that make them unsuitable for long-term climate impact studies. Recently, the long-term SM changes are computed based on either land-surface model like Global Land Data Assimilation System (GLDAS) or with the reanalysed data such as the European Centre for Medium Range Weather Forecast Reanalysis Version 5 (ERA5) (Deng et al. 2020; Lal et al. 2023). Due to the difficulties in SM measurements and limited data availability, modelled SM is employed to study the land–atmosphere interactions, feedbacks and agricultural droughts (Dorigo et al. 2017). However, models usually struggle to adequately capture regional phenomena due to uncertainties in parameters, such as soil properties, flaws in model structures, mismatch in the spatial scales and soil depth among

Table 1 Datasets with their resolution and source from which they are acquired

Data	Resolution	Source
MODIS LULC, NDVI, GPP and ET	500 m	(https://lpdaacsvc.cr.usgs.gov/)
ESA CCI Soil Moisture	0.25°×0.25°	(https://esa-soilmoisture-cci.org/)
GPM level–3 Precipitation	0.1°×0.1°	(https://daac.gsfc.nasa.gov/)
GLDAS Soil Moisture, Temperature and Soil Temperature	0.25°×0.25°	(https://daac.gsfc.nasa.gov/)
FLDAS Soil Heat Flux	0.1°×0.25°	(https://daac.gsfc.nasa.gov/)
IMD Precipitation	0.25°×0.25°	(https://www.imdpune.gov.in/index.html)
IMD Temperature	1°×1°	(https://www.imdpune.gov.in/index.html)
Net Irrigated Area	250 m	Ambika et al. (2016) Figshare:(https://dx.doi.org/10.6084/m9.figshare.3790611.v1)
Synthetic fertilisers, manures and biological fixation in soil		FAO/FAOSAT (https://www.fao.org/faostat/)
CMIP 6 GFDL data future projection of SM, T and P	1°×1°	(https://esgf-node.llnl.gov/projects/cmip6/)
CMIP 6 CNRM data future projection of SM, T and P	0.5°×0.5°	(https://esgf-node.llnl.gov/projects/cmip6/)
CMIP 6 HadGEM data future projection of SM, T and P	1.875°×1.25°	(https://esgf-node.llnl.gov/projects/cmip6/)
CMIP 6 CanESM data future projection of SM, T and P	2.81°×2.77°	(https://esgf-node.llnl.gov/projects/cmip6/)
Population dynamics	1 km	(https://sedac.ciesin.columbia.edu/)
Total Above Ground Production (TAGP)	0.1°×0.1°	(https://cds.climate.copernicus.eu/)
Gross sown area, area sown more than once, net irrigated area, food grain yield and food grain production		Ministry of Agriculture and Farmers Welfare, Government of India (http://apps.iasri.res.in/agridata/20data/HOME_20.HTML) (https://www.indiastat.com/)

the land surface models (LSM) and in situ measurements (Liu et al. 2011; Dorigo et al. 2017).

The advent of multi-satellite SM like the European Space Agency (ESA) Climate Change Initiative (CCI) is also a viable option for the same, as it exhibits a good agreement with both reanalyses and in situ measurements (Dorigo et al. 2017; Peng et al. 2023). The ESA CCI SM data (v07.1) are considered in our study (Gruber et al. 2019; Grillakis et al. 2021). Additionally, the active and passive instruments work best together because their responses to vegetation density differ. The passive instruments provide more accurate estimates in arid regions, whereas the active instruments perform better over areas with moderate vegetation (Hirschi et al. 2014; Raoult et al. 2018). Moreover, combining both measurements enables more reliable and accurate SM estimates for ecohydrological applications across various environmental conditions (Ma et al. 2024). Since the satellite retrieval is dependent on surface and sub-surface characteristics like soil texture and vegetation, the observations may be spatially uneven. Instrument drift and lifespan issues result in temporal inhomogeneity in the satellite data (Dorigo et al. 2017; Grillakis et al. 2021). Likewise, the combined product employs sensors with different temporal and spatial resolutions, spatial coverage, observation principles, and sensor calibration, add temporal inhomogeneity to the final dataset (Raoult et al. 2018). The blending/merging algorithms may also alter the long-term trends of the data (Liu et al. 2011; Gruber et al. 2019). In addition, in dense vegetation or low SM regions, satellite SM data have relatively higher uncertainty (de Jeu et al. 2008; Dorigo et al. 2017). To estimate changes in SM, and capture the role of drivers and their relation with terrestrial productivity, we also use process-based LSM-derived SM data from GLDAS Noah.

GLDAS near surface temperature data, a blend of National Ocean and Atmospheric Administration and Global Data Assimilation System (NOAA/GDAS) atmospheric analysis, are also considered (Xia et al. 2019). The soil temperature dataset used is based on GLDAS (Wang et al. 2016). The soil heat flux (SHF) is derived from the Famine Early Warning Systems Network (FEWS NET) Land Data Assimilation System (FLDAS) (Grillakis et al. 2021). The Global Precipitation Measurements (GPM, GPM_3IMERGDF L3), a multi-satellite daily precipitation data (mm/day), are too considered (Skofronick-Jackson et al. 2018). The ET data utilised here is the actual ET data from MODIS (MOD16 A3HGF). Further details of GPM, GLDAS and CCI are provided in the supplementary material. The precipitation (Pai et al. 2014) and temperature (Srivastava et al. 2009) data from the Indian Meteorological Department (IMD) are also used to complement our analyses (Table 1).

The future projection data of SM, P and T from the Coupled Model Intercomparison Project Phase 6 (CMIP6) models GFDL, CNRM, CanESM and HadGEM for high emissions scenarios (Shared Socioeconomic Pathways, SSP5.85) are considered (Eyring et al. 2016). The population dynamics SSP5 scenario (Fossil-fueled development)

data from Socioeconomic Data and Applications Centre (SEDAC) are also taken for our assessment (Jones and Neill 2020). The change between the two focal periods, i.e. 2015–2019 and 2020–2030, is estimated to find the near future changes in SM and its climate drivers. For the far future, the change between the two focal periods, i.e. 2015–2019 and 2090–2100, is estimated.

Vegetation and agriculture data

Moderate Resolution Imaging Spectroradiometer (MODIS) data are effective for studying large-scale terrestrial ecosystems (e.g. Chen et al. 2019; Kashyap et al. 2022). MODIS (MCD12Q1) Version 6 data provide global land cover types based on supervised classifications of reflectance data (Fig. S1). The MODIS Normalised Difference Vegetation Index (NDVI) (MOD13A1) is incorporated as a measure of surface greenness. The Terra and Aqua combined MODIS GPP (MOD17A2HGF) data are used to analyse the terrestrial productivity. The irrigation data (NIA) for India for the years 2000–2015 are taken from Ambika et al. (2016). The information regarding synthetic fertilisers and manures added to the soil and biological fixation are acquired from the Food and Agriculture Organization (FAO) for India for the period 2000–2018. The agricultural data such as GSA, area sown more than once, food grain yield and food grain production are collected from the reports of agricultural data book, Ministry of Agriculture and Farmers Welfare, Government of India. Crop productivity indicator in total above ground production (TAGP) of various food crops such as wheat, rain-fed rice, maize and soyabean from Copernicus Climate Change Service is also used (see Table 1).

Methodology

We first investigate the spatio-temporal variability of SM on regional, seasonal and decadal scales. Next, we examine the relation of SM with drivers based on correlation and partial correlation (PC) analysis. However, since correlation does not imply causation, we perform Granger causality to find the relationship between SM and its key climatic drivers. The relative contribution of the climatic drivers to SM variability is estimated based on random forest (RF) machine learning (ML) model. We find the changes in SM and terrestrial productivity (GPP) and major crops such as rice, wheat, maize and soya for food security implications. We also investigate the future changes in SM, its key climatic drivers and population. A schematic diagram representing the overall approach of the study is presented in Fig. S2 and the key steps in the methodology are detailed in the subsections.

Estimation of variability in soil moisture and drivers

Here, we estimate the variability in SM across various spatio-temporal scales ranging from seasonal, annual to decades. The seasons are defined as winter (December, January and February), summer (March, April and May), monsoon (June, July and August) and post-monsoon (September, October and November) for the last two decades (2000–2019). We find the changes in SM and its key climate drivers in recent decade (2010–2019) from the previous decade (2000–2009) based on image differencing technique. The change is estimated in terrestrial productivity (GPP) and compared to the changes in SM. The changes in grain yield, soil properties such as soil temperature, SHF, synthetic fertilisers added to the soil, manures added to the soil and biological fixation in the soil are also estimated as:

$$\%X_{R-P} = \frac{X_R - X_P}{X_P} \times 100$$

here, X is any variable such as SM, GPP, soil properties and others; R is the mean of X in the recent decade (2010–2019); and P is the mean of X in the previous decade (2000–2009).

The change in NIA is obtained by the pixel-wise image differencing technique on remotely sensed data for the Indian region for the years 2000–2015. Furthermore, the change in net irrigated area (ΔNIA) is analysed for each climate region of India. The percentage irrigated sown area (ISWA) is obtained by using GSA and NIA as:

$$ISWA = \left(\frac{NIA}{GSA}\right)100\%$$

Soil moisture and drivers: correlation, causation and contribution

Correlation analysis is performed to derive the response of SM to the climate drivers. Furthermore, partial correlation (PC) is computed to have a thorough understanding of the role of drivers in modifying the regional SM distribution. To test the relationship between two variables, the influence of third variable (covariate) must be eliminated. In simple correlation, the strength of the linear relationship between two variables is measured without considering the fact that both variables may be influenced by a third variable (covariate). The study of the linear relationship between two variables after excluding the effect of one or more independent variables is known as PC detailed in supplementary material. The influence of drivers to the soil moisture change is estimated as in Kashyap et al. (2022, 2023a), which is detailed in supplementary material.

Correlation analysis states the relation between two parameters, which does not imply causation. Therefore, to find the existence of causal links among SM and its key climate drivers (P, T and ET) and the associated temporal lag, Granger causality test is performed. This gives distinct causal relationship between two variables on the basis of "cause" and "effect." Rather than simple correlation among the effect/response and the cause/driver, Granger causality test is based on predictability. A causality is said to be Granger only if "our capacity to forecast future Y response increases by adding all relevant information except the current value of X." In this scenario, variable X is said to Granger cause Y. Also, "feedback" is established between "cause" and "effect" when X can Granger cause Y and Y can Granger cause X (Granger 1969). To perform Granger causality test, a bivariate model between two stationary time series (X and Y) is introduced.

$$Y_t = \sum_{i=1}^{n} a_i Y_{t-i} + \sum_{i=1}^{n} b_i X_{t-i} + \varepsilon_t$$

$$X_t = \sum_{i=1}^{n} c_i X_{t-i} + \sum_{i=1}^{n} d_i Y_{t-i} + \delta_t$$

where X and Y are two stationary time series; a, b, c and d are coefficients; and ε and δ are white noise. For X to Granger cause Y, $b_i \neq 0$; for feedback between X and Y, $d_i \neq 0$. To understand the temporal lag in Ganger causality, each variable is given a maximum lag of 4 months.

Due to its advantage in managing multidimensional data, ML has been used frequently in recent years to model systems with complex nonlinear correlation structures between the dependent and independent variables. RF is an ensemble model that combines boosting and regression trees to create a large number of simple tree models before combining them to a final optimised model. Based on the ML method RF, the relative contribution of key climate drivers (T, P and ET) and surface greenness (NDVI) to the SM variability is estimated in R Studio version 4.2.1 employing packages "randomForest" and "caret." In the RF model, a total of 500 decision trees are generated with two variable splitting allowed in each tree. Here, 70% of the data are used for training and 30% for testing. Also, the RF model is validated for the Indian region, where we compare the observed and the predicated data (Table S1) as in a previous study (Kashyap and Kuttippurath 2024). To examine the contribution and relative importance of each driver, a precision-based methodology is used. Using the independent data samples, it is possible to calculate the relative importance of each variable. The sample that was taken straight from the bag is first assessed for prediction accuracy. The values of the variables in the out-of-the-bag sample are then generated at random while the stability of all other variables is maintained. Then, using the average accuracy drop across all trees, the accuracy of prediction is evaluated. Additional outcome categories are created using the value indicator. A variable loses all predictive power when it is randomly shuffled. The importance of a variable indicates the reduction in its accuracy, if it were excluded.

Results

Soil moisture variability

The SM distribution averaged over the recent two decades (2000–2019) is shown in Fig. 1. The regions and specifications are shown in Fig. S1. ESA CCI exhibit lower (< 0.2 m^3/m^3) SM in North West (NW, Rajasthan and Gujrat), Indo Gangetic Plain (IGP, Punjab and Haryana) and Central India (CI). Higher (> 0.3 m^3/m^3) SM is exhibited by some areas in the eastern region of South India, NW (Gujrat) and northeast (NE). GLDAS data replicate the spatial patterns and capture seasonal variability in SM as done by ESA CCI (Fig. S2). Seasonally, the mean SM that serves as the indicator of gross soil water availability is higher (0.321 m^3/m^3) in post-monsoon due to favourable temperature (T, 21.46 ℃) and rainfall (P, 5 mm/day). Monsoon also exhibits higher SM (0.317 m^3/m^3) due to high rainfall (P, 7.5 mm/day). SM is lower in winter (0.2 m^3/m^3) owing to cold (15.58 ℃) and dry (P, 0.48 mm/day) conditions. Summer exhibits the lowest SM (0.161 m^3/m^3) owing to warmer (T, 27.37 ℃) and marginally wet (P, 1.41 mm/day) conditions. Majority of the Indian landmass exhibits low (< 0.2 m^3/m^3) SM in summer due to T above 30 ℃ and very small P (< 2.5 mm/day). The NW and east IGP regions show the smallest SM (< 0.15 m^3/m^3) due to little rain (0.5–2.5 mm/day) in winter. During monsoon, India receives high amount of P (> 5 mm/day) that leads to moderate and above levels of SM (> 0.25 m^3/m^3). Very high (> 0.3 m^3/m^3) SM is observed in NE and CI due to higher P (> 7.5 mm/day) there. In post-monsoon, the pattern is very similar to monsoon in GLDAS, but CCI exhibits lower spatial variability. The areas of higher precipitation (> 7.5 mm/day) show higher (> 0.3 m^3/m^3) SM (Figs. 1, S2, S3, S4, S5, S6).

The decadal variability in SM is shown in Fig. 2. Our analysis reveals a reduction of SM in each season (Fig. 2a) in recent decade (2010–2019) from the previous decade (2000–2009). In winter, areas of NW, eastern IGP and near western coast depict lower SM levels. During summer, there is a reduction in SM in some areas of IGP and CI, with most areas showing lower SM in recent decade (2010–2019). Monsoon has reduced levels of SM in most regions, except for hilly areas. In post-monsoon, most areas exhibit small SM levels, for which CI, eastern coastal areas

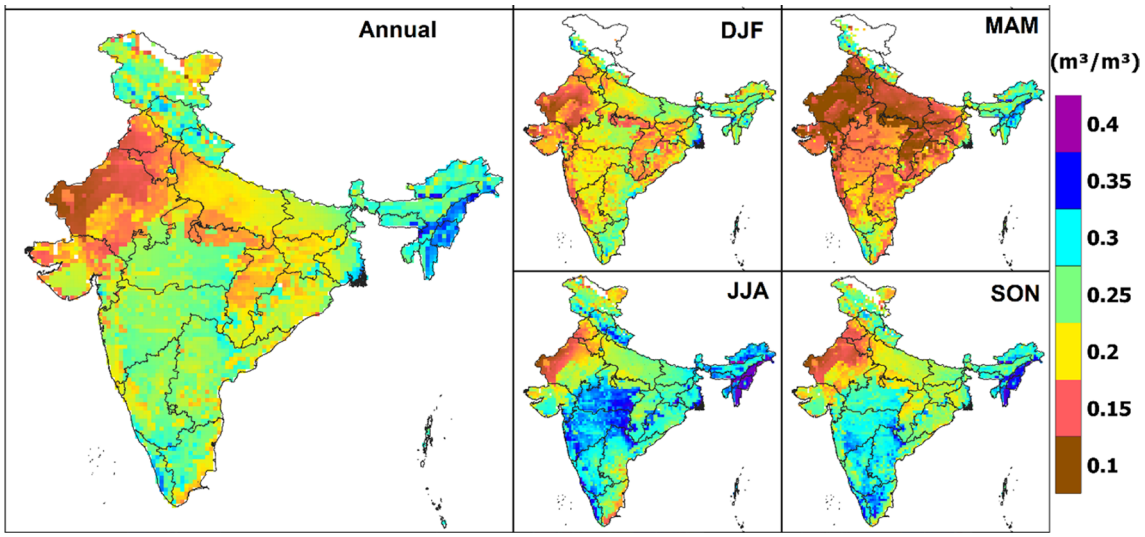

Fig. 1 Seasonal Variability in Soil Moisture (SM) in the Climate Change Initiative (CCI)-based volumetric soil moisture (m^3/m^3) during annual, winter (DJF: December, January and February), summer (MAM: March, April and May), monsoon (JJA: June, July and August) and post-monsoon (SON: September, October and November) seasons averaged over the period 2000–2019

and SI show dry conditions in comparison to the previous decade (2000–2009). The interannual variability in SM is also explored at seasonal and annual scales (Fig. 2b). Both measurements (CCI) and model (GLDAS) data capture temporal variability in SM during recent decades. To get a vivid understanding of the variability in SM, we examined its climate drivers (Fig. S7), and the results reveal that the temporal variability in SM is consistent with the spatio-temporal changes in P (increases) and T (decreases). There are some years such as 2002, 2009, 2012 and 2016 where the combined effect of warming and reduced P led to reduction in SM. SM has positive anomaly in years 2003–2008, 2010, 2011, 2013 and 2014, and negative anomaly in 2000–2002, 2009, 2012 and 2015–2019 (Fig. S7). El Niño years were severe drought years in comparison to the La Niña years (Roxy et al. 2015; Kumar et al. 2023). The years 2002, 2009 and 2015 were severe or extreme drought years in India (Kumar et al. 2006; Mishra 2020) that exhibited a decline in SM.

Generally, the years of negative anomaly in SM are estimated to have positive anomaly in ET, which is eventually driven by positive anomaly in T. Small anomaly in T can lead to a large anomaly in ET, and is reciprocated in SM anomaly. The relationship of SM with T and P is further analysed by segregating it into the areas of increasing (moistening) (Fig. S8a) and decreasing (drying) (Fig. S8b) SM. For the moistening regions, P and T distributions are very similar to that of SM (Fig. S7 and S8), but are not well correlated in the drying regions. The effect of lower P and higher T is highly pronounced in these regions. It is evident that there is a clear negative correlation between P and ET, and a clear positive correlation between T and ET. Therefore, persistent warming depletes moisture in the soil as analysed for the period 2012–2019.

Soil moisture changes and its drivers

The temporal evolution of SM is further explored at the regional scale incorporating both remote sensing (CCI) and model (GLDAS) estimates (Fig. 3). High interannual variability is captured by both the datasets. Most regions except for regions such as HR and NE exhibit similar patterns in both the datasets (Fig. 3a). There is a decline in SM in recent decade (2010–2019) from the previous decade (2000–2009) as shown in Fig. 3b. Except for NW, all five climatic homogenous regions (Fig. S1) exhibit a substantial decrease in SM. Among these regions, SI (7.67%), IGP (6%), SI (7.67%), CI (3.3%) and NE (2.37%) exhibit marked reduction in SM, as estimated from the CCI data. The GLDAS data also depict similar decline values in SM for each region. Both CCI (2.97%) and GLDAS (2.45%) data reveal an evident reduction in SM in recent decade (2010–2019) from the previous decade (2000–2009). In terms of the changes with respect to seasons, monsoon has a marked reduction in SM (4.5% in both data) in recent decade from the previous decade. Winter also exhibits a substantial decline in SM as shown in both CCI (2.08%) and GLDAS (3.15%). Limited reduction (1–2%) in post-monsoon and summer is estimated with CCI and GLDAS data in recent decade relative to the previous decade. The severe warming in monsoon (1.25 ℃/dec) is the primary cause of reduction in SM. In post-monsoon, the combined effect of reduced P (− 0.47 mm/day/dec) and increased T (0.26 ℃/dec) causes the decline in SM. In summer, enhanced warming (0.6 ℃/dec) has led to a dip in SM.

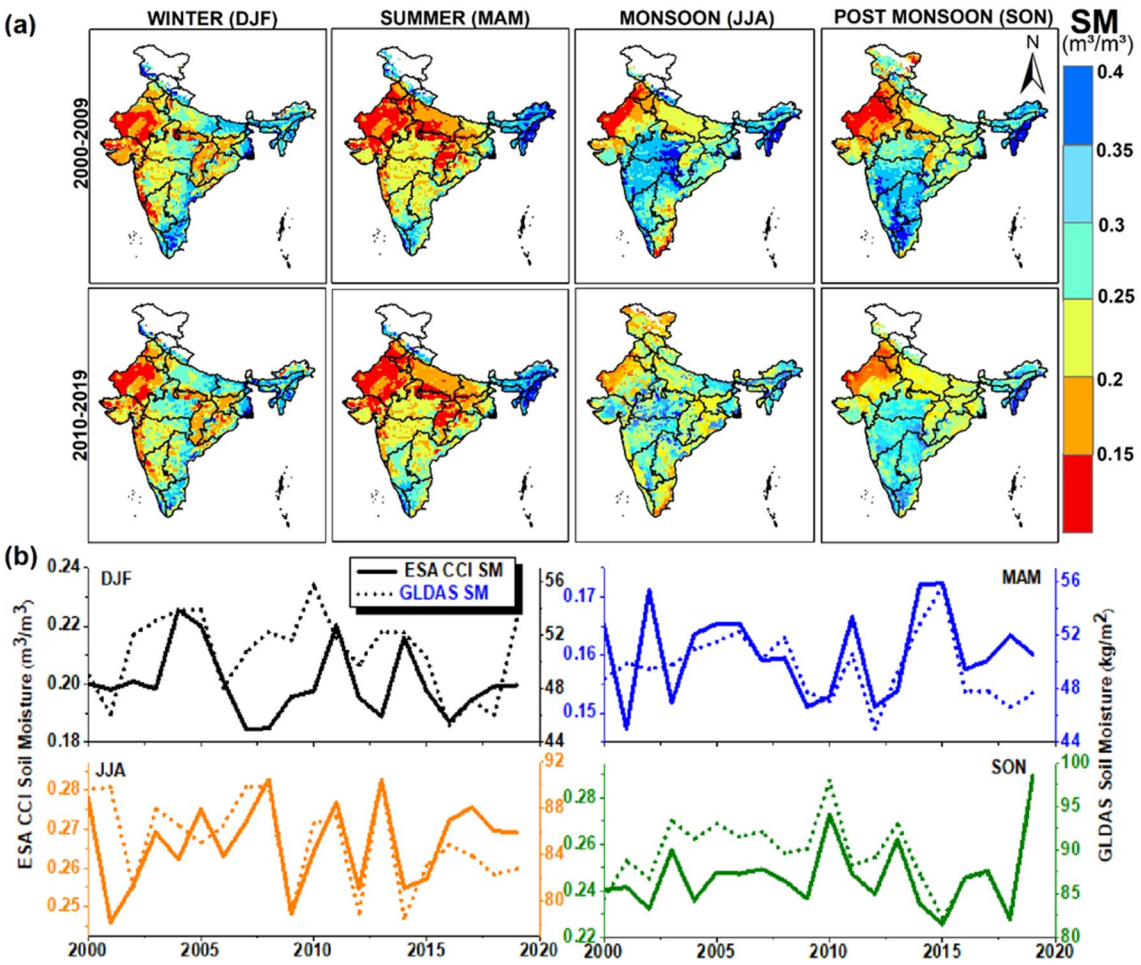

Fig. 2 Decadal and Interannual variability in SM. **a** Temporal evolution of volumetric soil moisture (m^3/m^3) in previous decade (2000–2009) and recent decade (2010–2019) based on the Climate Change Initiative (CCI) data. **b** Soil moisture variability based on both CCI and Global Land Data Assimilation System (GLDAS) during winter (DJF: December, January and February), summer (MAM: March, April and May), monsoon (JJA: June, July and August) and post-monsoon (SON: September, October and November) seasons for the period 2000–2019

Interestingly, despite the increasing P (0.014 mm/day/dec) and decreasing T (−0.04 ℃/dec), SM is declining in winter.

In recent decades, agricultural activities have greatly enhanced the SM-based drying (Liu et al. 2015; Samaniego et al. 2018). Rabi is a dry season due to very small amount of P in that period, in which crop growth is governed by subsurface moisture in terms of SM and groundwater. The excessive consumption of SM for agricultural activities in the dry season might be a reason for the reduction in SM. The interannual variability in GSA, NIA and ISA% is reciprocated in SM. The years such as 2009–2010 and 2012–2013 show a major dip in SM, which is also observed in GSA, NIA and ISA%. Likewise, the phase of enhanced SM in 2010–2011 and 2013–2014 is also reflected in the higher GSA, NIA and ISA (%). There is a drop in NIA and ISA% in 2005–2006, but the high GSA mask the large drop in SM in the same period (Fig. 4g).

Relation, causal links and contribution of key drivers

The role of climate drivers is very intricate and thus we thoroughly examine the role and contribution of key climate drives to SM changes using correlation analysis. We find that P ($r = 0.56$) influences SM positively, whereas T ($r = -0.44$) and ET ($r = -0.34$) have negative influence on SM (Fig. S9). The relative influence (positive/negative) of climate drivers on the long-term SM changes (Fig. 4a, b, c) exhibits that the NW region has an enhanced SM (moistening) due to positive influence of P. This influence is very strong as it dominates the negative influence of both T and ET in this arid region. The moistening in CI has a combined positive influence by all drivers. In NE, the positive influence of T is opposed by the negative influence of P and ET. In SI, the positive influence of P is dominated by the combined negative influence of T and ET, leading to reduced SM (drying) there.

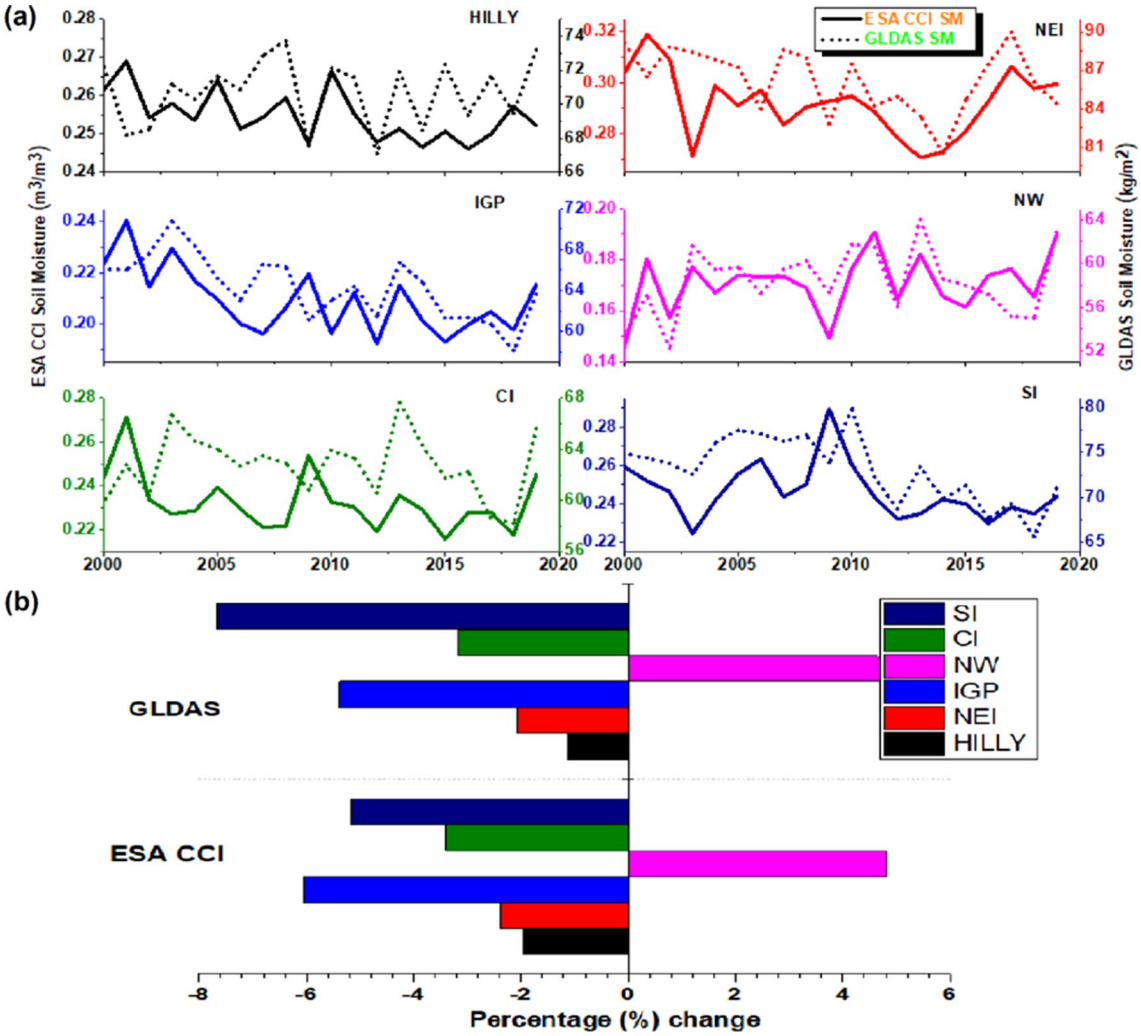

Fig. 3 Regional variability in SM. **a** Temporal evolution of soil moisture (SM) in the period 2000–2019 for six homogeneous climatic regions in (i) Hilly, (ii) North East (NE), (iii) Indo Gangetic Plains (IGP), (iv) North West (NW), (v) Central India (CI) and (vi) South India (SI) as derived from the Climate Change Initiative (CCI) and Global Land Data Assimilation System (GLDAS) data. **b** Percentage (%) change in SM in recent decade (2010–2019) from the previous decade (2000–2009) for the homogeneous regions as above derived from the Climate Change Initiative (CCI) and Global Land Data Assimilation System (GLDAS) data

Therefore, showering-induced moistening in NW and warming- induced moisture stress in SI and IGP are the two key mechanisms controlling the long-term SM changes in India.

The partial correlation (PC) analysis between SM and T with P as covariate (Fig. 4d) exhibits negative correlation in most regions. The negative correlation is very strong (> 0.5) in SI and some areas of IGP. Contrarily, cold regions such as HR and NE exhibit a small (0.25) positive correlation, but higher (> 0.5) in the western Himalaya. In the PC analysis between SM and ET with T as a covariate (Fig. 4e), majority of the regions exhibit positive correlation, which is highest in the west (0.75). The HR, NE and some regions in eastern IGP show negative correlation. In the PC between SM and P with T as covariate (Fig. 4f), most regions exhibit positive correlation, which is highest in CI and coastal regions (0.8). Some regions in HR, western Himalaya in particular, depict negative correlation. P and SM are well correlated (0.6) in SI and eastern IGP, where P has a positive influence, and T and ET have a negative influence on SM. The strong negative influence of T on SM in SI and eastern IGP, and the negative correlation between SM and ET, reduce SM, which is a major concern.

The relative contribution of each climate driver to SM variability is estimated using the ML-based RF technique (Fig. 5a) and we find that T (30.76%) is the dominant driver of SM variability followed by P (26.34%), ET (26.08%) and NDVI (16.82%). Therefore, T is the key driver of SM with P as the primary source and ET as the main sink. The results from Granger Causality (Fig. 5b) for IGP and SI reveal that the variability in SM is caused by all drivers in a lag of

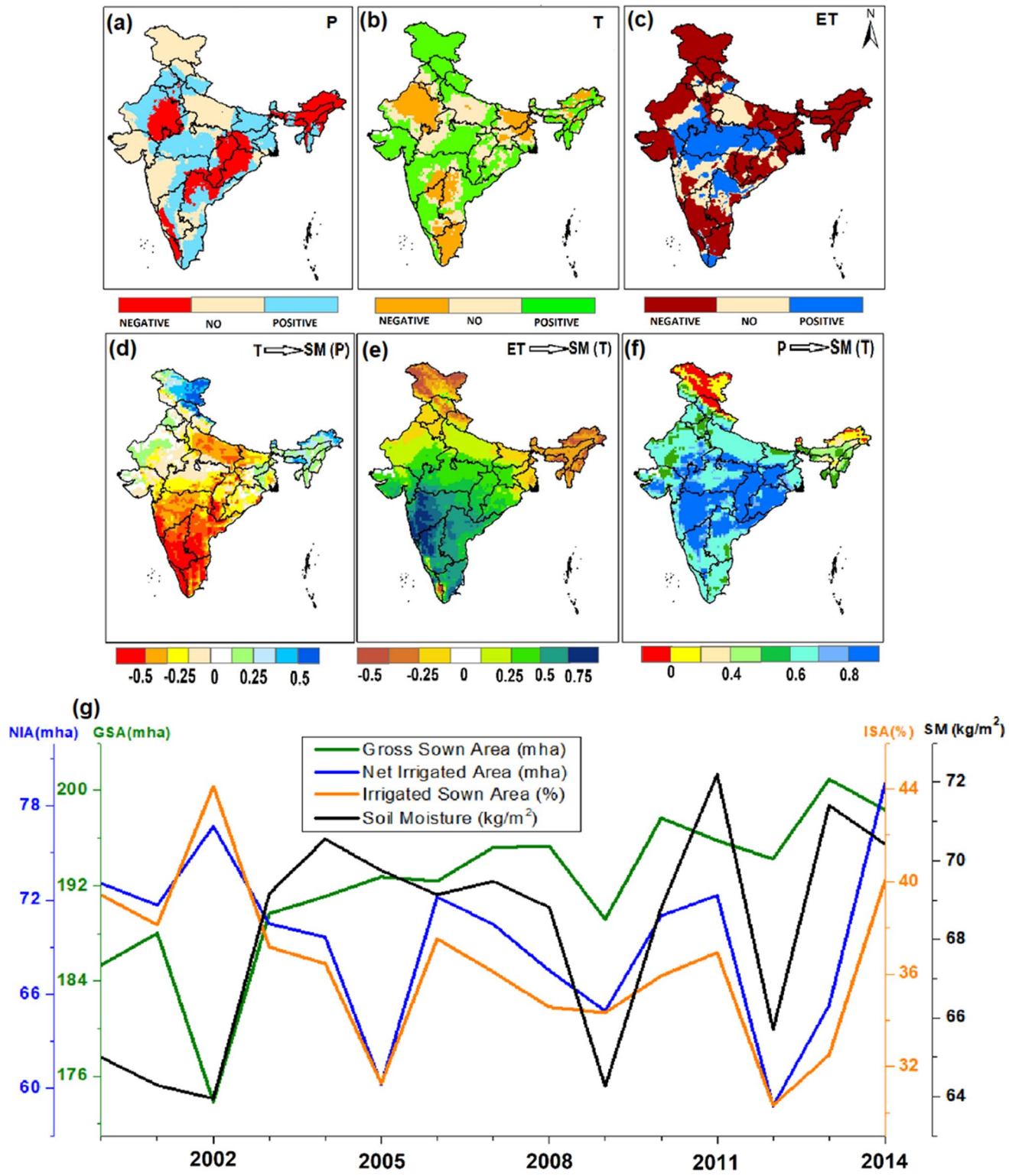

Fig. 4 Climate and Anthropogenic Drivers. **a** Relative influence (negative/positive) of the long-term changes in precipitation (drying/showering), **b** T (cooling/warming) and **c** evapotranspiration on long-term changes in soil moisture (drying/moistening) for the period 2000–2019. **d** The partial correlation between soil moisture (SM) and temperature (T) with precipitation (P) as covariate. **e** Soil moisture (SM) and evapotranspiration (ET) with temperature (T) as covariate. **f** Soil moisture (SM) and precipitation (P) with temperature (T) as covariate. **g** Variability of soil moisture (kg/m^2) with gross sown area (GSA), net irrigated area (NIA) and the percentage of irrigated sown area (ISA) during the period 2000–2014

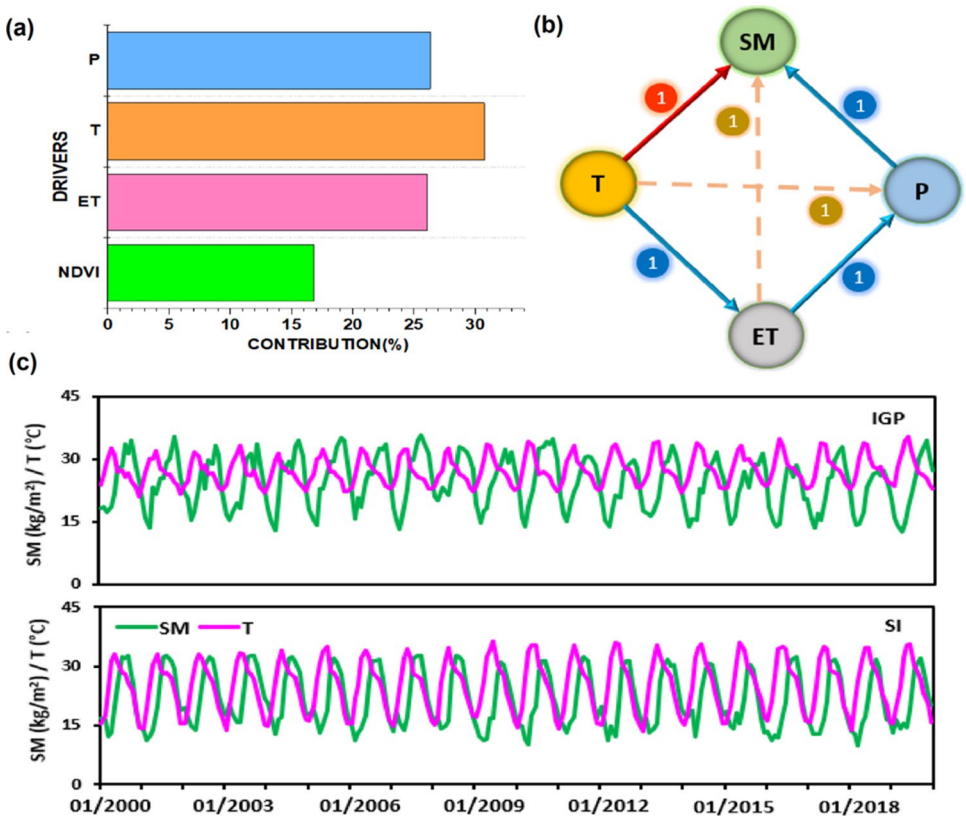

Fig. 5 Role of Climate drivers. **a** Machine Learning (ML) technique, Random Forest (RF)-based relative contribution of drivers precipitation (P), temperature (T), evapotranspiration (ET) and Normalised Difference Vegetation Index (NDVI) in soil moisture (SM) variability. **b** Granger Causality network graph with the links and lags among SM and its drivers (red line: negative link, blue line: positive link). **c** The monthly time series of SM and T for selected regions of Indo Gangetic Plain (IGP) and South India (SI)

1 month. However, there is a negative influence of T and ET in that region, which outplay the positive influence of P on SM. Also, T has a higher contribution in modifying SM, and SM-T have a Granger "cause and effect" relationship. The monthly time series of SM and T for IGP and SI exhibits the cycle of warming-induced moisture stress at a lag of 1 month (Fig. 5c).

Warming: a major driver for soil moisture stress

We here employ land T, soil T and SHF as three metrics to quantify warming. We find that T and soil T are very closely related (0.91), T and SHF (0.61), soil T and SHF (0.58) and also exhibit strong positive relationships. SM-T relation has a gradient from south to north, as it is largely negative in SI and some areas of CI. SM has a similar relation with soil T and SHF, for which soil T and SHF has a stronger negative control in SI (-0.4 to -0.8) and IGP (<-0.4) (Fig. S10). There is a predominant warming of land T (0.59 ℃/dec) and soil T (0.48 ℃/dec) in India during the period 2000–2019. The SHF is also increased (0.16 W/m^2/dec) during the same period. The spatial pattern of land T change is also replicated in the soil T with a substantial warming in SI and IGP. The SHF has also increased in SI, eastern Himalaya, NE and eastern areas of IGP (Fig. 6a, b, c). Therefore, land T, soil T and SHF show predominant warming in SI and some areas of IGP. Conversely, the land T and soil T changes show cooling in the forest areas of hilly region, NE, CI and Western Ghats. SHF is also reduced in NW and eastern areas in IGP. Higher temperatures generally lead to reduction in nutrients and water retention capacity, which degrade the soil. The application of synthetic fertilisers to replenish the soil has also found to be increased, about 34%, during the period 2000–2018. There has been an enhancement (7.6%) in the manures added to the soil in that period. In addition, the biological fixation in soil is highly increased (42%) during the period 2000–2018 (Fig. 6d). The higher soil T also promoted greater biological fixation, and therefore, soil warming is the major driver of the depleted soil nutrients, which is compensated by adding artificial agents such as synthetic fertilisers and manures to the soil. Although these would enhance the yield for a shorter period, they eventually degrade the soil.

Soil moisture stress and food security

There is a notable relationship between the grain yield and SM. In monsoon (June–September) season, SM is well related to the grain yield ($r=0.57$). This relationship is relatively stronger ($r=0.66$) in the late monsoon period (August–September), portraying the role of SM in the cropland productivity and annual grain yield (Mishra 2020). SM is the major driver that regulates photosynthetic activity and terrestrial primary productivity, as demonstrated in Fig. 7.

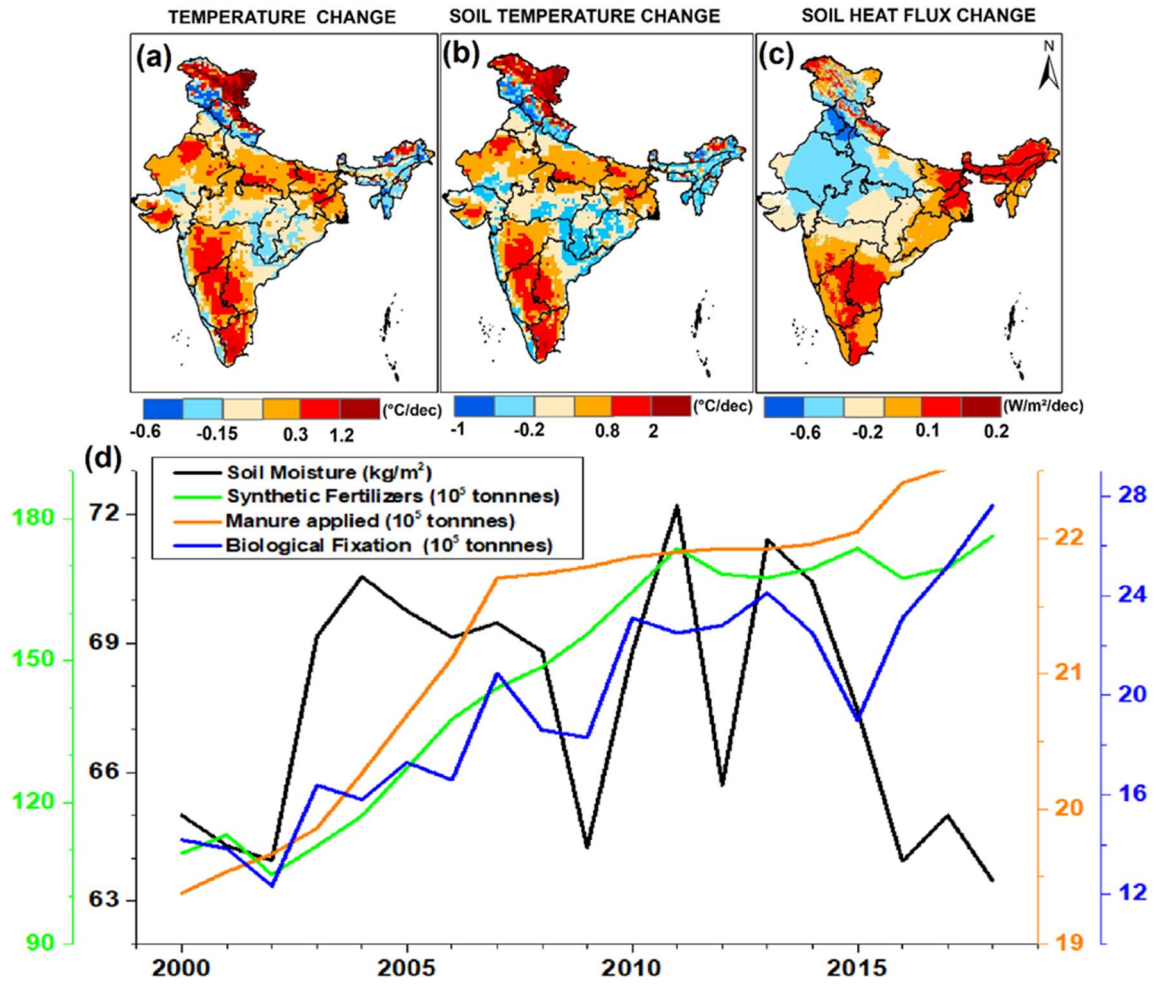

Fig. 6 Warming and anthropogenic drivers. The long-term change in (**a**) temperature (cooling/warming, ℃/dec), (**b**) soil temperature (℃/dec) and (**c**) soil heat flux (SHF, W/m^2/dec) over the period 2000–2019. **d** Temporal evolution of soil moisture, synthetic fertilisers added to the soil, manure applied to the soil and biological fixation in the soil during the period 2000–2018

The SM changes in both CCI and GLDAS data are consistent in most regions (Fig. S11). The enhanced SM (moistening) promotes increased GPP (greening) and this phenomenon is termed as moisture induced greening, which is predominant in NW. This region also has reduced SHF that promotes soil water retention. The negative influence of warming and ET reduce SM (drying) in SI and eastern areas of IGP. There is severe warming in these regions as found in both land and soil temperatures. SHF has also increased in these regions, leading to a reduction in SM, i.e. warming induced moisture stress, which reduces GPP (browning) in these areas.

Furthermore, it can be ascertained that ΔSM–ΔGPP coupling is more predominant for croplands (Fig. 7 and S1). Therefore, to get more insights on impact of SM drying on cropland productivity, we further investigate the change in yield of major food crops such as wheat, rain-fed rice, maize and soyabean in recent decade (2010–2019) from the previous decade (2000–2009) (Fig. S12). There is reduction in yield for wheat (Bihar (alluvium soil) and north Madhya Pradesh (black soil)) and rain-fed rice (West Bengal and SI (red and yellow soil)). Soyabean yield is reduced in its area of production with black soil in CI. Decrease in maize yield is observed in some areas (Bihar (alluvium soil) and Madhya Pradesh (black soil)). Therefore, the warming-induced moisture stress is a serious threat to cropland productivity in India, particularly in the agriculture intensive regions of SI and IGP.

To gain insights on the near future changes in SM and its drivers, we find the change in SM, T and P as projected from the historical (2015–2019) to near future (2020–2030), and population dynamics for the period 2000–2100. We find that most croplands in India will be experiencing severe SM drying (> 1 kg/m^2) and predominant warming (> 0.5℃) by 2030. Additionally, substantial P drying (> 0.2 mm/day) is also projected for the western, eastern and some CI and SI regions (Fig. 8 a, b, c). Furthermore, the changes in SM,

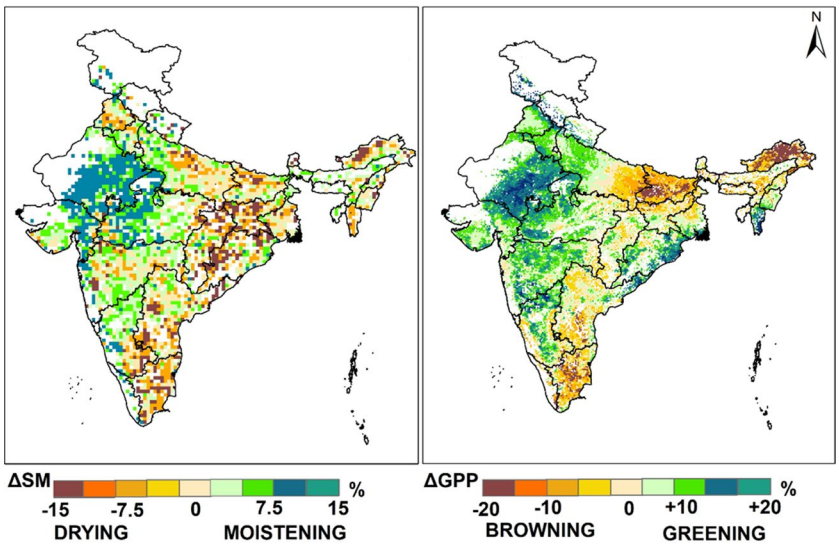

Fig. 7 Changes in soil moisture and terrestrial productivity. The long-term change (%) in soil moisture (increasing as moistening/decreasing as drying) and gross primary productivity (GPP) (enhanced/greening, reduced/browning) for the period 2000–2019

T and P as projected in the far future, i.e. end of the century (2090–2100) from the historical (2015–2019), reveal that warming-induced moisture stress is exhibited in the eastern region of India, particularly in the eastern IGP as they show SM drying, intense warming and decline in P (Fig. 8e, f, g). Also, there is a reduction in food grain yield in SI (rice), CI (soyabean and maze) and IGP (wheat) during recent decade (2010–2019) from the previous (2000–2009) (Fig. 8d). Interestingly, the eastern IGP suffers from warming-induced moisture stress that reduces cropland productivity (browning) there (Fig. S13). There is decline in major crops yield in regions of warming-induced moisture stress, which expand to the breadbasket of the world and threaten the food security of the most populous country in the world.

Discussion

Growing concerns of food security in the drying scenario

The livelihood of a significant portion of India's 1.4 billion population is based on agriculture (Ault 2020). Since the green revolution in the 1970s, food grain yield has increased significantly owing to improvements in available croplands, irrigation, seeds and fertiliser applications (Revadekar and Preethi 2012; Kuttippurath and Kashyap 2023). However, recent agricultural droughts and crop production in India are very well linked to the depleted SM (Mishra et al. 2014, Shah et al. 2021). SM has a major control on sustaining photosynthesis (Kashyap et al. 2022), productivity (Dubey and Ghosh 2023) and carbon sequestration potential (Kashyap et al. 2023a) in India. Additionally, utilising SM, the soil–plant continuum maintains ET and the land–atmosphere feedbacks during dry seasons in India (Sebastian et al. 2023). Thus, there is a strengthening of carbon–water cycle in India during recent decades in the rising moisture stress scenario (Kashyap and Kuttippurath 2024). Still, the changes in SM and its implication for food security are not adequately explored for India, a country that has a strong agrarian economy with unprecedented population growth.

This study incorporates both remote sensing measurements (CCI) as well as process-based LSM data (GLDAS) to estimate robust long-term SM dynamics, their mechanisms, relation with terrestrial productivity and implications on food security. To unravel the mechanism of warming-induced moisture stress, we also utilise the soil T and SHF data in addition to other climate drivers (P, T and ET). Our study not only investigates the impact of climate drivers on SM, but accounts also for the anthropogenic control in terms of GSA, NIA, ISA, synthetic fertilisers and manures added to the soil, and biological fixation. Unlike the conventional correlation and trend analysis, we incorporate a suite of mathematical and statistical techniques, including RF and Granger Causality to make our analysis robust. We find that SM drying is prevalent in much of the country in recent decade with hotspots in the eastern IGP and parts of SI. Also, the SM drying is very severe during the agricultural seasons of Kharif and Rabi, which is 9 and 6 times, respectively, of the global SM reduction rate (Peng et al. 2023). SM stress is also found in these regions by other studies (e.g. Pangaluru et al. 2019) and we attribute it to warming, consistent with Parida et al. (2020) and Kashyap et al. (2023a). Moreover, the CI and SI have significant dry season drying due to reduction in P and intense warming driven by the warming of Indian and Atlantic Oceans (Mishra 2020). However, increased P and reduced SHF in NW has led to enhanced SM there, called showering-induced moistening. Thus, showering-induced moistening in NW and warming-induced moisture stress in SI and eastern IGP are the two key mechanisms

that regulate the long-term SM changes in India. T is the most dominant driver of SM, and warming leads to higher ET that depletes SM despite the increase in P. In addition to climate change, irrigation has a significant impact on SM variability in dry seasons (Ambika and Mishra 2019). The impact of irrigation on SM is significant because surface and groundwater irrigation are used to make up for SM deficits during dry seasons in the irrigated lands. Henceforth, anthropogenic land management has a substantial impact on SM during dry seasons.

Implications and constraints

Despite the projected increase in the Indian summer monsoon P in the future, increased warming and reduced P during the dry seasons can result in severe deficit in SM in India (Mishra et al 2014; Mishra 2020). The frequency of simultaneous hot and dry extremes will increase by about five times in future (Im et al. 2017). SM drying depletes the terrestrial productivity in the croplands that lead to decline in the yields of major food crops such as wheat, rain-fed rice, maize and soyabean. Therefore, in the global warming context with rapidly growing population, warming-induced moisture stress is a serious threat to food security of India and similar agro-climatic countries/regions of the world. By the end of the 21st century, the breadbasket of IGP can be extremely vulnerable to warming-induced moisture stress. As India is a large exporter of food grains, decline in crop productivity in the breadbasket of the world can disrupt the global food security, particularly in the areas of rapidly growing population in Southeast Asia and Africa. Apart from food security, SM drying has adverse impacts on irrigation and groundwater. It can also trigger future climatic extremes such as heatwaves, fires and land degradation (Zhou et al. 2024).

The findings are based on the remote sensing, process-based LSM and reanalysis datasets. The ground-based SM measurements, flux towers for measuring terrestrial productivity and field-based crop yield measurements would enhance our analysis. Also, the findings are based on the specific datasets and statistical methods, which might vary from other studies that employ different datasets and statistical approach. Owing to the uncertainty of CCI estimates in the earlier decades (Dorigo et al. 2017), availability of MODIS satellite data since 2000 and the effects of COVID-induced lockdown on the terrestrial ecosystems in India (Kashyap et al. 2023b), our study period is restricted to 2000–2019.

Recommendations

The 1-month temporal lag of warming-induced moisture stress indicates the need for climate resilient agricultural practices. Additionally, bio-fortified and high-yielding seeds may be introduced. Change in sowing and harvesting dates of various crops might help in better yield. Crop diversification and organic farming are needed for maintaining good yield in the future warming-induced moisture stress scenario. Also, there is a constant need to improve the agricultural technologies to enhance the resilience of croplands to the changing climate. Better coordination among various agricultural sectors such as crops, agropastoral, agroforestry and livestock are required to establish a comprehensive landscape management system that accounts for sustainable and judicious use of land and water. Improved post-harvest storage of food grains and their distribution are required in the periods of reduced crop production.

In addition, planting water-efficient crops like millets (Ragi and Jowar) and sorghum in drying areas could be a way to counter the challenge of warming-induced moisture stress for food security. Also, crop switching like rice to pearl millet, sorghum in Kharif and wheat to sorghum in Rabi can be effective technique to reduce crop water consumption and improve nutritional value (Chakraborti et al. 2023). Incorporating a more conservative agricultural approach and improving agronomic management can be some of the other ways to combat this. Improved and more efficient irrigation facilities where better water management is ensured should be utilised. Additionally, mulching and crop row spacing are some of the examples of crop management practices that can be utilised to reduce SM drying as it impedes soil evaporation by lowering ET and improving soil and crop water retention ability. Also, better short-term and long-term forecasts of SM are very much needed to help the farmers to be better prepared to combat climate change induced threats. There is a need of more studies in the domain of intersection of carbon and water cycles. Some studies should focus on specific regions like IGP, which is the most irrigated breadbasket of the world. SI experience intense warming and drying in recent decades, which warrants more studies on the impact of changing climate on land resources.

Conclusions

Soil Moisture is the predominant driver of terrestrial photosynthesis, productivity, carbon sequestration and ecosystem health, and it maintains the land–atmosphere feedbacks during dry seasons in India. The warming world with erratic rainfall and enhanced ET can change the available SM. This is the first study that explores the SM dynamics based on both remote sensing (ESA CCI) and process-based land surface model (GLDAS) data by considering key climatic (P, T, ET and NDVI), anthropogenic (agricultural data, irrigation, fertilisers

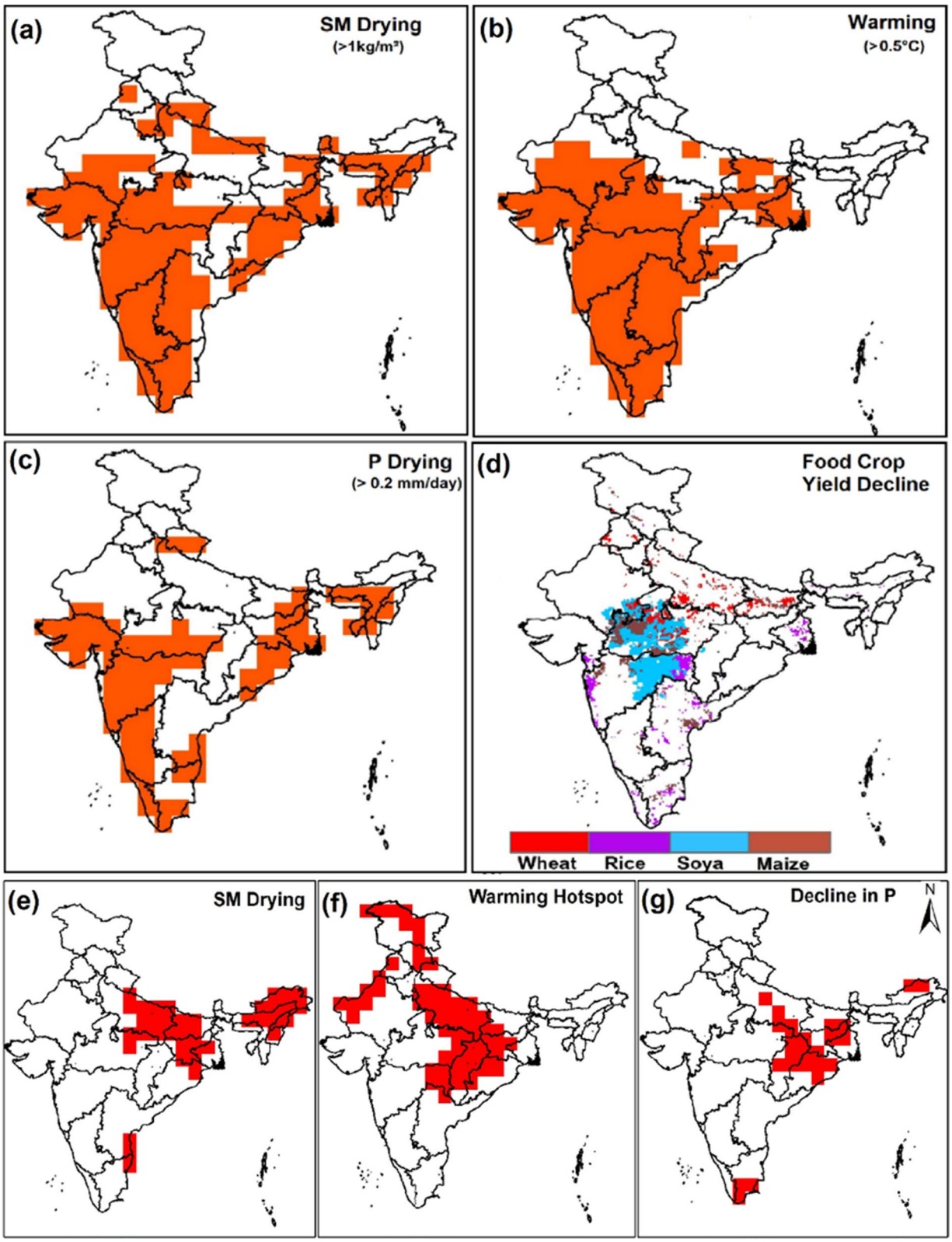

Fig. 8 Food security. The regions of (**a**) decrease in soil moisture (> 1 kg/m^2), (**b**) increase in temperature (> 0.5 ℃), (**c**) decrease in precipitation (> 0.2 mm/day) between the focal periods 2015–2019 and 2020–2030, (**d**) decline in the yield, i.e. total above ground production (TAGP) of major food crops in winter wheat, rain-fed rice, soyabean and maize grain during recent decade (2010–2019) in comparison to previous decade (2000–2009), (**e**) decrease in soil moisture, (**f**) increase in temperature (> top 10 percentile) and (**g**) decrease in precipitation between the periods 2015–2019 and 2090–2100

and manures) drivers and their implications on terrestrial productivity and food security of India. We find that SM peaks in post-monsoon as it is colder and sufficiently wet, but hits bottom in summer due to very warm and dry conditions. There is a soil moisture stress in all seasons in recent (2010–2019) decade in comparison to previous decade (2000–2009). The surface warming, along with enhanced soil T and SHF, drives reduction of SM in SI and eastern IGP: the agriculture-intensive areas of India. This mechanism of soil moisture decline is termed as warming-induced moisture stress. The SM variability is also consistent with that of the changes in GSA, NIA and ISA. The long-term SM and GPP changes show a good agreement for the croplands as the regions of decline in SM results in reduction of GPP (browning) and yields of major food crops such as wheat, rain-fed rice, maize and soyabean.

Henceforth, the warming-induced soil moisture stress is a serious threat to the cropland productivity in SI and eastern IGP. In a warming world, the ever-growing population would demand more food, but the warming-induced moisture stress is a major concern for food security in India and similar agricultureintensive regions of the world. This study adds new insights into the understanding of SM dynamics, particularly the SM drying due to warming and its implications on cropland productivity and food security of India and similar agrometeorological zones in the world. We employ a robust combination of remote sensing, process-based LSMs, reanalyses and a suite of statistical techniques including partial correlation, ML-based RF and Granger Causality for this analysis. Availability of more advanced observations, ML techniques and measurements of carbon–water fluxes would improve these analyses. These findings would help in drafting policy-making decisions for advancement in agricultural technologies and land management practices to counter the constant challenge of warminginduced moisture stress, in the scenario of rising population and anthropogenic climate change, through effective adaption and mitigation strategies.

Supplementary Information The online version contains supplementary material available at https://doi.org/10.1007/s11356-024-35107-7.

Acknowledgements We thank the Director, Indian Institute of Technology Kharagpur (IIT Kgp), Chairman of CORAL IIT Kgp and the Ministry of Education (MoE) for facilitating the study. RK acknowledges the support from Prime Minister's Research Fellowship (PMRF), MoE. We thank the NASA's LPDAAC team for providing the MODIS landcover, NDVI, ET and GPP products. ESA CCI for providing volumetric soil moisture data. Giovanni's online data system developed and maintained by the NASA GES DISC for providing the GPM level–3 precipitation data; GLDAS for providing land temperature, soil moisture content and soil temperature datasets; FLDAS for providing soil heat flux datasets; Krishnankutty Ambika A & Mishra V for making the high-resolution remote sensing-based irrigated area data; and Ministry of Agriculture and Farmers Welfare, Government of India, for providing all the agriculture data. We also sincerely thank FAO for providing soil data, IMD for providing the precipitation and temperature datasets.

Author contribution RK: conceptualization, methodology, data analyses, visualization, validation, software, writing—original draft and editing of the original draft. JK: conceptualization, methodology, visualization, supervision, writing—review and editing of the original draft.

Data availability All data are publicly available and are listed in Table 1.

Declarations

Ethics approval Not applicable.

Consent to participate Not applicable.

Consent for publication Not applicable.

Competing interests The authors declare no competing interests.

References

Ambika AK, Mishra V (2019) Observational evidence of irrigation influence on vegetation health and land surface temperature in India. Geophy Res Lett 46(22):13441–13451. https://doi.org/10.1029/2019GL084367

Ambika AK, Wardlow B, Mishra V (2016) Remotely sensed high resolution irrigated area mapping in India for 2000 to 2015. Sci Data 3(1):1–14. https://doi.org/10.1038/sdata.2016.118

Ault TR (2020) On the essentials of drought in a changing climate. Science 368:256–260. https://doi.org/10.1126/science.aaz5492

Bhimala KR, Rakesh V, Prasad KR, Mohapatra GN (2020) Identification of vegetation responses to soil moisture rainfall and LULC over different meteorological subdivisions in India using remote sensing data. Theor Appl Climatol 142(3):987–1001. https://doi.org/10.1007/s00704-020-03360-8

Chakraborti R, Davis KF, DeFries R, Rao ND, Joseph J, Ghosh S (2023) Crop switching for water sustainability in India's food bowl yields co-benefits for food security and farmers' profits. Nat Water 1(10):864–878. https://doi.org/10.1038/s44221-023-00135-z

Chen C et al (2019) China and India lead in greening of the world through land-use management. Nat Sustain 2(2):122–129. https://doi.org/10.1038/s41893-019-0220-7

de Jeu RA, Wagner W, Holmes TRH, Dolman AJ, Van De Giesen NC, Friesen J (2008) Global soil moisture patterns observed by space borne microwave radiometers and scatterometers. Surv Geophys 29:399–420. https://doi.org/10.1007/s10712-008-9044-0

Deng Y et al (2020) Variation trend of global soil moisture and its cause analysis. Ecol Indic 110:105939. https://doi.org/10.1016/j.ecolind.2019.105939

Dorigo et al (2017) ESA CCI Soil Moisture for improved Earth system understanding: state- of- the art and future directions. Remote Sens Environ 203:185–215. https://doi.org/10.1016/j.rse.2017.07.001

Dubey N, Ghosh S (2023) The relative role of soil moisture and vapor pressure deficit in affecting the Indian vegetation productivity. Environ Res Lett 18(6):064012. https://doi.org/10.1088/1748-9326/acd2ef

Entekhabi DN, Joku EG, O'neill PE, Kellogg KH, Crow WT, Edelstein WN, Van Zyl J (2010) The soil moisture active passive (SMAP) mission. Procd IEEE 98(5):704–716. https://doi.org/10.1109/JPROC.2010.2043918

Eyring V, Bony S, Meehl GA, Senior CA, Stevens B, Stouffe RJ, Taylor KE (2016) Overview of the Coupled Model Intercomparison Project Phase 6 (CMIP6) experimental design and organization. Geosci Model Dev 9(5):937–1958. https://doi.org/10.5194/gmd-9-1937-2016

Furtak K, Wolińska A (2023) The impact of extreme weather events as a consequence of climate change on the soil moisture and on the quality of the soil environment and agriculture-a review. CATENA 231:107378. https://doi.org/10.1016/j.catena.2023.107378

Granger CW (1969) Investigating causal relations by econometric models and cross–spectral methods Econometrica, pp 424–438. https://www.jstor.org/stable/1912791

Green JK, Seneviratne SI, Berg AM, Findell KL, Hagemann S, Lawrence DM, Gentine P (2019) Large influence of soil moisture on long-term terrestrial carbon uptake. Nature 565(7740):476–479. https://doi.org/10.1038/s41586-018-0848-x

Grillakis MG, Koutroulis AG, Alexakis DD, Polykretis C, Daliakopoulos IN (2021) Regionalizing root-zone soil moisture estimates from ESA CCI soil water index using machine learning and information on soil vegetation and climate. Water Resour Res 57(5):e2020WR029249. https://doi.org/10.1029/2020WR029249

Gruber A, Scanlon T, van der Schalie R, Wagner W, Dorigo W (2019) Evolution of the ESA CCI Soil Moisture climate data records and their underlying merging methodology. Earth Sys Sci Data 11(2):717–739. https://doi.org/10.5194/essd-11-717-2019

Hirschi M, Mueller B, Dorigo W, Seneviratne SI (2014) Using remotely sensed soil moisture for land-atmosphere coupling diagnostics: the role of surface vs root-zone soil moisture variability. Remote Sens Environ 154:246–252. https://doi.org/10.1016/j.rse.2014.08.030

Humphrey V, Berg A, Ciais P, Gentine P, Jung M, Reichstein M, Frankenberg C (2021) Soil moisture-atmosphere feedback dominates land carbon uptake variability. Nature 592(7852):65–69. https://doi.org/10.1038/s41586-021-03325-5

Im ES, Pal JS, Eltahir EA (2017) Deadly heat waves projected in the densely populated agricultural regions of South Asia. Sci Adv 3(8):e1603322. https://doi.org/10.1126/sciadv.1603322

Jha S, Das J, Sharma A, Hazra B, Goyal MK (2019) Probabilistic evaluation of vegetation drought likelihood and its implications to resilience across India. Glob Planet Chang 176:23–35. https://doi.org/10.1016/j.gloplacha.2019.01.014

Jones B, BCO Neill (2020). Global one-eighth degree population base year and projection grids based on the shared socioeconomic pathways, Revision 01. Palisades, New York: NASA Socioeconomic Data and Applications Center (SEDAC). https://doi.org/10.7927/m30p-j498. Accessed May, 2023

Kashyap R, Kuttippurath J (2024) Unraveling the sensitivity and response of ecosystems to rising moisture stress in India. Ecosyst Health Sustain 10:0180. https://doi.org/10.34133/ehs.0180

Kashyap R, Pandey AC, Kuttippurath J (2022) Photosynthetic trends in India derived from remote sensing measurements during 2000–2019: vegetation dynamics and key climate drivers. Geocarto Int 37(26):11813–11829. https://doi.org/10.1080/10106049.2022.2060325

Kashyap R, Kuttippurath J, Kumar P (2023a) Browning of vegetation in efficient carbon sink regions of India during the past two decades is driven by climate change and anthropogenic intrusions. J Environ Manag 336:117655. https://doi.org/10.1016/j.jenvman.2023.117655

Kashyap R, Kuttippurath J, Patel VK (2023b) Improved air quality leads to enhanced vegetation growth during the COVID–19 lockdown in India. Appl Geogr 151:102869. https://doi.org/10.1016/j.apgeog.2022.102869

Kerr YH, Waldteufel P, Wigneron JP, Delwart S, Cabot F, Boutin J, Mecklenburg S (2010) The SMOS mission: new tool for monitoring key elements of the global water cycle. Proceed IEEE 98(5):666–687. https://doi.org/10.1109/JPROC.2010.2043032

Krishnamurthy RPK, Fisher JB, Choularton RJ, Kareiva PM (2022) Anticipating drought-related food security changes. Nat Sustain 5(11):956–964. https://doi.org/10.1038/s41893-022-00962-0

Kumar KK, Rajagopalan B, Hoerling M, Bates G, Cane M (2006) Unraveling the mystery of Indian monsoon failure during El Niño. Science 314(5796):115–119. https://doi.org/10.1126/science.1131152

Kumar R, Kuttippurath J, Gopikrishnan GS, Kumar P, Varikoden H (2023) Enhanced surface temperature over India during 1980–2020 and future projections: causal links of the drivers and trends. npj Clim Atmos Sci 6(1):164. https://doi.org/10.1038/s41612-023-00494-0

Kuttippurath J, Kashyap R (2023) Greening of India: forests or croplands? Appl Geogr 161:103115. https://doi.org/10.1016/j.apgeog.2023.103115

Lal P, Shekhar A, Gharun M, Das NN (2023) Spatiotemporal evolution of global long-term patterns of soil moisture. Sci Tot Environ 867:161470. https://doi.org/10.1016/j.scitotenv.2023.161470

Liu YY et al (2011) Developing an improved soil moisture dataset by blending passive and active microwave satellite-based retrievals. Hydrol Earth Sys Sci 15(2):25–436. https://doi.org/10.5194/hess-15-425-2011

Liu Y et al (2015) Agriculture intensifies soil moisture decline in Northern China. Sci Rep 5(1):1–9. https://doi.org/10.1038/srep11261

Lobell DB, Burke MB, Tebaldi C, Mastrandrea MD, Falcon WP, Naylor RL (2008) Prioritizing climate change adaptation needs for food security in 2030. Science 319(5863):607–610. https://doi.org/10.1126/science.1152339

Ma H, Zeng J, Zhang X, Peng J, Li X, Fu P, Wigneron JP (2024) Surface soil moisture from combined active and passive microwave observations: integrating ASCAT and SMAP observations based on machine learning approaches. Rem Sens Environ 308:114197. https://doi.org/10.1016/j.rse.2024.114197

Mahto SS, Mishra V (2023) Increasing risk of simultaneous occurrence of flash drought in major global croplands. Environ Res Lett 18(4):044044. https://doi.org/10.1088/1748-9326/acc8ed

Marvel K, Cook BI, Bonfils CJ, Durack PJ, Smerdon JE, Williams AP (2019) Twentieth-century hydroclimate changes consistent with human influence. Nature 569(7754):59–65. https://doi.org/10.1038/s41586-019-1149-8

Mishra V (2020) Relative contribution of precipitation and air temperature on dry season drying in India, 1951–2018. J Geophys Res: Atmos 125(15):e2020JD032998. https://doi.org/10.1029/2020JD032998

Mishra V, Shah R, Thrasher B (2014) Soil moisture droughts under the retrospective and projected climate in India. J Hydrometeor 15(6):2267–2292. https://doi.org/10.1175/JHM-D-13-0177.1

Nair PJ, Chakraborty A, Varikoden H, Francis PA, Kuttippurath J (2018) The local and global climate forcings induced inhomogeneity of Indian rainfall. Sci Rep 8(1):6026. https://doi.org/10.1038/s41598-018-24021-x

Pai DS, Rajeevan M, Sreejith OP, Mukhopadhyay B, Satbha NS (2014) Development of a new high spatial resolution (0.25× 0.25) long period (1901–2010) daily gridded rainfall data set over India and its comparison with existing data sets over the region. Mausam 65(1):1–18. https://doi.org/10.54302/mausam.v65i1.851

Pangaluru K, Velicogna I, Mohajerani Y, Ciracì E, Charakola S, Basha G, Rao SVB (2019) Soil moisture variability in India: relationship of land surface–atmosphere fields using maximum covariance analysis. Remote Sens 11(3):335. https://doi.org/10.3390/rs11030335

Parida BR, Pandey AC, Patel NR (2020) Greening and browning trends of vegetation in India and their responses to climate and non-climate drivers. Climate 8(8):92. https://doi.org/10.3390/cli8080092

Patel VK, Kuttippurath J (2022) Significant increase in water vapour over India and Indian Ocean: implications for tropospheric warming and regional climate forcing. Sci Tot Environ 838:155885. https://doi.org/10.1016/j.scitotenv.2022.155885

Patel VK, Kuttippurath J, Kashyap R (2024) Rise in water vapour driven by moisture transport facilitates water availability for the greening of global deserts. Sci Tot Environ 946:174111. https://doi.org/10.1016/j.scitotenv.2024.174111

Peng C, Zeng J, Chen KS, Li Z, Ma H, Zhang X, Bi H (2023) Global spatiotemporal trend of satellite-based soil moisture and its influencing factors in the early 21st century. Rem Sens Environ 291:113569. https://doi.org/10.1016/j.rse.2023.113569

Raoult N, Delorme B, Ottlé C, Peylin P, Bastrikov V, Maugis P, Polcher J (2018) Confronting soil moisture dynamics from the ORCHIDEE land surface model with the ESA-CCI product: perspectives for data assimilation. Remote Sens 10(11):1786. https://doi.org/10.3390/rs10111786

Revadekar JV, Preethi B (2012) Statistical analysis of the relationship between summer monsoon precipitation extremes and foodgrain yield over India. Int J Climatol 32(3):419–429. https://doi.org/10.1002/joc.2282

Roxy MK, Ritika K, Terray P, Murtugudde R, Ashok K, Goswami BN (2015) Drying of Indian subcontinent by rapid Indian Ocean warming and a weakening land-sea thermal gradient. Nat Comms 6(1):1–10. https://doi.org/10.1038/ncomms8423

Samaniego L et al (2018) Anthropogenic warming exacerbates European soil moisture droughts. Nat Clim Chang 8(5):421–426. https://doi.org/10.1038/s41558-018-0138-5

Sebastian DE, Murtugudde R, Ghosh S (2023) Soil-vegetation moisture capacitor maintains dry season vegetation productivity over India. Sci Rep 13(1):888. https://doi.org/10.1038/s41598-022-27277-6

Seneviratne SI, Corti T, Davin EL, Hirschi M, Jaeger EB, Lehner I, Teuling AJ (2010) Investigating soil moisture-climate interactions in a changing climate: a review. Earth Sci Rev 99(3–4):125–161. https://doi.org/10.1016/j.earscirev.2010.02.004

Shah D, Shah HL, Dave HM, Mishra V (2021) Contrasting influence of human activities on agricultural and hydrological droughts in India. Sci Tot Environ 774:144959. https://doi.org/10.1016/j.scitotenv.2021.144959

Skofronick-Jackson G, Kirschbaum D, Petersen W, Huffman G, Kidd C, Stocker E, Kakar R (2018) The Global Precipitation Measurement (GPM) mission's scientific achievements and societal contributions: reviewing four years of advanced rain and snow observations. Q J R Meteorol Soc 144:27–48. https://doi.org/10.1002/qj.3313

Srivastava AK, Rajeevan M, Kshirsagar SR (2009) Development of a high resolution daily gridded Tdata set (1969–2005) for the Indian region. Atmos Sci Lett 10(4):249–254. https://doi.org/10.1002/asl.232

Trenberth KE, Dai A, Van Der Schrier G, Jones PD, Barichivich J, Briffa KR, Sheffield J (2014) Global warming and changes in drought. Nat Clim Chang 4(1):17–22. https://doi.org/10.1038/nclimate2067

Wang L, Li X, Chen Y, Yang K, Chen D, Zhou J, Huang J (2016) Validation of the global land data assimilation system based on measurements of soil temperature profiles. Agric for Meteorol 218:288–297. https://doi.org/10.1016/j.agrformet.2016.01.003

Xia Y et al (2019) Regional and global land data assimilation systems: innovations, challenges and prospects. J Meteorol Res 33(2):159–189. https://doi.org/10.1007/s13351-019-8172-4

Zhou S, Williams AP, Lintner BR, Berg AM, Zhang Y, Keenan TF, Gentine P (2021) Soil moisture-atmosphere feedbacks mitigate declining water availability in drylands. Nat Clim Chang 11(1):38–44. https://doi.org/10.1038/s41558-020-00945-z

Zhou J, Teuling AJ, Seneviratne SI, Hirsch AL (2024) Soil moisture-temperature coupling increases population exposure to future heatwaves. Earth's Future 12(7):e2024EF004697. https://doi.org/10.1029/2024EF004697

communications earth & environment

Article

A Nature Portfolio journal

https://doi.org/10.1038/s43247-025-02694-3

Ecological droughts increased in India with changing Indian summer monsoon and human interventions

Rahul Kashyap, Jayanarayanan Kuttippurath ✉ & Vikas Kumar Patel

Substantial ecological ramifications of moisture stress in ecosystems is called ecological droughts, and are largely unexplored for India. Here, we investigate ecological droughts, their drivers and implications in Indian Summer Monsoon during 2000–2019 based on remote sensing and machine learning. Ecological droughts are increasing in the ecologically fragile pristine forests and croplands that decline vegetation health in India. Meteorological aridity (23.9%) and ocean warming (18.2%) primarily drive the ecological droughts, as suggested by the Random Forest model. Causal analysis reveals that ocean warming indirectly triggers ecological droughts in India. The human intervention in forests also leads to their degradation. The rising ecological droughts due to changing vegetation-climate-human nexus in a shifting monsoon system is a concern for sustainability, food security and climate change mitigation in India. It is thus imperative to consider the ecological repercussions of droughts in policy making and combat their threats through judiciously engineered nature-based solutions.

Although they constitute about 5% of the natural disasters, droughts affect 55 million people every year and are projected to impact around 40% of the world population by 2030; making them the most hazardous and complex extreme events[1,2]. Droughts are conventionally defined as a period of a sustained decline in water availability below a certain threshold depending upon the region[3]. Based on the implications and indicators, droughts are typically classified as: meteorological (precipitation, P), hydrological (stream flow), agricultural (soil moisture, SM) and socio-economic (more demand than supply of water for human consumption)[3]. WMO defines meteorological droughts as deficit in P below 20th percentile for a minimum duration of 30 days[4]. Agricultural drought is the occurrence of insufficient SM (below 30–40% of the field capacity) typically for 2–4 weeks during the crop growth stage that has adverse impact on cropland yields, farm economics and food security[3,5]. Vegetation drought refers to reduced vegetation vigor in both natural vegetation and anthropogenic vegetation (croplands and plantations) due to decreased moisture availability (P and SM)[6–8]. Notable and large-scale ecological changes are becoming more frequent due to human-induced climate change. This is caused by erratic P, extreme high temperature (T), increased land and atmospheric evaporative demand, faster and longer-lasting droughts, and altered drought timings[2,5,6]. Current definitions of droughts, which focus on its impacts on hydroclimate, agriculture, water resources and society, have a limited perspective as it overlooks its ecological impacts[9,10].

Prolonged periods of water deficits that lead to changes in ecological conditions such as ecosystem structure, functioning, biodiversity and services beyond critical thresholds are termed as "ecological droughts"[11,12]. Rapidly changing climate, altered human water use and shifting climatic oscillations drive ecological droughts[10,12]. These changes have long-term ramifications such as hindered plant growth and development, decline in photosynthesis, changes in the rates of carbon, nutrient and water cycling, enhanced fires, insect outbreaks, and the extinction of local species[10–12]. Furthermore, ecological droughts have long-term (multiple years) impacts, in contrast to agricultural (seasonal) and vegetation (weekly to seasonal) droughts[10–12]. Moisture scarcity adversely affects photosynthesis and ecosystem functioning in natural ecosystems that are devoid of human water managements (e.g. irrigation), and eventually lead to ecological droughts[11–14]. Climate variability along with anthropogenic interventions make the complex, dynamic and auto-regulatory mechanism of ecological droughts across the globe[10–14].

Droughts lead to water scarcity, food insecurity, depleted forest resources and degradation of environment, which are severe in South Asia[15–18]. Meteorological droughts are widely studied for the Indian region, but ecological droughts remain largely unexplored. There were a few attempts to monitor vegetation health and its variability during meteorological droughts on regional[19–21] and pan India[22–24] scales. A minimum of 50% of the total area in 16 out of 24 major river basins is at a high risk of experiencing vegetation droughts due to depleted SM

CORAL, Indian Institute of Technology Kharagpur, Kharagpur, India. ✉e-mail: jayan@coral.iitkgp.ac.in

in India. Furthermore, more than half of the total area for each vegetation type exhibits a lack of resilience to vegetation droughts[7]. This highlights the vulnerable state of terrestrial ecosystems in India to moisture stress[17,18,25]. Since the Indian summer monsoon (ISM) contributes about 75% to the annual P, it plays a notable role in maintaining SM[26], natural vegetation growth and crop production in India[25,27,28]. Large-scale climate oscillations such as El Niño Southern Oscillation (ENSO) and Indian Ocean Dipole (IOD) greatly influence the ISM[29,30], vegetation health and ecosystem functioning in tropics[31,32] and India[33].

India is experiencing substantial changes in vegetation due to climate change and human influence[27,28,34,35]. India is largely greening due to improved irrigation and land management practices[36] and is the second largest contributor to the global greening[37]. However, browning is also observed in the efficient carbon sink regions of India and is a great concern[28]. India is one of the global hotspots of land-atmosphere interactions[38] and exhibits strengthening of carbon-water cycle coupling in the rising moisture stress context[17,18,25]. India is an agrarian economy with vast croplands and lush forests on which a huge population rely for their living. Therefore, in the climate change and increasing anthropogenic intervention scenario, ecological droughts are a potent threat for India's sustainability and food security, and demands a dedicated study. The science questions attempt to investigate here are: (i) What are the regions vulnerable to ecological droughts in India? (ii) What is the relation of various forms of aridity (meteorological, land evaporative and atmospheric) with ecological droughts in India? (iii) How does the ocean warming and climate oscillations impact vegetation health in India? (iv) How does the human-ecosystem interactions influence vegetation health in India? (v) What are the implications and recommendations to combat ecological droughts in India? To the best of our knowledge, this is the first comprehensive analysis of ecological droughts, drivers, mechanisms and implications for the region. Therefore, the findings would enable a better understanding of the ecological water demand and ecological ramifications of droughts, and the complex physical mechanisms involved in India and global regions of similar ecohydrology.

Results

Vegetation health and ecological drought vulnerability

Here, the Vegetation Condition Index (VCI), Temperature Condition Index (TCI) and Vegetation Health Index (VHI) during ISM months (June, July, August and September: JJAS) are presented to investigate the spatio-temporal variability in vegetation health and delineate the regions vulnerable to vegetation stress and ecological droughts during previous (2000–2009) and recent (2010–2019) decades, and the overall study period (2000–2019) (Fig. 1). Vegetation stress (VHI < 0.4) is predominant in regions of South India (SI) and North West (NW) as shown in Fig. 1. Southern regions experience severe vegetation stress (VHI < 0.2) in SI and are most vulnerable to ecological droughts as they have limited moisture availability, and generally support scanty vegetation (VCI, 0.2–0.4). These areas experience very high T, as reflected in higher TCI (> 0.6), which dries the moisture. The forests in the western Himalaya also experience vegetation stress (VHI < 0.2), with dense forest cover (VCI > 0.8). It is the very cold conditions (TCI < 0.4) that adversely affect vegetation health in this region and make vulnerable to ecological droughts. Contrarily, hilly areas (HR) in the eastern Himalaya, north east (NE) and some areas in Central India (CI), predominantly forests (VCI > 0.8), are least vulnerable to ecological droughts (VHI, 0.8–1) (Fig. 1a–c). Most of Indo-Gangetic Plain (IGP) have relatively healthier vegetation (VCI, 0.6–0.8) dominated by highly irrigated croplands, with less vulnerability to ecological droughts (VHI, 0.6–0.8). The rest of the vegetated regions in CI and eastern coast with warmer conditions show high TCI (0.6–0.8) with low vegetation stress (VCI, 0.4–0.6) and moderate vulnerability to ecological droughts (VHI, 0.4–0.6). There are changes in vegetation health and ecological droughts over the decades. In order to examine them, the study next looks into the relationship of ecological droughts with various forms of aridity.

Ecological droughts and aridity

This study considers the variability of moisture in terms of both P and SM in the vegetated Indian region during monsoon (JJAS) for the period 2000–2019 (Supplementary Fig. S1). Very small P (150–450 mm) and SM (40–60 kg/m^2) are observed in some areas of NW and SI. The rest of NW, some areas in SI show low P (450–750 mm) and SM (60–80 kg/m^2). These moisture deficit regions coincide with the vegetation stress there (VHI < 0.4) and are more vulnerable to ecological droughts. In contrast, the regions such as HR (eastern Himalaya), NE, Western Ghats and some areas in CI with ample P (1350–2700 mm) and SM (>100 kg/m^2) have vegetation in a better state (VHI > 0.8), and are less vulnerabile to ecological droughts. Interestingly, undeterred by considerable P (750–1050 mm) and SM (80–100 kg/m^2), some areas in the western CI and northern SI experience vegetation stress (VHI < 0.4), and are vulnerable to ecological droughts.

Therefore, three different aridity metrics: Evapotranspiration Ratio (ETR, evaporative aridity), Vapour Pressure Deficit (VPD, atmospheric aridity) and Palmer Drought Severity Index (PDSI, meteorological aridity) are also examined (Fig. 2a, b and Supplementary Fig. S1). The results reveal that the lowest ETR (0.3–0.45) is estimated in the western areas of NW and the southernmost SI. It indicates that these areas experience land evaporative stress, which lead to vegetation stress (VHI < 0.4) and are highly vulnerable to ecological droughts. These regions also experience a very high degree of atmospheric water demand (VPD, 1.5–2.5 kPa). The higher atmospheric aridity combined with higher temperature dry the land moisture. The highest ETR (0.9–1.0) is estimated for HR, NE, eastern IGP and eastern CI. The lowest (0.5–0 kPa) VPD is found in HR such as western Himalaya, some areas in NE and in the proximity of Western Ghats. These regions are less vulnerable to ecological droughts, except western Himalaya, where very cold conditions trigger vegetation stress. The rest of vegetated lands exhibit moderate ETR (0.6–0.75) and VPD (1.0–1.5 kPa), and are least vulnerable to ecological droughts (Fig. 2a, b). PDSI shows a distinct pattern in India during monsoon, with the lowest values (−3.5 to −0.5) in IGP and highest (1.0–2.5) in westernmost NW, SI, eastern coast and a small area in eastern Himalaya (Supplementary Fig. S1).

To explore the association between and among VHI and its drivers, Rotated Principal Component Analysis (RPCA) is performed with respect to the eigen values (Fig. 2d). The Principal Component 1 (PC1) is defined in rotated Principal Component Analysis (PCA) by SM (0.97), ETR (0.95), P (0.73) and VCI (0.95) with positive correlation, and a strong connection with VHI. In contrast, VPD (−0.93), T (−0.87) and SST (−0.63) are correlated negatively with PC1, indicating that VPD, T and SST negatively impact VHI. A high negative correlation is observed between VHI and VPD, and VHI and T. The moisture availability components SM, ETR and P have comparable variability as for VCI and VHI, as moisture is one of the key drivers of VCI and VHI during ISM in India. Principal Component 2 (PC2) is largely determined by the variability in VHI (0.97), TCI (0.82), PDSI (0.57) and SST (0.45). PC2 is also positively linked to VCI, P, T and ETR as they show similar variability like other drivers in PC2, including VHI. RPCA exhibits that moisture availability has a strong positive impact, but aridity, T and ocean heat have negative impact on the vegetation health, but opposite influence on ecological droughts.

Ecological droughts: temporal evolution with drivers, monsoon and climate oscillations

To further enhance our understanding of the changes in vegetation health and regions vulnerable to ecological droughts over the decades, the temporal evolution of VHI with aridity (ETR, PDSI and VPD), ocean heat (Sea Surface Temperature, SST), ISM and climatic oscillations i.e. Oceanic Niño Index (ONI), Indian Ocean Dipole (IOD) index i.e., Dipole Meridional Index (DMI), Pacific Meridional Mode (PMM) and North Atlantic Oscillation (NAO) are explored. The years of positive anomaly in VHI such as 2003, 2007, 2010–2012 and 2014–2019 are associated with non-ecological drought years. Contrarily, the years of marked negative anomaly in VHI during 2000–2002, 2004–2006, 2009, 2013 and 2015 indicate the

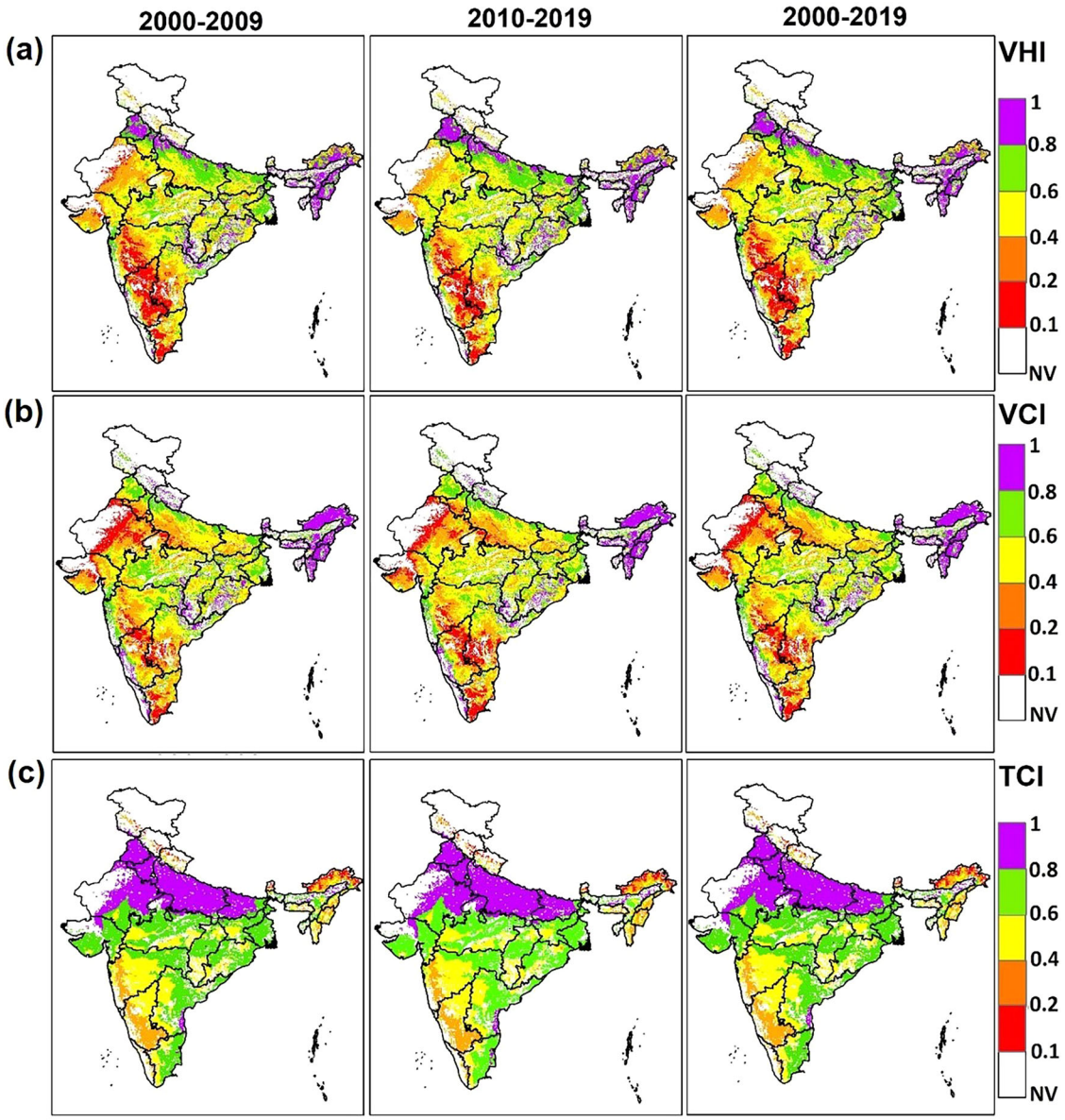

Fig. 1 | Vegetation health in India during Indian Summer Monsoon (ISM). **a** Vegetation Health Index (VHI), **b** Vegetation Condition Index (VCI) and **c** Temperature Condition Index (TCI) averaged for the Indian summer monsoon (ISM, June–September) season for the periods 2000–2009, 2010–2019 and 2000–2019.

ecological droughts that coincide with the years of high PDSI, VPD and low ETR. This signal is stronger in years 2002, 2009 and 2013 that indicates relatively severe ecological drought conditions (Fig. 2c). The years 2002, 2003, 2005, 2009, 2010, 2014–2017 and 2019 show lower P and higher SST, consistent with the drought years. Therefore, the years with high SST generally have negative VHI anomaly; suggesting the influence of ocean warming on triggering ecological droughts (Fig. 3d, e, and Supplementary Fig. S2). Our analyses of ONI and IOD depict vivid relationship with the VHI anomaly. The years of positive anomaly in ONI (i.e. El Niño years) and IOD such as 2002, 2004, 2009, 2012 and 2015 exhibit negative anomaly in VHI that lead to ecological droughts. In contrast, the years of negative anomaly in ONI (La Niña years) and IOD such as 2000, 2007, 2010, 2011, 2013 and 2016 coincide with the positive VHI anomaly (Fig. 3f and Supplementary Fig. S3). Likewise, there is a notable pattern of positive PMM (favours El Niño) and negative anomaly in VHI in 2004, 2009, 2016 and 2018. In contrast, the years of negative PMM (favours La Niña) have positive anomaly in VHI in 2008, 2011, and 2017 (Supplementary Fig. S4). Similarly, the positive phase of NAO (NAO^+) show negative anomaly in VHI in years 2002, 2009, 2013 and 2018 due delayed onset and weak ISM rainfall. Conversely, years 2003, 2008, 2010, 2014 and 2019 exhibit positive anomaly in VHI in the negative phase of NAO (NAO^-) that supports high ISM rainfall (Supplementary Fig. S5).

Since ISM carries moisture from the north Indian Ocean (NIO) and brings substantial amounts of rainfall in southeast Asia and India, it is highly important for agriculture and natural vegetation there. This study finds a significant increase in NIO SST in recent decade (2010–2019) as compared to its previous. The Indian Ocean Warm Pool (IOWP), a very warm area of the ocean, has been expanding and exhibit intensified warming. A comparable increase in SST is also noted in the West Pacific Warm Pool (WPWP), which also affect IOWP. Additionally, IOWP is expanding westward, as SST in the region has increased (0.25–0.5 °C) recent decade (2010–2019) from its previous (Fig. 3a–c). This suggests the westward shift of ISM and its associated heterogeneity in the rainfall distribution in India in recent decades, by which the western part may experience more rainfall, but moisture stress in the east result in enhanced ecological droughts there.

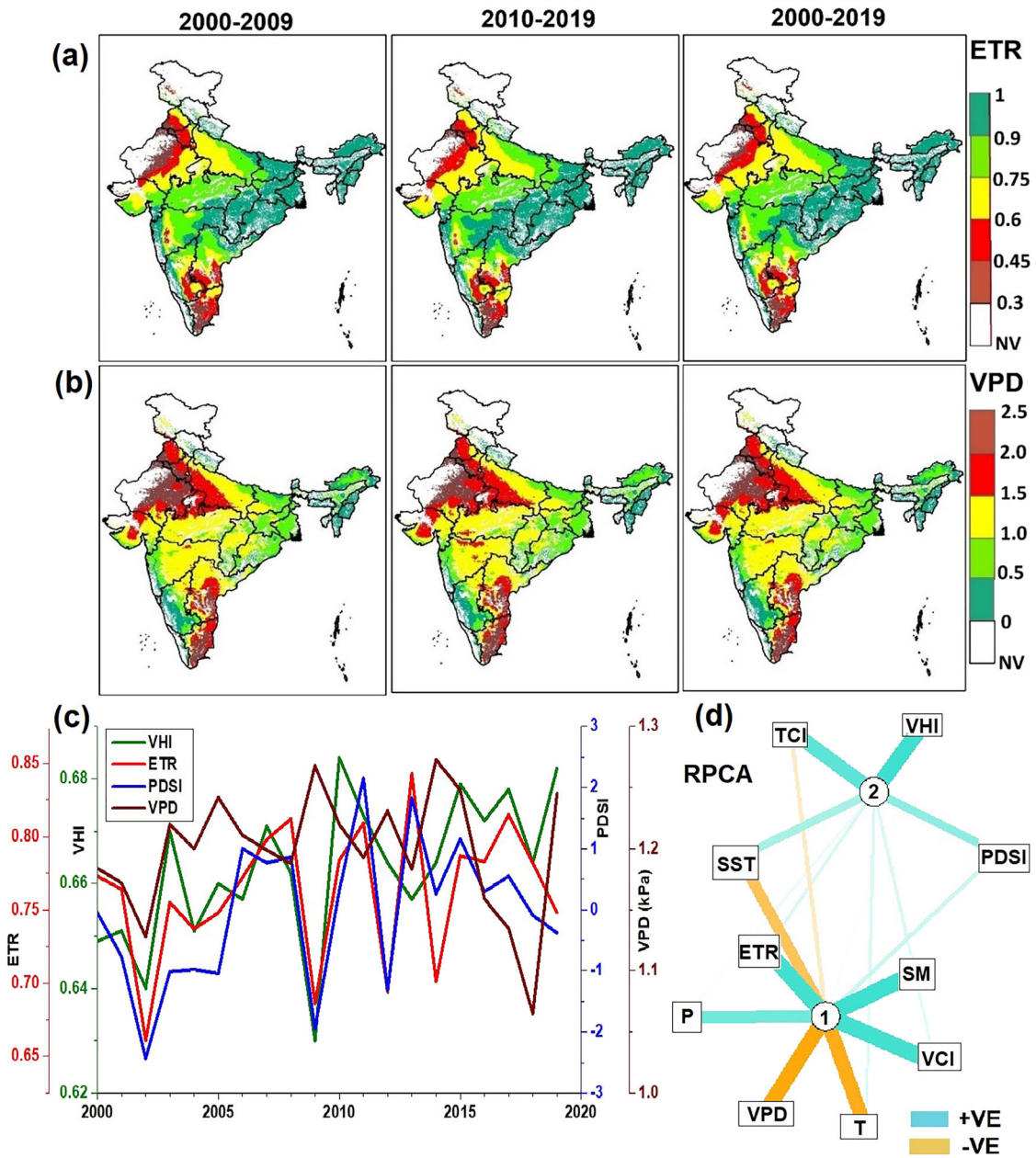

Fig. 2 | Vegetation health and aridity forms: spatio-temporal variability and relationships. a The Evapotranspiration Ratio (ETR), **b** Vapor Pressure Deficit (VPD) in kPa during Indian summer monsoon (ISM, from June to September) for the periods 2000–2009, 2010–2019 and 2000–2019. **c** The temporal evolution of Vegetation Health Index (VHI) with aridity forms such as ETR, VPD and Palmer Drought Severity Index (PDSI) for ISM during 2000–2019. **d** Rotated Principal Component analysis (RPCA) to examine the variability in VHI and its drivers: Precipitation (P), Soil Moisture (SM), Temperature (T), Sea Surface Temperature (SST), aridity forms (ETR, VPD and PDSI), Vegetation Condition Index (VCI) and Temperature Condition Index (TCI). Here, "1" and "2" denotes Principal Component 1 (PC1) and, PC2 respectively, "+VE" denotes positive correlation and "−VE" denotes negative correlation.

Contribution of drivers to ecological droughts

It is now known that climate drivers, aridity, monsoon, ocean heat and climatic oscillations have a notable influence on vegetation health and ecological droughts. However, the quantification and the pathways of physical mechanisms are to be explored. Here, Random Forest (RF) model is utilised to estimate the relative contribution of drivers in controlling VHI (Fig. 4a). The results reveal that PDSI (meteorological aridity) has the largest contribution (23.9%) in regulating VHI, followed by SST (18.2); suggesting the role of ocean warming on vegetation stress. Furthermore, ETR (14%) and VPD (12.4%) also contribute substantially and indicate the importance of land evaporative and atmospheric aridity, respectively, in driving vegetation health and ecological droughts in India. SM (11.1%), T (10.8%), and P (9.4%) also influence notably in VHI variability.

To quantify the influence of drivers on regional scale, this study estimates the relative contribution of drivers to VHI variability for various regions (Fig. 4a). Meteorological aridity (PDSI) is the dominant driver of VHI in most regions with stronger role in NW (27%) and CI (24.9%). Ocean warming (SST) also plays a substantial role in VHI variability in most regions with a higher influence in CI (19.6%), IGP (18.7%) and NE (18.4%). Land evaporative aridity (ETR) has a notable impact on VHI, particularly in NE (15.7%) and SI (15.2%). Atmospheric aridity (VPD) has a noticeable effect on VHI prominent in NE (17.4%) and HR (14.4%). Apart from aridity and ocean warming, fundamental climate drivers (P, T and SM) also play key roles in VHI variability. T has a marked impact in CI (12.5%), SI (12.2%) and HR (10.9%). SM plays an important role in IGP (16.7%) and SI (14.6%); whereas P is decisive to VHI variability in NW (14.2%) and HR (9.5%). The

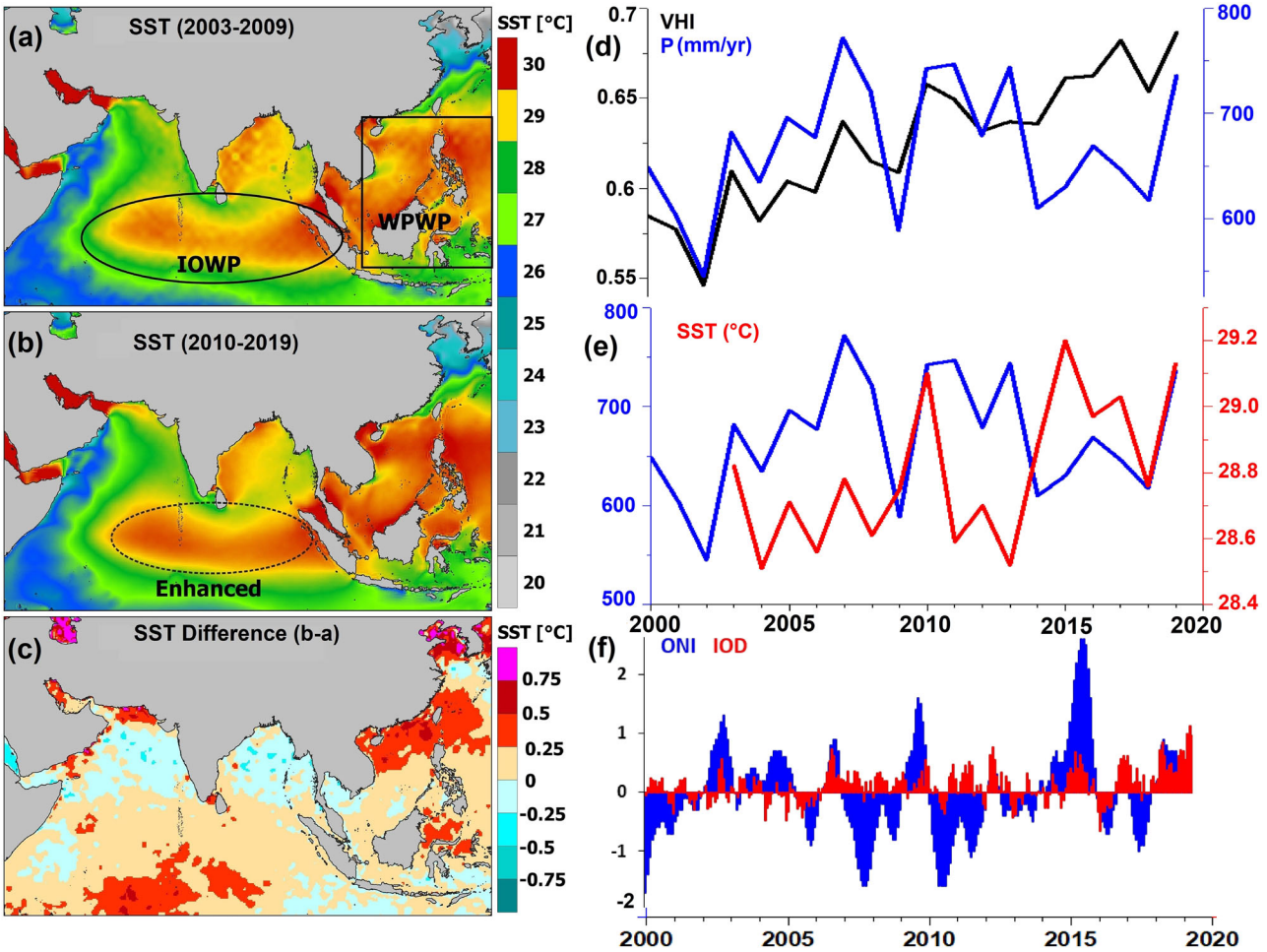

Fig. 3 | Vegetation health connection with ocean warming and climatic oscillations. a Sea Surface Temperature (SST) during the period 2003–2009, **b** 2010–2019, **c** Change in SST between b and a, here, WPWP is West Pacific Warm Pool and IOWP is Indian Ocean Warm Pool, temporal evolution of **d** Vegetation Health Index (VHI) with precipitation (P), **e** P and SST, **f** Oceanic Niño Index (ONI) and Indian Ocean Dipole (IOD) index during the period 2000–2019.

results from Multiple Linear Regression (MLR) (Supplementary Tables S1–S7) also exhibit similar findings wherein aridity (PDSI, VPD and ETR) and ocean heat (SST) are the major drivers of VHI, depending on region. Apart from these, T in HR, NE and CI; SM in IGP, NW and SI are the key drivers of VHI. Therefore, both RF and MLR reveal that aridity and ocean warming are the major controls of vegetation health and ecological droughts during ISM in india.

Relationships and causal links of drivers with ecological droughts

To examine the relationship of VHI with its drivers, this study employs correlation analyses (Fig. 4b). P (0.4) has a larger positive influence on VHI than SM (0.2) during monsoon (JJAS) season. ETR is positively correlated to VHI (0.63), as it has a strong positive relation with SM (0.7) and P (0.62), indicating the importance of the moisture availability for vegetation health. Contrarily, VPD (−0.61), PDSI (− 0.27) and T (−0.2) exhibit negative relation with VHI (Fig. 4b). SST (−0.88) exhibits a very strong negative influence on VHI as it has negative relation with moisture availability (SM, −0.45), and positive connection with T (0.5) and VPD (0.2). There is a strong relationship between various independent drivers, such as positive between P–SM (0.64), VPD–T (0.61) and negative between ETR–T (−0.84), SM–T (−0.8). Therefore, to thoroughly investigate the relationship of VHI with its drivers, this study employs partial correlation analyses (Fig. 4c). ETR has a strong positive relation with VHI even when T (0.86) and SM (0.7) are accounted. It helps to understand the larger influence of ETR on VHI, as also revealed by RF. VPD (−0.64) has a strong negative impact on VHI even when T is not accounted. Conversely, T (0.28) has a weaker and opposite relation with VHI without considering VPD. This explains the larger influence of VPD on VHI and the stronger control of VPD on T. Both ETR (0.4) and VPD (−0.38) hold their relation with VHI, despite the effect of one on the other. PDSI has a weak influence on VHI when P (0.15), T (0.22) and SM (0.23) are not accounted. VHI has a notable influence of P, T and SM without accounting for SST, but the relation is changed in case of SM (−0.45) and T (0.59). This is so as VHI has a high negative impact of SST (−0.92) even when land T is not considered.

Furthermore, to diagnose the connection of ecological droughts with its drivers and to unveil the complex non-linear atmosphere-land-ocean (ALO) interactions, this study utilises the causal discovery analysis of VHI with its potential drivers (Fig. 5). VHI has a positive causal link with ETR (0.4) at 3-months lag, as ETR has a very strong positive relation (0.8) with moisture availability (P and SM) and a strong negative (−0.8) link with T, as found from RPCA. Higher ETR suggests sufficient moisture availability that would support the vegetation growth. VHI shows a negative (−0.4) causal relationship with PDSI (at 1-month lag), as PDSI has a negative (−0.4) link with moisture availability (P and SM) at 3-month lag and a positive (0.4) connection with T (at 3-months lag). VHI also exhibits a very strong negative (−0.8) causal relation with VPD (at 3-months lag), wherein VPD has a negative ($r = -0.6$) relationship with moisture availability (P, SM and ETR), and all of these have a positive causal link with VHI. Apart from these, VHI has a direct positive (0.4) causal link with moisture availability (P and SM) at 3-months lag

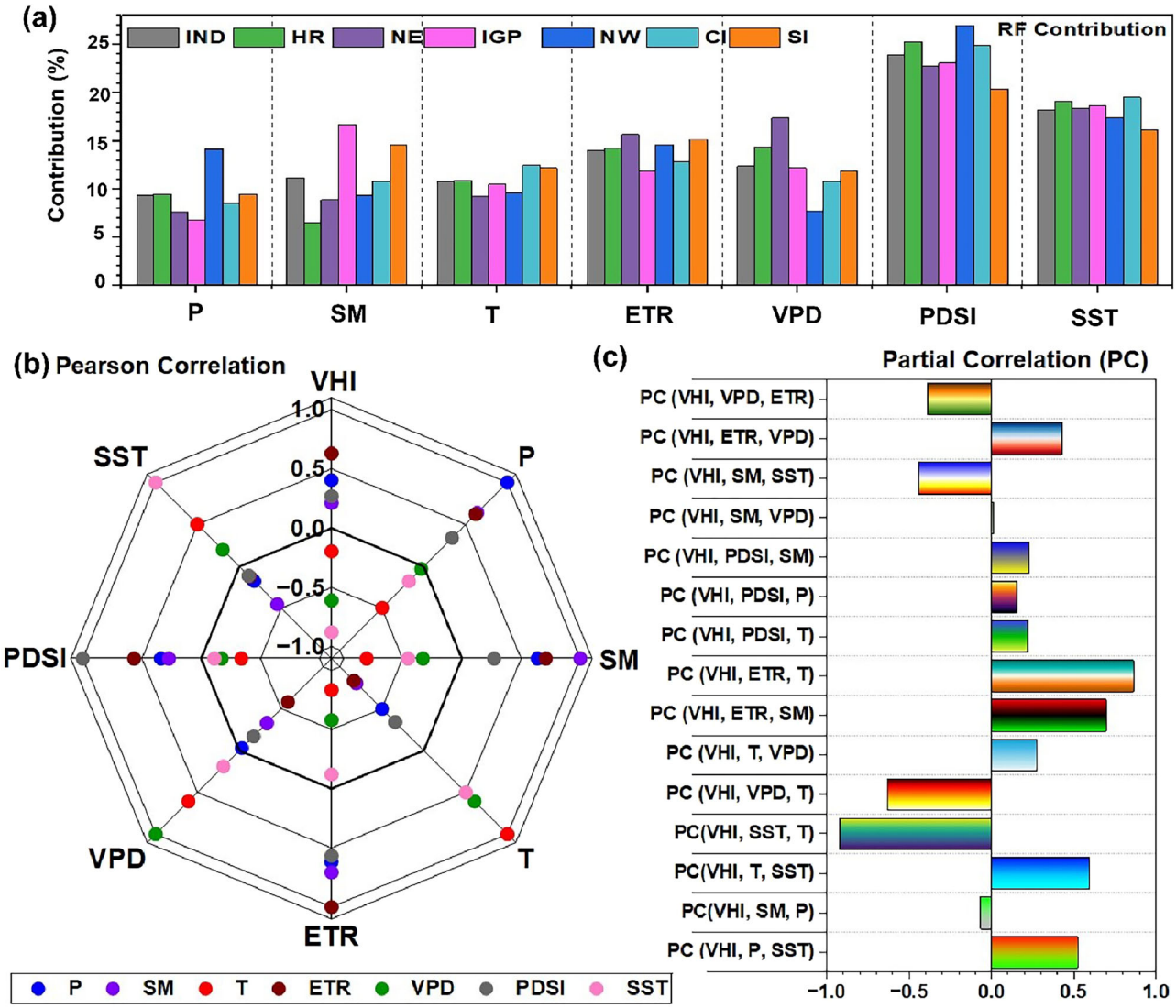

Fig. 4 | Vegetation health: relative contribution and relationship with drivers. **a** Random Forest (RF) based contribution of drivers: Precipitation (P), Soil Moisture (SM), Temperature (T), Evapotranspiration Ratio (ETR), Vapour Pressure Deficit (VPD), Palmer Drought Severity Index (PDSI) and Sea Surface Temperature (SST) to Vegetation Health Index (VHI) variability for various regions: as India (IND), Hilly Region (HR), Northeast (NE), Indo-Gangetic Plain (IGP), Northwest (NW), Central India (CI) and Southern India (SI). **b** Pearson Correlation, and **c** Partial Correlation (PC) between VHI and its drivers (P, SM,T, VPD, PDSI, ETR and SST) where PC (X, Y, Z) indicates partial correlation between X and Y limiting the effects of Z (covariate).

and a negative causal (−0.2) relation with T (3-months lag), as also depicted by RPCA. This is expected as water availability promotes vegetation growth, but higher T is detrimental to plant health in the tropical and temperate regions of India (Fig. 5a).

To enable vivid understanding of the underlying mechanisms and causal links, this study employs causal analysis for various regions (Fig. 5b–g). In most regions, aridity (PDSI, VPD and ETR) has a direct causal link with VHI, except for NW (only VPD), CI (no PDSI), and SI (no ETR). Key climate drivers (P, SM and T) also exhibit direct causal associations with VHI in most regions. In HR, SM does not have any direct causal link with VHI, as SM in this region is mostly very low or in the form of snow water equivalent. In NE, there is no direct causal link of T and VHI, but T impacts aridity that has a direct causal link with VHI. IGP and SI do not show direct causal relationship of P and VHI, and this might be due to the intensive irrigation in the vast croplands. However, P has a direct causal link with SM, T and PDSI that impacts VHI. Contrarily, VHI does not show any direct link with SST in any region, but it influences VHI indirectly through P, T and VPD as it has a positive link with all these. This is reasonable, as higher SST would increase T through heat transfer, and higher T would lead to enhanced land (low ETR) and atmospheric (high VPD) aridity. Therefore, atmosphere, land and oceans act as a complex interwoven system that triggers increased vegetation stress and ecological droughts during ISM in India.

Rising ecological droughts triggers browning

The long-term change in ecological droughts along with their drivers (Fig. 6) and its impact on vegetation dynamics (Fig. 7) are investigated here. VHI is estimated to have increased by 2.3% in recent decade (2010–2019) in comparison to the previous decade (2000–2009) during ISM (Fig. 6). Concurrently, there is greening (+5% VCI) supported by improved moisture availability through enhanced P (+3.2%) and ETR (+2.8%); reduction in VPD (−1.2%). However, simultaneously, SM has reduced by 2.7% due to increase in thermal stress (+0.3% TCI) (Fig. 6a). Therefore, for clear understanding of the mechanisms, the decadal changes in these indicators are explored on regional scales (Fig. 6b). There is a notable improvement in VHI for NW (+5.4%) due to enhanced greening (+10.1% VCI) and reduced thermal stress on vegetation (−1.4% TCI). Improved VHI in NW is also facilitated by substantial improvement in moisture

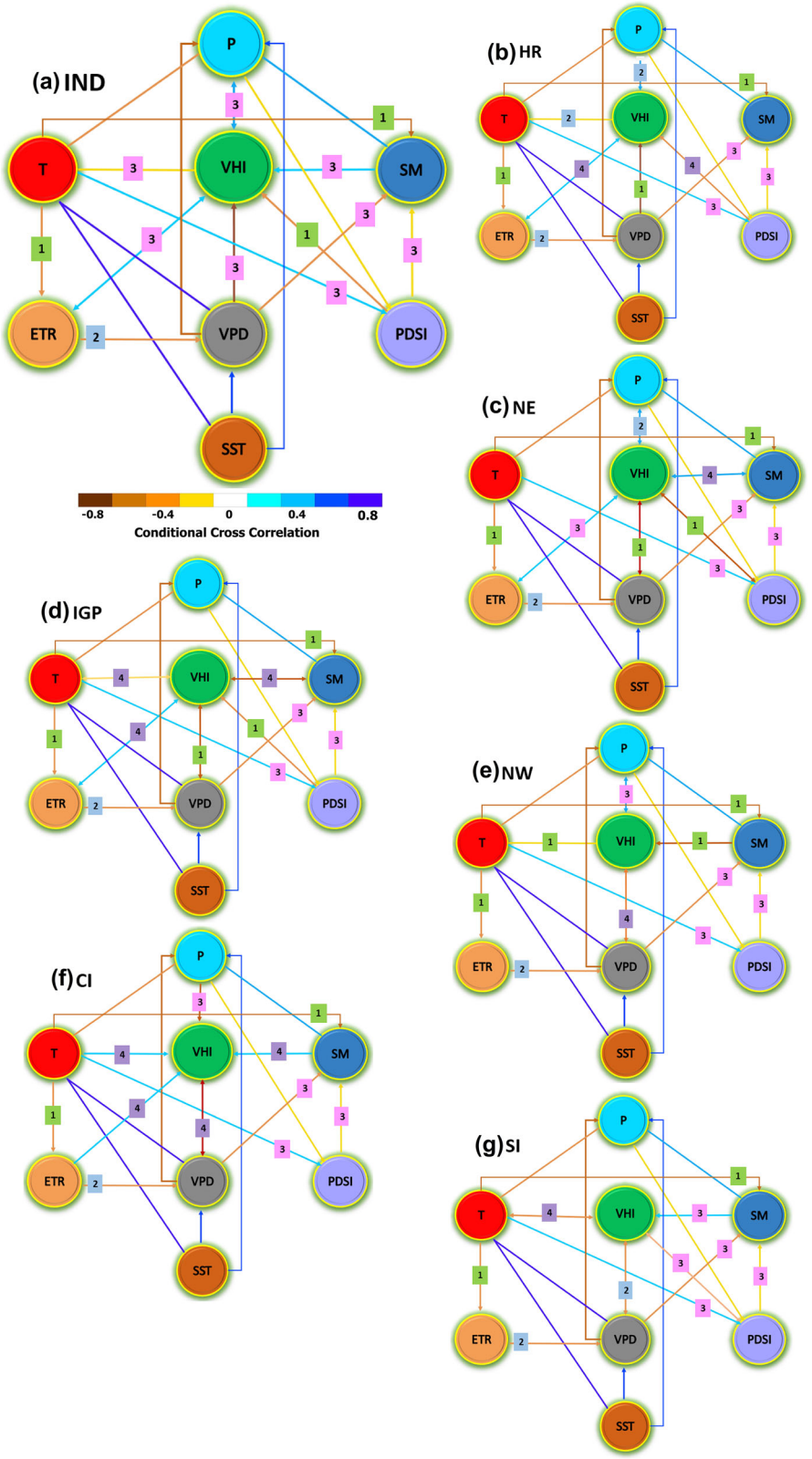

Fig. 5 | Vegetation health and drivers: causal relationships. Causal graphs representing the causal links for Vegetation Health Index (VHI) with its drivers in Precipitation (P), Soil Moisture (SM), Temperature (T), Evapotranspiration Ratio (ETR), Vapour Pressure Deficit (VPD), Palmer Drought Severity Index (PDSI) and Sea Surface Temperature (SST) and interrelationship among them for **a** India (IND) and various bioclimatic regions: **b** Hilly Region (HR), **c** Northeast (NE), **d** Indo-Gangetic Plain (IGP), **e** Northwest (NW), **f** Central India (CI) and **g** Southern India (SI).

availability exhibited by enhanced P (+18.8%), SM (+2.5%), ETR (+8%) and depleted VPD (−1.1%). Likewise, IGP exhibits enhanced VHI (2.5%) as there is marked greening (+5.5% VCI) due to enhanced water availability in this region as P (2.3%), SM (3.4%) and ETR (2.4%) show a noticeable rise, and a decline (−1.5%) in VPD in recent decade. Similarly, CI shows enhanced VHI (+2.2%) due to increased VCI (4.4%), P (5.5%) and TCI (0.5%). In addition, the reduction in VPD (−1.8%) has led to an increase in ETR (1.8%) in recent decade there. HR shows enhanced VHI (0.6%) owing to the increase in VCI (0.9%), enhanced P (3.9%) and decrease in TCI, as indicated by the marginal rise in ETR (0.2%) in recent decade. NW, much of CI and some areas in IGP are estimated to have reduced meteorological aridity (PDSI).

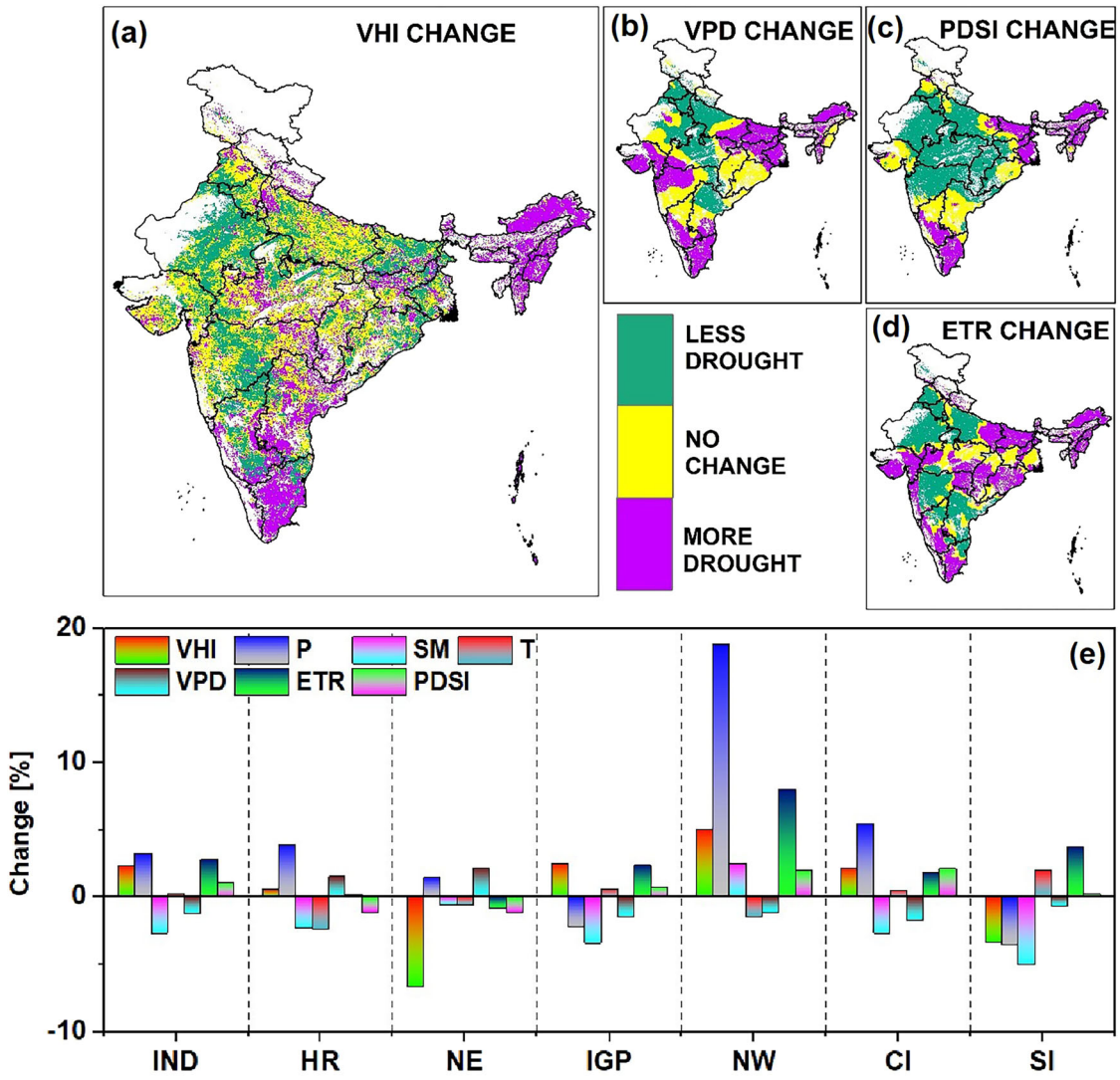

Fig. 6 | Changes in ecological droughts and drivers. The long-term change in various drought indices: **a** Ecological: Vegetation Health Index (VHI), **b** Atmospheric: Vapour Pressure Deficit (VPD), **c** Meteorological: Palmer Drought Severity Index (PDSI) and **d** Land Evaporative: Evapotranspiration Ratio (ETR) in recent decade (2010–2019) from the previous decade (2000–2009). **e** Percentage (%) change in VHI and its drivers in aridity forms (VPD, ETR, and PDSI), key climatic factors [Precipitation (P), Soil Moisture (SM), Temperature (T)], and Sea Surface Temperature (SST) for various regions: as India (IND), Hilly Region (HR), Northeast (NE), Indo-Gangetic Plain (IGP), Northwest (NW), Central India (CI) and Southern India (SI) in recent decade (2010–2019) from the previous decade (2000–2009).

In contrast, VHI has substantially decreased in NE (−6.6%), although this region shows marginal greening (VCI is +1.7%) due to reduced thermal stress (−0.5% TCI) and enhanced P (1.5%). Simultaneously, increased aridity, i.e. VPD (+2.2%) and ETR (−1.7%) has depleted SM (−0.5%) in NE. In SI, VHI is reduced notably (3.4%) due to strong browning (−8.7% VCI) due to a substantial reduction in moisture availability, i.e. P (−3.5%) and SM (−5%). This is driven by an enhancement in thermal stress (+ 2.1% TCI), and aridity i.e. VPD (+1.6%) and ETR (−3.7%). PDSI is increased in the southern areas in SI, eastern IGP, HR (eastern Himalaya) and NE in recent decade from the previous. Additionally, the browning areas are HR in the eastern Himalaya, NE, eastern areas of IGP and the southern regions of SI. Interestingly, the ecological droughts have increased in all these regions, as illustrated in Fig. 7. Therefore, greening facilitated by improved moisture availability and better thermal conditions support improved vegetation health and reduced ecological droughts in the western regions of the country. On the other hand, the threat of ecological drought has increased in NE, eastern IGP and SI during ISM due to enhanced aridity, increased moisture stress, and thermal stress in recent decades, which triggers browning there.

Declining forest health due to anthropogenic intrusions

The ecological droughts are increasing predominantly in intensive croplands of eastern IGP and forests in India. In terms of forests, ecological droughts are rising in south western Himalaya, eastern Himalaya, NE, some areas in CI and Western Ghats (Fig. 8a). The ecological drought driven browning is evident in the regions of increased ecological droughts, except for some areas in southern NE (Fig. 8b). To explore the human modifications of natural ecosystems, this study employs two indices; Human Modification Index (HMI) and Forest Landscape Integrity Index (FLII). The forests in western Himalaya, NE, CI, and Western Ghats and SI exhibit large human modifications (HMI > 0.4). The forests in CI show substantial modifications (HMI > 0.4), with a low integrity score (FLII = 5.5). Similarly, IGP shows the weakest integrity (FLII = 3.9) and high human alterations (HMI = 0.38). The FLII of forests in southern NE, some areas in western Himalaya, CI and Western Ghats exhibit low integrity or high forest fragmentation (Fig. 8c, d). Also, this analysis finds large increase in human population in the forest regions of India during 2000–2019 (Supplementary Fig. S8). The population explosion (40–60%) is dominant in the forests of HR, NE, IGP, CI and

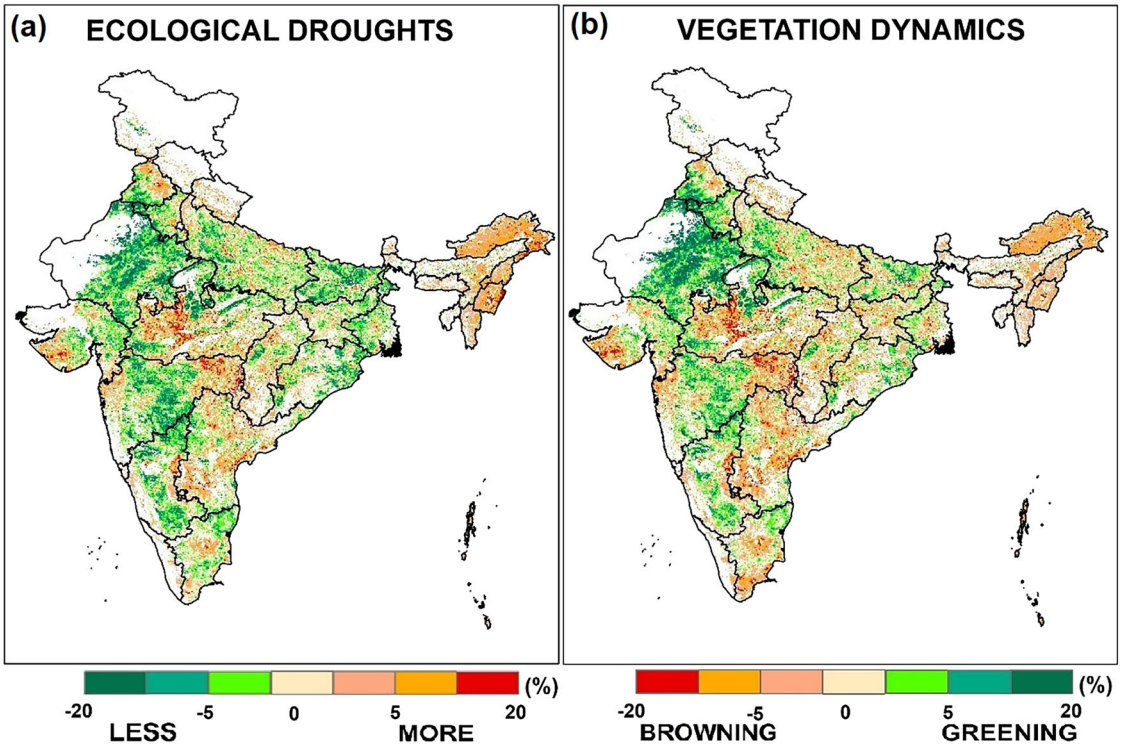

Fig. 7 | Changes in ecological droughts and vegetation dynamics. The long-term change (%) in **a** ecological droughts (less/more) based on the Vegetation Health Index (VHI) and **b** vegetation dynamics (greening/browning) based on the the Normalized Difference Vegetation Index (NDVI) in recent decade (2010–2019) from the previous decade (2000–2009).

Western Ghats that exhibit severe human modifications and forest fragmentation (Fig. 8 and Supplementary Fig. S6).

Discussion

Previous drought management strategies were based on the response of hydrological, hydroclimatic, agricultural and socio-economic factors to droughts[3,5,6,9]. Ecological drought is put forward as an ecological response linked to long-term moisture stress, and it expands the existing understanding of droughts[10–12]. The ecological ramifications of droughts are not being adequately addressed[9–12]. The impact of climate change-induced changes in vegetation can surpass the direct effects of climate change in certain areas with enhanced ecological droughts, even with more rainfall[10,39]. Ecological droughts in northwest China are increasing westward affecting larger areas, longer durations, higher frequency, and greater severity in the 21st century[13]. Ecosystem water balance model suggests that ecological droughts will be more in the southern and less in the northern drylands of the United States and Canada[40]. When comparing the meteorological droughts to ecological droughts in northwest China, ecological droughts last longer than meteorological droughts[13]. Furthermore, the duration of transition from meteorological to ecological drought was shorter during summer (2.7 months) and longer during winter (7 months). However, the transition is more likely during summer than winter in China[14].

In the changing climate and enhanced human influences, vegetation exhibits substantial changes in India during recent decades[27,28,34–37]. Concurrently, India is one of the global hotspots of land-atmosphere interactions[38], and exhibits a very strong connection between the carbon and water cycles[17,18,25]. Also, India is the most inhabited country with more than 1.4 billion people whose livelihood is largely depend on agricultural yields and forest goods. Furthermore, droughts are more intense and common in recent decades due to strengthened land-atmosphere coupling in India[41]. Erratic rainfall[30], unprecedented warming[42], shifting monsoon[43] and enhanced aridity[17,18] in recent decades make the ecological ramifications of droughts very severe, but are not adequately addressed for India. However, there are numerous challenges such as the diversity of vegetation and bioclimatic regions, complex land-atmosphere interactions, data scarcity and extensive computational needs to conduct such studies for the Indian region[17,18,25]. In addition, droughts are inherently intricate, which pose challenges in accurately assessing their effects on terrestrial ecosystems. The ecosystem water demands are very diverse and depend upon many factors such as biomes, biological hierarchy, prevailing climate, topography, drought stage and characteristics and ecosystem services[7,10,17,18]. Thus, the ecological ramifications of droughts are very complex as ecosystems exhibit diverse reactions to droughts[10–14]. Therefore, this is a dedicated assessment of ecological droughts, and we expose the high vulnerability regions, analyse its underlying drivers, mechanisms and investigate its impact on vegetation dynamics in India during ISM and its implications for sustainability. This study is based on a suite of advanced statistical and ML techniques employed on satellite measurements, reanalyses and models.

This study finds that forests in western Himalaya, and croplands in northwest (NW) and southern regions of south India (SI) are vulnerable to vegetation stress and ecological droughts. The ecological droughts are increasing in Himalaya, NE, eastern IGP, CI and southern SI due to increase in land evaporative (ETR), meteorological (PDSI) and atmospheric (VPD) aridity in recent decade (2010–2019) from the previous (2000–2009). Interestingly, these are the regions with ample moisture and optimum warmth to support vegetation, yet they are subjected to ecological droughts now. The increase in ecological droughts in these regions drives browning during monsoon, particularly in the croplands of eastern IGP and southern SI, and forests of Himalaya, NE and CI. These croplands in eastern IGP and SI are browning due to warming-induced soil moisture stress in recent decades[17,34]. The Himalaya and NE are regions of highly efficient carbon sinks and have become ecologically fragile and vulnerable now due to climate change and anthropogenic intrusions[28,44,45]. Apart from the rising

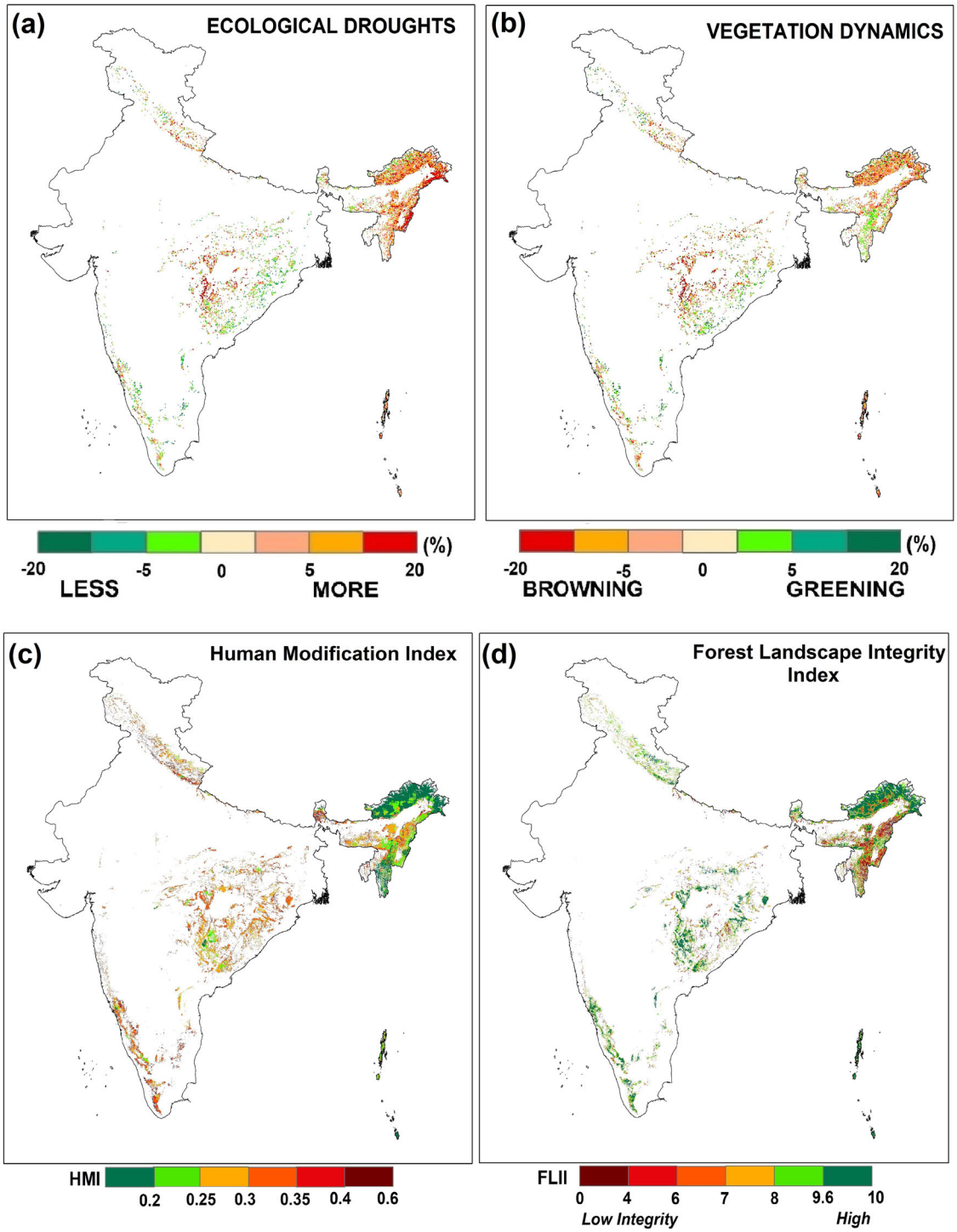

Fig. 8 | Changes in ecological droughts, vegetation dynamics and anthropogenic interventions in forests. The long-term change (%) in **a** ecological drought and **b** vegetation dynamics in recent decade (2010–2019) from the previous decade (2000–2009). **c** Human Modification Index (HMI). **d** Forest Landscape Integrity Index (FLII) for Indian forest ecosystems during the year 2016 and 2019, respectively.

aridity, the ocean warming also contributes to the enhancement in ecological droughts in India. The high SST would increase land T through the transfer of oceanic heat to land, which reduces VHI through TCI. In addition, high land T enhances ET, which would deplete SM and trigger ecological droughts. Also, the warming of Indian Ocean is the major cause for weakening of ISM rain over the Himalayan foothills, northern and central-east regions of India[29]. Furthermore, warming in the warmer region of NIO (IOWP) is intensified and WPWP is also getting stronger and moving westward[46]. These hint at the potential westward shift of ISM[43] that leads to increase in ecological droughts and browning, mainly in eastern and southern India and dryland greening in northwest India[47]. The multiple algorithms such as correlation, partial correlation, PCA, causal analysis and RF yield coherent results across India and various bioclimatic regions, which are also consistent with previous findings[17,25,28].

The climatic oscillations impact hydroclimatic conditions through ISM and its associated rainfall that regulates moisture availability[29,30] and vegetation health in India[32,33]. The teleconnections like ENSO in its warm phase (El Niño) leads to dry and hot conditions, and promote ecological

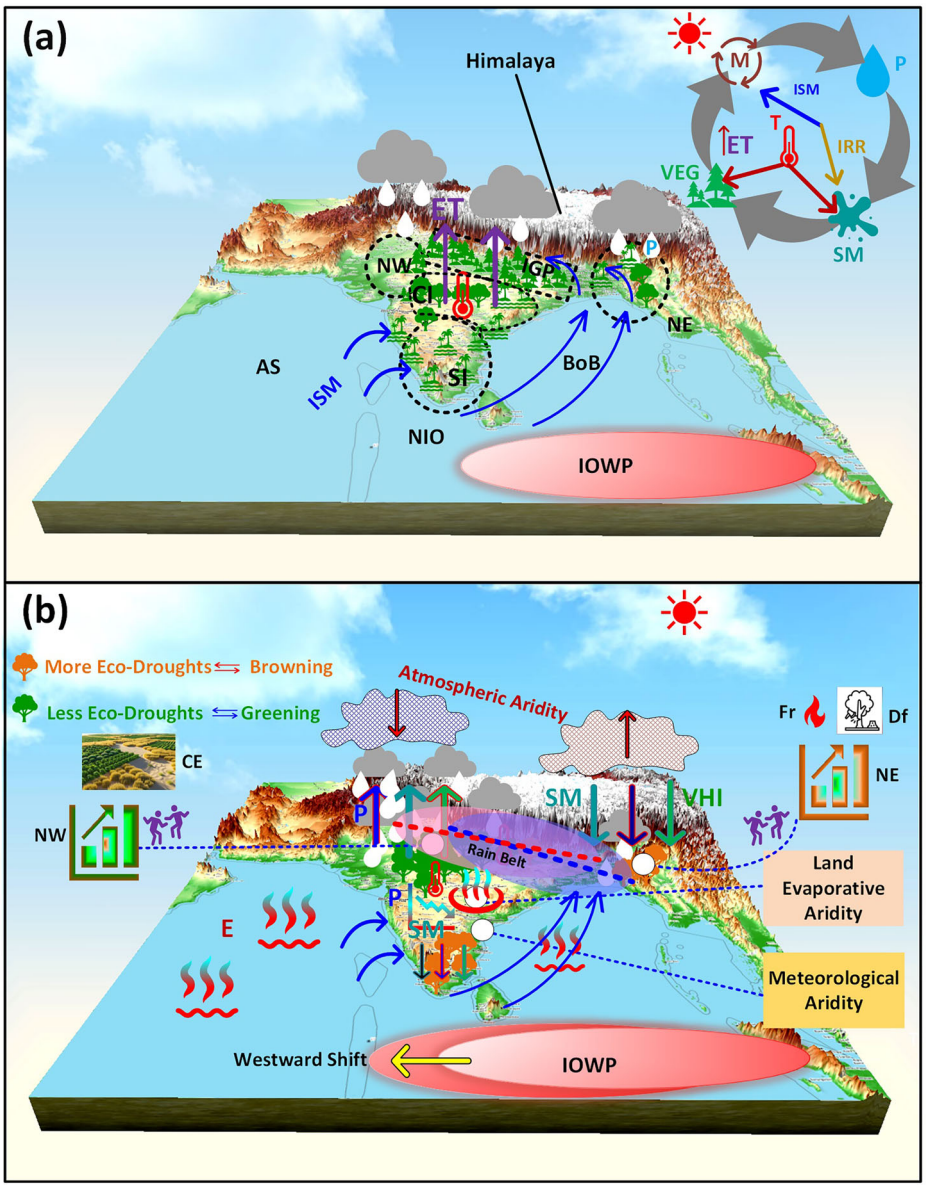

Fig. 9 | Concept diagram. An illustration showing **a** general state of atmosphere, land and ocean (ALO) interactions and **b** state of ALO interactions during rising ecological droughts due to climate change and human interventions. Here, M Moisture, P Precipitation, SM Soil Moisture, IRR Irrigation, VEG Vegetation, ISM Indian Summer Monsoon; ET Evapotranspiration, E Evaporation, T Temperature, NIO North Indian Ocean, BoB Bay of Bengal, AS Arabian Sea, NW North west, NE North east, IGP Indo-Gangetic Plain, SI Southern India, FR Wildfires, DF Deforestation, CE Cropland Expansion. Here, solid blue arrows represent the ISM winds, dashed blue line represents actual rain region and dashed red line represents the shifted rain region that indicates westward shift of ISM.

droughts in India. The IOD also impacts regional weather processes and interannual climate variability in India, in which the negative IOD (nIOD) suppresses convection and weakens the ISM rainfall along with higher temperatures[30,48] that favours ecological droughts. Other climatic oscillations such as PMM and NAO mainly act as precursors of the ISM rainfall. PMM influence teleconnections like ENSO with positive PMM favouring El Niño development and weakens the regional walker circulation over the Pacific, which displaces the westerlies towards Indian Ocean and leads to weak ISM rainfall[48,49], triggering ecological droughts in India. NAO also impacts ISM rainfall indirectly as they alter upper tropospheric wind patterns over India for which the positive phase of NAO (NAO^+) delays onset and reduces the strength of ISM rainfall, promotes dryness[48,50] and ecological droughts in the region. In short, the El Niño, nIOD, positive PMM and NAO^+ years are the periods of ecological droughts in India.

This study finds that the ecological droughts are increasing in the forests of HR, NE, CI and Western Ghats. These regions exhibit forest degradation and have high anthropogenic intrusions, including traditional agricultural practices (slash and burn, and shifting jhum cultivation) and land use and land cover changes (LULCC)[45], accompanied by natural hazards such as landslides[51] and wildfires[44,52]. Large scale human modifications of natural ecosystems lead to increase in forest integrity (intactness) loss that would eventually disrupt the land-atmosphere interactions. The regional recycling of moisture through forests is greatly perturbed and cause moisture stress in the rising aridity scenario that have substantial ecological ramifications and leads to ecological droughts. Furthermore, growing human alteration of natural ecosystems results in deforestation and forest degradation that cause browning and decline in forest health. Additionally, rising ecological droughts also decline vegetation vigor and functioning; triggering browning. Thus, more ecological droughts and browning trigger each other as a feedback loop. In short, the rising aridity, ocean warming, westward shift of the ISM and human modifications drive more ecological droughts that leads to browning in the intensive croplands of eastern IGP, southern SI and forests in Himalaya, NE, CI and Western Ghats, as depicted in Fig. 9a, b.

The rising ecological droughts in India are driving browning of pristine forests and intensive croplands during the moisture rich monsoon season. The browning owing to ecological droughts would result in weakened forest carbon sinks[28] and reduced crop yields[15,17]. Browning will decline the health and functioning of the terrestrial ecosystems[11–13,18]. Also, ecological droughts lead to tree mortality due to mechanisms such as carbon starvation and

hydraulic failure[53]. This will also decline the evapotranspiration that would constrain the cooling effects and promote regional warming[54]. Persistent ecological droughts would alter the regional plant species composition and promote growth of more moisture resistant plant species[10,11]. The human influence on natural ecosystems has resulted in large-scale forest fragmentation and degradation in India that can greatly threaten the regional biodiversity[45,55]. In the drier and warmer world with increasing human intervention on the natural ecosystems would lead to more severe and frequent fires in central and southern India[56]. Also, the decline in forest health would weaken the land-atmosphere feedbacks like the regional moisture recycling. Furthermore, stronger, frequent and persistent ecological droughts can lead to forest to grassland transition in India[57], as in some regions of Amazon[58]. Growing ecological droughts can weaken the carbon sink potential of Indian forests in the future[57]. Some vulnerable ecosystems might not completely recover ever and lead to a chain of destabilisation and ecosystem collapse. This can lead to release of stored carbon, and rise the atmospheric carbon dioxide (CO_2) that would further increase the global warming. Forests serve as vital resources, and their degradation would adversely affect the ecosystem goods and services, and the lives of forest dwellers. Increase in ecological droughts that drive decline in crop yield is a great threat to food security in the population explosion scenario. This can also lead to a hike in global prices of major food grains as India is one of the key breadbaskets of the world. Therefore, the rising ecological droughts due to enhanced aridity, changing monsoon climate, and human activities on natural ecosystems is a great concern for food security and sustainability.

It may be feasible to alleviate the effects of ecological droughts by implementing modifications to policies, management practises and water infrastructure. Using the conventional engineered solutions may harm the vulnerable natural systems. There is a need of proactive resource management strategy such as forest thinning that align with natural processes and can enhance them to effectively mitigate ecological drought vulnerability. "Nature-based solutions (NbS)" refer to investments made to safeguard and rehabilitate natural systems and offer potential for mitigating the risks linked to ecological droughts. However, these approaches are mostly lacking in drought planning, and their effectiveness and cost are seldom measured or compared to infrastructure-based mitigation strategies. Typically, human activities prioritise the demand for water over the needs of ecosystems[11,12]. Henceforth, it is imperative to incorporate ecosystem services and vulnerability assessment into the planning to effectively tackle ecological droughts. To adequately tackle them, management policies should integrate both ecosystem services and vulnerability assessment of droughts. Furthermore, one of the approaches can be planting drought resilient plants in areas vulnerable to ecological droughts. Water-efficient crops (e.g. millets and sorghum) can be grown as a counter strategy. Also, to reduce crop water consumption, crop switching and water-efficient irrigation facilities should be employed[59]. Additionally, there is a need to preserve the readily plant-available water in the soil by utilising conservative agricultural practices such as crop row spacing, mulching, and low or no till farming[17,18]. In the growing human population scenario with limited land area, approaches like agroforestry should be promoted for judicial utilisation of the available resources to attain sustainability. There is a need of scientific restoration of degraded landscapes through efficient land management and forest conservational approaches. In addition, the indigenous vulnerable ecosystems should be preserved and protected against ecological droughts by improving their resilience against moisture stress.

It is high time to integrate ecological droughts in the climate policies and give due respect in various climate change adaptation and mitigation strategies. The ecological implications of droughts should be considered in legislations to combat their threats such as prevention of crop failures, famines, degeneration and fragmentation of forests, and socio-economic issues. Remote sensing data should be integrated with existing available ground-based measurements and previous government reports to delineate the regions vulnerable to the increasing risk of ecological droughts. Landscape level ecosystem planning and restoration efforts should be practiced, centred around the Ecosystem-based Adaptation (EbA) strategies such as REDD+ (Reducing Emissions from Deforestation and Forest Degradation, 2008), the Bonn Challenge (2011), Land Degradation Neutrality (LDN) goals (2015), and the Trillion Trees Initiative (2020). Efforts should be made for plantation of indigenous structurally diverse plant species as a buffer against ecological droughts in the vulnerable regions. There is an urgent need to align the ecological drought adaption strategies and regional planning with mainstream government policies and sustainability targets in the near future. Also, more studies are needed on ecological droughts, its mechanisms and implications in a warmer and drier Earth. Future studies should focus on carbon stock monitoring and forest carbon dynamics[60]. Further research should be conducted on the forecast of ecological droughts, its adaption and mitigation strategies especially for the Indian region, as a large population depends upon agriculture and forest driven ecosystem goods and services for living there.

This study is centred around remote sensing measurements that have their own limitations such as atmospheric and soil background noises, changes in satellite orbit, and replacement of sensors along with saturation and insufficient sensitivity in dense canopy. The land surface model results used in the study are also constrained as they are largely global models and might not be very efficient in capturing regional dynamics. Ground-based measurements are very limited in the Indian region, but would certainly enhance our results, if available. The statistical and ML techniques employed in the study have their own limitations, as they are data driven and require more measurements to train and test to yield robust outcomes. Also, the data utilised have certain uncertainty that is inherited in the results. The temporal span of the study is limited to the years from 2000 to 2019 based on the availability of the MODIS (since 2000) and various other datasets. In addition, this analysis period is restricted up to 2019 to avoid the anomalies owing to the COVID-19 lockdown in the vegetation, meteorological and other related data, which if included, would corrupt the long-term changes and training data for the ML model[61].

Conclusions

To the best of our knowledge, this study is the first attempt to explore the complex non-linear interactions among atmosphere-land-ocean (ALO) through investigation of ecological droughts, their drivers, long-term changes and implications on vegetation dynamics in India during ISM in recent decades (2000–2019). It finds an increase in ecological droughts in ecologically sensitive regions such as Himalaya, NE, eastern IGP, CI and southern SI in recent decades. These regions are also the hotspots of increase in meteorological, land evaporative and atmospheric aridity. Meteorological aridity and ocean warming are two of the dominant drivers of ecological droughts in India as per the ML based RF model. Causal analysis reveals that the ocean warming indirectly triggers ecological droughts as it affects moisture availability, thermal conditions and atmospheric aridity. Furthermore, potential westward shift of the summer monsoon system triggers more ecological droughts in eastern and southern India. Henceforth, the rising ecological droughts due to enhanced aridity, ocean warming and human interventions drives browning during the ISM season in India. Monsoon is the crucial season for agricultural activities and growth of forests in India, and thus, the ecological droughts during ISM are a big threat to socio-economic fabric of the country. Therefore, rising ecological droughts due to changing vegetation-climate-human nexus in a shifting monsoon climate can be a serious concern for environmental sustainability in India as a millions of people rely on agriculture and forest-based ecosystem goods and services. Rising ecological droughts and browning during the ISM season can also disturb the ecohydrological balance, moisture recycling and land-atmosphere feedbacks. This study, henceforth, unveils the complex non-linear links between the atmosphere, biosphere and hydrosphere through various statistical and ML techniques. The findings will help in effective planning for mitigation and adaption of the adverse impacts of droughts on ecosystems in India and is applicable to similar bioclimatic regions of the world. There is a need for efficient monitoring of the carbon-water cycle interactions, improved climate risk management,

Table 1 | Data table

Data	Resolution	Purpose/use	Source
MODIS LULC	500 m	LULC data to extract Forest and Cropland	(https://lpdaacsvc.cr.usgs.gov/)
MODIS NDVI	500 m	NDVI & calculation of VCI	(https://lpdaacsvc.cr.usgs.gov /)
MODIS LST	500 m	LST & calculation of TCI	(https://lpdaacsvc.cr.usgs.gov /)
MODIS SST	4 km	Ocean heat content changes	(https://lpdaacsvc.cr.usgs.gov /)
GPM Precipitation	0.1° × 0.1 °	Precipitation variability and change	(https://daac.gsfc.nasa.gov/)
GLDAS Soil Moisture	0.25° × 0.25°	Soil Moisture variability and change	(https://daac.gsfc.nasa.gov/)
GLDAS Air Temperature	0.25° × 0.25°	Air Temperature variability and change	(https://daac.gsfc.nasa.gov/)
TerraClimate AET	4 km	Calculation of land evaporative aridity and change	(https://www.climatologylab.org/terraclimate.html)
TerraClimate PET	4 km	Calculation of land evaporative aridity and change	(https://www.climatologylab.org/terraclimate.html)
TerraClimate PDSI	4 km	Calculation of meteorological aridity and change	(https://www.climatologylab.org/terraclimate.html)
TerraClimate VPD	4 km	Calculation of atmospheric aridity and change	(https://www.climatologylab.org/terraclimate.html)
Human Modification Index (HMI)	1 km	To investigate human modification of forests	(https://sedac.ciesin.columbia.edu/)
Forest Landscape Integrity Index (FLII)	300 m	To investigate the impact of human on forests	(www.forestlandscapeintegrity.com)
WorldPop	1 km	To investigate change in human population in forests	(https://www.worldpop.org/)
NOAA ONI		To account for role of ENSO	(https://origin.cpc.ncep.noaa.gov/)
NOAA IOD (DMI)		To account for role of IOD	(https://psl.noaa.gov/gcos_wgsp/Timeseries/)
NOAA PMM		To account for role of PMM	(https://psl.noaa.gov/data/timeseries/month/)
NOAA NAO		To account for role of NAO	(https://www.cpc.ncep.noaa.gov/products/precip/CWlink/pna/norm.nao.monthly.b5001.curren620t.ascii.table)

Datasets with their resolution, purpose and source are mentioned.

land management practices, and policies in the context of anthropogenic climate change in India to achieve sustainability and food security.

Methods

Detection of ecological droughts

Remote sensing-based indices have emerged as effective techniques for monitoring droughts[6,10,62,63]. NDVI has been extensively used for detecting vegetation dynamics[34,36,45] and drought assessment[6,7,62,63]. Recently, VHI is widely used as an ecological drought indicator[6,8,14,64] which is based on the combination of VCI and TCI. VHI is highly efficient for the detection of ecological droughts as it incorporates the climate and topographical features such as slope and soil[19]. Also, the crop yield and VHI show a high coherence, which is stronger in the important crop growth stages[64]. VHI is a stronger indicator of ecosystem health and crop yield than the vegetation indices such as NDVI, Enhanced Vegetation Index (EVI) and Leaf Area Index (LAI), as they are proxies to the surface greenness and plant biomass[6,8,14,64]. Therefore, VHI is employed as an indicator for vegetation health, and delineation of regions under vegetation stress and vulnerable to ecological droughts in India during ISM (June, July, August, and September: JJAS) months for recent decades (2000–2019).

All datasets, specifications and sources are listed in Table 1. An overview of the methodology employed in this study is illustrated in Supplementary Fig. S7. All analyses are performed for the vegetated land comprising of croplands and forest regions. The other land cover types were masked out based on the Moderate Resolution Imaging Spectroradiometer (MODIS) land use and land cover (LULC) data for the year 2019 (Supplementary Fig. S8). VHI is estimated by linearly combining VCI and TCI. VCI is based on pixel-wise normalization of the NDVI values, which represents the variation or the proximity of current NDVI to the minimum NDVI estimated over a period of time[65]. Here, VCI is estimated from MODIS NDVI data using the relation (Eq. (1))

$$\mathrm{VCI} = \frac{\mathrm{NDVI_i} - \mathrm{NDVI_{min}}}{\mathrm{NDVI_{max}} - \mathrm{NDVI_{min}}} \quad (1)$$

Where, $\mathrm{NDVI_i}$, $\mathrm{NDVI_{max}}$ and $\mathrm{NDVI_{min}}$ are the mean, maximum and minimum values of NDVI, respectively.

TCI gives the temperature induced stress on vegetation and is estimated as VCI, where Land Surface Temperature (LST) data from MODIS are used at same resolution (Eq. (2))

$$\mathrm{TCI} = \frac{\mathrm{LST_i} - \mathrm{LST_{min}}}{\mathrm{LST_{max}} - \mathrm{LST_{min}}} \quad (2)$$

Where, $\mathrm{LST_i}$, $\mathrm{LST_{max}}$ and $\mathrm{LST_{min}}$ are mean, maximum and minimum values of LST, respectively.

VHI is derived from VCI and TCI based on the relationship (Eq. (3))

$$\mathrm{VHI} = (a.\mathrm{VCI}) + (b.\mathrm{TCI}) \quad (3)$$

Where, a and b are weights; and b is 1-a. Here, both a and b are taken as 0.5 each as per the convention[64].

VHI is normally represented in terms of 0–100, but for convenience as an indicator for ecological droughts, here it is scaled it to 0–1 (Eq. (4))

$$\mathrm{VHI_n} = \frac{\mathrm{VHI_i} - \mathrm{VHI_{min}}}{\mathrm{VHI_{max}} - \mathrm{VHI_{min}}} \quad (4)$$

Here, $\mathrm{VHI_n}$, $\mathrm{VHI_i}$, $\mathrm{VHI_{min}}$ and $\mathrm{VHI_{max}}$ are the normalised, mean, minimum and maximum and minimum values of VHI, respectively.

To examine the spatio-temporal changes, the analyses are divided into three focal periods: (i) 2000–2009 (previous decade), (ii) 2010–2019 (recent decade) and (iii) 2000–2019 (the complete study period). The decadal change in VHI and all its drivers is also estimated based on the pixel-wise image differencing technique. The change in different parameters during the period (2000–2019) is quantified in terms of percentage, as per the equation (Eq. (5))

$$\%X_{R-P} = \frac{X_R - X_P}{X_P} \times 100 \quad (5)$$

Here, X is any variable, R is the mean of X in recent decade (2010–2019) and P is the mean of X in the previous decade (2000–2019).

Quantification of aridity

Sufficient moisture availability in an ideal scenario for healthy crops that can be evaporated is called potential evapotranspiration (ETp), and the moisture supply to plants to be evaporated that is influenced by weather conditions, water availability and crop health is termed as the actual evapotranspiration (ETa)[66,67]. The ETR, indicates evaporative or land aridity, is also called as evaporative stress index (ESI) that considers the moisture availability on the land surface readily available to be evaporated[68]. The TerraClimate ETa and ETp data are taken to compute ETR as per the equation (Eq. (6))

$$ETR = \frac{ETa}{ETp} \quad (6)$$

Apart from this, the drought indices in terms of PDSI and VPD from TerraClimate are also considered to examine the meteorological and atmospheric aridity, respectively[69,70]. PDSI is a comparative measure that integrates past P, current moisture levels (P and SM), and moisture requirements (ETp)[69]. VPD is regarded as a reliable indicator of atmospheric aridity as it is a measure of "atmospheric moisture demand" estimated as the difference between saturated (SVP) and actual atmospheric vapour pressure (AVP) at a specific temperature[71] as per the equation (Eq. (7))

$$VPD = SVP - AVP \quad (7)$$

VPD impacts vegetation water stress, canopy photosynthesis, and global carbon and climate feedback by regulating vegetation stomatal aperture[70–72].

Accounting for climatic oscillations

To account for the role of large-scale circulation, the El Niño Southern Oscillation (ENSO) Index and Oceanic Niño Index (ONI) based on the Dipole Mode Index (DMI) are taken, and the 3-month anomaly of Jun-Jul-Aug (JJA) and Jul-Aug-Sep (JAS) are averaged to make ONI for the Indian summer monsoon (JJAS). To estimate the influence of Indian Ocean Dipole (IOD) on monsoon variability and its effect on terrestrial vegetation, the IOD index is considered. Apart from these, two other climatic oscillations that are regarded as precursors indirectly influence ISM i.e. Pacific Meridional Mode (PMM) and North Atlantic Oscillation (NAO) are also considered for pre-monsoon (MAM: March, April and May) period[48,49].

Correlation and partial correlation

To understand the relationship among ecological drought and its drivers, Parsons's correlation analysis is performed. Since there are a number of drivers with certain degree of autocorrelation, this study employs partial correlation (PC) to account for specific relations limiting the role of covariates. The linear relationship between two variables after excluding the effect of one or more independent variables (covariate) is known as PC, and is computed as (Eq. (8)):

$$r_{xy.z} = \left(\frac{r_{xy} - r_{xz} \cdot r_{yz}}{\sqrt{1 - r_{xz}^2} \cdot \sqrt{1 - r_{yz}^2}} \right) \quad (8)$$

Here, r_{xy} = correlation coefficient of between variable x and variable y, $r_{xy.z}$ = first order partial correlation between variable x and y by elimination of covariate (z) from the other variables (x and y).

Principal component analysis

Furthermore, PCA is performed to better understand the link between drivers and VHI. PCA is popular in the climate science for performing the teleconnection analyses[73]. The varimax method is used to derive principal components (PCs). The PCs are decided based on the computed eigen values. The linear transformation of PCs wherein the prominent relationships are highlighted and the underlying autocorrelations are eliminated[74]. Here, rotated PCA (RPCA) using varimax rotation technique is employed to enhance the inference, and to segregate the key drivers of VHI variability as detailed in Supplementary Information (Supplementary Text 1). However, in some instances, PCA does not provide easily explainable results for physical processes that are not directly connected and is more suitable to explain the variability[75]. Furthermore, to gain better understanding of drivers and their influence on ecological droughts, causal discovery is employed, as detailed below.

Causality

To investigate the complex interactions in ecological systems, correlation-based method may not be sufficient as it is not a causation. Also, it is insufficient when there is influence of a third variable (covariate, z) between the relationship of two (x and y), and certain degree of autocorrelation exists among the variables[76]. To explore the complex non-linear links between the atmosphere-land-oceans (ALO) interactions accounting for hidden drivers, specific paths and temporal lags, this study employs causal discovery. Peter and Clarke's Momentary Conditional Independence (PCMCI), a Machine Learning (ML) algorithm from the family of widely used Pearl Causality (PC) framework, is utilised to explore the causal links between VHI with its drivers, and the interrelationships among them[28,77]. PCMCI works at two stages, for which, initially it estimates partial correlation between two timeseries for identification of driver's parents based on iterative conditional independence test at various lags. Then, it evaluates the statistical significance of the causal relationships based on momentary conditional independence (MCI) tests, followed by the estimation of strength of causal links using multiple linear regression (MLR). The PCMCI method utilises various statistical tests to ascertain causality, including linear partial correlations (Par-Corr) and nonlinear independence tests such as Gaussian Process regressions Distance Correlation (GPDC), and Conditional Mutual Information (CMI). In this study, the PCMI+ based causal discovery is performed at 5% statistical significance ($\acute{\alpha}$) with a 4-month maximum allowable lag (τ_{max}) to quantify the non-linear relation among the multiple drivers of regional ALO interactions as detailed in Supplementary Information (Supplementary Text 2).

Contribution of drivers to ecological droughts

In recent years, ML has been extensively employed to examine the intricate nonlinear relationship between the dependent and independent variables owing to its suitability for multidimensional data. Random Forest (RF) is a decision tree-based ML algorithm usually made with unpruned RF regression trees that are used to make strong predictions[78]. This study utilises the RF model in R Studio version 4.2.1 based on packages "randomForest" and "caret" to estimate the relative contribution of individual drivers to VHI variability[17,18]. In the RF model, a total of 500 decision trees are generated with two variable splitting allowed in each tree. Here, 70% of the data are split for training and 30% for testing. A variable relevance indicates the

degree to which its exclusion reduces accuracy, as per the equation (Eq. (9))

$$I_x = \sum_{k=1}^{K}\left[\frac{1}{\mathrm{K}}(MSE_k{}^{xprem} - MSE_k)\right] \quad (9)$$

Here, I_x is the variable importance or contribution, K is the number of trees in the forest, $MSE_k{}^{xprem}$ is the estimation error with predictor x being eliminated for the k^{th} decision tree, and MSE_k is the forecasting error with all predictors included in the k^{th} decision tree.

The spatial autocorrelation between the training and testing data is estimated, and the spatial cross validation is found by dividing the study area of Indian vegetated land into six homogeneous bioclimatic zones (HR, NE, IGP, NW, CI and SI) (Supplementary Fig. S8 and Supplementary Table S8). The RF model is run for Indian vegetated land and each of these homogeneous bioclimatic zones to estimate the relative contribution of drivers to the VHI variability as detailed in Supplementary Information (Supplementary Text 3). Additionally, MLR is also employed to determine the contribution of drivers to the VHI variability, together with the standard errors for Indian vegetated land and its bioclimatic zones to complement the findings from the RF model, as presented in Supplementary Information (Supplementary Tables S1–S7). The drivers considered are P, temperature (T), SM, ETR, VPD, PDSI and sea surface temperature (SST). The P data are sourced from the Global Precipitation Measurement (GPM), while the SM and T data are obtained from the Global Land Data Assimilation System (GLDAS). Here, the SST data are from MODIS as detailed in Table 1.

Quantification of human influence

To assess anthropogenic intrusions on natural ecosystems, this study employs two indices[57]: the Human Modification Index (HMI) and the Forest Landscape Integrity Index (FLII). HMI is sourced from the Socioeconomic Data and Applications Centre (SEDAC) and ranges from 0 to 1, reflecting the cumulative extent of human alteration of land, encompassing 13 anthropogenic stressors categorised into five groups: (i) human settlement, (ii) agriculture, (iii) transportation, (iv) mining and energy production, and (v) electrical infrastructure[79] for the year 2016. FLII represents the inaugural assessment of the ecological integrity of global forests, incorporating both observed and inferred human pressures (such as infrastructure, agriculture, and tree cover loss) and accounts for the degradation of forest connectivity (the ratio of current to potential forest connectivity) for the year 2019. The scale spans from 0 to 10, categorising low as 0–6, moderate as 6–9.6, and high as 9.6–10[80]. Also, the human population count data are obtained from WorldPop that employs dasymetric redistribution based on RF model. As a proxy for human interference in natural ecosystems, the change in human population in the year 2019 from 2000 is estimated by pixel wise image differencing technique for the forest regions[57].

Data availability

All data are publicly available and are listed in Table 1.

Code availability

Data processing is performed in R Studio (version 4.2.1) and ArcGIS (version 10.4). The plots and charts are created in and ArcGIS (version 10.4), OriginPro (version 9), Maps3D (https://maps3d.io/) and Microsoft Visio (https://www.microsoft.com/en-in/microsoft-365/visio/flowchart-software), QGIS, and The R codes for MLR, RF can be obtained from https://github.com/RahulKashyap1803. The source code for the PCMCI$^+$ causal discovery is available at https://github.com/jakobrunge/tigramite.

Received: 7 March 2025; Accepted: 12 August 2025;
Published online: 28 October 2025

References

1. Erian, W. et al. GAR special report on drought 2021. United Nations Office for Disaster Risk Reduction. https://collections.unu.edu/view/UNU:8334 (2021).
2. Singh, J. et al. Enhanced risk of concurrent regional droughts with increased ENSO variability and warming. *Nat. Clim. Change* **12**, 163–170 (2022).
3. Mishra, A. K. & Singh, V. P. A review of drought concepts. *J. Hydrol.* **391**, 202–216 (2010).
4. Svoboda, M., Hayes, M. & Wood, D. Standardized precipitation index: user guide. (WMO-No. 1090). Geneva, Switzerland: WMO. https://library.wmo.int/doc_num.php?explnum_id=7768 (2012).
5. Wu, H. et al. Decreasing dynamic predictability of global agricultural drought with warming climate. *Nat. Clim. Change* **15**, 411–419 (2025).
6. Zeng, J. et al. Improving the drought monitoring capability of VHI at the global scale via ensemble indices for various vegetation types from 2001 to 2018. *Weather Clim. Extrem.* **35**, 100412 (2022).
7. Jha, S., Das, J., Sharma, A., Hazra, B. & Goyal, M. K. Probabilistic evaluation of vegetation drought likelihood and its implications to resilience across India. *Glob. Planet. Change* **176**, 23–35 (2019).
8. Weng, Z., Niu, J., Guan, H. & Kang, S. Three-dimensional linkage between meteorological drought and vegetation drought across China. *Sci. Tot. Environ.* **859**, 160300 (2023).
9. Slette, I. J. et al. How ecologists define drought, and why we should do better. *Glob. Change Biol.* **25**, 3193–3200 (2019).
10. Cui, J., Chen, A., Huntingford, C. & Piao, S. Integrating ecosystem water demands into drought monitoring and assessment under climate change. *Nat. Water* **2**, 215–218 (2024).
11. Crausbay, S. D. et al. Defining ecological drought for the twenty–first century. *Bull. Am. Meteorol. Soc.* **98**, 2543–2550 (2017).
12. Crausbay, S. D. et al. Unfamiliar territory: Emerging themes for ecological drought research and management. *One Earth* **3**, 337–353 (2020).
13. Jiang, T., Su, X., Singh, V. P. & Zhang, G. Spatio–temporal pattern of ecological droughts and their impacts on health of vegetation in Northwestern China. *J. Environ. Manag.* **305**, 114356 (2022).
14. Wang, F. et al. Dynamic variations of terrestrial ecological drought and propagation analysis with meteorological drought across the mainland China. *Sci. Tot. Environ.* **896**, 165314 (2023).
15. Lesk, C., Rowhani, P. & Ramankutty, N. Influence of extreme weather disasters on global crop production. *Nature* **529**, 84–87 (2016).
16. Mahto, S. S. & Mishra, V. Increasing risk of simultaneous occurrence of flash drought in major global croplands. *Environ. Res. Lett.* **18**, 044044 (2023).
17. Kashyap, R. & Kuttippurath, J. Warming–induced soil moisture stress threatens food security in India. *Environ. Sci. Poll. Res.* **31**, 59202–59218 (2024).
18. Kashyap, R. & Kuttippurath, J. Unraveling the sensitivity and response of ecosystems to rising moisture stress in India. *Ecosyst. Health Sustain.* **10**, 0180 (2024).
19. Bhuiyan, C., Saha, A. K., Bandyopadhyay, N. & Kogan, F. N. Analyzing the impact of thermal stress on vegetation health and agricultural drought–a case study from Gujarat, India. *GISci. Rem. Sens.* **54**, 678–699 (2017).
20. Mishra, D., Goswami, S., Matin, S. & Sarup, J. Analyzing the extent of drought in the Rajasthan state of India using vegetation condition index and standardized precipitation index. *Model. Earth Sys. Environ.* **8**, 601–610 (2022).
21. Masroor, M. et al. Analysing the relationship between drought and soil erosion using vegetation health index and RUSLE models in Godavari middle sub–basin, India. *Geosci. Front.* **13**, 101312 (2022).

22. Singh, R. P., Roy, S. & Kogan, F. Vegetation and temperature condition indices from NOAA AVHRR data for drought monitoring over India. *Int. J. Remote Sens.* **24**, 4393–4402 (2003).
23. Kundu, A., Dwivedi, S. & Dutta, D. Monitoring the vegetation health over India during contrasting monsoon years using satellite remote sensing indices. *Arab. J. Geosci.* **9**, 1–15 (2016).
24. Ambika, A. K. & Mishra, V. Observational evidence of irrigation influence on vegetation health and land surface temperature in India. *Geophys. Res. Lett.* **46**, 13441–13451 (2019).
25. Dubey, N. & Ghosh, S. The relative role of soil moisture and vapor pressure deficit in affecting the Indian vegetation productivity. *Environ. Res. Lett.* **18**, 064012 (2023).
26. Sebastian, D. E., Murtugudde, R. & Ghosh, S. Soil–vegetation moisture capacitor maintains dry season vegetation productivity over India. *Sci. Rep.* **13**, 888 (2023).
27. Kashyap, R., Pandey, A. C. & Kuttippurath, J. Photosynthetic trends in India derived from remote sensing measurements during 2000–2019: vegetation dynamics and key climate drivers. *Geocarto Int.* **37**, 11813–11829 (2022).
28. Kashyap, R., Kuttippurath, J. & Kumar, P. Browning of vegetation in efficient carbon sink regions of India during the past two decades is driven by climate change and anthropogenic intrusions. *J. Environ. Manag.* **336**, 117655 (2023).
29. Roxy, M. K. et al. Drying of Indian subcontinent by rapid Indian Ocean warming and a weakening land–sea thermal gradient. *Nat. Commun.* **6**, 1–10 (2015).
30. Pachore, A., Remesan, R. & Kuttippurath, J. Flash drought teleconnection with the large-scale climate drivers in the homogeneous rainfall regions of India. *Int. J. Climatol.* **45**, e8711 (2025).
31. Bastos, A., Running, S. W., Gouveia, C. & Trigo, R. M. The global NPP dependence on ENSO: La Niña and the extraordinary year of 2011. *J. Geophys. Res. Biogeosci.* **118**, 1247–1255 (2013).
32. Wigneron, J. P. et al. Tropical forests did not recover from the strong 2015–2016 El Niño event. *Sci. Adv.* **6**, eaay4603 (2020).
33. Kashyap, R. & Kuttippurath, J. Tropical cyclones enhance photosynthesis in moisture–stressed regions of India. *npj Clim. Atmos. Sci.* **8**, 115 (2025).
34. Parida, B. R., Pandey, A. C. & Patel, N. R. Greening and browning trends of vegetation in India and their responses to climatic and non–climatic drivers. *Climate* **8**, 92 (2020).
35. Sarmah, S. et al. Mismatches between vegetation greening and primary productivity trends in South Asia-a satellite evidence. *Int. J. Appl. Earth Obs. Geoinfo.* **104**, 102561 (2021).
36. Kuttippurath, J. & Kashyap, R. Greening of India: forests or croplands?. *Appl. Geogr.* **161**, 103115 (2023).
37. Chen et al. China and India lead in greening of the world through land–use management. *Nat. Sustain.* **2**, 122–129 (2019).
38. Humphrey, V. et al. Soil moisture–atmosphere feedback dominates land carbon uptake variability. *Nature* **592**, 65–69 (2021).
39. Tietjen, B. et al. Climate change-induced vegetation shifts lead to more ecological droughts despite projected rainfall increases in many global temperate drylands. *Glob. Change Biol.* **23**, 2743–2754 (2017).
40. Bradford, J. B., Schlaepfer, D. R., Lauenroth, W. K. & Palmquist, K. A. Robust ecological drought projections for drylands in the 21st century. *Glob. Change Biol.* **26**, 3906–3919 (2020).
41. Mahto, S. S. & Mishra, V. Flash drought intensification due to enhanced land–atmospheric coupling in India. *J. Clim.* **37**, 5291–5307 (2024).
42. Kumar, R., Kuttippurath, J., Gopikrishnan, G. S., Kumar, P. & Varikoden, H. Enhanced surface temperature over India during 1980–2020 and future projections: causal links of the drivers and trends. *npj Clim. Atmos. Sci.* **6**, 164 (2023).
43. Rajesh, P. V. & Goswami, B. N. Climate change and potential demise of the Indian deserts. *Earths Fut.***11**, e2022EF003459 (2023).
44. Sannigrahi, S. et al. Examining the effects of forest fire on terrestrial carbon emission and ecosystem production in India using remote sensing approaches. *Sci. Tot. Environ.* **725**, 138331 (2020).
45. Sparsha, S. & Parida, B. R. Vegetation browning trend progressively leading to forest degradation in eastern himalaya in response to climatic and anthropogenic drivers. *Remote Sens. Appl. Soci. Environ.* **35**, 101209 (2024).
46. Peter, R., Kuttippurath, J., Chakraborty, K. & Sunanda, N. A high concentration CO2 pool over the Indo–Pacific Warm Pool. *Sci. Rep.* **13**, 4314 (2023).
47. Kashyap, R., Kuttippurath, J. & Patel, V. K. Agriculture intensification and moisture–induced Thar desert greening: implications for energy balance, socio–economy, and biodiversity. *GISci. Remote Sens.* **62**, 2483458 (2025).
48. Athira, K. S. et al. Regional and temporal variability of Indian summer monsoon rainfall in relation to El Niño southern oscillation. *Sci. Rep.* **13**, 12643 (2023).
49. Hari, V., Ghosh, S., Zhang, W. & Kumar, R. Strong influence of north Pacific Ocean variability on Indian summer heatwaves. *Nat. Commun.* **13**, 5349 (2022).
50. Yadav, R. K., Srinivas, G. & Chowdary, J. S. Atlantic Niño modulation of the Indian summer monsoon through Asian jet. *npj Clim. Atmos. Sci.* **1**, 23 (2018).
51. Kashyap, R., Pandey, A. C. & Parida, B. R. Spatio–temporal variability of monsoon precipitation and their effect on precipitation triggered landslides in relation to relief in Himalayas. *Spat. Info Res.* **29**, 857–869 (2021).
52. Kashyap, R. & Pandey, A. C. Spatio–temporal variability assessment of pre–monsoon temperature to deduce their impact on Forest Fire events in relation to relief across Himalayan region. *J. Geomat.* **15**, 106–114 (2021).
53. McDowell, N. G. et al. Mechanisms of woody–plant mortality under rising drought, CO2 and vapour pressure deficit. *Nat. Rev. Earth Environ.* **3**, 294–308 (2022).
54. Yang, Y. et al. Evapotranspiration on a greening Earth. *Nat. Rev. Earth Environ.* **4**, 626–641 (2023).
55. Reddy, C. S. et al. Assessment and monitoring of deforestation and forest fragmentation in South Asia since the 1930s. *Glob. Planet. Change* **161**, 132–148 (2018).
56. Bar, S. et al. Investigation of fire regime dynamics and modeling of burn area over India for the twenty-first century. *Environ. Sci. Poll. Res.* **31**, 53839–53855 (2024).
57. Kashyap, R. & Kuttippurath, J. Weakening of forest carbon stocks due to declining Ecosystem Photosynthetic Efficiency under the current and future climate change scenarios in India. *Resour. Conserv. Recycl.* **222**, 108478 (2025).
58. Staal, A. et al. Hysteresis of tropical forests in the 21st century. *Nat. Commun.* **11**, 4978 (2020).
59. Chakraborti, R. et al. Crop switching for water sustainability in India's food bowl yields co–benefits for food security and farmers' profits. *Nat. Water* **1**, 864–878 (2023).
60. Wigneron, J. P. et al. Global carbon balance of the forest: satellite-based L-VOD results over the last decade. *Front. Remote Sens.* **5**, 1338618 (2024).
61. Kashyap, R., Kuttippurath, J. & Patel, V. K. Improved air quality leads to enhanced vegetation growth during the COVID–19 lockdown in India. *Appl. Geogr.* **151**, 102869 (2023).
62. West, H., Quinn, N. & Horswell, M. Remote sensing for drought monitoring and impact assessment: Progress, past challenges and future opportunities. *Rem. Sens. Environ.* **232**, 111291 (2019).
63. Liu, Q., Zhang, S., Zhang, H., Bai, Y. & Zhang, J. Monitoring drought using composite drought indices based on remote sensing. *Sci. Tot. Environ.* **711**, 134585 (2020).

64. Bento, V. A., Gouveia, C. M., DaCamara, C. C. & Trigo, I. F. A climatological assessment of drought impact on vegetation health index. *Agric. Meteorol.* **259**, 286–295 (2018).
65. Kogan, F. N. Application of vegetation index and brightness temperature for drought detection. *Adv. Space Res.* **15**, 91–100 (1995).
66. Otkin, J. A., Zhong, Y., Lorenz, D., Anderson, M. C. & Hain, C. Exploring seasonal and regional relationships between the Evaporative Stress Index and surface weather and soil moisture anomalies across the United States. *Hydrol. Earth Sys. Sci.* **22**, 5373–5386 (2018).
67. Liu, Y. et al. The divergence between potential and actual evapotranspiration: an insight from climate, water, and vegetation change. *Sci. Tot. Environ.* **807**, 150648 (2022).
68. Anderson, M. C. et al. The Evaporative Stress Index as an indicator of agricultural drought in Brazil: an assessment based on crop yield impacts. *Rem. Sens. Environ.* **174**, 82–99 (2016).
69. Song, X., Song, Y. & Chen, Y. Secular trend of global drought since 1950. *Environ. Res. Lett.* **15**, 094073 (2020).
70. Fu, Z. et al. Atmospheric dryness reduces photosynthesis along a large range of soil water deficits. *Nat. Commun.* **13**, 989 (2022).
71. Grossiord, C. et al. Plant responses to rising vapor pressure deficit. *N. Phytol.* **226**, 1550–1566 (2020).
72. Yuan, W. et al. Increased atmospheric vapor pressure deficit reduces global vegetation growth. *Sci. Adv.* **5**, eaax1396 (2019).
73. Mezzina, B., Garcia–Serrano, J., Blade, I. & Kucharski, F. Dynamics of the ENSO teleconnection and NAO variability in the North Atlantic–European late winter. *J. Clim.* **33**, 907–923 (2020).
74. Huth, R. & Beranová, R. How to recognize a true mode of atmospheric circulation variability. *Earth Space Sci.* **8**, e2020EA001275 (2021).
75. Spensberger, C., Reeder, M. J., Spengler, T. & Patterson, M. The connection between the Southern Annular Mode and a feature–based perspective on Southern Hemisphere midlatitude winter variability. *J. Clim.* **33**, 115–129 (2020).
76. Runge, J. et al. Inferring causation from time series in Earth system sciences. *Nat. Commun.* **10**, 1–13 (2019).
77. Krich, C. et al. Estimating causal networks in biosphere–atmosphere interaction with the PCMCI approach. *Biogeosci* **17**, 1033–1061 (2020).
78. Breiman, L. Random forests. *Mach. Learn.* **45**, 5–32 (2001).
79. Kennedy, C. M., Oakleaf, J. R., Theobald, D. M., Baruch-Mordo, S. & Kiesecker, J. Managing the middle: a shift in conservation priorities based on the global human modification gradient. *Glob. Change Biol.* **25**, 811–826 (2019).
80. Grantham, H. S. et al. Anthropogenic modification of forests means only 40% of remaining forests have high ecosystem integrity. *Nat. Commun.* **11**, 5978 (2020).

Acknowledgements

We thank the Director, Indian Institute of Technology Kharagpur (IIT Kgp), Chairman of CORAL IIT Kgp and the Ministry of Education (MoE) for facilitating the study. RK acknowledges the support from PMRF, MoE and VKP acknowledges the support from MoE, IIT KGP. We thank the NASA's LPDAAC team for providing the MODIS landcover, NDVI, LST and SST products. NASA GES DISC for providing the GPM level–3 precipitation data, GLDAS air temperature and soil moisture. We thank TerraClimate for providing AET, PET, PDSI, VPD datasets, WorldPop for population count, NOAA for providing ONI, IOD, PMM, and NAO data, SEDAC for HMI data and Prof. Hedley Grantham for making FLII datasets available publicly.

Author contributions

R.K.: Conceptualization, Methodology, Data Analyses, Visualization, Validation, Software, Writing–original draft and editing of the original draft. J.K.: Conceptualization, Methodology, Supervision, Validation, Visualization, review and editing of the original draft. V.K.P.: Data Analyses, Software and Visualization.

Competing interests

The authors declare no competing interests.

Additional information

Supplementary information The online version contains supplementary material available at https://doi.org/10.1038/s43247-025-02694-3.

Correspondence and requests for materials should be addressed to Jayanarayanan Kuttippurath.

Peer review information *Communications Earth & Environment* thanks Songyan Zhu and the other, anonymous, reviewer(s) for their contribution to the peer review of this work. Primary Handling Editors: Min-Hui Lo and Aliénor Lavergne. A peer review file is available.